Maser Hunting in the Galactic Plane

A thesis submitted to The University of Manchester for the degree of
Doctor of Philosophy
in the Faculty of Engineering and Physical Sciences

2010

Lyshia Quinn

School of Physics and Astronomy

Contents

List of Figures

List of Tables

The University of Manchester

ABSTRACT OF THESIS submitted by Lyshia Quinn
for the Degree of Doctor of Philosophy and entitled
Maser Hunting in the Galactic Plane. July 2010

The process of massive star formation greatly influences its surroundings through their outflows, vast UV output and shocks from their supernova death. They form at great distances from the Earth, enshrouded by dust and gas and have relatively short life-times. Astrophysical masers which form in these environments may act as locators of the star forming regions. The aim of this thesis is to study massive star formation using masers to probe these regions. The three main masers used in this thesis are the Class I and Class II methanol masers and the 6035 MHz ex-OH maser. The methanol masers are divided into two groups, Class I and Class II, based on their distance from a central source. The Class I masers are separated 1-2 pc from a central source, the central source is the star forming region. The Class II masers are associated close to a star forming source. They are often associated with a 6035 MHz ex-OH maser. The 6035 MHz ex-OH masers are less common than the 6668 MHz Class I methanol masers. They are often found at sites of the 6668 MHz Class I masers and 1665/7 MHz OH masers. This thesis presents two maser surveys, the Methanol Multibeam (MMB) survey and the Class I survey. The MMB survey is currently surveying the entire Galactic Plane for the 6668 MHz Class II methanol maser and the 6035 MHz ex-OH maser. Over 60% of the survey in the Southern hemisphere is now complete using the Parkes telescope. Over 900 6668 MHz Class I methanol masers and 110 6035 MHz ex-OH masers have been detected, with all of these masers pinpoint the location of newly forming high mass stars. Follow up observations to determine the precise locations of the 6668 MHz methanol and 6035 MHz ex-OH masers are currently underway. The first ever unbiased Class I survey has observed 1 sq degree of the Galactic Plane for

the 44 GHz Class I methanol masers using the Mopra telescope in Australia. The 44 GHz Class II methanol masers are hypothesised to be associated with the outflows of high mass stellar objects. The Class I survey has detected 25 44 GHz methanol masers, with 23 being new detections. A smaller survey for 36 GHz Class I masers was also conducted using the Mopra telescope centered on the region with the highest population of 44 GHz Class I masers.

A second part of the thesis involved analysing APEX Telescope Large Area Survey of the GALaxy (ATLASGAL) for the submillimeter clumps. ATLASGAL is currently observing ±1° in latitude and -80° and 20° in longitude in the Galactic plane, providing an unbiased view of star formation at the submillimeter wavelength. A section of the Galactic plane will be analysed to determine the submillimeter clumps. These clumps will be compared with the 6668 MHz methanol masers and the 6035 MHz ex-OH masers found in the MMB to see if there are any differences with the clumps with and without a maser. The results are presented within.

Declaration

I declare that no portion of the work referred to in the thesis has been submitted in support of an application for another degree or qualification of this or any other university or other institute of learning.

Copyright Statement

That's what gravity does Johnathon!

I. Bonnell, 2007

What would happen if everyone decided not to come into work all the time? Eh?

A. J. Markwick

Dedication

I dedicate this thesis to my wonderful, amazing and patient Mom and Dad,

Marie and Gerry Quinn

Acknowledgements

First and foremost, I would like to thank my third and main supervisor, Dr. Gary Fuller, for putting up with my numerous tantrums and long car journeys to Narrabri. Without his patience and guidance this thesis would never have been completed. I would like to thank my second supervisor, Prof. Phil Diamond for getting Gary to be my supervisor. A special thanks has to go to my first supervisor, Dr. Jim Cohen, who suddenly and unfortunately passed away in November 2006. Jim Cohen is the reason why I chose a project in masers and the MMB. It only took 5 minutes for Jim to tell me about masers, after which I had completely forgotten about doing an electronics PhD. Of course, a big thank you to Dr. Jim Caswell, for teaching me so much about masers and always having to answer! Also, a big thank you to all the staff at Parkes, Mopra and the ATCA for always making sure I was taken care of during the, sometimes weeks long, observations. Take good care of my hula hoops at Parkes!

I have to thank my wonderful friends who have made me laugh through the good and bad times, Roisin Ni Chuimin, Nadya Kunawicz, David Tideswell, Shari Breen, Danny Wong McSweeney, Andrew Markwick, Cormac Purcell and Stewart Williams. A special thanks to Neil Jackson for giving me the Marie Curie fellowship, so I could achieve the highest ever amount of expenses of any student. A big thank you to Robert Kay for all the coffees and long chats about the birds in Australia.

A huge thank you to my wonderful family, Mom, Dad, Pavla, Jack and Pheobe, for all their love and support throughout the PhD. Thank you for always supporting and encouraging me throughout the years. Dad, I promise I'll get a job really soon!

A massive thank you to my wonderful boyfriends' family, Gaynor, Nicola and Jessica, who have always been there with hugs, lovely food and gin cocktails to keep me

smiling. The final and biggest thank you to my wonderful patient boyfriend David Andrew Louden. Thank you for always cheering me up, making me laugh and smile and always believing in me.

This thesis was typeset with LaTeX.

Supporting Publications

The 6-GHz methanol multibeam maser catalogue - I. Galactic Centre region, longitudes 345 to 6

Caswell, J. L.; Fuller, G. A.; Green, J. A.; Avison, A.; Breen, S. L.; Brooks, K. J.; Burton, M. G.; Chrysostomou, A.; Cox, J.; Diamond, P. J.; Ellingsen, S. P.; Gray, M. D.; Hoare, M. G.; Masheder, M. R. W.; McClure-Griffiths, N. M.; Pestalozzi, M. R.; Phillips, C. J.; Quinn, L.; Thompson, M. A.; Voronkov, M. A.; Walsh, A. J.; Ward-Thompson, D.; Wong-McSweeney, D.; Yates, J. A.; Cohen, R. J.

MNRAS, May 2010

Masers associated with high-mass star formation regions in the Large Magellanic Cloud

Ellingsen, S. P.; Breen, S. L.; Caswell, J. L.; Quinn, L. J.; Fuller, G. A.

MNRAS, May 2010

High-Mass Star Formation in the Near and Far 3 kpc Arms

Green, J. A.; McClure-Griffiths, N. M.; Caswell, J. L.; Ellingsen, S. P.; Fuller, G. A.; Quinn, L.; Voronkov, M. A.

ApJ, May 2009

The 6-GHz multibeam maser survey - I. Techniques

Green, J. A.; Caswell, J. L.; Fuller, G. A.; Avison, A.; Breen, S. L.; Brooks, K.; Burton, M. G.; Chrysostomou, A.; Cox, J.; Diamond, P. J.; Ellingsen, S. P.; Gray, M. D.; Hoare, M. G.; Masheder, M. R. W.; McClure-Griffiths, N. M.; Pestalozzi, M.; Phillips, C.; Quinn, L.; Thompson, M. A.; Voronkov, M. A.; Walsh, A.; Ward-Thompson, D.; Wong-McSweeney, D.; Yates, J. A.; Cohen, R. J.

MNRAS, January 2009

Multibeam maser survey of methanol and excited OH in the Magellanic Clouds: new detections and maser abundance estimates

Green, J. A.; Caswell, J. L.; Fuller, G. A.; Breen, S. L.; Brooks, K.; Burton, M. G.; Chrysostomou, A.; Cox, J.; Diamond, P. J.; Ellingsen, S. P.; Gray, M. D.; Hoare, M. G.; Masheder, M. R. W.; McClure-Griffiths, N.; Pestalozzi, M.; Phillips, C.; Quinn, L.; Thompson, M. A.; Voronkov, M.; Walsh, A.; Ward-Thompson, D.; Wong-McSweeney, D.; Yates, J. A.; Cohen, R. J.

MNRAS, April 2008

Figure 1: The Parkes radio telescopes used by the author for this work.

1

Introduction

For centuries people have looked at the night sky and been greeted by the light from distant stars. Throughout history, these stars have played an important part in human life, from using them as navigational and orientational tools, to our solar calendar.

Massive stars greatly influence and shape their surroundings. From their birth in a giant molecular cloud of dust and gas, to a life of nuclear fusion and mass loss due to solar winds. Ending with a supernova death that sends shock waves throughout the interstellar medium (ISM) and scatters the stars' mass through the surrounding regions.

There are observational difficulties associated with high mass stars. High mass stars are rare, they form at large distances from the Earth where their birth is enshrouded in dust and gas. They form on relatively short timescales and in clusters. Clustering is an issue as it causes confusion when observing a star forming region and the feedback effects of neighbouring stars also adds to the complexity of their formation.

To study massive star formation, we first need to locate where it is taking place. It is possible to detect locations of massive star formation using astrophysical masers, the subject of this thesis, as tracers. These masers not only provide the locations of massive star forming regions but also probe the chemisty and physics of these environ-

ments.

1.0.1 Star Forming Environments

High and low mass stars begin their lives within a molecular cloud. Molecular clouds are inhomogeneous objects with masses ranging from a few solar masses to $\sim 10^6$ $M_\odot$. The less massive of these are often called dark clouds and usually result in low mass stars (Blitz 2001). Molecular clouds with masses greater than 10^4 $M_\odot$ are typically called giant molecular clouds (GMCs) and are the breeding ground for massive star formation. The Orion Nebula and W3 in the constellation Cassiopeia are examples of GMCs with active star formation. Once a massive star has ignited, its ultraviolet photon flux ionises the surrounding dust and gas, creating complex regions known as ultra compact HII regions (UC HII). The stars that create these regions are among the brightest and most massive stars in the galaxy.

Giant Molecular Clouds

A molecular cloud is a region of condensed interstellar dust and gas comprised mostly of molecules of H, C, N & O. They are the coldest (10-20 K), densest (10^6 to 10^{10} particles/cm^3) regions of the ISM. As stated above they have masses greater than $10^4 M_\odot$, typical diameters of 50 pc, and can extend all the way up to 100 pc in the case of elongated clouds (Blitz 2001).

Giant molecular clouds contain density enhancements, called clumps. These clumps do not have uniform density and are observed to have very dense, warm sub-structures called ‘cores’ (e.g., Purcell et al. 2006). It is these cores that collapse to form stars. Radio and infrared observations of these regions provide the most useful information as the dust and gas of the GMC hide the birth of the star from optical and often near-infrared (IR) views. Once the star has ignited, a combination of its stellar wind and ionising radiation breaks up the molecules and drives the gas and dust away, allowing

it to become visible.

UC HII Regions

An UC HII region is an expanding bubble of ionised gas surrounding a protostellar core. It is formed when the protostar begins to emit UV photons which ionise and heat the surrounding molecular gas. UC HII regions are strongly associated with sites of massive star formation. UC HII regions around young OB stars, are typically < 0.1 pc in diameter, have electron densities of 10^4 cm^{-3} and temperatures of 10^4 K (Tielens 2005; Wood and Churchwell 1989b). The ionised region is constantly expanding into the surrounding HI region (cool gas, mainly neutral hydrogen), to form a HII region. A UC HII region cannot be observed optically as it is hidden within its parent cloud of dust and gas. Observations of these regions are best taken in the radio and infrared regimes.

1.1 Star Formation

Star formation may be divided into two groups by mass. Low mass stars of mass <8 $M_\odot$, will end their lives as white dwarfs. The second is high mass stars, the main focus of this work. These stars have masses >8 $M_\odot$ and are known to be as large as 150 $M_\odot$. To explain the differences between the formation routes of both groups, low mass star formation must first be discussed.

1.1.1 Low Mass Star Formation

A cold (10 K) dense (~100 cm^{-3}) molecular core undergoes gravitational collapse to form a protostar. The core must increase its density by twenty orders of magnitude and decrease its radius by seven orders of magnitude during its collapse (Murdin 2001).

At first the dust and gas are optically thin, meaning the core can stay isothermal and

dynamically collapse. The mass at the centre collapses faster and builds up quicker, thus its density is greater than the outer regions. The inner regions of the collapse form a protostellar core, which becomes optically thick to its own radiation and heats up.

The protostellar core is now surrounded by a thick infalling envelope of dust and gas - a process called accretion. The core begins to gain mass from the infalling envelope. The infalling matter must dissipate its gravitational potential energy before it reaches the star. This provides a luminosity of:

$$L_{acc} = \frac{G\dot{M}M_{\star}}{R_{\star}} \tag{1.1}$$

where, L_{acc} is the accretion luminosity, $M_{\star}$ and $R_{\star}$ are the mass and radius of the protostellar core and $\dot{M}$ is the accretion rate.

At this point the protostellar core would have a mass of $\sim 10^{-2} M_{\odot}$, once the core reaches 0.2 - 0.3 $M_{\odot}$ it will begin nuclear fusion and deuterium burning. The core is fully convective, so the newly accreted material gets mixed into the core and nuclear burning continues. Accretion continues until the core reaches 10^7 K and hydrogen burning starts; it is then a Main Sequence star.

The evolutionary status of a low mass star may be determined from the shape of its spectral energy distribution (SED), particularly at infrared wavelengths. From their SEDs, YSOs may be classified into four broad classes (Lada and Wilking 1984; Andre et al. 1993). The SEDs of each class are shown in Figure 1.1.

Class 0

Class 0 SEDs peak in the submillimetre range of the spectrum, $\sim 150\ \mu$m. Most are not detected shortward of 20 micron and they resemble a single-temperature blackbody spectrum. This tells us that the emission is dominated by emission from cold dust (20-30K). The luminosity from Class 0 YSOs is due to the release of the infalling material

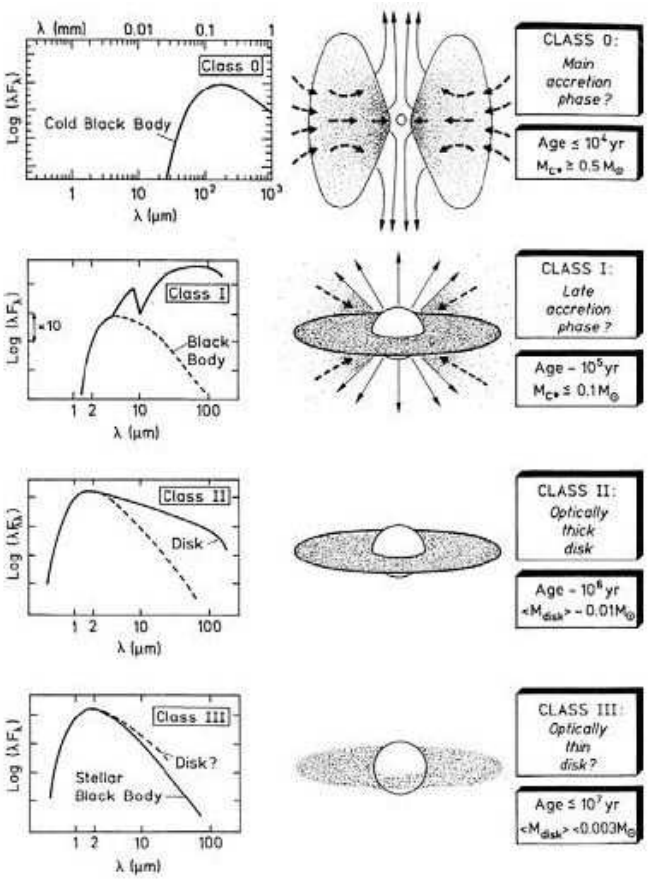

Figure 1.1: Diagram showing the four different classes of young stellar objects and their respective SEDs. From Bachiller (1996).

(Bachiller 1996). They are associated with bipolar molecular outflows. Class 0 objects are quite rare and they make up $\sim$ 10% of embedded sources.

Class I

As accretion onto the core continues, the temperature rises, the peak of the SED moves to the far-IR ($\sim$ 100 μm). The SED corresponds to a 50-100 K blackbody from the accreting envelope and a 200-400 K component from the disk (Purcell et al. 2006a). They are associated with jets and outflows and their lifetimes are estimated at $1 - 5 \times 10^5$yr (Lada et al. 2001).

Class II

As the star reaches Class II status, the stellar winds have dispersed much of the surrounding envelope, exposing the disk. The SED peaks in the mid-infrared band at $\sim$2 μm. Longward of 2 microns Class II SEDs are dominated by an excess emission in the infrared, which indicates the presence of circumstellar material associated with the star. At this stage the protostar may be observed at optical and near-infrared wavelengths and is called a T Tauri star. Class II objects differ from Class I sources, as they lack the large infall of dust and gas.

Class III

These SEDs peak in the visible and infrared. The SED is fit well by a reddened black body spectrum corresponding to a reddened photosphere of a star at the zero-age Main Sequence. The star is still surrounded by an optically thin debris disk (Lada et al. 2001). Class III YSOs have an age of $\sim 10^7$ yrs.

1.1.2 High Mass Star Formation

High mass stars are extremely important for shaping the galaxy. They produce vast amounts of UV radiation which heats the ISM. During a massive star's life it will produce the heaviest elements in the universe and replenish the ISM with this enriched material during its supernova death. Massive stars shape their surroundings through the jets, outflows, solar winds and shocks they produce. The heavy elements produced by the star are also responsible for the cooling of the ISM.

Once gravitational collapse of the core occurs, the mass moves to the centre, building up the protostar. As the mass of the protostar increases, its density and temperature rises towards hydrogen burning, and its radius decreases. As the core contracts the gravitational potential energy is released as luminosity, this is the Kelvin-Helmholtz

mechanism (Zinnecker and Yorke 2007). The timescale for the contraction, until the core has the conditions for fusion, is the Kelvin-Helmholtz timescale, t_{KH}:

$$t_{KH} \sim \frac{GM_\star^2}{R_\star L_\star} \tag{1.2}$$

where G is the gravitational constant, $M_\star$ is the mass, $L_\star$ is the luminosity and $R_\star$ is the radius of the protostar. As the luminosity grows, especially once nuclear fusion begins, the outward radiation pressure eventually overcomes the inward gravitational collapse, reversing the infall of the envelope. The luminosity required to balance the inward force of gravity is called the Eddington Luminosity, L_{Edd} (Krumholz et al. 2004).

$$L_{Edd} = \frac{4\pi cGM_\star m}{\kappa} \tag{1.3}$$

where c is the speed of light, m is the mass of the particle and κ is the opacity coefficient. The opacity coefficient, κ, is a constant which is established by the density, temperature and composition of the material. The accretion timescale, t_{acc} is the time taken for the mass to accrete onto the protostar, for it to gain the mass and thus temperature and density required for nuclear fusion.

The main difference between high and low mass star formation is, for high mass star formation the Kelvin-Helmholtz timescale is less than the accretion timescale, meaning the protostellar core begins nuclear fusion before accretion onto the protostellar core is finished.

We know that when a protostellar core reaches $\sim$ 8 $M_\odot$ it exerts enough radiation pressure to disperse the surrounding dust and gas and stop the accretion (Keto 2003). However, we have observed stars of 8-100 $M_\odot$, so there must be another method to form stars > 8 $M_\odot$.

There are two main theories for the formation of massive stars. The first is a scaled

up version of low mass star formation with enhanced accretion (Yorke and Sonnhalter 2002; McKee and Tan 2003; Krumholz et al. 2005a). Enhanced accretion means that the accretion disk around the central object is very thick, so the centre of the disk can still accrete onto the core whilst sheltered by the outer disk layers. And some of the radiation pressure from the core escapes from the bipolar outflows which puncture the surrounding material along the polar axis (Krumholz et al. 2005b)

The second theory is based on competitive accretion and mergers (Bonnell et al. 1998; Bally 2002; Bonnell et al. 2004). Competivite accretion is when the stars in a cluster accrete from a shared reservoir of unbound gas in the clump. In a core densely populated by evolving protostars, competitive accretion may become the dominant way to increase mass. There is also the possibility that protostellar cores coalesce in these densely populated clusters, forming the most massive stars.

There are several differences between the two scenarios which may be explored by observations. One follows that, a scaled-up version of the low mass star formation scenario would have highly collimated outflows, something that would most likely not happen in competitive accretion scenarios. Observations of high mass outflows provide different results. Some observations find collimated outflows from B stars (Gibb et al. 2003; Su et al. 2004), whilst others observed molecular outflows that are less collimated than low mass outflows (Ridge and Moore 2001; Wu et al. 2004). The observations of the less collimated outflows may be the result of the great distance at which they are located. The degree of collimation in massive stellar objects is yet to be determined.

1.1.3 From Molecular Cloud to UCHII Region

The massive star formation process begins with a starless clump of ~10000 $M_{\odot}$. This clump contains even higher density cores. Stars form in these cores, at densities of 10^6

H cm^{-3}, radii of $\leq$ 0.1 pc and temperatures of 10-15 K (Jappsen et al. 2003; Krumholz 2006). McKee and Tan (2003) suggest that these cores are supported by turbulence, whilst Bonnell et al. (1997, 2001) argue the cores are more of a transient phase due to random motions of the gravitationally bound cloud.

The next stage begins when the core undergoes gravitational collapse. As the mass rushes to the centre, the formation of the protostar begins. This stage is usually observed with mid-infrared and continuum emission. Beuther et al. (2005) observed a core without any mid-infrared emission but with signs of molecular outflows, indicating the onset of protostar formation. This is the hot core stage and is associated with 6668 MHz methanol maser emission (Purcell et al. 2006a).

The main accretion stage is next. As the protostellar core increases, it starts to ionise its surrounding region, but the growth of the ionising UC HII region is impeded by the infalling material. Excited hydroxyl (ex-OH) and ground state hydroxyl (OH) masers (section 1.4), at 6035 and 1665/7 MHz respectively, are observed along with the 6668 MHz methanol maser at this stage (Edris et al. 2007; Cohen et al. 2006).

As the protostellar core grows, its output of UV photons increases and it continutes to ionises its surroundings to become a UC HII region.

1.2 Astrophysical Masers

Astrophysical masers are found in the most interesting regions in space: star forming regions, comets, supernova remnants and evolved stars. They are readily identified by their highly beamed non-thermal intensity from their relatively compact environment (Cohen 1995). They arise from population inversions in the energy levels of molecules,

pumped by far infrared photons, collisions or chemical reactions (Gray 1999). Population inversion arises when the upper energy states have a higher population than the ground state. Their highly collimated beam can reveal details of gas and dust filled regions of star formation which were previously unknown. A study by Edris et al. (2007) has shown that high resolution observations of OH and methanol masers can identify previously unknown high mass protostellar objects and circumstellar disks. The OH masers in the disks can be used to obtain a magnetic field reading of these circumstellar disks. Masers can also identify where regions of high mass star formation exist and can tell us about galactic structure (Green et al. 2009c).

The big question is whether it is possible to identify the evolutionary stage of a protostar by the presence of a particular maser. We do know a lot about masers, such as, SiO masers are found in regions of shocked gas and closest to oxygen rich stars as they need the highest temperature to be released from the grain (Beuther et al. 2007; Gray 2007). Formaldehyde (H_2CO) masers are proposed to trace the warm molecular gas in the vicinity of massive star formation (Araya et al. 2006), water (H_2O) masers are found in the outflow of high and low mass stars (Breen et al. 2010) and 6668 MHz methanol (CH_3OH) masers are only associated with high mass protostars (Minier et al. 2001; Walsh et al. 2003). However, a conclusive evolutionary maser clock is still yet to be agreed upon.

To understand what masers tell us about their environments we must first understand how masers form.

1.2.1 Radative Transfer and the Einstein coefficients

To understand how masers form, we must start with the equation of radiative transfer.

$$\frac{dI_\nu}{ds} = -\kappa_\nu I_\nu + \epsilon_\nu \tag{1.4}$$

where I_ν is the specific intensity of radiation, ϵ_ν is the emissivity, and κ_ν is the absorption coefficient. The emissivity, ϵ_ν, is the ability of a material to radiate absorbed energy and the absorption coefficient, κ_ν, is the measure of how easily energy can pass through a material.

We consider a two level system, (Figure 1.2), with populations n_1 and n_2 in the respective levels (Cohen 1995). The emissivity is

$$\epsilon_\nu = n_2 A_{21} \frac{h\nu_{21}}{4} f(\nu) \tag{1.5}$$

A_{21} is the Einstein coefficient of spontaneous emission, ν_{21} is the frequency of the

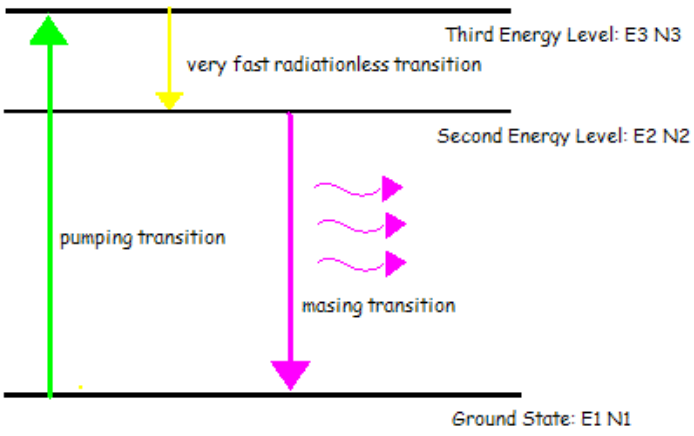

Figure 1.2: A simple two level system. E_1, E_2 and E_3 are the first three energy levels and N_1, N_2 and N_3 are the populations of those levels.

emitted photons, $f(\nu)$ is the normalised line profile. The absorption coefficient:

$$\kappa_\nu = (n_1 B_{12} - n_2 B_{21}) \frac{h\nu_{21}}{c} f(\nu) \tag{1.6}$$

B_{12} is the Einstein coefficient for absorption and B_{21} is the coefficient for stimulated emission. They are related by

$$A_{21} = B_{21} \frac{8h\nu^3}{\pi c^3} \tag{1.7}$$

$$B_{12} = \frac{g_2}{g_1} B_{21} \tag{1.8}$$

where g_1 and g_2 are the statistical weights of the upper and lower states. The ratio of stimulated emission to spontaneous emission increases with the cube of the wavelength, therefore it is $\sim 10^{18}$ times larger for radio waves than visible light (Cohen 1989). Stimulated emission has the effects of reducing the absorption coefficient $k\nu$, which is quite substantial at radio wavelengths.

1.2.2 Population Inversion

The populations of each level are calculated by:

$$\frac{n_2}{n_1} = \frac{g_2}{g_1} \exp\left(-\mathrm{h}\nu_{21}/\mathrm{kT_{ex}}\right) \tag{1.9}$$

where T_{ex} is the excitation temperature. At radio frequencies $h\nu/k$ is the order of 0.1K so for a gas at local thermal equilibrium (LTE) the factor is very small and stimulated emission almost cancels absorption. The net absorption of the system is the difference of two very large numbers, this causes the radiative transfer to be very sensitive to very small changes.

A very small shift from Maxwell-Boltzman distribution, which describes the speed, or kinetic energy, of a molecular specie at thermodynamic equilibruim, can cause a population inversion ($n_2/n_1 > g_2/g_1$) and absorption becomes negligible. The radiation passing through the gas becomes amplified and a maser is created. The solution to the equation of radiative transfer is:

$$I_\nu = I_\nu(0)\exp(-\tau_\nu) + \int_0^\tau \frac{\mathrm{j}_\nu}{\kappa_\nu} \exp\left[-(\tau_\nu - \tau_\nu')\right] \mathrm{d}\tau_\nu' \tag{1.10}$$

where $I_\nu(0)$ is the intensity entering the gas, τ_ν is the optical depth and j_ν is the total radiation emitted per unit mass per until time (Cohen 1989).

Normally the optical depth is positive and the radiation reaching the observer would be background radiation $I_\nu(0)$, which is attenuated by a factor exponential τ_ν plus the emission/absorption of the cloud. For a maser, the absorption coefficient is negative along with the optical depth. The optical depth can reach -25 magnitudes, which leads to gain factors 10^{10}. Growth will continue as long as population inversion can be maintained against the losses by stimulated emission. This describes an unsaturated maser.

1.2.3 Unsaturated Maser

The characteristics of an unsaturated maser are line narrowing, beaming and rapid variability. Exponential gain in the system amplifies the line profile function $f(\nu)$, which is a Gaussian, but reduced in width. The radiation travelling through the centre of the cloud is amplified to a greater degree resulting in the beaming effect observed, because of this the apparent angular size of the cloud is reduced by a factor of $(1-\tau_\nu)^{1/2}$ (Goldreich and Keeley 1972). As the gain of the maser is exponentially proportional to the population inversion and path length, any little changes in either are amplified, resulting in rapid variability.

1.2.4 Saturated Maser

The exponential growth of a maser is limited as the radiation grows more intense, stimulated emission begins to reduce population inversion and hence gain. This is said to be a saturated maser, although only parts of the maser will be actually saturated. The levels of population of each state in the maser are governed by the rate equations

$$\frac{dn_2}{dt} = -n_2 A_{21} - (n_2 - n_1)B_{21}J + P_2(n - n_1 - n_2) - \Gamma_2 n_1 \tag{1.11}$$

$$\frac{dn_1}{dt} = -n_2 A_{21} - (n_2 - n_1)B_{21}J + P_1(n - n_1 - n_2) - \Gamma_1 n_1 \tag{1.12}$$

where n is the total density, P_i is the pump rate into all other levels besides 1 and 2. Γ_i is the loss rate of i and

$$J = \frac{1}{4\pi}\int\int I_\nu d\nu d\Omega \tag{1.13}$$

is the number of maser photons crossing unit volume per second. The population inversion depends on the loss and the pump rates as spontaneous emission is negligible in comparison with the other terms. Therefore the maser saturates where

$$J \sim \frac{\Gamma_2}{2B_{21}} = \frac{\Gamma_2}{A_{21}}\frac{4h\nu^3}{\pi c^3} \tag{1.14}$$

In a maser, there is typically more than one beam; saturation of a maser is very good at turning the weaker transitions off. However this does not increase the main beam by much (Cohen 1989). Saturation affects the line profile by re-broadening it to non-thermal values.

1.3 Methanol & Hydroxyl Masers

Our understanding of space has come a long way since hydroxyl (OH) was first detected in absorption by Weinreb (1963). This was a time when it was believed there were no molecules greater than two atoms in space. In 1965, Weaver et al. conducted observations of OH towards several sources including W51, W75 & W3. They found several sources had narrow (0.5-1 km s^{-1}) spikes of OH emission. Not knowing that it was produced by population inversion, they called it ‘mysterium’. Fortunately it was soon realised that the narrow emission was a maser, but rather unfortunately they dropped the name mysterium. The work in this thesis is concentrated on the Class I 44 GHz methanol, Class II 6668 MHz methanol and 6035 MHz excited hydroxyl (ex-OH) masers.

1.3.1 The Class I and Class II Methanol Maser

Since the first detection of a methanol maser by Barrett et al. (1971) observations of a plethora of methanol maser transitions have been made. The most common methanol masers are the 6.7, 12.1 and 44 GHz transitions, which are known to trace young forming stars (Menten 1991).

Based on observational results, the methanol masers have been divided into two classes (Batrla and Menten 1988). The Class I masers include the $4_{-1} - 3_0E$ 36 GHz, $7_0 - 6_1A^+$ 44 GHz and the $8_0 - 7_1A^+$ 95-GHz transitions and were originally classified as being offset from known centres of star formation, Class II methanol masers and other molecular masers such as OH and H_2O. Class II methanol masers, such as the $5_1 - 6_0A^+$ 6.7 and $2_0 - 3_{-1}E$ 12.1 GHz masers, the brightest of the known methanol masers, are observed at known centres of star formation, close to OH and H_2O maser emission and FIR emission.

From theoretical modelling, this class difference is explained as differences in the pumping of the maser populations (Cragg et al 1999, 2002; Voronkov 2006). The Class I masers are pumped collisionally, which is most efficient in regions with both low gas and radiation temperature (Voronkov et al. 2006; Kurtz et al. 2004). The Class II methanol masers are pumped by FIR radiation from a forming star; hence they are found closer to the site of star formation than the Class I masers.

Twenty years ago, H_2O masers, known tracers of outflows, were the most popular method of locating forming stars (Wood and Churchwell 1989a). The discovery of the 6668 MHz Class II methanol maser (Menten 1991), indicated an earlier stage of evolution of the protostar than the H_2O masers. The 6668 MHz methanol maser is uniquely associated with high mass protostars (Minier et al. 2003). As they are widespread through the Galactic Plane and relatively strong ($\sim$ few Jy), there have been several

successful surveys of them (Pestalozzi et al. 2005; Caswell 1996; Szymczak et al. 2002). The work by Walsh et al. (1999) showed that the 6668 MHz masers are associated with high mass star forming regions, however, they are offset from known centres of star formation (UCHII regions, H_2O masers). Purcell et al. (2006b) expanded on this work to show that 6668 MHz masers are in fact associated with hot cores, an earlier evolutionary stage than UCHII regions. The location of the 6668 MHz methanol maser in the star forming region is still up for debate. For example, it has been argued the methanol masers arise in outflows (De Buizer et al. 2009) or disks (Pestalozzi et al. 2009).

The 7_0 - 6_1 A^+ Class I 44 GHz methanol maser was first detected by Morimoto et al. (1985) towards the Sgr B2 and W51 regions, which are known regions of high mass star formation. Since then there have been several large scale surveys for the 44 GHz methanol maser by Bachiller et al. (1990); Haschick et al. (1990); Kalenskii et al. (1992); Slysh et al. (1994). These surveys resulted in over 100 detections of 44 GHz methanol masers towards HII regions, late-type stars, H_2O masers, CH_3OH masers and IRAS sources. There were zero detections of the 44 GHz methanol maser (or any other methanol maser) towards a late type star.

A recent statistical analysis by Val'Tts and Larionov (2007) of 160 Class I methanol masers found that 24% of the Class I masers are associated with a bipolar outflow. Considering that Class I masers are thought to arise close to outflows this seems like a very low percentage. However, a more recent detailed statistical analysis by Chen et al. (2009), found that two-thirds of high mass outflows have Class I masers and 50% of the masers in the Chen et al. (2009) sample are associated with outflows. From this Chen et al. (2009) believe they have solidified the relationship between Class I masers and outflows. This suggestion has been backed up by the recent results of Kalenskii et al. (2010) who made detections of three 44 GHz Class I methanol masers towards bipolar outflows. These results are all the more interesting as they are from low mass

star forming regions.

Observations over the past several years suggest that the class system may not be as clear cut as originally supposed. Kurtz et al. (2004) performed the highest angular resolution search for 44 GHz masers in 44 star forming regions with the VLA. In 22 of the fields the median distance between the Class I 44 GHz methanol maser and HII regions was found to be 0.2 pc. This is much smaller than the 1-2 pc separation expected from Bartla & Menten (1991).

The 6668 MHz methanol maser is one of the subjects of the Methanol Multibeam (MMB) survey, a Galactic plane survey (see Chapter 2). The first results of the MMB survey are presented in Chapter 3. The catalogue of 6668 MHz masers detected in the MMB is presented in Appendix 1. The first unbiased survey of 44 GHz Class I methanol masers was undertaken for this thesis and is discussed in Chaper 5.

1.3.2 The 6035 MHz Excited Hydroxyl Maser

Unlike methanol masers, hydroxyl masers are found in a wide variety of regions such as the early and late stages of stellar evolution and in comets. The $^2\Pi_{3/2}, J = 5/2 F = 3 - 3$ 6035 MHz excited hydroxyl (ex-OH) maser is the strongest of the excited OH masers (Caswell 1998). The ex-OH maser is strongly associated with the 6668 MHz methanol maser (Caswell 2001) and is also found coincident with the 1665 MHz OH maser, both of which are typically stronger (Caswell 2001). The 6035 MHz is also commonly observed with a 6031 MHz ex-OH maser companion and 1720 MHz ex-OH masers also preferentially occur at site of 6035 MHz masers (Caswell 2003). All of these associations may be explained by the theoretical models of Cragg et al. (2002).

The models of Cragg et al. (2002) show that the 6035 MHz ex-OH maser occurs in the low gas temperature, $T_k = 30$ K, high density, $n_H = 10^{8.5} \mathrm{cm}^{-3}$, high specific column

density $N_{OH}/\Delta V > 10^{10.3}$ cm^{-3} and is independent of dust temperature (Figure 1.3). Collisions must be important for the 6035 MHz maser as it is not seen at low gas densities. Figure 1.3 shows that the model accounts for the presence of the 1665 MHz OH maser with the 6035 MHz ex-OH maser. Sites where the 6035 MHz occur without the 1665 MHz maser are likely sites of high density. The occurrence of the 1720 MHz maser is also accounted for by the model, (Figure 1.3), although the model suggests that the 1720 MHz maser only occurs in sites with strong 1665 and 6035 MHz maser emission, which is not always the case when observed. The Cragg et al. (2002) models also see the regular occurrence of the 6031 MHz ex-OH alongside the 6035 MHz ex-OH maser, but is always weaker than the 6035 MHz, which is a situation typically seen in observations .

The 6035 MHz maser undergoes Zeeman splitting in the presence of a magnetic field. This causes a slight shift between the right and left hand circularly polarised spectra, at a given position. The shift between the right and left polarisation spectra is proportional to the magnetic field. Thus, the 6035 MHz ex-OH masers are capable of measuring the magnetic field in massive star forming regions.

The separation between the right and left circularly polarised spectra is usually $\sim 0.1 km\ s^{-1}$. A separation of of 0.060 km s^{-1} is caused by a magnetic field strength of 1 mG (Caswell 1998). Figure 1.4 shows G300.969+1.148, a 6035 MHz maser from this work with Zeeman splitting indicating a magnetic field of 3.17 mG.

Caswell and Vaile (1995); Caswell (1998, 2003) have undertaken the most extensive surveys of 6035 MHz ex-OH to date, targeting sites of 1665 MHz OH and 6668 MHz methanol masers. This work presents the first unbiased survey for 6035 MHz ex-OH masers, part of the MMB survey, in Chapter 4.

The 6035 MHz ex-OH maser is closely associated with 6668 MHz methanol masers,

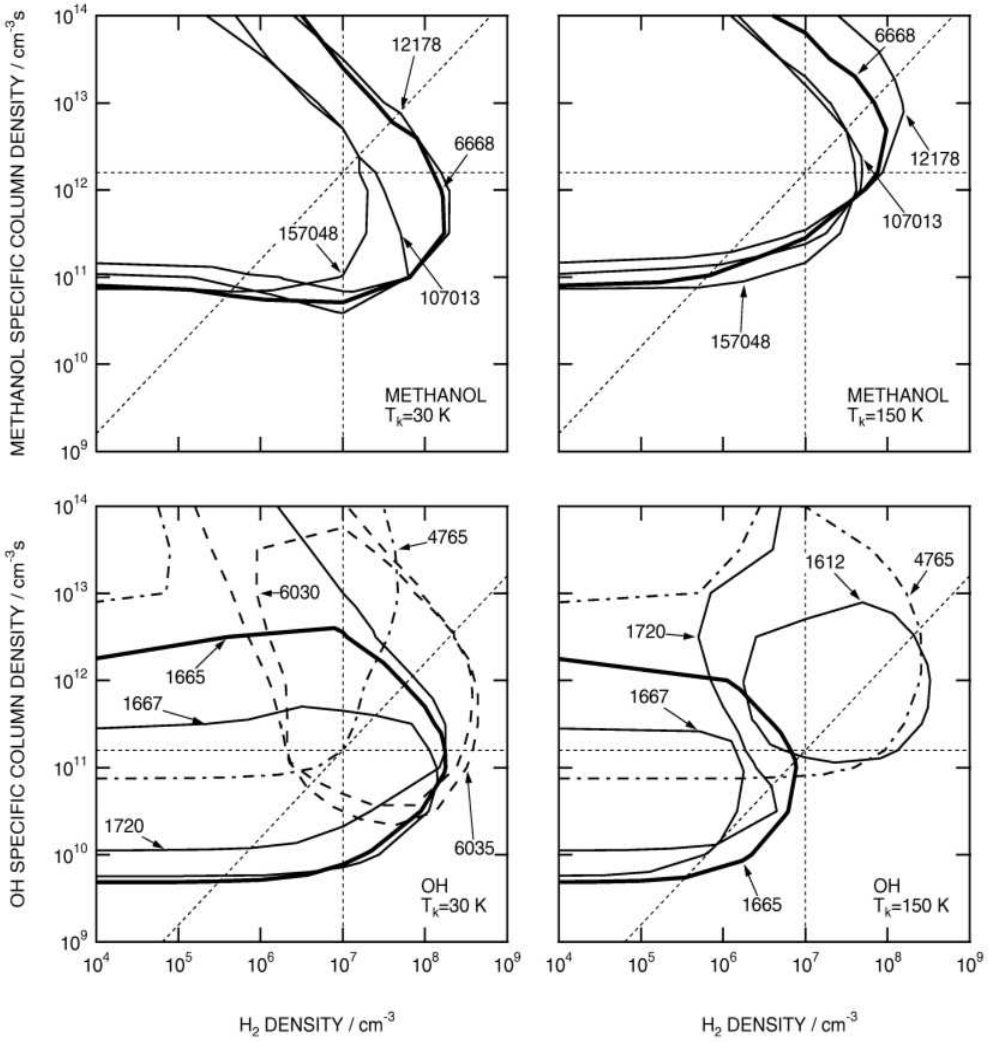

Figure 1.3: (Figure 1 from Cragg et al. 2002). Contour plot showing regions where selected masers of methanol and OH become active, as a function of hydrogen density n_H and specific column density of the maser molecule N/ΔV, for T_k =30 K (left-hand panels) and T_k =150 K (right-hand panels). Contours are labelled with the line frequency in MHz. For each maser a single contour representing a brightness temperature of 10^4 K is drawn, with no masers appearing above this threshold in the bottom right regions of the plots.

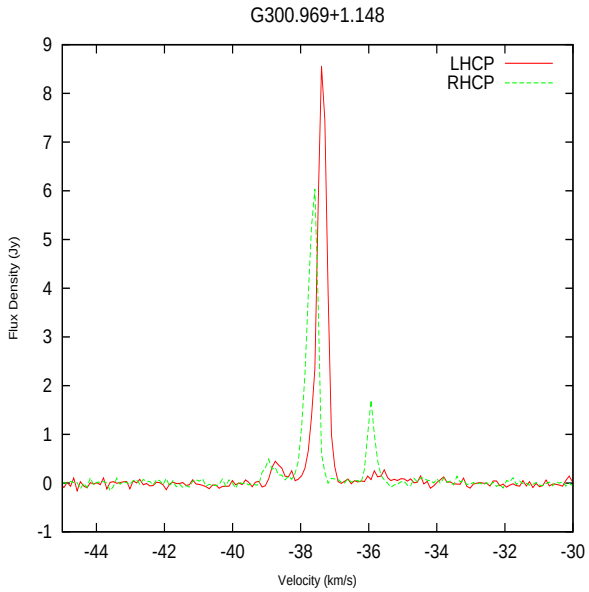

Figure 1.4: G300.969+1.148, a 6035 MHz ex-OH maser. The Zeeman splitting of the peaks, caused by the presence of a magnetic field, is visible.

with ~ 80% of the ex-OH masers having a methanol association (Caswell 1998). From the point of view of the 6668 MHz methanol maser, only ~ 10% of them have an associated 6035 MHz ex-OH maser. Therefore the question must be asked, are 6035 MHz ex-OH masers a transitent phase in the evolution of the protostellar object? Or is there a physical difference in the sources which host the 6035 MHz ex-OH and 6668 MHz methanol maser? We aim to answer this question in this work.

1.4 Infrared, Radio and Submillimeter Surveys

A full comparison of the methanol and ex-OH masers with other surveys is presented throughout this work. The main surveys used for comparison are GLIMPSE, ATLASGAL and CORNISH, for reasons explained below.

Infrared Astronomical Satellite (IRAS) conducted an all sky survey at 12, 25, 60 & 100 μm. It detected about ~350,000 infrared sources. GLIMPSE is a legacy program

of the Spitzer Space Telescope, that surveyed $10° < l < 60°$, $|b| \leq 2°$ of the Galactic plane at 3.6, 4.5, 5.0 & 8.0 μm at a resolution of 1.4-1.9″ (Benjamin et al. 2003). Comparing the masers with the GLIMPSE sources potentially allows us to identify their exciting source. A recent discovery in the GLIMPSE survey are Extended Green Objects (EGOs), are extended 4.5 μm sources (the 4.5 μm band is usually denoted as green in the three colour displays). EGOs are thought to trace shocked molecular gas in outflows (Cyganowski et al. 2008a). Cyganowski et al. (2008a, 2009) have shown that EGOs are associated with infrared dark clouds (IRDCs), 6668 MHz methanol and 44 GHz methanol masers. Cyganowski et al. (2008a, 2009) suggest that the EGOs are pinpointing outflows from young massive stars.

The Co-Ordinated Radio 'N' Infrared Survey for High-mass star formation (CORNISH) survey is a 5 GHz radio continuum survey of the northern GLIMPSE region, $10° < l < 60°$ and $|b| = 1°$. Using the NRAO Very Large Array (VLA) CORNISH aims to detect UCHII regions across the Galactic plane. The UCHIIs detected in the CORNISH survey are compared with the 6035 ex-OH and 6668 MHz methanol masers in Chapter 4.

The APEX Telescope Large Area Survey: the GALaxy (ATLASGAL) is a survey of the inner Galactic plane, $+20° > l > -80°$ and $|b| = 2°$, at 870 μm (Schuller et al. 2009). ATLASGAL is carried out using the APEX telescope on the Chajnantor plateau in Chile. At 870 μm it traces the cold dust and gas in the galactic plane, the homes of star formation. The 6668 MHz methanol masers are compared to the 870 μm continuum emission found by ATLASGAL in the $6° > l > -6°$ and $|b| = 1°$ region in Chapter 6.

1.5 Thesis Aim

The overall aim of this work is to study high mass star formation, primarily high mass star formation in the Galactic plane. The main focus of this thesis is the Methanol

Mulitbeam Survey (MMB), which is locating sites of massive star formation using the 6668 MHz Class II methanol and 6035 MHz ex-OH masers. The Class I survey of 44 GHz Class I methanol masers is also pin-pointing sites of star formation using the masers positions. The Class I survey is also pin-pointing the location of low mass star forming regions to be studied in greater detail.

The last section of this thesis work focuses on comparing the ATLASGAL survey with the 6668 MHz Class II methanol and 6035 MHz ex-OH masers. As this work aims to study the formation of high mass stars, ATLASGAL provides information about the clumps in which the stars form, from which masses may be derived. The clumps with and without masers may then be studied in detail to discover new elements of sites that lend themselves to high mass star formation.

1.6 Thesis Overview

Chapter 2 presents the telescopes used for this work and describes the MMB survey. The first results of the MMB survey are discussed in Chapter 3. The main focus of this thesis, the 6035 MHz ex-OH masers from the MMB, are presented and discussed in Chapter 4. The first unbiased survey for 44 GHz Class I masers is presented in Chapter 5. The analysis of the ATLASGAL clump finding algorithms and the comparison of the molecular clouds found in the $6^\circ > l > -6^\circ$ and $|b|=1^\circ$ ATLASGAL region and the 6668 MHz methanol masers from the MMB are presented in Chapter 6. Finally, the summary and conclusions of this thesis are presented in Chapter 7.

2

Radio Telescopes & Survey Techniques

Several radio telescopes have been used to collect data for this thesis, both single dish and interferometers. The MMB project involved using the Parkes 64 m single dish telescope in Australia, the Very Large Array (VLA) in America and the Australia Telescope Compact Array (ATCA) interferometers. The Class I project used the 22 m Mopra telescope in Australia.

2.1 Single Dish Radio Telescopes

Radio telescopes underwent a huge development during the Second World War - although, not for outer space uses. Today they remain an important part of radio astronomy, even with the prevalence of interferometers.

The single dish telescopes used in this thesis work are the 64-m Parkes radio telescope and the Mopra 22-m telescope, both located in Australia. Both telescopeshave a parabolic dish which reflects radio waves onto an antenna at the principal focus of the dish. The in-coming radio waves are very weak, thus focussing them onto the antenna from the reflecting dish makes them more intense. The reciever and amplifiers boost the weak signal to a more detectable level. The amplifiers are cooled to a very low temperature to ensure to minimum interference from the thermal noise. The amplified

signal is carried to the main computers to be stored and analysed at a later time.

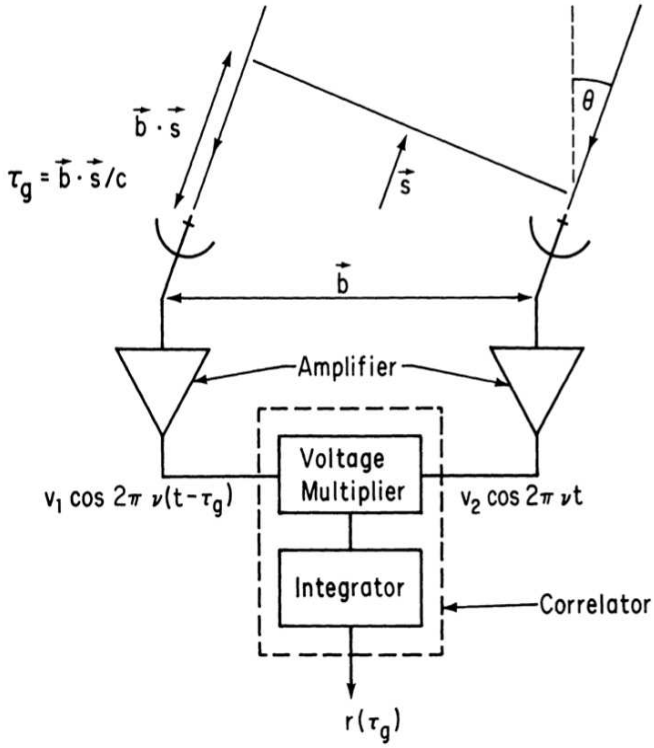

Figure 2.1: A simplified interferometer with two antennas, from Thompson (1999).

2.2 Radio Telescopes

As the need for resolution increases so does the diameter of our radio telescopes, the largest single dish is the 305 m diameter Arecibo telescope. It is a tough engineering feat to construct a radio telescope with a diameter greater than 100 m, but to obtain the resolution required for many astronomical observations we need very large (>1000 m) telescopes. It is cheaper and easier to build several smaller telescopes that work together, providing a much greater effective area resulting in the required resolution to observe astrophysical objects in greater detail. Such a group of telescopes is called an interferometer.

An interferometer collects and correlates signals from each antenna to produce an interference pattern, the inverse Fourier Transform of this interference pattern is the radio source brightness distribution - the map of the source. To understand how this is accomplished we shall consider a two element interferometer, consisting of two antennas separated by a distance much greater than the telescope's diameter, (Figure 2.1). The two antennas are separated by a distance **b** called the baseline and they point toward the distant radio source in the direction indicated by the unit vector **s**. The wavefront from the observed radio source arrives at the antennas at different times. This time delay is called the geometric delay, τ_g, and is defined by Equation 2.1,

$$\tau_g = b \cdot \frac{s}{c} \tag{2.1}$$

where c is the speed of light. The signals are collected by the dish and pass through the receiver to the amplifier which selects the desired frequency, ν and the frequency width, $\Delta\nu$, the bandwidth. The signals are next combined in the correlator (the time delay is adjusted for before the signals are correlated). The first step in the correlator is to multiply the voltages and then to perform a time averaged integration. Each of the wavefronts from the antennas to the correlator are $V_1(t)$ and $V_2(t)$:

$$V_1 = v_1 \cos 2\pi\nu t\left(t - \tau_g\right) \tag{2.2}$$

$$V_2 = v_2 \cos 2\pi\nu t \tag{2.3}$$

The signal received by each antenna pair is called a visibility, it contains phase and amplitude information about the radio source. The combination of the visibilities produces an interference pattern from which the the radio source may be imaged and its precise position determined. Thus, each visibility is one component of the Fourier Transform of the source brightness distribution.

The baseline has components u, v, w; w points in the direction of interest, u and v point towards the East and North respectively, as may be seen in Figure 2.2. The positions on

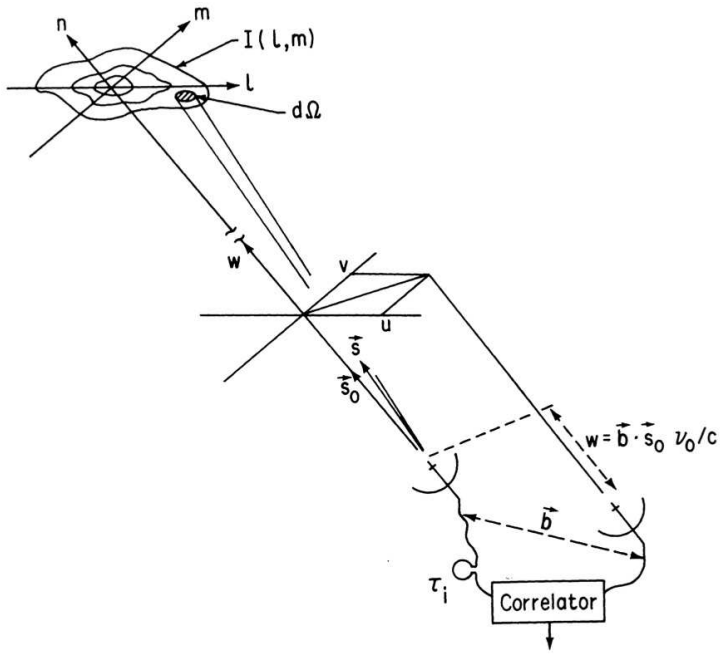

Figure 2.2: The image displayes the baseline components: u,v & w and the sky componments: l, m & n, from Thompson (1999)

the sky are measured in l and m, they are the directional cosines measured with respect to the u and v axes. Each visibility measured is one point on the u-v plane. The u-v plane can be imagined as the view the radio source has of the interferometer. As the Earth rotates this view changes, so different visibilities are observed making elliptical tracks as seen in Figure 2.3 the u-v plane of the 6035 MHz observations for this thesis.

The u-v data is a multiplication of the visibility function, V(u,v), and a sampling function. A 'dirty image' is produced from the calibrated set of visibilities, which are interpolated onto a grid, and then Fast Fourier Transformed. The Fourier Transform of the point spread function is the 'dirty beam' (Figure 2.4), which needs to be subtracted. As the synthesised beam does not fully sample the u-v plane it is lacking information about the source intensity distribution. In terms of u, v, l & m the visibility function is defined as:

$$V(u,v) = \int\int I(l,m)\, e^{-2\pi i(ul+vm)} dl\, dm \qquad (2.4)$$

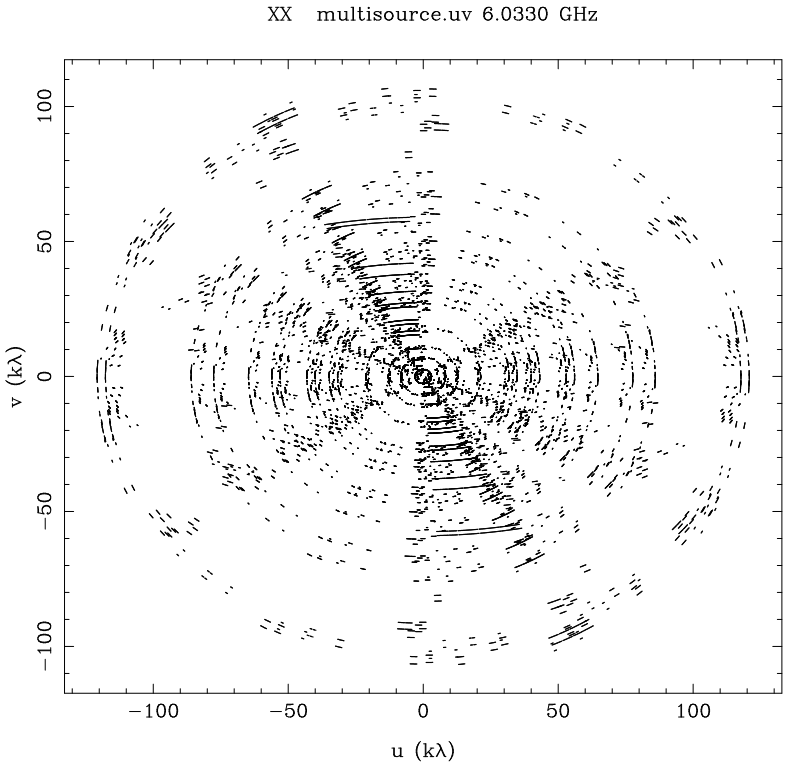

Figure 2.3: The U-V coverage of the 6035 MHz ex-OH observations at the ATCA

The visibility function is a Fourier Transform of the measured sky intensity distribution, thus using the inverse Fourier Transform we can retrieve the sky intensity distribution:

$$I(l,m) = \int\int V(u,v)\, e^{2\pi i(ul+vm)} du\, dv \tag{2.5}$$

To obtain the true image a deconvolution algorithm is used. This deconvolution algorithm accounts for the unsampled regions of the u-v plane. A non-linear algorithm is used to interpolate the gaps in the data. The two most common algorithms are called CLEAN and Maximum Entropy Method (MEM). The solution to the deconvolution process is not a unique one, there are indeed several solutions. As masers are point sources the process is somewhat easier as we know what it should look like, although there is no substitute for good u-v coverage. The deconvolution process produces a model of the source. The final step is to restore the image by convolving the model with a Gaussian, producing a science ready image, Figure 2.5.

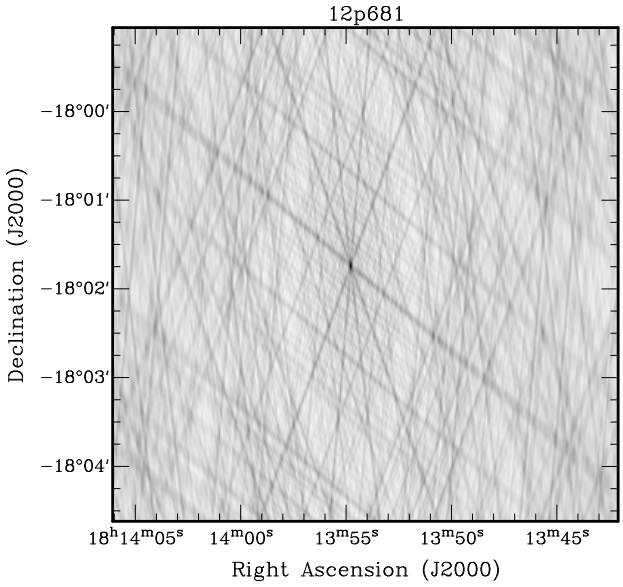

Figure 2.4: The dirty beam from the 6035 MHz ex-OH ATCA observations of source G12.681-0.182

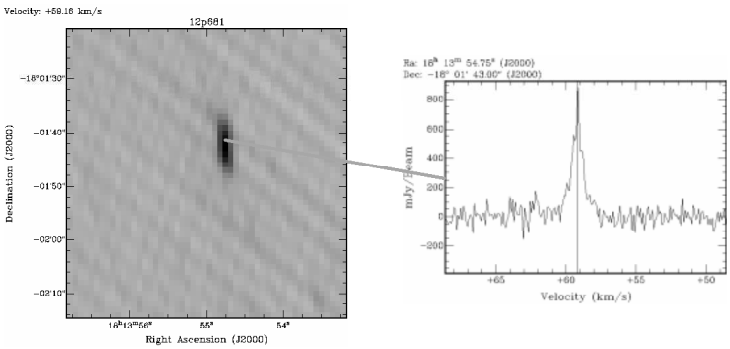

Figure 2.5: The final cleaned image of the maser at G12.681-0.182 and its spectrum to the right.

2.2.1 Calibrating the Data

As the wavefront passes through the Earth's atmosphere it is attenuated; the water vapour causing the waves to be scattered. It is vital to know how the atmosphere is

changing so we can track it and adjust for it. For this reason we observe phase calibrator sources, which are staple sources for which we know the exact position, intensity and shape.

The main calibrations performed on the data are the amplitude, phase and bandpass. The bandpass is the instrumental response which needs to be subtracted - especially for spectral line observations such as masers. The bandpass and amplitude calibrations are usually performed at the start/end of the observations. The phase needs to be tracked much more frequently, usually phase calibrators are observed every 20-30 minutes. For the 6035 MHz observations, the phase calibrator was observed before and after every 4 masers. The phase calibrator is chosen to be close to the masers position so excessive time is not lost on telescope slewing.

Once the u-v data is calibrated it is ready for imaging.

2.2.2 Single Dish or Interferometer?

Not all observations require the level of resolution provided by an interferometer. When deciding what type of telescope to use you need to consider several factors: resolution, point source or extended structure, are you mapping a region or pointing at a specific source, are you looking for a specific spectral line (NH_3, CO), if so which telescope have the receivers to obtain the necessary frequencies and bandwidth. There is also the more trivial issue of the desired region being accessible from the North or South hemisphere.

The MMB survey covers the North and South hemispheres making use of telescopes in both hemispheres. The Parkes single dish telescope and the Australian Telescope Compact Array (ATCA) are used for the Southern hemisphere and the single dish Effelsberg 100 m telescope in Germany along with the Very Large Array (VLA) are used

for the Northern hemisphere observations. The Class I survey at l =30° is accessible from the North and South hemisphere so either the ATCA or VLA may be used for the follow up observations.

In terms of studying star formation, single dish and interferometers are both equally important. Using the Scuba single dish telescope at the JCMT, Hatchell et al. (2005) observed the dust in the Perseus molecular cloud at 850 and 450 μm and the gas at $C^{18}O$. Ninety-one protostars and pre-stellar cores were detected from the observations. Star formation properties were determined for the molecular cloud such as: the large and small scale structure and filaments of the clouds, mass estimates using the continuum and the $C^{18}O$ observations, column densities of clusters and filaments and the number of stars forming in clusters. Using the single dish observations Hatchell et al. (2005) characterised the Perseus molecular cloud on a large scale. For this thesis, 960 sq degrees of the Galactic plane was observed for the MMB survey with the Parkes single dish telescope, it was subsequently reduced and analysed (see section *). The Class I maser survey was also observed using the Mopra single dish telescope as was the ATLASGAL continuum survey, using APEX (see Chapter 6 for a detailed comparison of the 6668 MHz methanol masers and ATLSGAL continuum survey).

As massive stars form in clusters, we require interferometers to study single objects in greater detail. General applications of interferometers for studying massive star formation include: studying protostellar disks (Zhang et al. 2001; Manoj et al. 2007), studying spectral lines in hot cores and protostars (Schilke et al. 2000), investigating chemical evolution of star forming regions using molecules (Longmore et al. 2007; Tideswell et al. 2010), studies of molecular outflows (Gibb et al. 2003) and observations of infall tracers, to see if a prestellar core is still accreting mass (Park et al. 2000). In this thesis, the ATCA and VLA interferometers were used to obtain precise positions of 6035 MHz ex-OH masers and the ATCA was also used to observe 5 GHz continuum at all the Class I maser source-sites.

2.3 Interferometer Data Reduction

The interferometric data in this thesis are from the VLA and the ATCA. The VLA uses the AIPS reduction package whilst the ATCA uses Miriad for data processing. Both reduction packages have their own advantages and disadvantages. You are more in control of every aspect using AIPS, but it is a long process. Miriad is more of a 'black box', but it is easier, quicker and more intuitive to use. The same method is used to process data using both tools, it is as follows:

1. Load the data (atload)
2. Calibrate the bandpass (mfcal)
3. Check the bandpass solutions by viewing it (gpplt, uvspec, uvplt)
4. Copy the bandpass solutions to the phase calibrator (task)
5. Calculate the gain calibration using the phase calibrator (task)
6. Check the solution quality (uvplt, gpplt)
7. Calibrate the primary flux calibrator, 1934-638 (mfcal)
8. 'Bootstrap' the output to the phase calibrator
9. Copy the phase calibrator solutions to the target sources - the masers (gpcopy)
11. Remove the continuum from the sources (uvlin)
12. Invert the source (invert)
13. Clean the source - fill in the u-v gaps (clean)
14. Restore the image (restor)
15. View the image in Kvis.

2.4 The Methanol Multibeam Survey

This section describes the telescopes, observing and data reduction techniques employed for this survey. The MMB is a joint project between the UK and Australia. A specially built 6-7 GHz receiver was constructed for the project. The aim of the MMB project is to survey the Galactic plane in 180°> l>180° & -2°< b<2° for 6668 MHz Class II methanol masers and 6035 MHz ex-OH masers. The receiver is currently at the Parkes telescope. Observing in the l=0° - 60° and l=186° - 360° longitude range has been completed and the receiver will shortly be moved to the 100 m Effelsberg telescope in Germany to complete the Northern hemisphere observations.

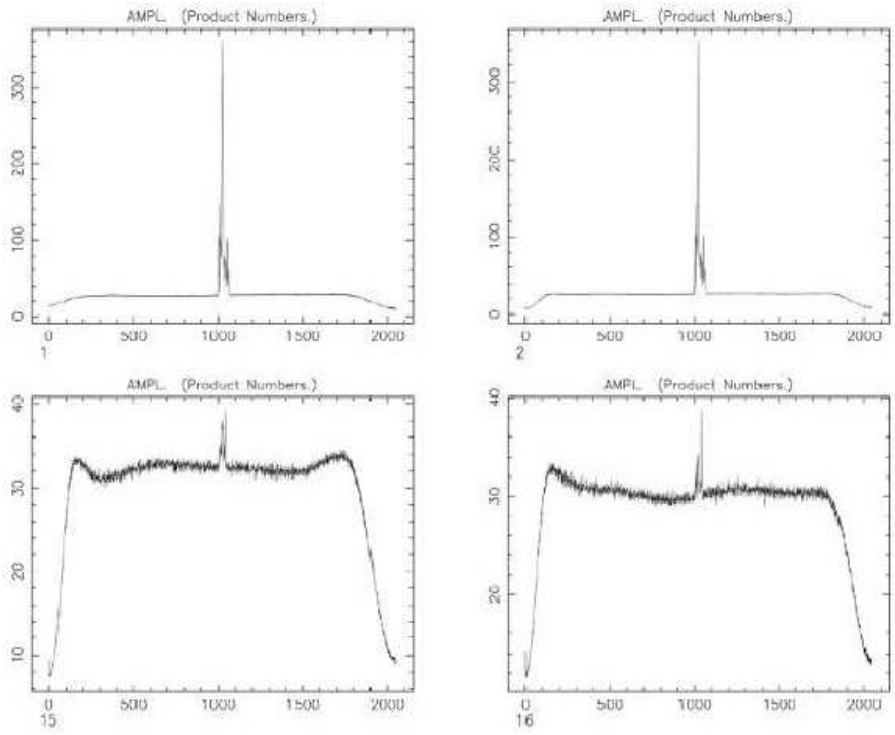

Figure 2.6: The first 6668 MHz methanol and 6035 MHz ex-OH maser detection with the MMB receiver.

2.4.1 Multibeam Receiver

The multibeam receiver was jointly built by the Jodrell Bank Observatory and the Australia National Telescope Facility (ATNF). The receiver has seven dual circular polarisation beams. They are arranged in a hexagonal pattern around the central feed (Figure 2.7).

The low noise amplifiers are Indium-Phosphide High Electron Mobility Transistors (HEMTS) and provide a 1 GHz bandwidth. A 500 Hz switched noise diode is used for continuous calibration in the presence of varying incoming power levels. The receiver is mounted 27 m above the dish at the prime focus. It was successfully commissioned at Parkes on the 21st of January 2006 and had first light on the 22nd of January (Figure 2.6).

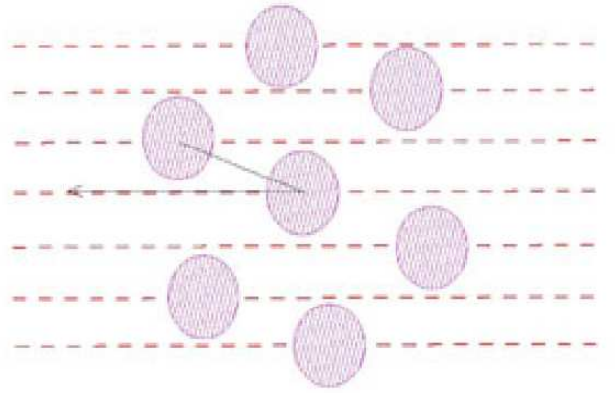

Figure 2.7: The orientation of the 7 beam 6-7 GHz reciever.

2.4.2 MMB Survey Techniques

The completed MMB survey will cover -180° < l < 180° in longitude and -2° < b<2° in latitude and observed the 6668 MHz methanol and 6035 MHz ex-OH transitions simutaneously. The southern section of the MMB, which is now completed, spans from

-174° < l < 60°. The survey region is divided into 2° latitude by 4° longitude blocks. In the final reduction of the data, adjacent data cubes are combined so there are no rough edges, ensuring no masers at an edge of a cube are missed.

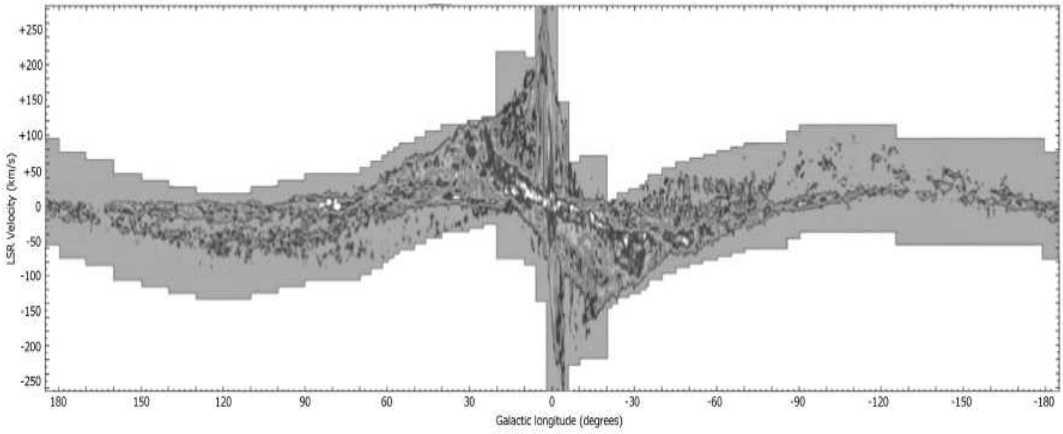

Figure 2.8: The Galactic CO emission from Dame er al (2001)

On the Parkes telescope, the total footprint of the receiver is ~15 arcmins, adjacent beams are separated by 6.4 arcmin. The FWHM of each beam is 3.2 arcmin at 6668 MHz and 3.4 at 6.035 GHz. For this hexagonal feed configuration an orientation of 19.1° to the scan direction, the Galactic plane, maintains equally spaced tracks for seven beams (Condon et al. 1989).

The correlator has 2048 frequency channels for each intermediate frequency (IF) and polarisation. The 4 MHz bandwidth gives a velocity coverage of 180 kms^{-1} and resolution of 0.0879 kms^{-1} at 6668 GHz and 200 kms^{-1} velocity coverage and 0.0971 kms^{-1} velocity resolution at 6.035 GHz. These are well within the ~0.2-0.3 kms^{-1} maser linewidths. To determine the velocity coverage required for the observations at different longitudes, the CO Galactic emission data from Dame et al. (2001) was utilised (Figure 2.8). For the regions covering the Galactic centre, 20° > l> 6°, multiple velocity settings were required to cover all the CO emission.

	Ex-OH	Methanol
Rest Frequency (MHz)	6035	6668
Beamwidth (arcmin)	3.4	3.2
Velocity coverage (km/s)	200	180
Velocity spacing (km/s)	0.0971	0.0875
Average system noise (Jy)	59.9	60.1
Typical survey noise (Jy)	0.17	0.17
Positional accuracy (arcsec)	0.5	0.5

Table 2.1: The MMB Survey characterisitics.

Individual Blocks

Scans were directed along lines of constant latitude at a rate of 0.1° min^{-1}, dumping spectra every 5s. Tracking of the paralactic angle was updated continuously. Each full scan is comprised of one pass forward before shifting 1.07' and scanning one pass back in the opposite direction to ensure the whole region was mapped. A larger displacement of 15 arcmin occurs for the next scan pair. One block is fully sampled in 32 scans, taking ~10 hrs. Across a block the sensitivity varies by ±3.5 %, however, this is worse when observing a strong continuum source which raises the system temperature. The pointing accuracy is ~15 arcsec.

The noise diode is used throughout the observations. Each of the 28 channels (7 beams, 2 frequencies, 2 polarisations) have different flux density values. To measure these values and to check for pointing offsets, the continuum source 1934-638 was observed most days. For this a 'SPOT' schedule scanned each beam over 1934-638 in RA and DEC. At 6668 MHz 1934-638 is assumed to have a flux of 3.9 Jy and 4.4 Jy at 6.035 GHz.

Calibration checks were also carried out by performing pointed observations, 'MX',

on known sources such as G300.969+1.148, which has a 6668 MHz and 6035 MHz maser. [1] Each maser that was detected in the data was subject to a pointed 'MX' observation, with each beam on source for ~1 min. This provided 7 minutes of integration time and a 1 sigma noise of ~0.1 Jy.

2.4.3 Data Reduction

The data was processed using Livedata and Gridzilla, glish based programs developed by Mark Calebrata at the ATNF. There are several steps involved in the data processing as the data are composed of the signal (possibly including a maser), noise, bandpass and possible baseline ripples. The bandpass is the strongest of these features and is removed first, next the data is flux density calibrated followed by baseline calibration and finally the data is constructed into a viewable cube.

Livedata

Livedata removes the effects of the bandpass, performs flux density calibrations and fits a polynomial to the data for baseline reduction. Usually a reference source is observed alongside the target to calibrate the bandpass. For this galactic survey, it is possible to estimate the bandpass. This eliminates the need to interleaf constant bandpass reference sources within the scanning, thus saving significant time.

In one scan there are 240 spectra each with 2048 channels. For each channel the median is calculated from the 240 spectra. This reference spectrum is constructed from the median of each channel. The reference spectra is then subtracted from each spectra in the scan. Even if a maser were in the scan, it would only last ~15 channels, so would not affect the median value or the bandpass. This method was proved to work from the HIPASS Parkes Survey (Barnes et al. 2001).

[1] The term MX comes from the LGM-118 Peacekeeper:"MX missile" (for Missile-eXperimental)

Following the bandpass removal the data were flux density calibrated using the values obtained from the SPOT 1934-638 observations. There are 28 values from the SPOT; seven beams, two polarisations and two frequencies.

Lastly, a fourth order polynomial was fitted to the data and the first and last 100 channels were removed. The fourth order polynomial fit was low enough not to distort any emission or absorption features.

Gridzilla

Gridzilla produces a viewable data cube from the 32 scans comprising of a 2° by 4° block. This is achieved by gridding individual spectra onto a grid to produce a position-position-velocity cube, reconstructing the flux at a certain position on the sky. The process determines which spectra contribute to a pixel and calculates the pixel value based on the input data and weights.

Gridzilla Settings	Parkes - MMB
Velocity range	-100 - 100 km/s (varies at Galactic Centre)
IF 1 (methanol)	6668.5192 MHz
IF 2 (ex-OH)	6035.0932 MHz
Beamwidth	4.4 arcmin
FWHM	4.4 arcmin
Cutoff radius	2.2 arcmin

Table 2.2: Gridzilla Parameters for the MMB

A smoothing radius is chosen to determine how many spectra contribute to each pixel value. The smoothing radius also determines the gridded beamsize and final image noise level. Testing carried out by Barnes et al. (2001) during the HIPASS survey have found that a smoothing radius which is too small does not produce a sufficient robust-

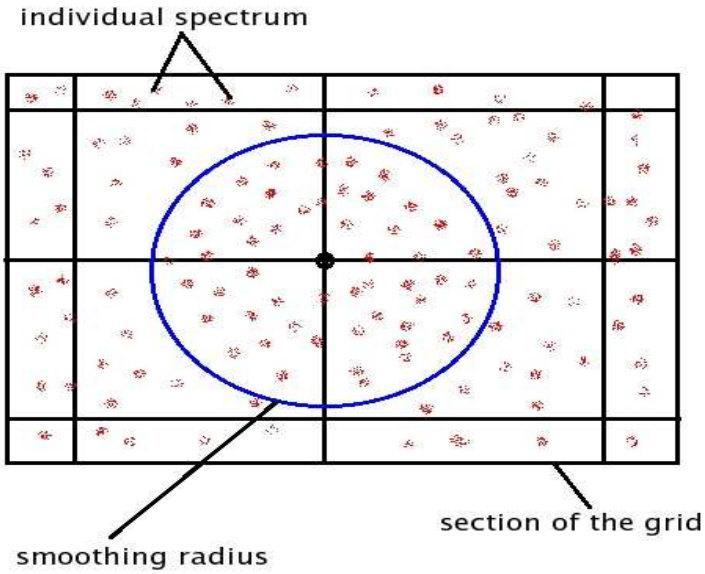

Figure 2.9: A grid with individual spectra that will contribute to the final pixels. The weighting a spectrum has is inversely proportional to its distance from the pixel - the further away, the less weighting it has.

ness whilst one that is too large will cause a loss of positional accuracy and resolution. A top-hat smoothing kernel of radius 4.4 arcmin and a cutoff of 2.2 arcmin was used and the size of the pixels are determined by the Nyquist relation (Green et al. 2009a).

A weighted mean is used to determine how the spectra contribute to the pixel in determining the flux. A beam weighting of 2, weighs the spectra by the square of the beam response, which is calculated for the distance of each spectra from the pixel, (Figure 2.9). Typically 50 spectra contribute to each pixel, 25 from each polarisation. Pixels were chosen to be 1 arcmin, which over-samples relative to the Nyquist requirements. The final gridded cube can be positioned against a reference point or automatically sized based on the length and number of scans. For initial cube processing at Parkes the autosize is used but the final stitched cubes have offset centres so they are gridded together to get rid of the jagged edges. These gridded cubes cut out the risk of losing any sources at the edges of the cubes.

Cubes were produced for total intensity (Stokes parameter I) for the 6668 MHz methanol data, combining the right and left hand circular polarisations. For the 6035 MHz data, separate cubes of right and left circular polarisation were made as they are generally highly polarised.
The optimisation of Livedata and Gridzilla was performed by the MMB team during the first observing run at Parkes.

2.5 Source Detection

In the survey, not only are each of the cubes run through a source detection algorithm code, but each and every cube is also viewed by eye. This ensures that any false positives concluded to be a source by the detection program are eliminated. Also, this program (along with several other Starlink source detection programs) missed a large number of sources when they were close in position and velocity to a strong (>20 Jy) source. Therefore, viewing the cubes by eye led to finding many more sources than if just run through the detection program. Figure 2.11 shows four maser detections found by the source detection program, but when viewed by eye they were deemed to be just noise. Figure 2.10 shows the bright central maser at G348.00+0.00, the masers surrounding it were not picked up by the detection program, but by eye.

2.5.1 Source Detection Algorithm

The source detection algorithm is based on the ATNF spectral line analysis package called ASAP. The ASAP one dimensional routine was run on each of the 2.2° by 4° cubes, containing 32,000 pixels. The spectrum of each pixel is compared with a baseline estimated from a linear fit to the intensity as a function of velocity for ~100 channels, centred on the pixel in question. The ~100 channel width is smaller than any baseline ripple but much greater than any maser feature.

-a = 2	Averaging: The number of consecutive spectral channels that will be averaged to check for broad emission
-c= 3	The number of spectral channels that should be above the threshold to be considered a detection
-t = 4.7	A detection threshold in terms of RMS in the spectra
-p = 1	Minimum number of pixels in an image
-d =1	Minimum distance in pixels between peaks of different line ranges to split the source in two.
-r	All velocity ranges will be present in the programs output (default)
-s	Produces spectra of the detections (default)

Table 2.3: Inputs for the source detection program

To class as a detection, three consecutive channels must be 4.7 times the root mean square deviation of the baseline fit in question, $4.7/\sqrt{3}$ per channel. This threshold was found to be high enough to limit the number of false positives whilst low enough to guarantee we are detecting the weaker masers (>0.8 Jy).

Once the threshold is reached, the algorithm searches for more emission in both directions of the spectrum until the difference between the channel flux density and the linear baseline fit changed sign. Once a line was detected the channels were excluded

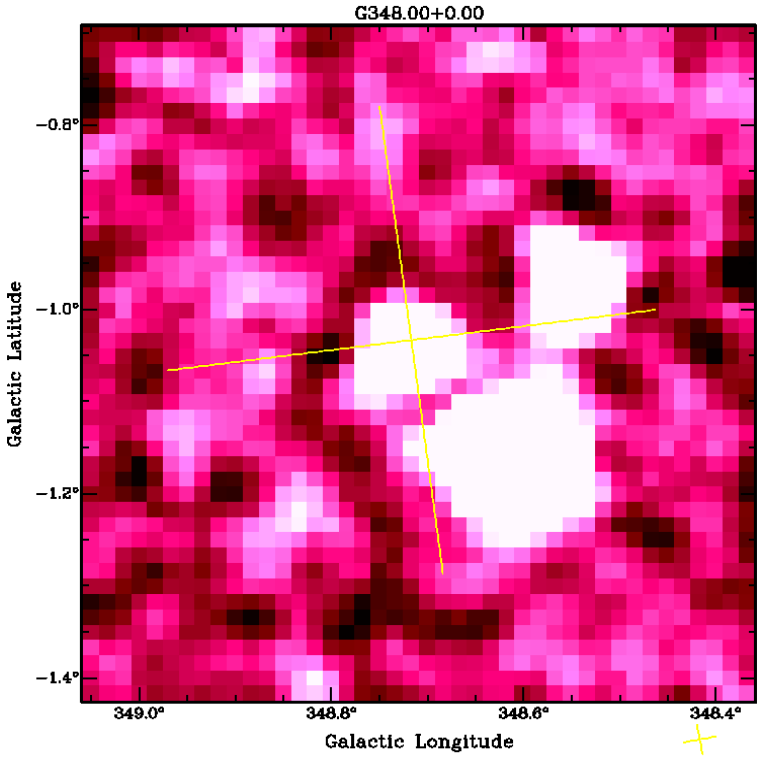

Figure 2.10: An excerpt of the G348.00+0.00 Parkes data cube, showing the maser (marked by the annotation) which was picked up by the source finding algorithm and the two other masers to the East which were missed by the algorithm but spotted in the visual detection.

and the baseline fit was recalculated. When the end of the spectrum was reached the process started again.

When a detection was made in a pixel all neighbouring pixels were searched for emission. If more than one distinct spectral line was found their separation distance was compared. If the separation was greater than 1 pixel (1 arcmin) then they were deemed separate sources, if the separation was less than this they were combined into one source. On several occasions the detection program incorrectly grouped sources into one source. However, these instances were rectified by the visual inspection of the cubes. The algorithm inputs are summarised in Table 2.3

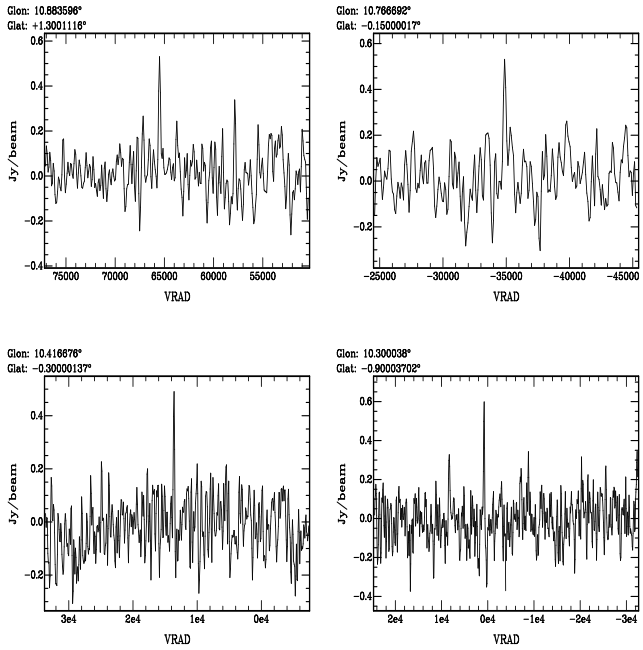

Figure 2.11: False maser detections from the Source detection algorithm.

During the course of the data processing and detection, there were >100 sources which were difficult to classify as real or false. They were on or below the detection limit, looked real in the spectrum but not particularly in the cube. These sources were observed in targeted observations to determine if they were real or not. We found only ∼4% of these sources to be real.

2.5.2 Source Detection Efficiency

The efficiency of the maser detection was explored using test cubes and simulated masers. A real empty data cube spanning from latitude l=220° to l=G222° was injected with simulated masers at flux densities of 0.5, 0.6, 0.7, 0.8, 0.9, 1.0 & 1.1 Jy. Forty masers were constructed and put into 14 simulated cubes. They were processed in the same way using the source detection program and 'by eye' visual inspection. The results were grouped into two samples: algorithm detections - detections made by the program and catalogued sources - detections deemed real by eye. The results are

Input Flux (Jy)	Percentage of sources below threshold	Algorithm detections	Completeness of algorithm (%)	Catalogued sources	Total completeness (%)
0.5	58.8	3	8±4	0	0
0.6	36.9	11	28±8	7	18±7
0.7	18.74	25	63±13	14	35±9
0.8	7.4	35	88±15	34	85±15
0.9	2.3	37	93±15	36	90±15
1.0	≤0.1	36	90±15	32	80±14
1.1	≤0.1	40	100±16	36	90±15

Table 2.4: Comparison of the number of simulated sources versus those detected by the source algorithm.

summarised in Table 2.4

3

The Methanol Multibeam Survey

3.1 The Methanol Multibeam Survey

The Methanol MultiBeam (MMB) project is a Galactic plane survey for 6668 MHz methanol and 6035 MHz ex-OH masers (Green et al. 2009b), as described in Chapter 2. My role in the survey include; carrying out a majority of the Parkes observing (> 100 days), reducing all of the Parkes single dish 6668 MHz methanol and 6035 MHz ex-OH data; running the source detection algorithm on all the 6668 MHz methanol and 6035 MHz ex-OH data; visually inspecting all of the 6668 MHz methanol and 6035 MHz ex-OH data cubes; producing the single dish catalogues for the 6668 MHz methanol and 6035 MHz ex-OH masers and leading the 6035 MHz ex-OH maser follow up survey.

There have been 953 6668 MHz methanol masers and 118 6035 ex-OH masers detected by the MMB survey so far (Caswell et al. 2010). The first results catalogue of the 6668 MHz methanol maser detections between 345° and 6° in longitude have been published (Caswell et al. 2010), The MMB has also discovered the first evidence of high mass star formation in the near and far 3 kpc spiral arms (Green et al. 2009c). The MMB has also completed the first unbiased survey of the LMC and SMC for 6668

MHz methanol and 6035 MHz ex-OH (Green et al. 2008). Table 3.1 shows an extract of the full 6668 MHz methanol maser table, the full table of the Parkes results is displayed in Appendix 1.

3.2 High Mass Star Formation in the 3 kpc Spiral Arms

An important feature of the 6668 MHz methanol masers is that they exclusively trace regions of high mass star formation (Minier et al. 2003; Walsh et al. 2003; Purcell et al. 2006b). A second, is that the peak velocity of the 6668 MHz methanol maser is usually within a few km $s^{-1}$from the peak velocity of CS(2-1) emission. CS(2-1) is a known tracer of dense gas, therefore the methanol masers have a good velocity correlation with their parent molecular cloud (Larionov et al. 2001). Using the velocity and longitude of a 6668 MHz methanol maser, it is possible to estimate a distance for it, hence telling in which spiral arm it is located.

The near 3 kpc spiral arm was not believed to host high mass star formation (Lockman 1980) and the newly discovered, far 3kpc arm (Dame and Thaddeus 2008) was also believed to lack high mass star formation. The narrow thickness of the CO and HI in the two arms was the assumed reason for the lack of massive star formation.

The MMB has detected 42 6668 MHz methanol masers in the region defined (-15° < l < 15°) by Dame and Thaddeus (2008) (Figure 3.1). The peak velocity of these masers velocities matching the CO emission velocities in the 3 kpc arms and are associated with the longitude-latitude distribution of the velocity integrated CO emission, (Figure 3.2). Thus, there are forty-two methanol masers in the near and far 3 kpc spiral arms, based on their longitudinal positions and velocities. Since 6668 MHz methanol masers are only observed at sites of massive star formation, we have been able to conclude that there must be high mass star formation in the near and far 3 kpc arms. It also shows the assumption that this location is devoid of massive star formation, based

Source Name	Parkes Gal L	Parkes Gal B	Parkes:RA (J2000)	Parkes:Dec. (J2000)	Peak Flux (Jy)	Parkes Vp (km s^{-1})	Vstart (km s^{-1})	Vstop (km s^{-1})	Vrange	Status
G0.092-0.663	0.083	-0.667	17:48:25.57	-29:12:38.10	24.80	23.5	10.0	25.0	15.0	New
G0.167-0.446	0.167	-0.450	17:47:46.43	-29:01:38.31	4.44	13.8	9.5	17.0	7.5	New
G0.212-0.001	0.217	0.000	17:46:08.07	-28:45:04.24	3.47	49.3	41.0	50.5	9.5	Known
G0.315-0.201	0.317	-0.217	17:47:12.98	-28:46:41.47	72.16	19.4	14.0	27.0	13.0	Known
G0.316-0.201	0.317	-0.200	17:47:09.16::	-28:46:09.40	0.60	21.0	20.0	22.0	2.0	Known
G0.376+0.040	0.367	0.033	17:46:21.61	-28:36:20.56	2.32	37.0	35.0	40.0	5.0	Known
G0.409-0.504	0.400	-0.517	17:48:35.13	-28:51:42.92	2.77	25.3	24.5	27.0	2.5	New
G0.475-0.010	0.467	-0.017	17:46:47.48	-28:32:46.38	3.43	28.8	23.0	31.0	8.0	Known
G0.496+0.188	0.500	0.183	17:46:05.55	-28:24:49.76	32.14	0.8	-12.0	2.0	14.0	Known
G0.546-0.852	0.550	-0.850	17:50:14.65	-28:54:16.78	62.83	11.8	8.0	20.0	12.0	Known
G0.645-0.042	0.650	-0.067	17:47:25.11	-28:24:55.26	76.08	49.5	46.0	53.0	7.0	Known
G0.666-0.029	0.666	-0.050	17:47:24.07	-28:23:22.64	32.90	70.0	68.0	73.0	5.0	Known
G0.695-0.038	0.700	-0.050	17:47:28.31	-28:21:50.24	36.41	68.6	64.0	75.0	11.0	Known
G0.836+0.184	0.833	0.167	17:46:56.62	-28:08:15.43	8.99	3.6	2.0	5.0	3.0	Known
G1.008-0.237	1.000	-0.250	17:48:57.17	-28:12:37.41	15.23	1.6	1.0	7.0	6.0	New
G1.147-0.124	1.133	-0.133	17:48:48.66	-28:02:09.55	2.97	-15.3	-20.5	-14.0	6.5	Known
G1.329+0.150	1.317	0.133	17:48:12.32	-27:44:28.84	1.56	-12.0	-13.5	-11.0	2.5	New
G1.719-0.088	1.717	-0.100	17:50:02.29	-27:31:06.76	9.81	-8.0	-9.0	-4.5	4.5	New
G2.143+0.009	2.150	0.017	17:50:35.25	-27:05:12.09	6.70	62.7	54.0	65.0	11.0	Known
G2.521-0.220	2.520	-0.233	17:52:23.59	-26:53:56.93	0.70	4.2	-7.5	5.0	12.5	New
G2.536+0.198	2.533	0.200	17:50:45.71	-26:39:48.76	36.41	3.2	2.0	20.5	18.5	Known
G2.591-0.029	2.600	-0.033	17:51:48.74	-26:43:31.82	1.69	-8.2	-9.5	-4.0	5.5	New
G2.615+0.134	2.617	0.133	17:51:12.54	-26:37:33.78	1.10	94.5	93.5	104.0	10.5	New
G2.703+0.040	2.700	0.050	17:51:43.20	-26:35:49.11	9.00	93.6	91.5	98.0	6.5	New

Table 3.1: An extract of the 6668 MHz methanol masers detected by the Parkes telescope in the MMB survey. The rest of the masers are listed in Appendix 1.

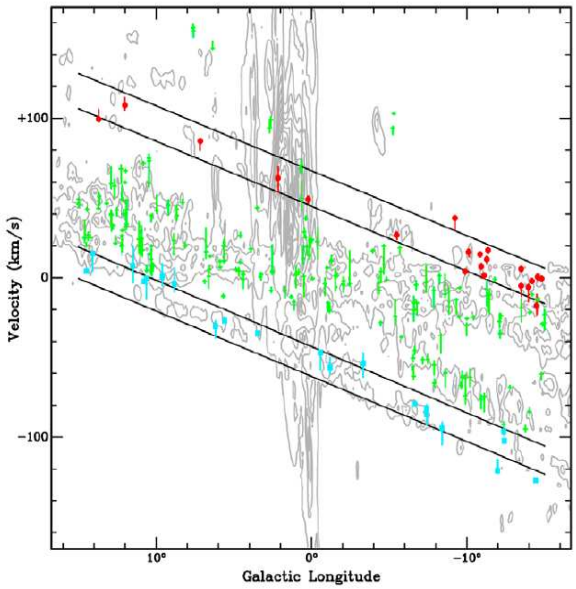

Figure 3.1: The longitude-velocity diagram of the methanol masers (symbols) and the CO emission (contours) of Dame and Thaddeus (2008). The black lines delineate the near and far 3 kpc arms (Dame and Thaddeus 2008). The blue symbols show the 6668 MHz methanol masers in the near 3 kpc arm, the red symbols are the methanol masers in the far 3 kpc arm and the green symbols are the masers not associated with the near or far arm.

on the thickness of the CO and HI, is incorrect.

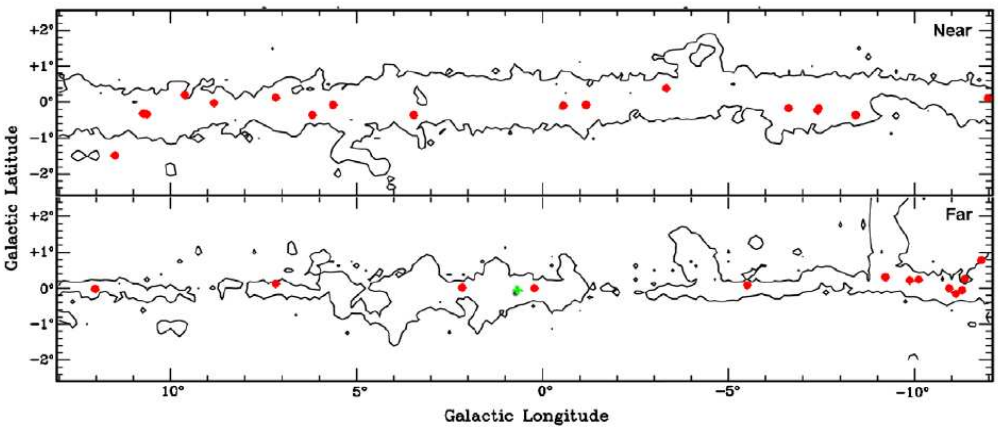

Figure 3.2: Longitude-latitude velocity distribution of CO (1-0) from Dame and Thaddeus (2008). Overlayed in red are the methanol masers associated with the near and far arms. The green crosses are the masers associated with Sgr B2.

3.3 MMB Survey in the Magellanic Clouds

The MMB has conducted the first complete survey of the Large (LMC) and Small (SMC) Magellanic Clouds for 6668 MHz methanol and 6035 MHz ex-OH masers. Regions known to host high mass star formation were also targeted for higher sensitivity searches (Table 3.2). The survey revealed a fourth 6668 MHz methanol maser and a second 6035 MHz ex-OH maser in the LMC. There were no detections in the SMC.

A number of masers have been detected in the LMC since the eighties; initially ground state OH and water masers, (Caswell and Haynes 1981; Haynes and Caswell 1981; Scalise and Braz 1982; Whiteoak et al. 1983; Whiteoak and Gardner 1986), followed by methanol maser detections (Sinclair et al. 1992; Ellingsen et al. 1994; Beasley et al. 1996). The SMC has also been a target for maser observation, searching for 6668 MHz methanol, ground state OH and 22-GHz water masers (Ellingsen et al. 1994; Beasley et al. 1996). There have only been two maser detections in the SMC, both of water masers (Scalise and Braz 1982). The detection rates and emission strengths of all the masers are lower than in our own Galaxy.

3.3.1 LMC & SMC Observations

The survey regions were defined to cover the CO and HI distributions of Fukui et al. (2001) and Staveley-Smith et al. (2003). The LMC observations took place over a longitude of 275° < l < 283° and latitude of -30° < b < -37°, this covered four blocks of 56 scans each. Figure 3.3 shows the LMC observed region with the CO clouds and HI emission respectively. A first pass of observations was carried out, giving a rms noise of ~0.22 Jy. All of the 6668 MHz methanol and 6035 MHz ex-OH masers are located in the central two blocks, along with the majority of CO clouds (as shown in Figure 3.3), as this is where one would expect to locate any more masers, scanning was focused on the two central blocks. A total of four passes were carried out on the central two blocks, giving an rms noise of ~0.06 Jy. In addition to the mapping observations, 11 regions were targeted in the LMC, for more sensitive pointed observations (Table 3.2). These regions were chosen as they are known to host high mass star formation tracers such as water, OH, methanol masers or HII regions. A region of 299° <l < 305° and -42° < b < -46° was mapped in the SMC, with two passes reaching a rms noise level of ~0.13 Jy.

3.3.2 Results

Two known 6668 MHz methanol masers at IRAS 05011-6815 and N105a and the one known 6035 MHz OH source at N160a, were detected from the mapping of the LMC. There were no detections at either 6668 MHz methanol or 6035 MHz OH transitions, in the SMC. From the targeted observations in the LMC, (Table 3.2), three known 6668 MHz methanol masers at N11, N150a & IRAS 05011-6815 were detected (Figure 3.5). A new 6668 MHz methanol maser was detected at the site of a known 6035 MHz OH maser at N157a (Figure 3.5), and a new 6035 MHz ex-OH maser was detected in a pointing towards N157a, all in the LMC. There were no detections from the pointings towards the SMC.

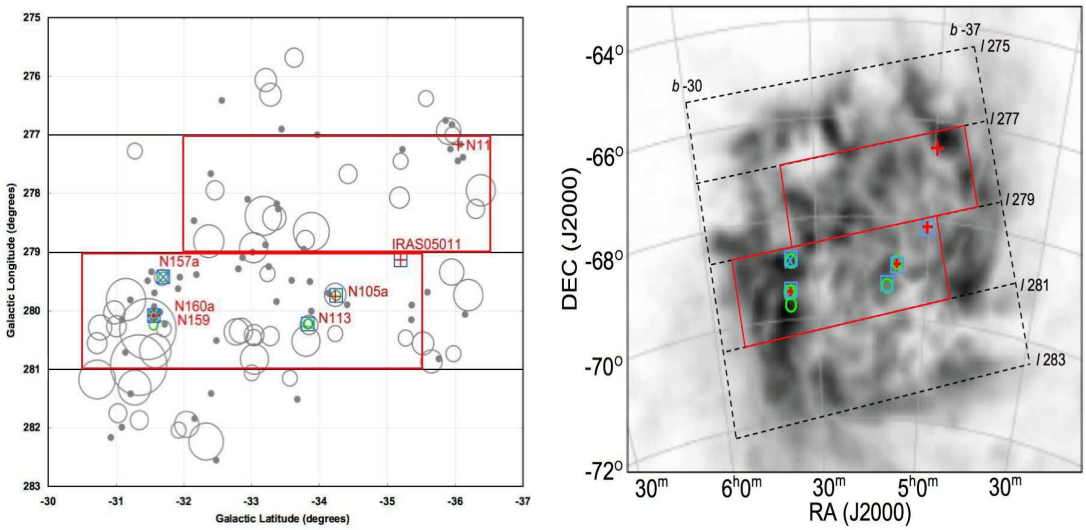

Figure 3.3: On the left: Surveyed region with CO clouds from Fukui et al. (2001). Grey dots and grey circles represent small and large CO clouds. Blue squares are ground state OH masers, green circles are water masers, blue crosses are 6035 MHz ex-OH masers and red pluses are 6668 MHz methanol masers. The red line show the region surveyed to a higher sensitivity. On the right: Peak brightness temperature of the HI in the LMC, overlaid with the maser positions, identified as before

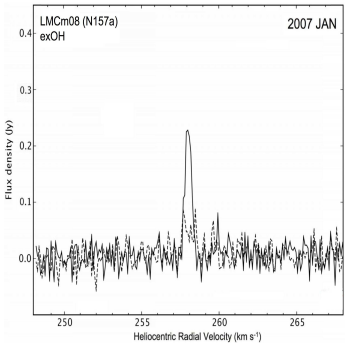

Figure 3.4: Parkes spectra of the new 6035 MHz ex-OH maser detected toward N157a (LSR velocity). The dashed line is the LHC and the solid line is the RHC.

Maser site number	RA (J2000)	DEC (J2000)	6668 MHz Methanol V_{helio} S_{peak} (km s^{-1}) (Jy)	6035 MHz OH V_{helio} S_{peak} (km s^{-1}) (Jy)	Other Known Transitions[a]
LMCm01	04 56 47.10 (0.03)	-66 24 31.7 (0.2)	301.0 0.33	- -	-
LMCm02	05 01 01.85 (0.06)	-68 10 28.3 (0.3)	268.0 3.78	- -	1665-/1667 MHz OH[7]
LMCm03	05 09 52.00 (0.04)	-68 53 28.6 (0.3)	- -	- -	1665-/1667 MHz OH[2,5,7]
					22-GHz H_2O[4,6,8]
LMCm04	05 09 58.66 (0.03)	-68 54 34.1 (0.2)	252.0 0.25	- -	-
LMCm05	05 13 25.18 (0.07)	-69 22 46.0 (0.4)	- -	- -	1665 MHz OH[7]
					22-GHz H_2O[6,8]
LMCm06	05 13 17.67 (0.07)	-69 22 21.4 (0.4)	- -	- -	22-GHz H_2O[8]
LMCm07	05 38 46.65 (0.07)	-69 04 45.5 (0.4)	- -	- -	22-GHz H_2O[4,6,8]
LMCm08	05 38 45.00 (0.03)	-69 05 07.4 (0.2)	- -	258.0 0.22	-
LMCm09	05 39 29.41 (0.07)	-69 47 18.9 (0.4)	- -	- -	22-GHz H_2O[3,8]
LMCm10	05 39 43.92 (0.10)	-69 38 33.6 (0.6)	- -	- -	22-GHz H_2O[6,8]
LMCm11	05 39 38.94 (0.03)	-69 39 10.8 (0.2)	248.0 0.20	248.5 0.39	1665 MHz OH[1,5,7]
					22-GHz H_2O[4,6,8]

Table 3.2: Four 6668 MHz methanol masers and two 6035 MHz OH masers in the LMC with additional data on other species.

Comparing the star formation rates of Israel (1980), the metalicity and the masses of the LMC, SMC and our own Galaxy we can estimate the number of masers the LMC and SMC would be expected to have. With the star formation rates of the SMC, LMC and Milky way being 0.4, 0.08 and 3.5 M yr^{-1}, the LMC should have nine times less masers and the SMC ~40 fewer masers. This range fits for the OH and water masers in the LMC, but the methanol masers are ~5 times under abundant.

What could be the cause of this deficiency in methanol masers? We know that maser emission is affected by metallicity and the UV field, but just how much we do not know. Without a high enough abundances of methanol, masers cannot form and without a strong enough UV field the molecules cannot by excited and reach a stage of population inversion required for maser action (Cragg et al. 2002). The metallicities of the LMC and SMC are known to be ~44% and ~28% of the solar neighborhood (Massey 2003). If the lower metallicity results in fewer complex molecules, maybe there is a shortage of methanol to produce the masers. The factor of 5 under abundance may be explained by the lower levels of oxygen and carbon in the LMC, reported by Beasley et al. (1996).

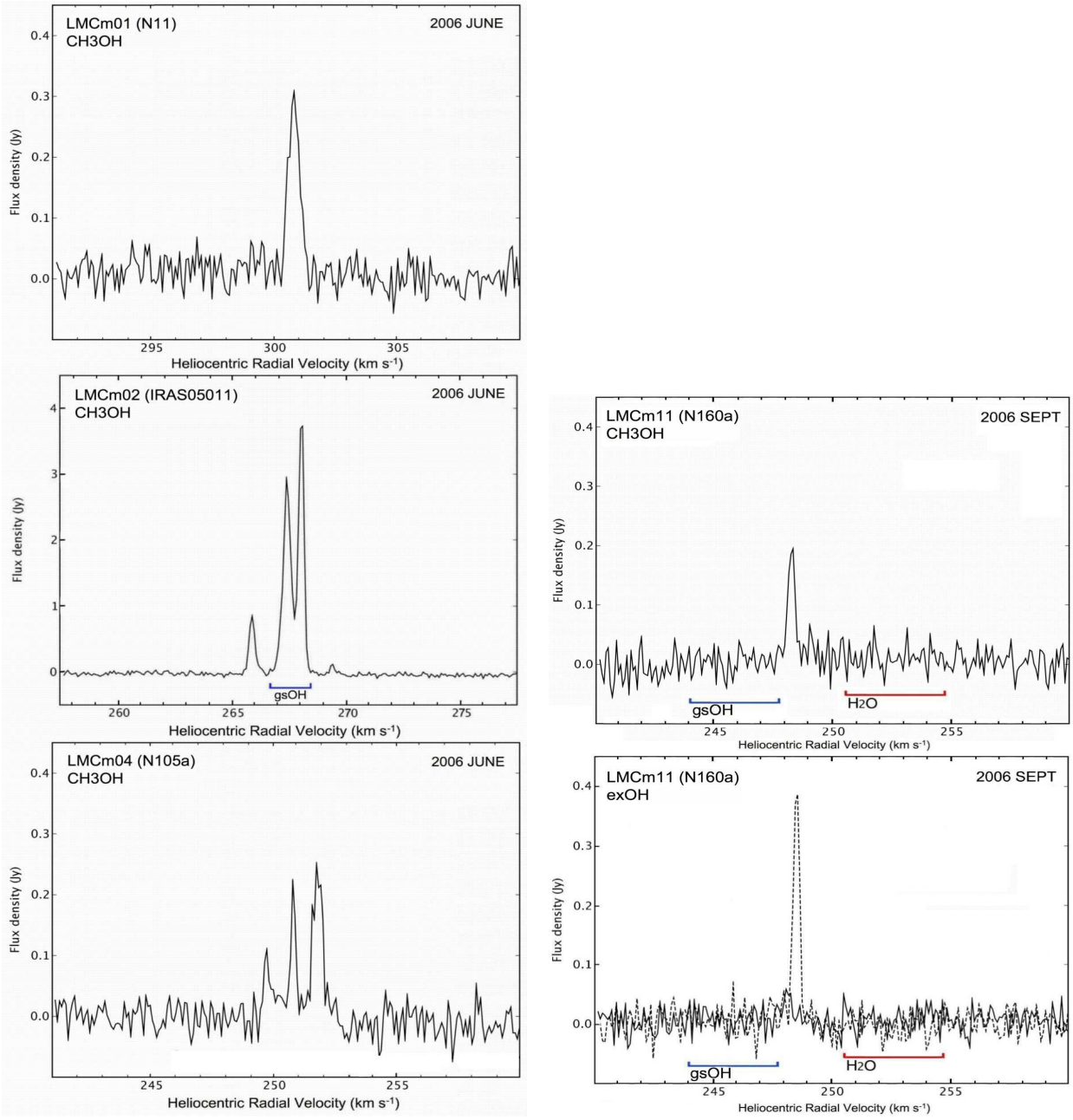

Figure 3.5: Left: the three known 6668 MHz methanol masers, taken at Parkes. Right: the newly detected 6668 MHz methanol and 6035 ex-OH masers from the LMC survey. The horizontal lines represent the velocity range of the ground state OH (gsOH) and water (H_2O) masers.

4

MMB: 6035 MHz Excited Hydroxyl Maser

The 6035 & 6031 MHz ex-OH masers detected in the MMB survey by the Parkes telescope are presented in Tables 4.1 to 4.5 and Tables 4.13 & 4.14. All of the results of the interferometric observations of the 6035 MHz ex-OH masers conducted with the ATCA, (as described in Chapter 2), are also presented and discussed in this Chapter. Each 6035 MHz ex-OH maser is discussed individually in the following section. The 6035 & 6031 MHz ex-OH maser spectra is presented in Figures 4.1 to 4.22. The properties of the ex-OH masers are discussed in section 4.4, followed by a detailed comparison of the ex-OH masers to the 6668 MHz methanol masers detected in the MMB, 1665/7 MHz OH masers and the infrared GLIMPSE and CORNISH surveys, the tables comparing the positions of the 6035 MHz ex-OH masers to 6668 MHz methanol, 6031 MHz ex-OH and 1665/7 MHz OH masers are shown in Tables 4.6 to 4.10

4.1 6035 MHz Ex-OH Maser Results

118 ex-OH masers have been detected in the region 180°< l < 56°, |b|=≤2°, 43 of which are new and 75 are known sources. The detections were made two ways: in the Parkes survey results or from an MX observation on a 6668 MHz methanol maser

position. The majority of new detections, 27, of 6035 MHz masers were found from MX's on methanol masers. The observations of the forty 6035 MHz ex-OH maser ATCA observations are presented in Tables 4.11 & 4.12 and discussed immediately afterwards.

4.1.1 Individual Maser Analysis and Spectra

The following section discusses each ex-OH maser separately and details it in relation to previous observations, 6031 MHz, 1665/7 MHz and 6668 MHz maser association, and with GLIMPSE and CORNISH. A full discussion on these relationships as a whole follows in the subsequent sections. For simplicity, the following reference abbreviations have been used: Caswell & Vaile (1995): CV95, Caswell (1998): C98, Forester & Caswell (1998): FC98, Caswell (2001): C01, Caswell (2003): C03. All references to methanol masers are the Class II 6668 MHz methanol maser unless otherwise stated. All of the GLIMPSE images refered to in the text below are located in Appendix 2.

G0.666-0.029 & G0.666-0.035

Both of these masers are known from CV95 and both have an accompanying 6031 MHz maser. The spectrum of the 6035 MHz masers is very entangled. G0.666-0.035, the weaker of the two masers is responsible for the emission in the 60-68 km s^{-1} range, whilst the stronger ranges from 68-74 km s^{-1}. The GLIMPSE image shows the G0.666-0.035 is coincident with a strong source while G0.666-0.029 is associated with an IRDC.

G4.682+0.278

This is a new maser discovered from an MX on a methanol maser, is offset 21″ from the methanol maser. No 6031 MHz emission was detected. The ex-OH maser is at a peak velocity of 2 km s^{-1}, whilst the methanol maser has three peaks from 2-5 km s^{-1}. Both masers are probably associated with the same star forming region. Interestingly, the

GLIMPSE image shows the methanol maser is associated with a bright source whilst the ex-OH maser is located in a region without any obvious source.

G6.881+0.093

This new source is coincident with 6668 MHz methanol, 6031 MHz ex-OH and 1665 MHz OH masers within 1″. The 1665 MHz detection is a new ATCA detection with a peak flux density of 1.6 Jy. Both of the ex-OH masers have the same velocity range and the 6035 MHz maser is four times the intensity of the 6031 MHz emission. This is an interesting source as the 6035 MHz maser emission intensity is comparable to the methanol and 1665 MHz OH maser. Usually the 6035 MHz ex-OH emission intensity is much lower than the 6668 MHz methanol and 1665/7 MHz OH masers (C98). The GLIMPSE images shows the masers are coincident with a reddened GLIMPSE source, on the cusp of an IRDC.

G8.267+0.486

This new ex-OH maser is very unusual as no 6668 MHz methanol maser was detected in the Parkes data and no methanol or 1665/7 MHz OH was detected at ATCA. It does have a 6031 MHz companion at a similar velocity. The GLIMPSE image is equally as interesting, showing the ex-OH maser in an IRDC with slight EGO emission (Appendix 2).

G8.669-0.356

A known maser detected by CV95. It is spatially coincident with a 6668 MHz methanol maser. The spectrum profile remains the same as the CV95 spectrum but with a slight increase in the flux density. The masers sit in between two clumps of EGO emission (Appendix 2).

G9.620+0.194

This is a new single peaked detection. It is spatially coincident with the brightest

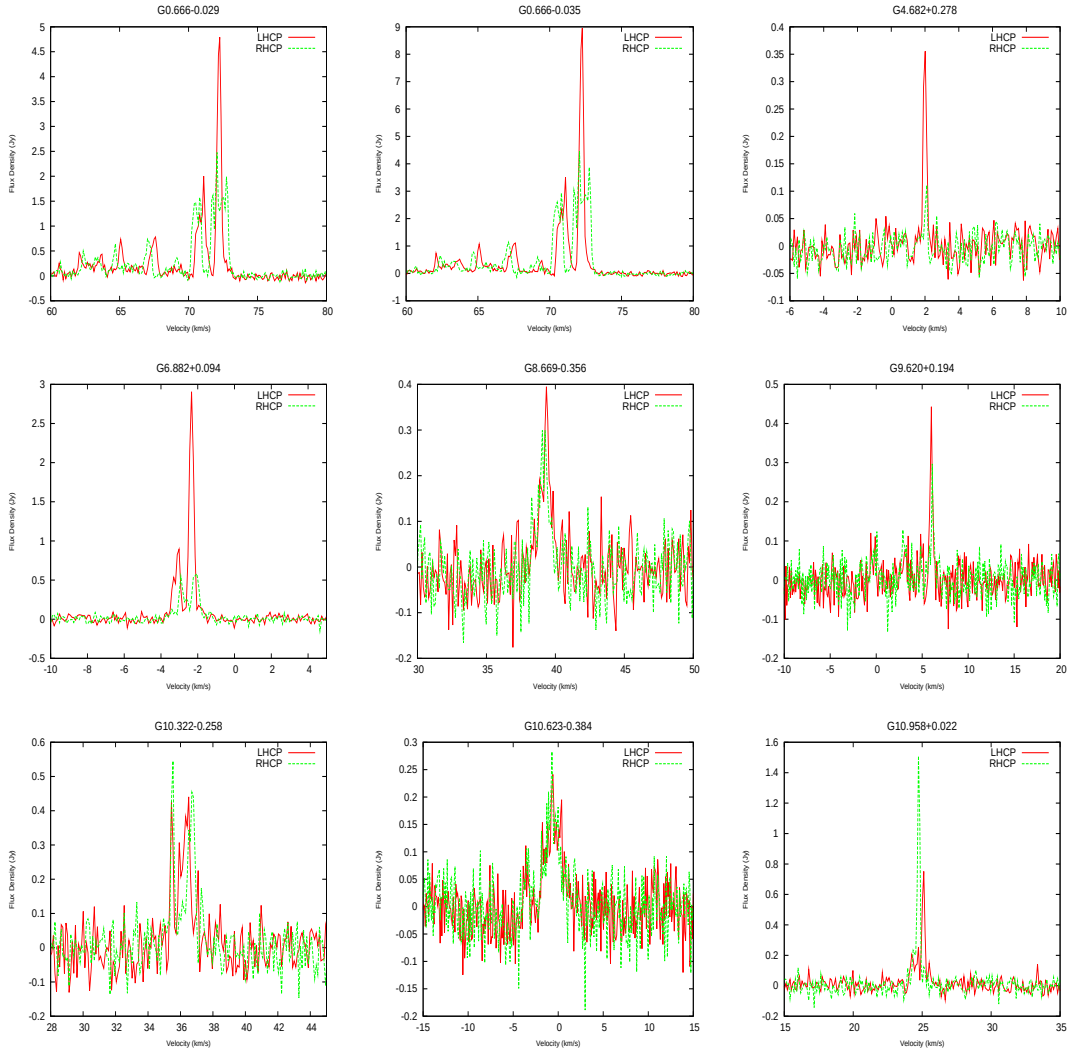

Figure 4.1: Spectra of 6035 MHz ex-OH masers detected by the Parkes telescope for the MMB survey.

known methanol maser. 1665/7 MHz masers are also present, detected by C98. The GLIMPSE three colour image shows the OH and surrounding methanol masers are coincident with three clumps of bright EGO emission, which is interesting as previous observations by Cyganowski et al. (2008a) all show the 6668 MHz methanol masers are not coincident with the EGOs.

G10.322-0.258

A new source, 5.1″ from a 6668 MHz methanol maser. It does not appear to be polarized. The GLIMPSE data show the methanol maser is coincident with a bright source whilst the ex-OH maser is on the edge of the source. No 6031 MHz emission was detected.

G10.623-0.384

A known maser, the profile is similar to that of CV95 and C2003. It is 11.7″ away from a methanol maser. There is also 1665/7 MHz OH emission at the location of the ex-OH maser as determined by C98. The GLIMPSE image shows the 6035 MHz and 1665/7 MHz masers sit on top of EGO emission, 10″ to the west a methanol maser is located on the edge of some EGO emission. The ex-OH maser is 0.9″ from a UC HII region of 305 mJy, detected by the CORNISH survey.

G10.958+0.022

This is a new detection which is spatially coincident with a methanol maser and new 1665 MHz OH maser detected with ATCA. The spectrum is multi-peaked and shows clear Zeeman splitting. The GLIMPSE image shows the ex-OH, OH and methanol masers coincident with a bright GLIMPSE source. This maser is separated by 0.91″ from an HII region of 109 mJy, detected by CORNISH (Figure 4.42).

G11.034+0.062

A known maser detected by CV95 & C03. The spectrum is very different from CV95, the flux density has increased six-fold and the peak at -26 km s^{-1} has disappeared below the detection threshold. The masers are all coincident with a bright GLIMPSE source. The masers are separated by 2.6″ from a UC HII region of 21 mJy, detected by CORNISH.

G11.904-0.141

First detected by CV95, the spectrum remains largely unchanged, with a slight in-

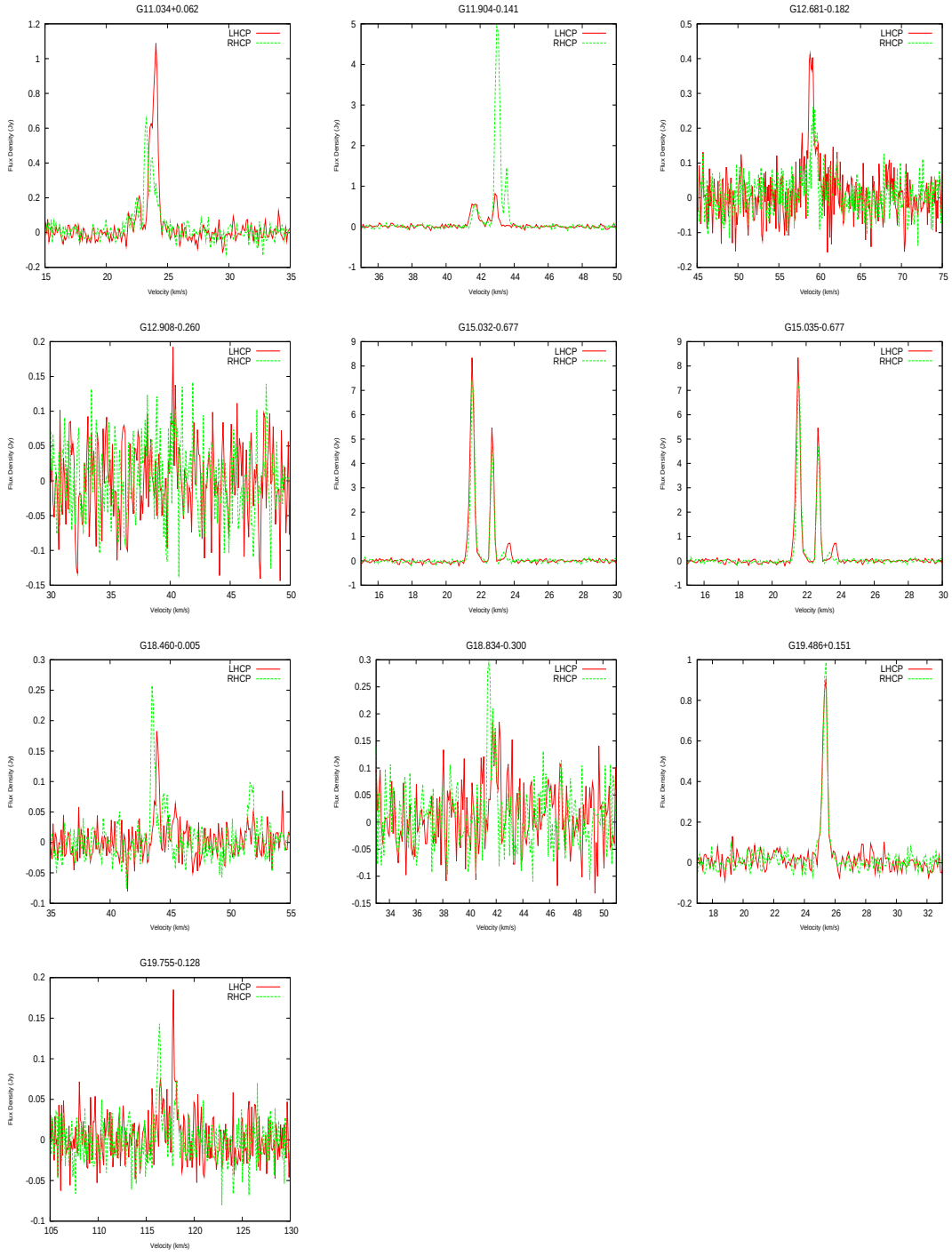

Figure 4.2: Spectra of 6035 MHz ex-OH masers detected by the Parkes telescope for the MMB survey.

crease in flux density. It is coincident with a methanol maser. There has not been any 6031 MHz detection, but 1665/7 MHz OH masers have been detected at the same location. The GLIMPSE images shows the methanol and OH masers coincide with a bright GLIMPSE source. The masers are coincident with a UC HII region detected in the CORNISH survey. The UC HII region has an integrated flux density of 11 mJy

G12.681-0.182

This is a new source, coincident with a methanol maser and 1665/7 MHz OH masers. The peak velocity of the 6035 MHz maser agrees with the peak velocity of the methanol maser. The methanol maser exhibits several features across a ∼10 km s^{-1} velocity spread. The single peak of the 6035 MHz maser matches up with the strongest methanol peak at -58 km s^{-1} .

G12.908-0.260

A new detection, the position matches previously detected 1665/7 MHz maser emission from C98, it is 1.1″ from a methanol maser. No 6031 MHz emission was detected. The three colour GLIMPSE image shows the OH masers are coincident with the centre of a bright source whilst the methanol maser is slightly offset.

G18.460-0.005

A new source separated 1.6″ from a methanol maser. There is a velocity difference of ∼5 km s^{-1} between the peak of the methanol and ex-OH maser. Figure 4.3 shows the 6035 MHz ex-OH maser and 6668 MHz maser spectra. The methanol and ex-OH maser lie on the edge of a bright GLIMSPE source.

G18.836-0.300

This is a new detection separated 9″ from a methanol maser. 6031 MHz emission is also detected. The ex-OH maser is on the edge of a bright GLIMPSE source whilst the

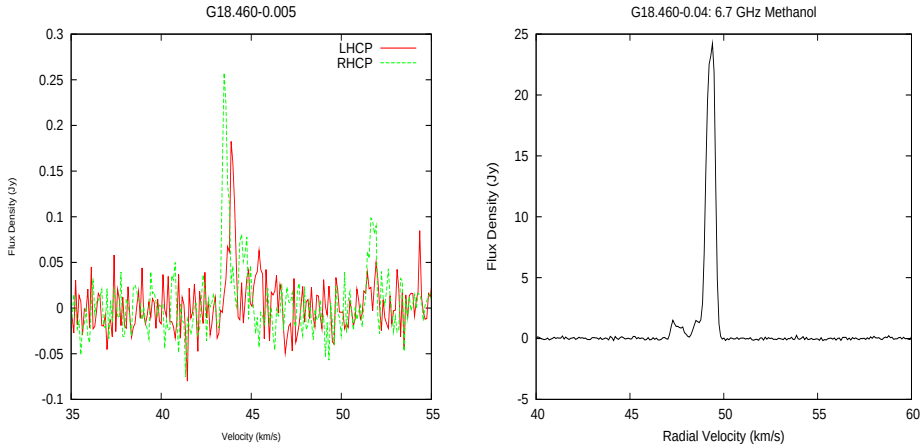

Figure 4.3: The spectra of the 6035 MHz ex-OH maser (left) and the 6668 MHz methanol maser (right), the difference between the peaks is clearly visible.

methanol maser is coincident with it (Appendix 2).

G19.486+0.151

This is a known maser, first detected by CV95 and again in C03. It is not associated with a methanol maser. The intensity and profile structure remain very similar to CV95 and C03. It has an accompanying 6031 MHz maser which is one-third the flux density of the 6035 MHz transition. A 1665 MHz maser is also detected at this location (priv. comm. Jim Caswell). The GLIMPSE three colour image shows the three OH masers residing on top of a small EGO which is $\sim 5''$ from bright source.

G19.755-0.128

This is a new detection, with no associated 6031 MHz emission. It is coincident with a methanol maser and whilst the velocity ranges of the emission match, the peak velocity of the ex-OH and methanol masers differ by 5 km s^{-1}. The GLIMPSE image shows both masers are coincident with a bright GLIMPSE source. The masers are associated with an HII region, detected by CORNISH.

G20.237+0.065

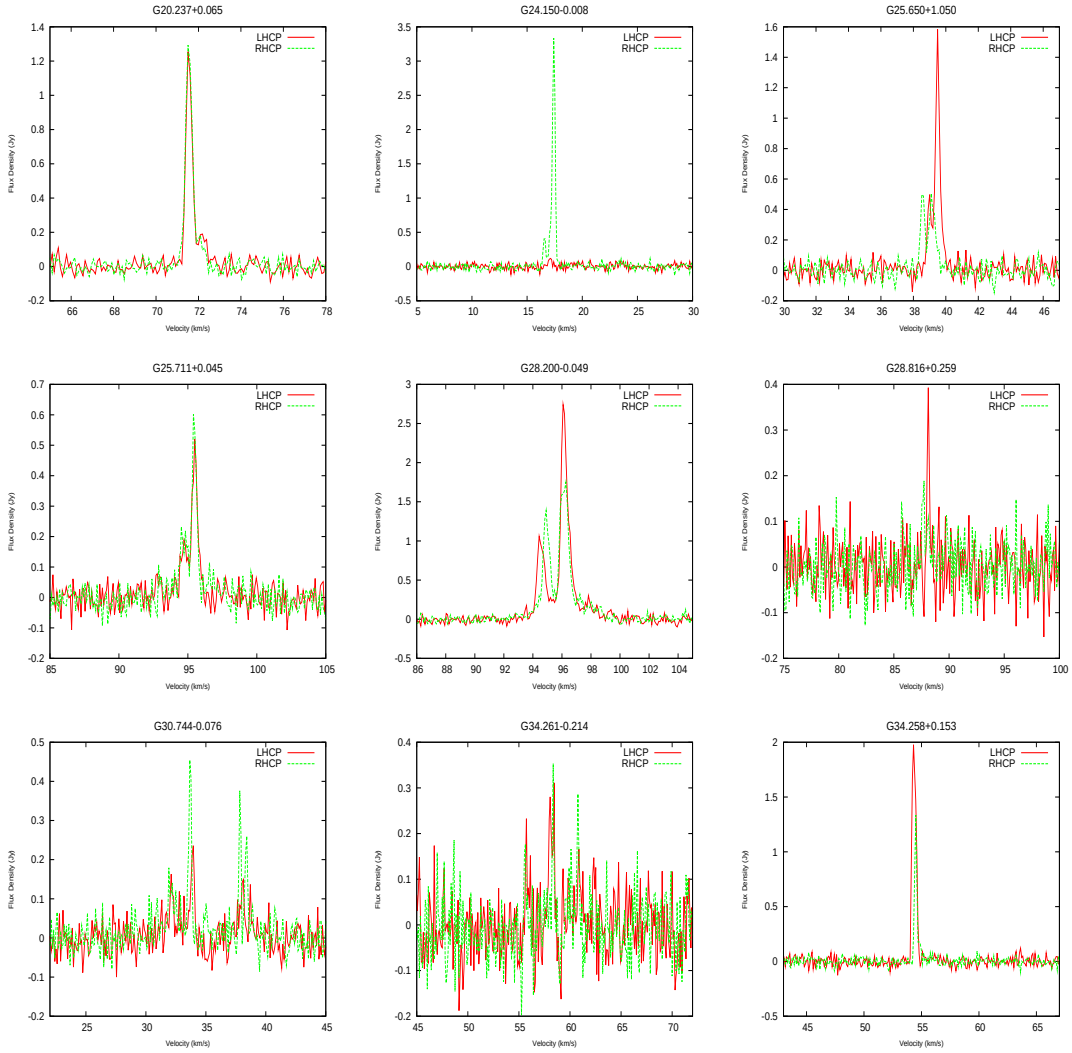

Figure 4.4: Spectra of 6035 MHz ex-OH masers detected by the Parkes telescope for the MMB survey.

This maser is known and coincident with 6031 MHz maser emission, 1665/7 MHZ OH masers (C98) and a methanol maser. The spectrum remains similar to CV95, the 6031 MHz is also stable and the flux density is one sixth of the 6035 MHz maser. The GLIMPSE images shows the masers lie on a compact GLIMPSE source with some EGO emission. Another methanol maser, without any OH emission is visible ∼5″ to the left.

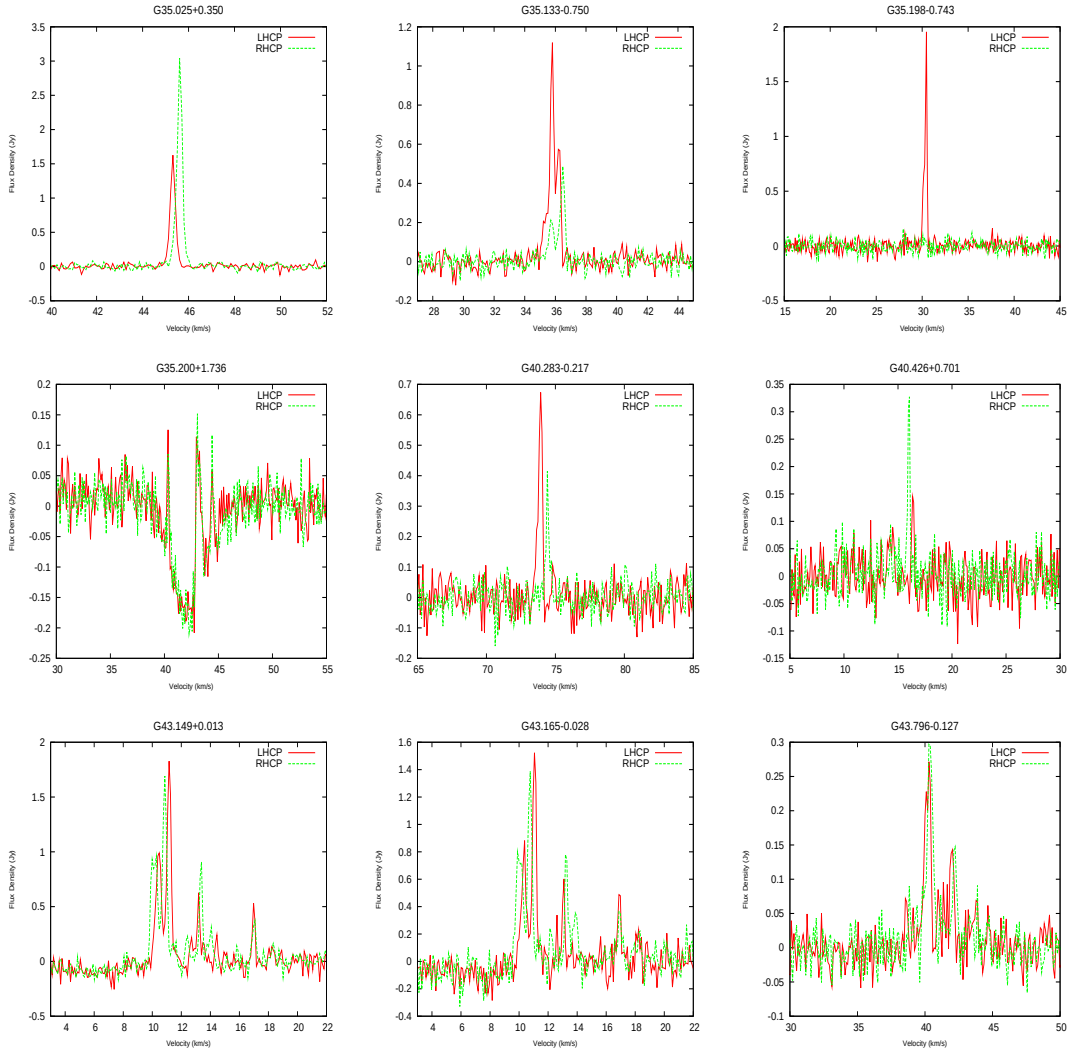

Figure 4.5: Spectra of 6035 MHz ex-OH masers detected by the Parkes telescope for the MMB survey.

G24.150-0.008

A new detection dominated by emission from the right hand circular polarisation (RCHP). It is 10″ away from a methanol maser. The GLIMPSE image shows the methanol and ex-OH masers on either side of a clump of EGO emission, with the methanol maser closer to the EGO.

G25.771+0.045

This is a new source 5″ away from a methanol maser. It does not have any 6031 MHz maser emission. The methanol maser is on the edge of EGO emission whilst the ex-OH maser is offset ~3″.

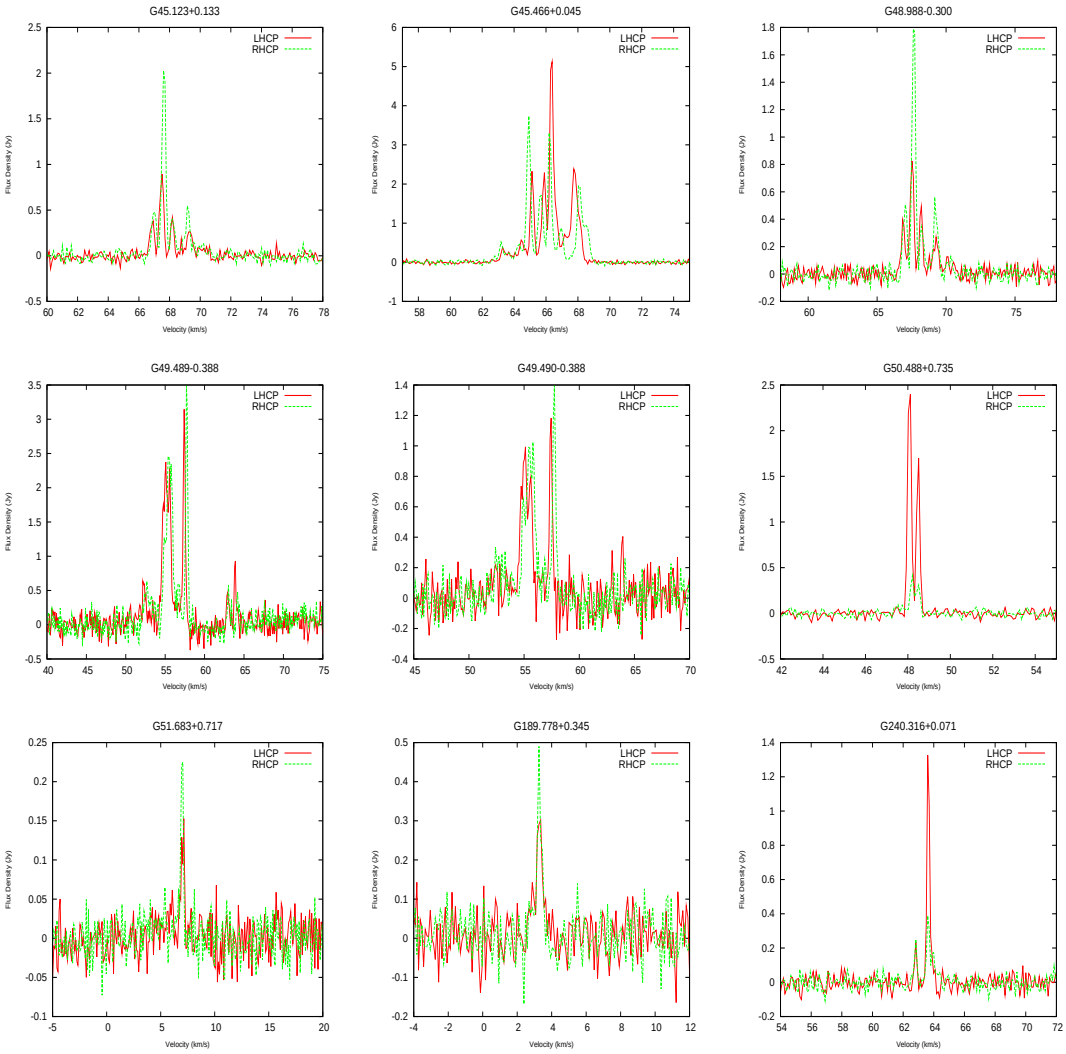

Figure 4.6: Spectra of 6035 MHz ex-OH masers detected by the Parkes telescope for the MMB survey.

G28.200-0.049

This is a new detection and also displays 6031 MHz maser emission. Two strong peaks are visible in the 6035 MHz spectrum and there appears to be Zeeman splitting in the

peak at 94 km s^{-1}. The 6031 MHz maser appears to display some thermal emission. In the GLIMSPE image the ex-OH masers are coincident with the centre of a bright source whilst the methanol maser is offset to the edge. The ex-OH maser is offset by 0.87″ from the peak of a UC HII region, detected by the CORNISH survey. The UC HII regions has an integrated flux of 161 mJy.

G30.771-804

This is a new detection, no 6031 MHz emission was detected. It is separated by 1.3″ from a methanol maser. The GLIMPSE image shows both of the masers on the edge of a bright source, with this bright source lying on the edge of an IRDC filament.

G32.744-0.076

A known maser first detected by CV95. It does not have any 6031 MHz maser emission but is coincident with 1665/7 MHz OH masers (priv. comm. Jim Caswell) and a methanol maser. The spectrum of the 6035 MHz maser shows several features spread over ~8 km s^{-1}. The peaks at 38 km s^{-1} are new features since CV95. The masers are coincident with bright EGO emission and offset by 0.52″ from a UC HII region of 8 mJy integrated flux density, detected by CORNISH.

G34.258+0.153

A known maser detected by CV95. It has newly detected 6031 MHz maser emission and at 1.2 Jy it is over half the flux density of the 2.0 Jy 6035 MHz emission. 1665/7 MHz maser emission is also detected at the same location (priv. commun. Jim Caswell). The OH masers are coincident with a bright GLIMPSE source whilst the methanol maser is offset in a region without any luminous sources. The ex-OH maser is separated by 0.22″ from the peak of a UC HII region detected by CORNISH, the UC HII region has an integrated flux density of 34 mJy. The spectrum of the 6035 MHz maser has varied from the CV95 spectrum, Figure 4.8. A peak at 54.8 km s^{-1} is now visible, which does not match to any of the emission peaks in the C98 spectrum.

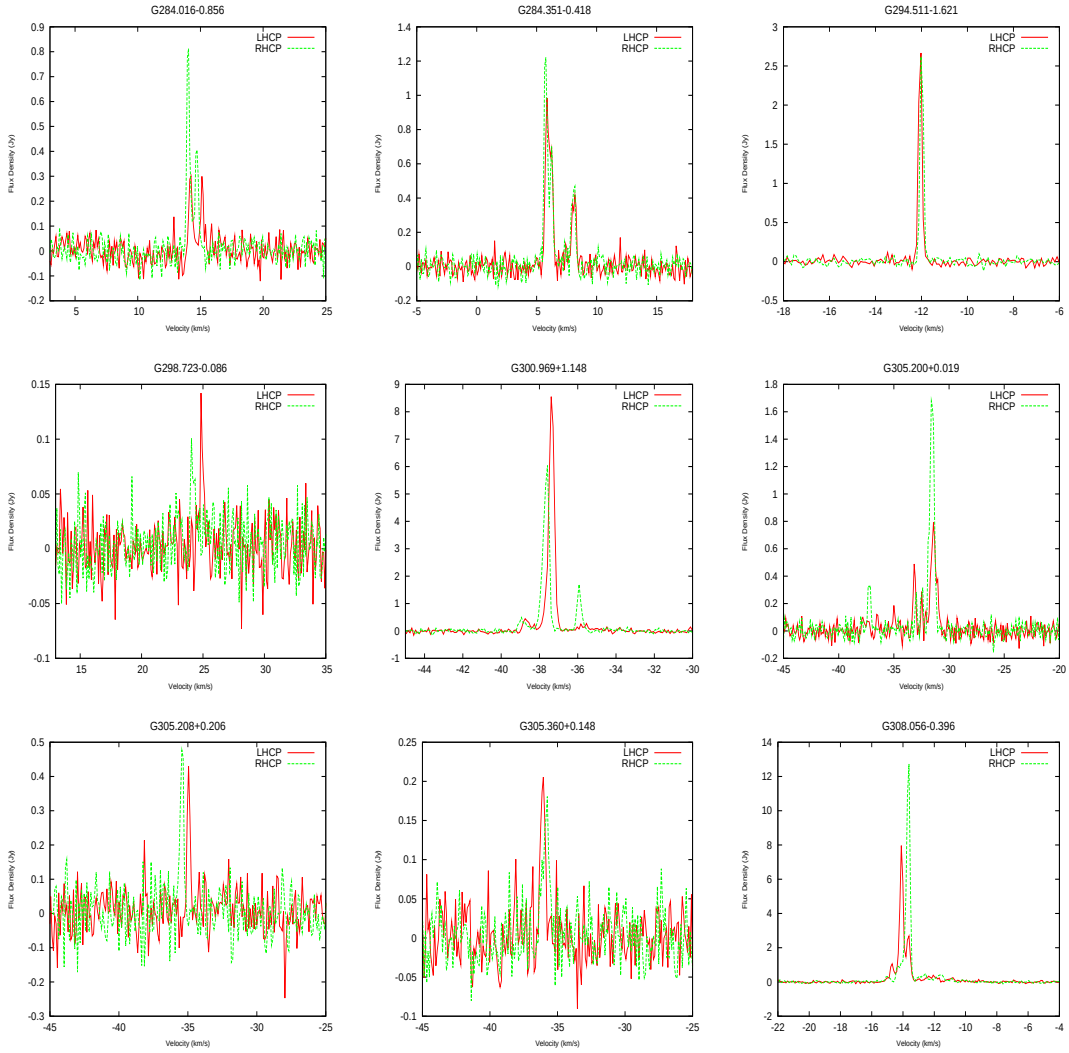

Figure 4.7: Spectra of 6035 MHz ex-OH masers detected by the Parkes telescope for the MMB survey.

G34.261-0.214

A new maser, separated from the methanol maser by 23″. No 6031 MHz emission was detected. The ex-OH maser covers the 55-62 km s^{-1} range, whilst the methanol maser is at a lower velocity range of 49-56 km s^{-1}. The GLIMPSE three colour image shows the ex-OH maser to the North of a bright GLIMPSE source, the methanol maser is to the South-West but it not associated with any bright source. The methanol maser is

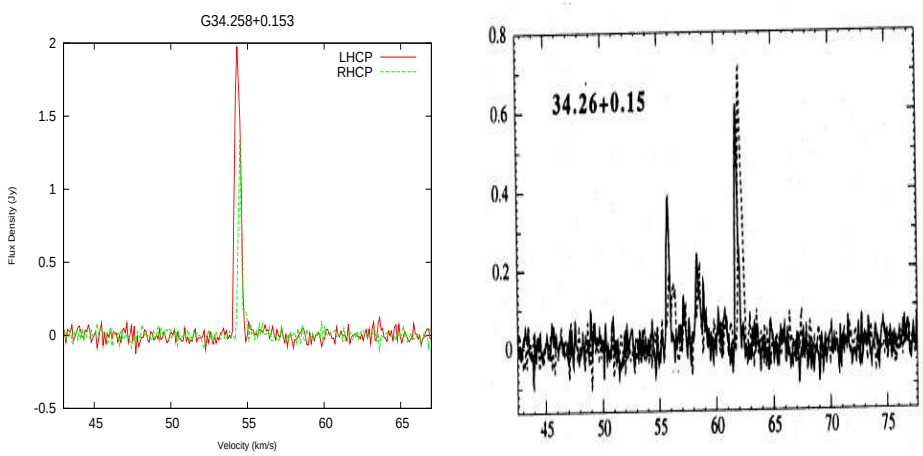

Figure 4.8: G34.258+0.153: The spectrum on the left was taken in 2009 and the one on the right in by Caswell (1998). In 2009 the peak at 54.8 km s^{-1} does not match any of the 1998 maser emission.

possibly tracing a less evolved massive star forming region than the ex-OH maser.

G35.025+0.350

A known maser from CV95 with an estimated kinematic distance of either 3.0 or 13.3 kpc (near or far) from C03. The source also contains 1665/7 MHz OH emission coincident with the ex-OH emission (priv. comm. Jim Caswell). GLIMPSE images show the ex-OH and OH masers are coincident with strong EGO emission, whilst the nearest methanol maser is off-set by 9.4″. No 6031 MHz emission was detected. The ex-OH maser is 2.76 ″ from the peak of an UC HII region of 11 mJy integrated flux density, detected by CORNISH.

G35.198-0.743

A known maser, detected by CV95 which is coincident with a methanol maser. 6031 MHz emission was not detected. 1665/7 MHz OH masers have also been observed at this location (priv. comm. Jim Caswell). The intensity in the LHCP has increased four-fold since CV95. The GLIMPSE image shows the masers are all located in an IRDC.

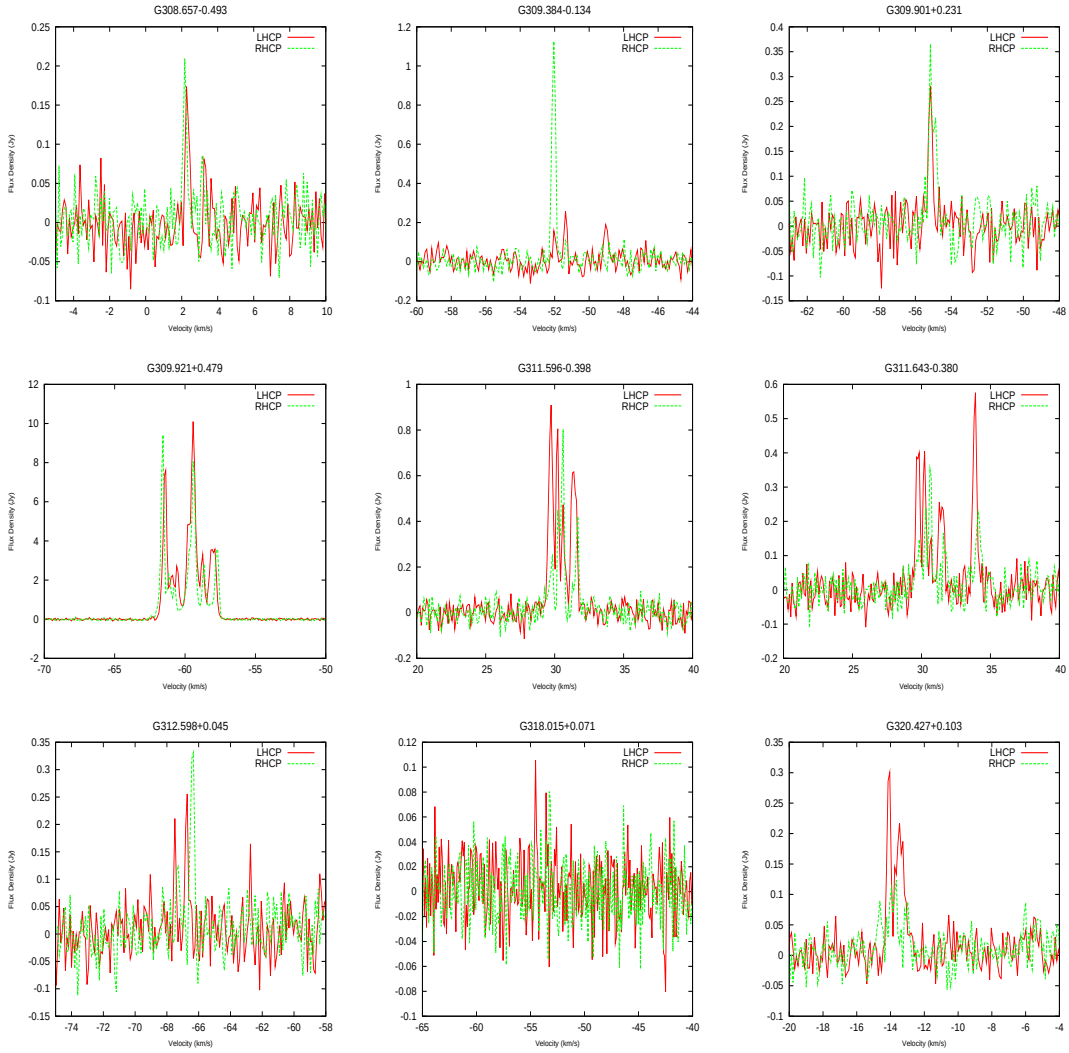

Figure 4.9: Spectra of 6035 MHz ex-OH masers detected by the Parkes telescope for the MMB survey.

G35.200-1.736

This is a known source from CV95. It has an accompanying 6031 MHz ex-OH maser. The flux density of the 6035 MHz maser has decreased by a third since 1995. The spectrum also contains a noticeable absorption feature. However, it was determined by C2001 the absorption feature is not associated with the maser and is in fact 15″ away,

but is picked in the single dish data.

G35.133-0.750

This is a new source coincident with a methanol maser. The GLIMPSE image shows the masers are located in a dark cloud without any visible emission.

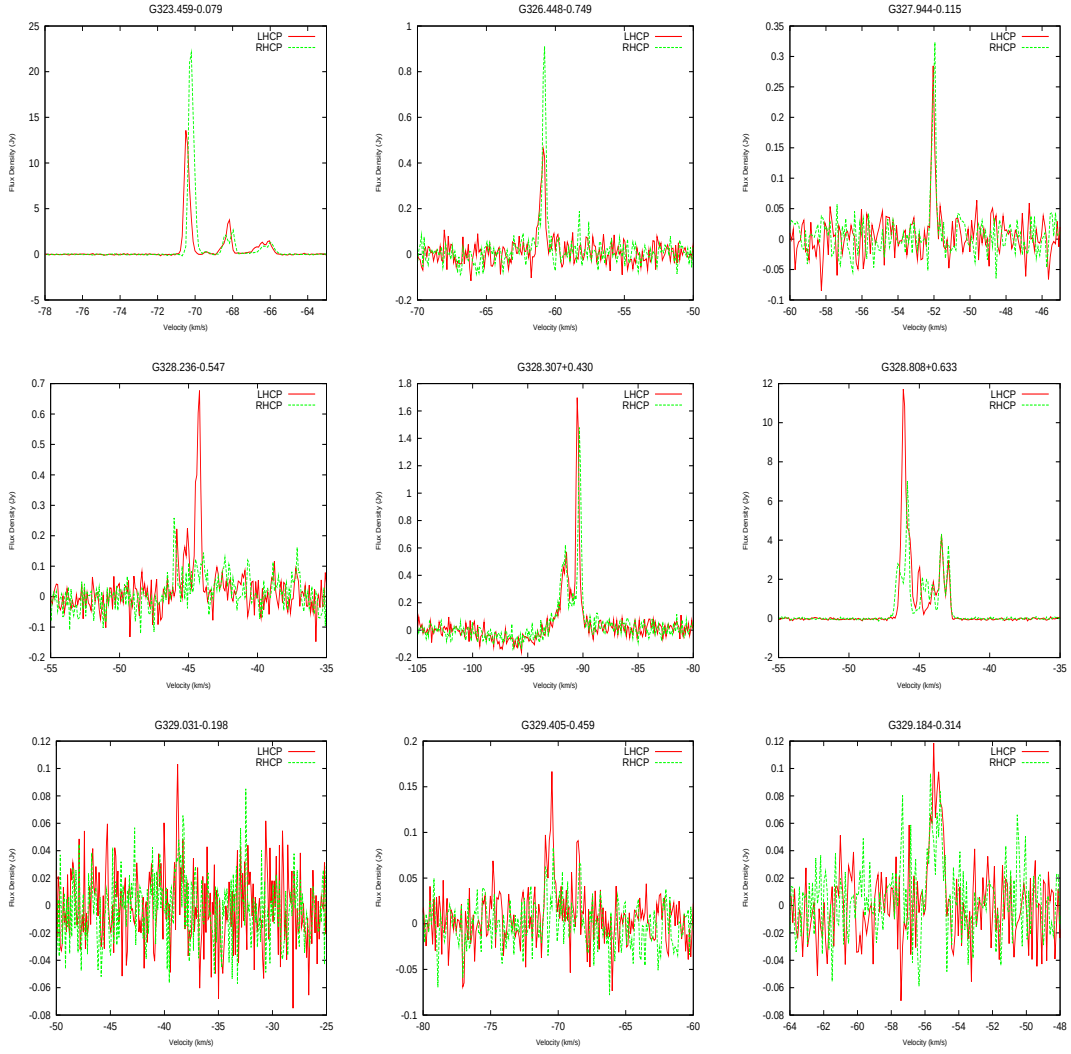

Figure 4.10: Spectra of 6035 MHz ex-OH masers detected by the Parkes telescope for the MMB survey.

G40.283-0.217

A new detection, without any 6031 MHz emission. It is coincident with a methanol maser and the velocity peaks of the 6035 MHz ex-OH and methanol maser match. Both masers lie in a dark GLIMPSE region which is ~5″ from a bright source.

G40.426+0.701

A known maser, (CV95), with a separation of 1.5″ from a methanol maser. The profile has varied significantly from CV95 and C03. The LHCP emission has doubled in flux density whilst the RHCP emission has remained the same. The GLIMSPE image shows the methanol maser lining up with the centre of a bright source and the ex-OH maser on the edge of the source. The ex-OH maser is offset by 2.85 ″ from the peak of a UC HII region detected by CORNISH. The integrated flux of the HII region is 8 mJy.

G43.149+0.013

This is a known maser which is in the W49 complex. It is 2.1″ from a methanol maser. The profile of the spectrum is very similar to CV95, with a slight increase in the flux density. The ex-OH and methanol maser lie on the edge of a bright GLIMPSE source. The ex-OH maser is 1.93″ from the peak of a UC HII region identified by the CORNISH survey. The UC HII region has an integrated flux density of 42 mJy.

G43.167-0.004

This is a known ex-OH maser. It is without an 6031 MHz companion, but is coincident with a methanol maser. The methanol and 6035 MHz ex-OH maser display several features. The methanol maser velocity range extends from -5 to 23 km s^{-1}, the ex-OH maser shows possible very weak emission at -5 km s^{-1} and and extends to 19 km s^{-1}. If the weak feature at -5 km s^{-1} is to be believed in the ex-OH maser, then it has the largest velocity spread of the sample, (Figure 4.12). The peaks of the masers occur at the same velocity. The 6035 MHz ex-OH maser is offset by 4.9″ from a UC HII region detected by the CORNISH survey with an integrated flux density of 2661 mJy.

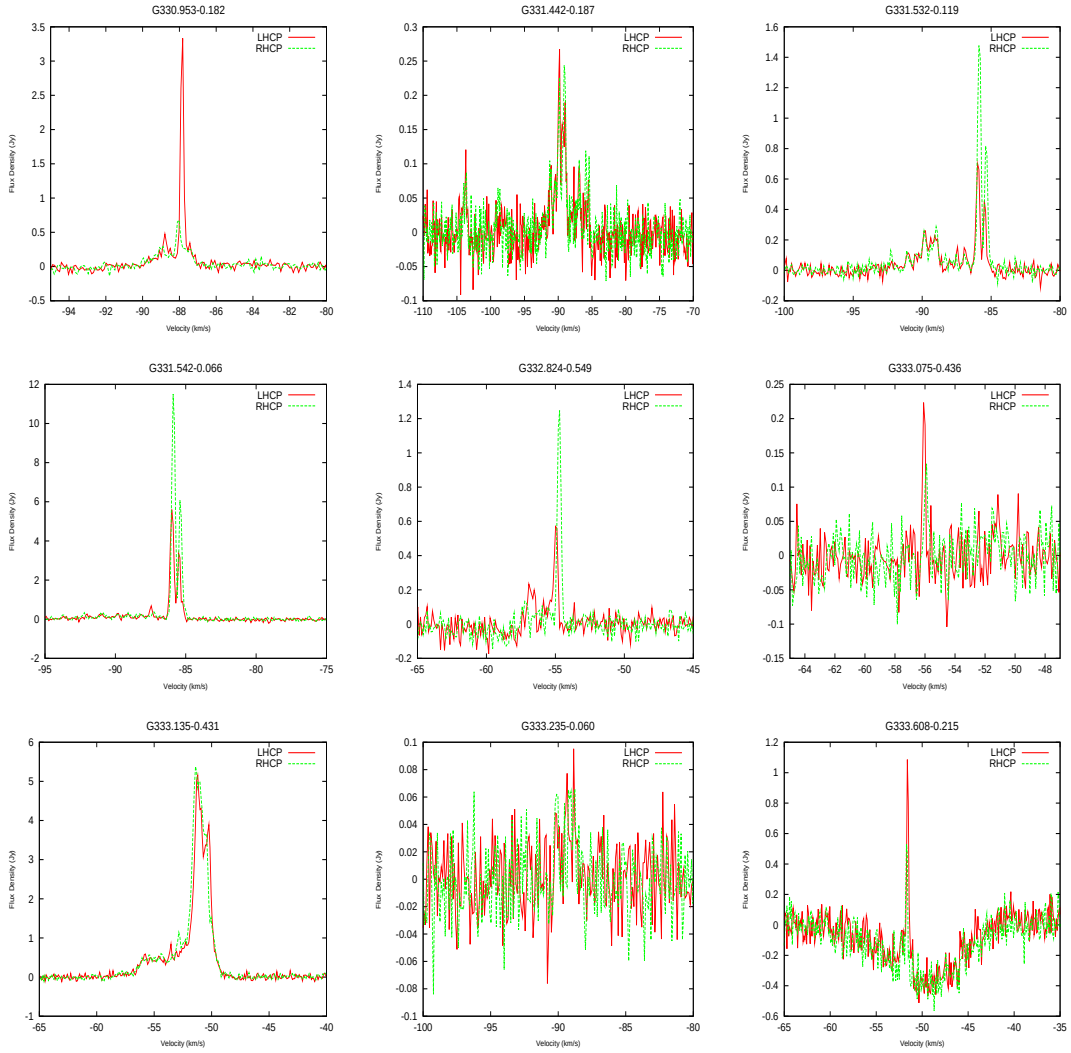

Figure 4.11: Spectra of 6035 MHz ex-OH masers detected by the Parkes telescope for the MMB survey.

G43.796-0.127

This is a known maser from CV95. The profile of the spectrum has changed dramatically from CV95, with the three dominant peaks blending into two peaks and several smaller features now visible, Figure 4.13. The flux density has remained similar. Both the ex-OH and methanol maser lie on the edge of a GLIMPSE source. The ex-OH maser is offset from the peak of an UC HII region by 2″. The UC HII region was

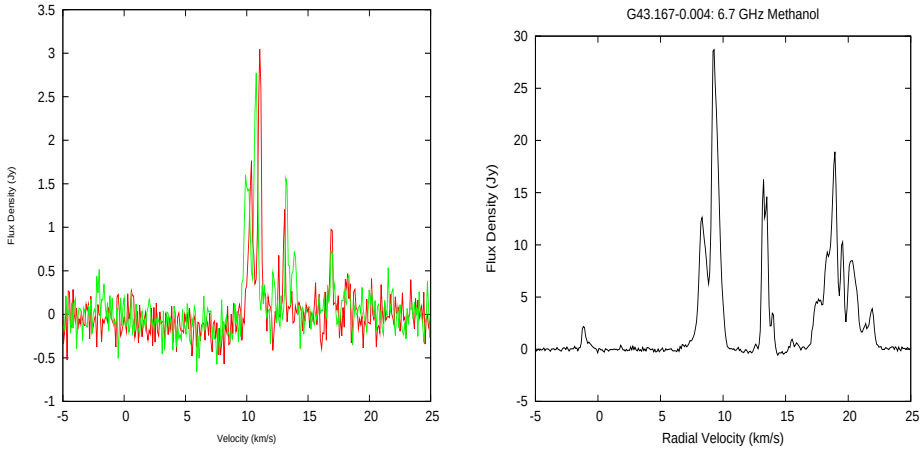

Figure 4.12: G43.167-0.004: The spectra of the 6035 MHz ex-OH maser (left) and the 6668 MHz methanol maser (right). The ex-OH maser displays and extremely wide range, comparable with the 6668 MHz methanol maser. It may be seen that the peaks of both maser match in velocity.

detected by CORNISH and has an integrated flux density of 24 mJy.

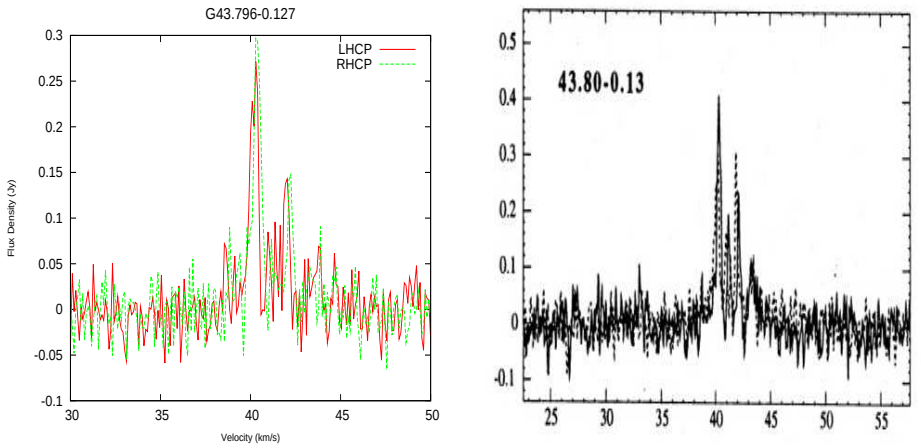

Figure 4.13: The spectra of the G43.796-0.127 ex-OH maser, from 2009 on the left and 1995 on the right, several small changes in the profile have occured.

G45.123+0.133

This is a known maser from CV95. It was varied significantly since it was observed in 1995. The four blended peaks that were visible in 1995 are now several separate peaks.

The flux density has increased by 25%. The GLIMPSE image shows the ex-OH maser is coincident with a strong source whilst the methanol maser 14″ away is associated with a dark GLIMPSE region. The methanol maser is possibly associated with a deeply embedded source. The ex-OH is separated by 4.18″ from a UC HII region of 2967 mJy integrated flux density. The HII region was identified by the CORNISH survey.

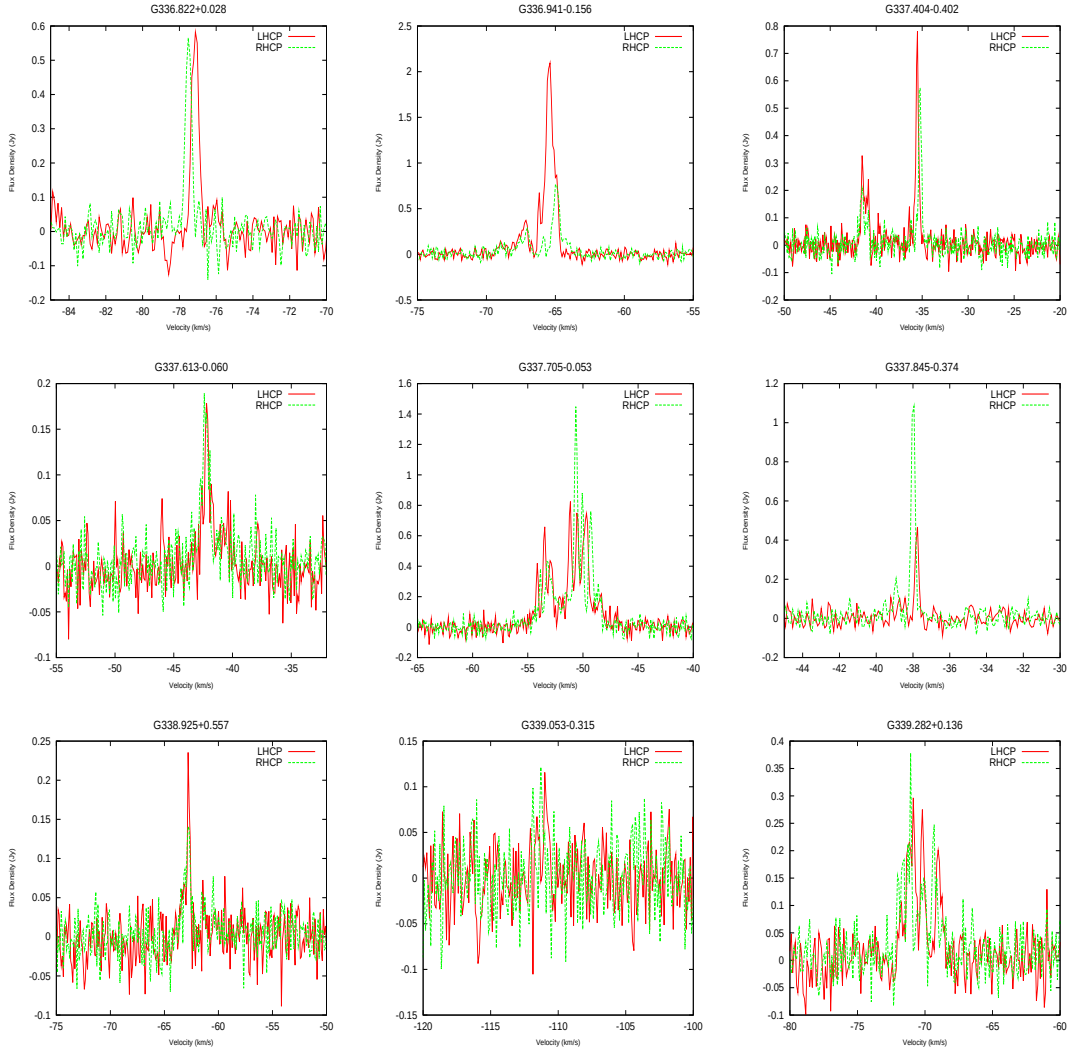

Figure 4.14: Spectra of 6035 MHz ex-OH masers detected by the Parkes telescope for the MMB survey.

G45.466+0.045

Known maser, discovered by CV95. The nearest 6668 MHz methanol maser is offset by 28″. The position of the ex-OH maser agrees with the 1665 MHz OH maser from FC98. The 6031 MHz ex-OH maser is also detected at one fifth of the 6035 MHz OH maser flux density. The GLIMPSE image shows the ex-OH maser is associated with a bright source with visible EGO emission, the methanol maser is to the North and is associated with a more compact GLIMPSE object. The ex-OH maser is offset by 1.34″ from a UC HII Region of 61 mJy integrated flux density. The UC HII region was identified by the CORNISH survey.

G48.993-0.298

This is a new maser discovered from the survey. It is without any 6031 MHz emission. The spectrum displays several peaks clustered between 66-71 km s^{-1}. It is separated by 24″ from a methanol maser, it is a very interesting source, as the ex-OH maser spectrum is more complex than the single spiked methanol spectra, but also, the 6035 MHz maser is more than twice the flux density of the methanol maser (Figure 4.15). From the GLIMPSE image it looks to be on the edge of an IRDC.

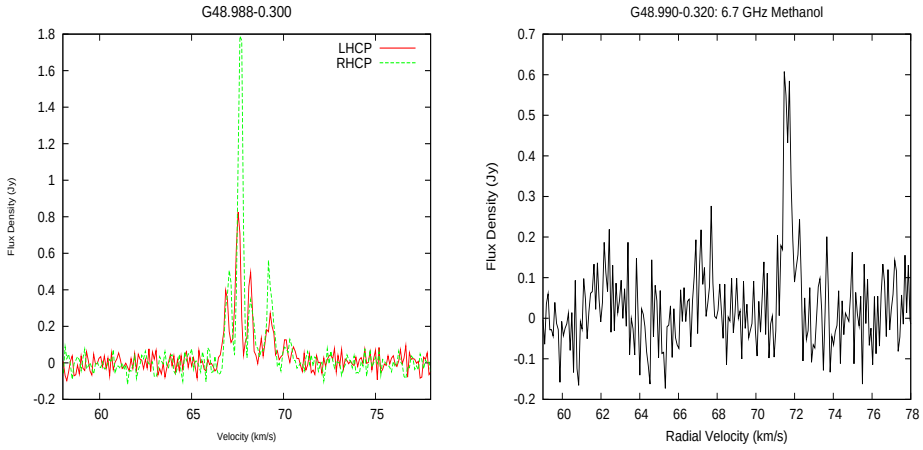

Figure 4.15: The spectrum on the left is of the 6035 MHz ex-OH maser at G48.993-0.298 and the spectrum on the right is of a Class II 6668 MHz methanol maser at G48.990-0.320. Interestingly the ex-OH maser has a more complex spectrum than the methanol maser and is stronger.

G49.489-0.388 & 49.493-0.388

Both of these known masers are in the W51 complex. No 6031 MHz emission was detected this time, although a 1 Jy detection was made by C03. The profile of the ex-OH maser has changed significantly since C03. The broad peak at 55 km s^{-1} in C03 is now seen to contain several separate peaks of similar flux density. The peaks at 56 km s^{-1} have now increased by 25%, whilst the peaks at the lower velocity of 55 km s^{-1} have decreased by 50%. The OH masers appear to be coincident with a small EGO.

G50.488+0.735

This new maser is a very interesting source, it has no accompanying 6031- or 1665/7 MHz OH maser, neither does it have a 6668 MHz maser. In the GLIMSPE image it is not associated with any strong or obvious source. It is certainly a source worthy of further investigation. It is discussed further in the GLIMPSE section 4.7.

G51.683+0.717

A new detection, without any 6031 MHz emission. It is spatially coincident with a methanol maser.

G189.030+0.783

This is a new detection. The ex-OH spectrum shows four peaks with one central dominant peak at 3.7 km s^{-1}. Interestingly, the methanol maser peaks at a velocity of 8.9 km s^{-1}.

G240.316+0.071

A known maser first detected by CV95. It is without any 6031 MHz emission. The spectrum profile remains stable from CV95, except the flux density of the strongest LHCP component at 63.8 km s^{-1} has decreased from 2.0 Jy to 1.4 Jy, whilst the peak at 63 km s^{-1} has remained the same intensity.

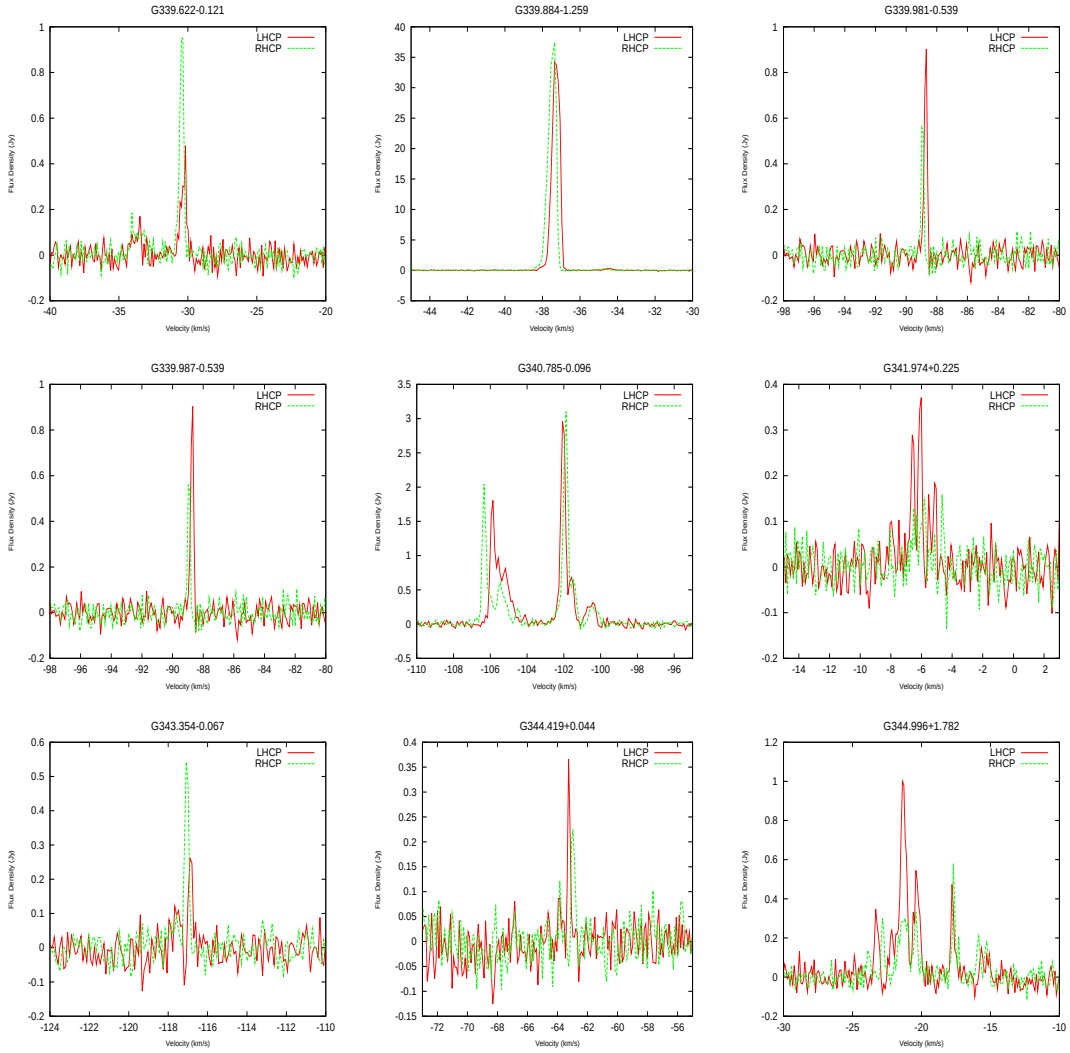

Figure 4.16: Spectra of 6035 MHz ex-OH masers detected by the Parkes telescope for the MMB survey.

G284.016-0.856

This is an interesting new detection as it does not have an accompanying methanol maser or 6031 MHz ex-OH emission. As the 6035 MHz ex-OH maser is seldom without either a methanol or 6031 MHz ex-OH maser, definitely warrants further investigation to determine if this is an extreme source.

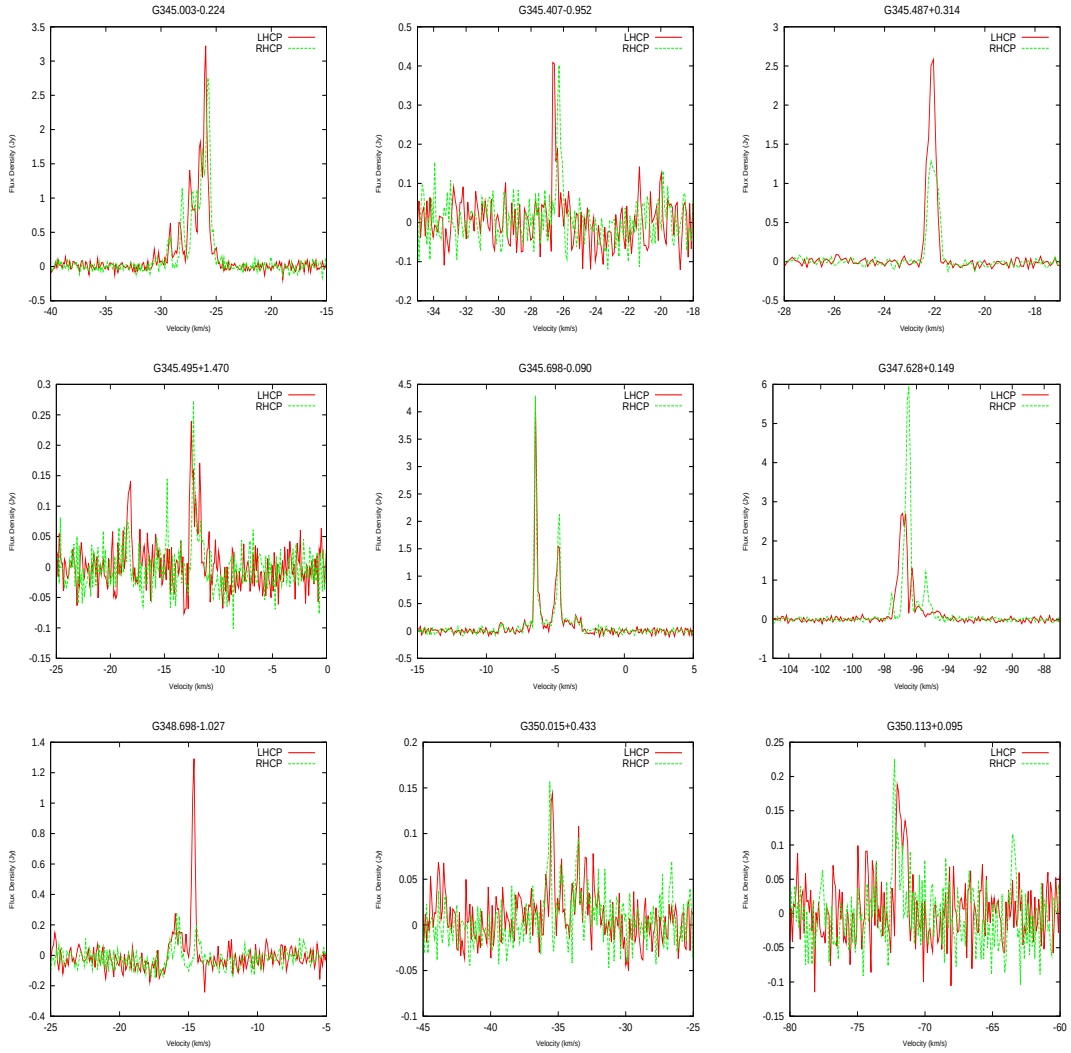

Figure 4.17: Spectra of 6035 MHz ex-OH masers detected by the Parkes telescope for the MMB survey.

G284.351-0.418

This is a known source from CV95 and C03 and 6031 MHz emission was also detected. It is also known, from C98, to harbour 1665/7 MHz masers. The 6035 and 6031 MHz have two peaks at the same velocity. Interestingly, the flux density of the 6031 MHz maser is almost as high as the 6035 MHz maser, with the 6031 MHz at 1 Jy and the other at 1.2 Jy. The 6035 and 6031 MHz masers have both developed the second peak at 8 km s^{-1} since the source was observed in C03. A kinematic distance

is estimated to be 5.5 kpc by C03.

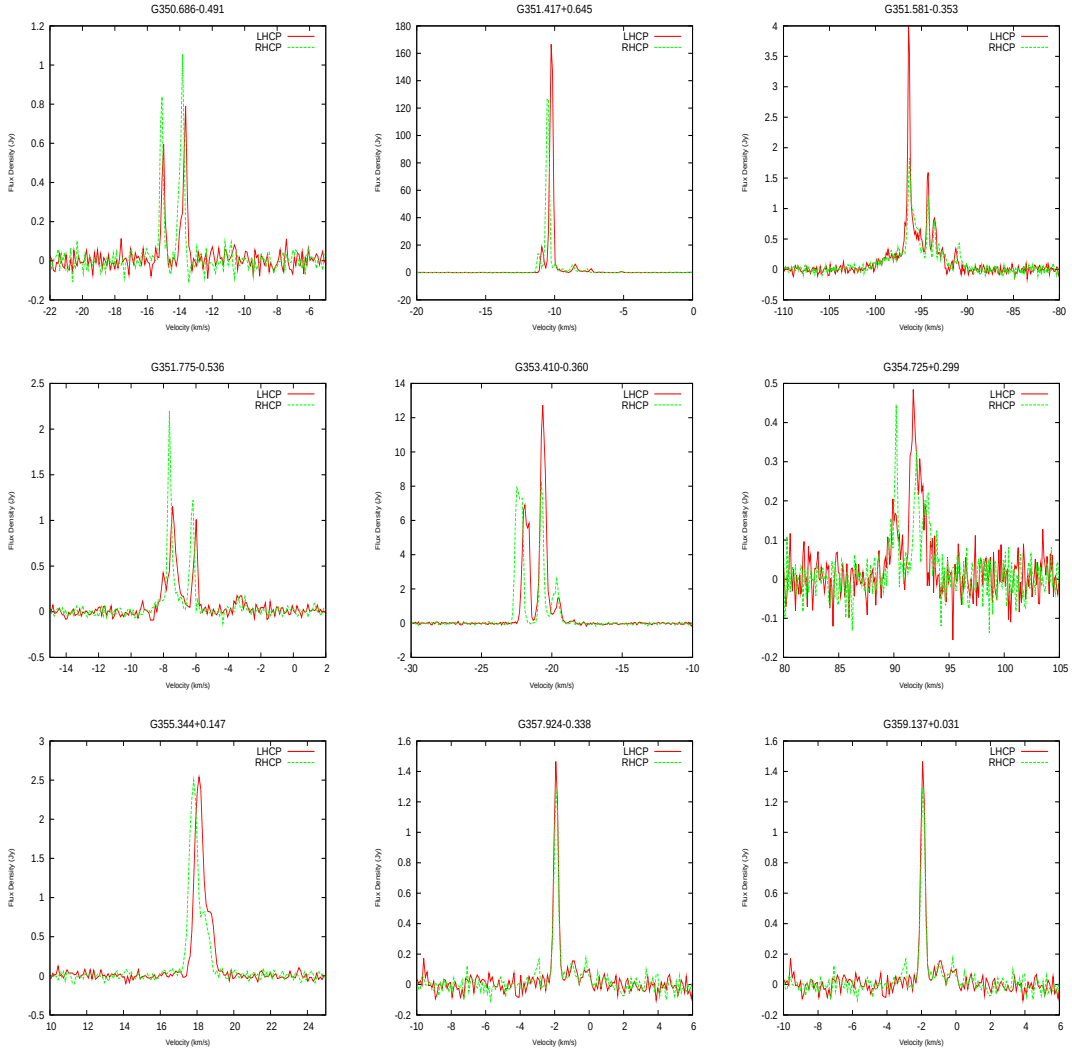

Figure 4.18: Spectra of 6035 MHz ex-OH masers detected by the Parkes telescope for the MMB survey.

G294.511-1.621

This maser was first detected by C98, it is coincident with a methanol maser and 1665/7 MHz OH emission (C98). It is a single peaked maser with decreasing flux density since C95, but the spectrum profile remains the same.

G298.723-0.086

A new detection which is coincident with a methanol maser and without any 6031 MHz emission. The peak velocities of the masers are different by ∼1 km s^{-1}.

G300.969+1.148

This maser had both the 6035 and 6031 MHz maser emission first detected by CV95. 1665/7 MHz emission is also present at this location as detected by C98. The intensity of the 6035 MHz maser has doubled since CV95 and a new peak has emerged at -36 km s^{-1}. A 6031 MHz maser is also present and is two-thirds the flux density of the 6035 MHz maser, which is unusually high.

G305.200+0.019

A known maser, first detected by CV95, without an 6031 MHz detection. Two peaks are still visible in the spectrum but have both changed since CV95. The peak at -31 km s^{-1} has doubled in intensity whilst the peak at -34 km s^{-1} has dropped five-fold.

G305.208+0.206

This is a new detection, without any 6031 MHz emission but with 1665/7 MHz OH maser emission at the same location. It is coincident with a methanol maser. The spectrum shows Zeeman splitting giving a magnetic field of -8.2 mG.

G305.360+0.148

A new detection without any 6031 MHz maser emission. It is 9.6″ away from a methanol maser, the ex-OH and methanol maser have a velocity difference of ∼1 km s^{-1}.

G308.056-0.396

A strong new detection at 20 Jy. It is separated 1.3″ from a methanol maser. The ex-OH maser ranges from -10,-15 km s^{-1} with the peak in the -13 km s^{-1} range. The

methanol maser peaks at -11 km s^{-1}.

G308.657-0.493

This is a new source, which was initially found from an MX on a methanol maser using the Parkes telescope, however, interferometric observations have shown that the ex-OH maser is over 60″ from the methanol maser.

G309.384-0.134

A new detection with a separation of 1.5″ from the methanol maser. No 6031 MHz emission was detected. The ex-OH peaks at a velocity of -52 km s^{-1} whilst the methanol peaks at -49.9 km s^{-1}.

G309.901+0.231

This is a new detection, its position closely matches with a methanol maser, 1″ away. No 6031 MHz emission was detected.

G309.921+0.479

A known maser detected by CV95. Known 6031 MHz emission was also detected. This location also contains 1665/7 MHz OH emission, detected by C98. The 6035 MHz spectrum has several peaks spread over ∼7 km s^{-1}. The flux density has doubled since C03, with the main peaks at -62 & -59 km s^{-1} remaining dominant. The 6031 MHz profile remains the same although the intensity has increased by a third.

G311.596-0.398

known maser from CV95, CW03. The spectrum is similar to the one taken in C01. There are a multitude of peaks between 28-31 km s^{-1}. There is no 6031 MHz or 1665/7 MHz masers present.

G311.643-0.380

This maser was first detected by CV95. 1665/7 MHz OH masers are also present at this location, detected by C98. There remains no 6031 MHz emission. The spectrum has significantly changed since CV95, with the emergence of several new peaks.

G312.598+0.045

A new detection, without any 6031 MHz emission. C98 detected 1665/7 MHz emission at this location and it is also coincident with a methanol maser. The spectrum has two peaks, both peaks appear to has Zeeman splitting, but of different strengths.

G318.050+0.087

A new weak detection, without any 6031 MHz emission detected. 1665/7 MHz OH maser emission is also present and detected by CV98.

G320.427+0.103

This is a new source with several peaks over ~5 km s^{-1}. No 6031 MHz emission was detected. It is separated by 1.3″ from a methanol maser.

G323.459-0.079

This is a known maser from CV95. The spectrum contains three distinct emission ranges. The profile has stayed the same but the flux density of all three peaks has increased, with the largest change in the strongest peak which has increased from 22 Jy to 48 Jy. The 6031 MHz emission profile mimics the 6035 MHz emission. The source also contains 1665/7 MHz emission at the same location detected by C98.

G326.448-0.749

A new detection separated by 2.2″ from a methanol maser. No 6031 MHz emission was detected. The ex-OH maser peaks at -62 km s^{-1} whilst the methanol maser peaks at -71 km s^{-1}.

G327.944-0.115

This is a new detection without any 6031 MHz emission. The spectrum shows a single unpolarised spike. The velocity peak of the ex-OH and methanol maser, which is 2.4″ away, agree.

G328.307+0.430

Known maser from CV95, CW03. The spectrum closely resembles the spectrum taken in CV03, with the flux density staying stable. Although the wide absorption between -100 km s^{-1} and -95 km s^{-1} is more pronounced since CV03. The 6031 MHz maser was not detected to a noise level of 0.15 Jy.

G328.808+0.633

This is actually two known masers, G328.808+0.0633 & G328.809+0.633, with the 1665/7 MHz OH maser emission associated with the G328.809+0.633 source (C03). G328.809+0.633 is responsible for the emission between -48 and -45 km s^{-1} and G328.808+0.0633 for the rest. The spectrum is similar to the one taken in C2003. Interestingly, in C03 a 6031 MHz maser was detected at 2.2 Jy, but is not detected here to a noise level of 0.1 Jy.

G329.031-0.198

This is a new weak detection. It has matching 1665/7 MHz OH maser emission at the same location (C98) and is also coincident with a methanol maser. There is no detectable 6031 MHz emission.

G329.184-0.314

A new detection, with matching 1665/7 MHz OH maser emission at the same location (priv. commun. Jim Caswell). While it is 2.3″ away from a methanol maser, the ex-OH and methanol maser agree in peak velocities.

G329.405-0.459

A known ex-OH maser first detected by CV95. There is no detection of 6031 MHz, but there are 1665/7 MHz OH masers present at the same location. The spectrum profile and flux density remains similar to CV95.

G330.953-0.182

A known maser detected by CV95, 1665/7 MHz OH emission is also detected at the same location by C98. The spectral profile has remained the same structure, but with a three-fold flux density increase. Broad emission is also visible from -90,-86 km s^{-1}.

G331.442-0.187

A new detection which is coincident with a methanol maser. The velocity ranges of the masers match, but the peak velocities of the masers differ by 3.5 km s^{-1}.

G331.556-0.121

A new detection that is without any detectable 6031 MHz emission. 1665/7 MHz OH maser emission has also been detected at this location by C98. The spectrum shows two regions of emission, one detection at -89 km s^{-1} that is weak, wide and multi-peaked. The other is at -85.5 km s^{-1}, a two peaked feature.

G331.542-0.66

This is a known maser detected by CV95, the spectrum profile remains largely unchanged except in the current observations the 6031 MHz maser emission is no longer visible. The 6035 MHz emission has more than doubled, in strength, going from 6 Jy to 17 Jy. It is coincident with a methanol maser.

G332.826-0.549

This maser was first detected by C01, it is unusually offset from a 1665 MHz OH maser by 7″ but is coincident with a methanol maser. The spectrum profile remains constant

from C01, but the intensity has doubled.

G333.068-0.047

This is a new detection, without any 6031 MHz emission. It is a weak single peaked detection with Zeeman splitting giving a magnetic field of 4.8 mG.

G333.135-0.431

A known maser detected by C98, with matching 6031 MHz emission. The 6035 MHz spectrum remains unchanged whilst a second peak at -55 km s^{-1} is now visible in the 6031 MHz emission. There is still broad emission visible in both spectra.

G333.235-0.060

This is a new detection with a matching 1665/7 MHz OH maser detection at the same location (priv. commun. Jim Caswell). The peak velocity of the methanol maser 2.6″ away matches the OH maser peak velocity.

G336.822+0.028

This is a known source, with no detectable 6031 MHz emission. C98 only detected a 1665 MHz OH maser. The GLIMPSE images shows the masers are located on the edge of a bright source, which in turn is on the edge of an IRDC.

G336.941-0.156

A known maser, detected by CV95. The profile remains similar with a flux density increase of 50%. There is also a known 6031 MHz maser present at location (CV95) along with 1665/7 emission (priv. commun. Jim Caswell).

G337.404-0.402

A known maser detected by CV95. 1665/7 MHz maser emission is also detected at the same location by C98. The spectrum shows two distinct features ∼6 km s^{-1} apart. The

spectrum has not changed from CV95. C01 confirmed that both peaks are only 0.6″ apart and they 'straddle the peak' of a compact HII region of size 1.1 x 0.9 arcsec^2 and integrated flux density of 130 mJy at 6 GHz.

G337.613-0.060

This is a known source detected by CV95 and C03, and is without 6031 MHz emission. The flux density has decreased a factor of 6 since the CV95 spectrum, but the profile remains the same.

G337.705-0.053

A known maser, without any 6031 MHz emission but with 1665/7 MHz OH maser emission at the same location. The spectrum profile has remained similar to CV95 except for an increase in flux density of ~50%. The ex-OH maser is also coincident with a methanol maser. All the masers lie on a compact GLIMPSE source.

G337.845-0.374

A new source separated by 6.4″ from a methanol maser. It does not have any 6031 MHz emission. The GLIMPSE images shows the ex-OH maser is on the edge of a bright GLIMPSE source whilst the methanol maser 6.4″ away is associated with an IRDC. They both are likely too be in the same star forming region.

G338.925+0.557

A known maser detected by CV95. There is no 6031 MHz maser emission present. The spectrum profile remains unchanged from CV95, although the flux density has decreased by 50%.

G339.053-0.315

A known maser detected by CV95. The detection remains weak as it was in C03, it has continued to decrease since its detection in CV95. The GLIMPSE image shows

the masers lie on the edge of some weak EGO emission.

G339.282+0.136

This maser was first detected by Caswell (2001), the overall spectrum profile and flux density have remained constant since then. No 6031 MHz emission has been detected. 1665/7 MHz OH maser emission is also detected at this site by C98. All the masers are coincident with a bright GLIMPSE source.

G339.622-0.121

A known maser which is coincident with a methanol maser and 1665/7 MHz OH emission. The spectrum shows two features, a strong and weak peak which are still visible from the CV95 spectrum, with a slight increase in flux density. The masers are associated with a very bright GLIMSPE source.

G339.884-1.259

The discovery of a flare in the 1665 MHz OH maser in this location (Caswell & Reynolds, unpublished data) led to a search for the 6035 and 6031 MHz ex-OH masers. The intensity of the ex-OH maser has continued to rise with the 6035 MHz going from 25 Jy to 68 Jy and the 6031 MHz increasing an impressive 3 Jy to 48 Jy. These OH masers are also coincident with a methanol maser.

G339.981-0.539

A new detection, without any 6031 MHz emission. It is 2.4″ away from a methanol maser, the velocity peaks of both masers agree. The ex-OH maser appears to be associated with a small EGO clump, whilst the methanol maser is offset. Both appear to be on the edge of an IRDC.

G340.785-0.096

First detected by CV95, no 6031 MHz emission has been detected. The spectrum re-

mains similar, exect that the peak at -106 km s^{-1} has doubled in intensity. C98 detected 1665/7 MHz maser emission at the same location, all coincident with a methanol maser to 0.4″. All the masers lie among several clumps of EGO emission.

G341.974+0.225

This is a new maser with several peaks between the velocity range -7 to -4 km s^{-1}. There is no detectable 6035 MHz emission. The nearest methanol maser is ∼30″ away and at a velocity of -11 km s^{-1}. From the GLIMPSE image the ex-OH maser is associated with a bright source, whilst the methanol maser, in the North-East corner, is not associated with any bright emission.

G343.354-0.067

This is a new detection of a 6035 MHz ex-OH maser. It is 2.3″ from a methanol maser, with both masers matching in peak velocity. The GLIMPSE image shows the ex-OH maser on the cusp of a bright source whilst the methanol maser is located in a infrared darker region.

G344.419+0.44

A known maser detected by CV95, with 1665/7 MHz OH emission, but without 6031 MHz emission. The two features of the spectrum have changed oppositely to each other. The peak at -73 km s^{-1} is no longer visible above the detection threshold whilst the peak at -64 km s^{-1} has doubled in intensity.

G345.003-0.224

A known maser first detected by CV95, it also displays 6031 MHz emission. C98 also detected 1665/7 MHz OH masers at this location. The peaks of the 6035 MHz emission are now more distinct than the C03 spectrum, as the flux density has also increased by a factor of two. The 6031 MHz maser emission has also increased in flux density by at least a factor of two. The strongest peak of the 6035 MHz emission at -26

km s^{-1} is mimicked by the 6031 MHz emission. The GLIMPSE image shows the OH masers are coincident with a bright source, whilst a methanol maser is offset by ∼25″ to the North in a darker region, without any obvious sources.

G345.010+1.792

A known source, first detected by Smits (1994). It is coincident with a methanol maser. Since 1994 it has continued to decrease in flux density, when observed by CV98, C03 and here. The flux density has decreased four-fold since CV95, however it has retained the same profile. 6031 MHz and 1665/7 MHz OH masers are also detected at this location by CV98 and C98 respectively. The 6031 MHz emission has decreased in flux density from 1.4 Jy to 0.5 Jy. The GLIMPSE image shows the masers are all on the edge of a bright source with EGO emission present.

G345.495+1.470

A new detection, 45.6″ from the nearest methanol maser. No 6031 MHz emission was detected at this location. The 6035 MHz maser emission is spread over ∼10 km s^{-1}, which is rather high for an ex-OH maser.

G345.487+0.314

A known maser detected by CV95. It also contains a 6031 MHz maser which is one-fifth the intensity of the 6035 MHz maser. The profile of the spectra for the ex-OH masers have remained constant since C03. In the GLIMPSE image, the ex-OH masers line up with a bright source whilst the methanol is offset, in a less luminous region.

G345.407-0.952

First detected by CV95, 1665/7 MHz is also present at this location (C98). The two features of the spectrum have undergone opposing changes, with the peak at -73 km s^{-1} no longer visible. All the masers line up with a bright GLIMPSE source.

G345.698-0.090

Known maser from CV95 and CV03, with known a 6031 MHz maser too. The 6031 maser spectrum and flux density appears to have stayed stable from CV03. However, the 6035 MHz spectrum is decidedly different as the strengths of the two peaks seem to have switched; the peak at -7 km s^{-1} has doubled in intensity, whilst the peak at -4 km s^{-1} has decreased slightly.

G347-628+0.149

A known maser, first detected by C95, 6031 MHz emission is also present and previously known. The spectral profile remains the same as CV95, except for 50% increase in the flux density. 1665/7 MHz OH maser emission is also detected at the same location by C98. The GLIMPSE image shows the OH masers lie on the centre of an EGO with the methanol maser ∼0.5″ away, on its edge.

G348.698-1.027

Known from CV95 and CW03. The spectrum is similar to the CW03 spectrum except that the main feature at -14.8 km s^{-1} has doubled in flux density from 0.6 Jy to 1.3 Jy. Maser emission at 1665/7 is also present.

G350.015+0.433

This is a new detection. Its position coincides with known 1665/7 MHz OH masers from C98. It is separated by 1″ from a methanol maser. The GLIMPSE image shows the OH and methanol masers coincide with a very bright object.

G350.113+0.095

A known source, discovered by CV95. The profile of the spectrum remains largely unchanged except the flux density has increased by a third. No 6031 MHz emission was detected. This source also contains 1665/7 MHz OH maser emission (C98). The GLIMPSE image shows the ex-OH and OH masers are associated with weak EGO

emission. This maser is not associated with a methanol maser, with the closest greater than 50″ away.

G350.686-0.491

A known ex-OH maser first detected by CV95. No 6031 MHz emission has been detected. The two peaks of the spectrum have had opposing changes since C03. The intensity of the peak at -15 km s^{-1} remains the same but the intensity of the peak at -14.5 km s^{-1} has tripled.

G351.417+0.645

This is a known source with the 6035 and 6031 MHz maser emission detected by CV95. The ex-OH masers are coincident with a methanol maser. 1665/7 MHz OH masers are also located in the same region, detected by C98. The masers are centred on a bright GLIMPSE source, another methanol maser is visible in the North-West corner in a darker region, possibly associated with a less evolved massive star.

G351.581-0.353

Known 6035 & 6031 MHz masers at this location, 1665/7 also present (C98). The intensity of the peaks have varied since CV95. The OH masers are also coincident with a methanol maser. All the masers are coincident with an EGO.

G351.775-0.536

A known maser first detected by CV95, also has 1665/7 MHz OH maser emission at the same location (priv. comm. Jim Caswell). The maser has doubled in intensity since CV95 but has retained its profile. It is also coincident with a methanol maser. All the masers lie on the edge of a bright GLIMPSE source, with EGO emission dotted around.

G353.410-0.360

When this maser was first detected by Smits (2004), the 6031 MHz maser was unusu-

ally brighter than the 6035 MHz maser. Now, the 6031 MHz masers is one-seventh the strength of the 6035 MHz ex-OH maser. 1665/7 MHz OH emission is also detected at the same location. The four maser transitions all lie on a dark region in the GLIMPSE image, but next to several bright sources $\sim$3″ away.

G354.725+0.299

This is a new detection and also has 1665/7 MHz emission in the same location, detected by C98. The spectrum displays two strong peaks over a $\sim$6 km s^{-1} range, with the velocity of the strongest peak lining up with the velocity of the methanol peak. The OH masers are on the edge of a bright GLIMPSE source whilst the methanol maser lies in a less luminous region 3.7″ away.

G355.344+0.147

Known 6035 and 6031 MHz ex-OH masers at this location were first detected by CV95. This source is also home to 1665/7 MHz OH maser emission (C98). The spectra of both masers remains unchanged. The OH masers lie on a bright GLIMPSE source whilst two methanol masers are offset by several arcseconds in darker GLIMSPE regions.

G357.924-0.338

This is a new single peaked detection with a matching 6031 MHz detection. It is separated by 3″ from a methanol maser. In GLIMPSE, the ex-OH maser is on the edge of three bright sources and the methanol is located in the South-East in a less luminous region, but probably the same star forming region.

G359.137+0.031

A known maser from CV95, the profile of the spectrum profile is exactly the same as C95 except the intensity has doubled to 1.6 Jy. Its position coincides with 1665/7 MHz emission detected by C98. The GLIMPSE image shows the OH masers are coincident

with a compact source and a methanol maser is coincident with a second source ~3″ away.

4.1.2 6035 MHz Ex-OH ATCA Results

The newly discovered 6035 MHz masers were subject to interferometric follow up observations to obtain their precise positions. The 6035 MHz masers in the Southern hemisphere were observed with the ATCA and the Northern sources were observed with the eVLA.

The observations were taken from January 7-11th 2009, fourty 6035 MHz ex-OH masers were observed using the ATCA. Tables 4.11 and 4.12 displays the results, which include the galactic source name, the peak positions, the major and minor beam widths and the positional angle. As may be seen in, the sources with are close to a declination of 0° have the most elongated beams, knowing this would be the case, these sources were also observed by the eVLA.

During the three days of observations, the bandpass and flux calibrator were observed first. Every four sources were interleafed with observations on a phase calibrator, with a typical cycle time of twelve minutes between the phase observations and source observations. the data reduction started with the flux, phase and bandpass calibrations being applied to the calibrators. The solutions from these were copied and applied to the sources. Folling this, the sources were cleaned and imaged. Each of the sources were analysed and the peak flux position was taken as the resulting locations.

The remaining northern sources and the masers with elogonated beams were observed with the eVLA. Unfortunatley, the eVLA data can not be processed and imaged due to technical issues.

	Right Hand Circular Polarisation						Left Hand Circular Polarisation					
Source Name	RA (J2000)	DEC (J2000)	Peak Flux Density (Jy)	Vel Peak (km s^{-1})	Vel Range (km s^{-1})	RMS (Jy)	Peak Flux Density (Jy)	Vel Peak (km s^{-1})	Vel Range (km s^{-1})	RMS (Jy)	Magnetic Field (mG)	Status
G0.666-0.029	17:47:18.64	-28:22:54.6	17.91	72.27	10.71	0.12	8.91	72.07	10.94	0.10	-	C03
G0.666-0.035	17:47:20.14	-28:23:06.2	9.58	72.26	11.13	0.12	4.96	72.06	10.97	0.10	-	C03
G4.682+0.278	17:55:18.81	-24:46:24.0	0.71	2.12	1.19	0.05	0.22	2.11	0.84	0.05	0.17	new
G6.882+0.094	18:00:49.36	-22:57:38.8	5.81	-2.34	1.47	0.08	1.16	-2.05	1.43	0.08	4.8	new
G8.267+0.486	18:02:18.71	-21:33:48.7	5.82	0.56	5.66	0.11	1.42	0.36	6.07	0.12	-0.2	new
G8.669-0.356	18:06:19.00	-21:37:32.7	0.66	39.31	2.32	0.09	0.58	39.31	2.00	0.09	-0.2	C03
G9.620+0.194	18:06:14.92	-20:31:39.6	0.89	6.00	1.20	0.07	-	-	-	0.07	0.17	new
G10.322-0.258	18:09:23.30	-20:08:01.8	0.75	36.59	4.53	0.06	1.15	35.62	2.46	0.08	-	new
G10.623-0.384	18:10:28.65	-19:55:49.6	0.50	-0.53	5.85	0.08	0.44	-0.73	5.14	0.08	-	C03
G10.958+0.022	18:09:39.32	-19:26:28.0	1.50	25.12	2.56	0.08	3.02	24.73	1.57	0.08	-6.5	new
G11.034+0.062	18:09:39.85	-19:21:20.1	2.18	24.05	2.94	0.08	1.31	23.27	3.24	0.08	-	C03
G11.904-0.141	18:12:11.44	-18:41:29.0	1.64	42.88	2.38	0.07	9.87	42.97	2.63	0.08	0.17	C03
G12.681-0.182	18:13:54.75	-18:01:46.6	0.83	58.82	3.49	0.11	0.52	58.00	1.32	0.09	-	new
G12.908-0.260	18:14:39.53	-17:52:01.1	0.38	-57.16	10.62	0.11	-	-	-	0.11		C98
G15.035-0.677	18:20:24.81	-16:11:34.1	16.68	21.52	3.22	0.12	14.58	21.52	2.82	0.13	-	C03
G18.460-0.005	18:24:36.40	-12:51:09.6	0.37	43.51	1.05	0.04	0.52	44.11	2.18	0.04	-10	new
G18.836-0.300	18:26:23.69	-12:39:30.9	0.35	41.69	1.41	0.04	0.60	41.50	1.57	0.05	-3.17	new
G19.486+0.151	18:26:00.39	-11:52:21.9	1.81	25.41	1.18	0.07	1.98	25.41	1.23	0.07	-	C03
G19.755-0.128	18:27:31.66	-11:45:55.0	0.37	115.7	0.97	0.05	0.29	116.39	2.66	0.05	-	new
G20.237+0.065	18:27:44.56	-11:14:54.6	2.51	71.51	1.62	0.08	2.59	71.51	1.64	0.07	-	C03
G24+150-0.008	18:35:20.98	-07:48:46.9	-	-	-	0.14	6.82	17.35	2.40	0.14	-	new
G25.650+1.050	18:34:20.91	-05:59:40.4	2.50	39.58	1.72	0.07	0.72	38.71	1.78	0.06	-7.33	new
G25.715+0.047	18:38:03.18	-06:23:52.9	1.04	95.50	1.89	0.08	1.20	95.40	1.76	0.07	-0.17	new
G28.200-0.049	18:42:58.07	-04:13:57.0	5.48	96.08	5.04	0.07	3.50	96.27	5.80	0.07	7.8	C03
G28.816+0.359	18:42:38.39	-03:29:55.2	0.60	87.72	0.78	0.07	0.27	88.00	1.45	0.06	-4.7	new

Table 4.1: Properties of the 6035 MHz ex-OH masers from the Parkes MX's and accurate positions. CO3: Caswell (2003), C98: Caswell (1998), CV95: Caswell & Vaile (1995).

			Right Hand Circular Polarisation				Left Hand Circular Polarisation					
Source Name	RA	DEC	Peak Flux	Vel Peak	Vel Range	RMS	Peak Flux	Vel Peak	Vel Range	RMS	Magnetic Field	Status
	(J2000)	(J2000)	Density (Jy)	(km s^{-1})	(km s^{-1})	(Jy)	Density (Jy)	(km s^{-1})	(km s^{-1})	(Jy)	(mG)	
G32.744-0.076	18:51:21.88	-00:12:05.5	0.47	33.95	9.13	0.07	0.91	33.66	7.40	0.07	-4.8	C03
G34.258+0.153a	18:53:18.68	01:15:00.3	0.46	58.19	7.20	0.09	0.71	58.48	7.33	0.08	4.8	C03
G34.258+0.153b	18:53:18.68	01:15:00.0	3.95	54.31	1.14	0.08	2.67	54.50	0.94	0.06	4.8	C03
G34.261-0.214	18:54:37.35	01:05:07.2	0.62	58.45	3.95	0.12	0.71	58.35	3.80	0.12	-	new
G35.025+0.350	18:54:00.66	02:01:19.3	3.25	45.32	1.41	0.06	6.09	45.61	0.98	0.08	0.17	C03
G35.133-0.750	18:58:07.48	01:36:59.5	2.24	35.80	1.71	0.08	0.98	36.48	1.82	0.07	3.9	
G35.198-0.743	18:58:13.06	01:40:37.7	1.95	30.46	1.19	0.04	-	-	-	0.04		- C03
G35.200-1.736	19:01:45.55	01:13:33.3	0.43	44.34	4.95	0.10	0.50	42.98	3.94	0.08	-	C03
G40.283-0.217	19:05:40.76	06:26:21.9	0.86	73.88	0.94	0.06	-	-	-	0.06	-7.3	new
G40.426+0.701	19:02:39.62	06:59:12.0	0.29	15.08	2.79	0.05	0.49	16.04	2.32	0.05	4.2	C03
G43.149+0.013	19:10:11.05	09:05:22.1	3.65	11.16	9.38	0.10	3.38	10.86	8.14	0.09	-	C03
G43.165-0.028	19:10:21.68	09:05:04.0	3.05	11.06	9.99	0.18	2.77	10.77	9.37	0.17	-	C03
G43.796-0.127	19:11:53.97	09:35:51.8	0.54	40.29	3.95	0.04	0.59	40.29	4.27	0.04	-	C03
G45.123+0.133	19:13:27.80	10:53:39.1	1.79	67.51	3.51	0.09	4.06	67.60	3.16	0.09	0.17	C03
G45.466+0.045	19:14:25.66	11:09:26.5	10.25	66.38	5.50	0.06	7.48	64.93	6.34	0.07	-	C03
G48.988-0.300	19:22:26.05	14:06:30.9	1.65	67.53	3.59	0.08	3.58	67.63	4.02	0.08	-	new
G49.490-0.388	19:23:43.93	14:30:34.9	2.36	57.45	3.12	0.21	2.79	57.74	5.93	0.19	4.8	C03
G49.489-0.388	19:23:43.85	14:30:29.9	6.29	57.40	12.29	0.24	6.98	57.70	12.73	0.25	-	C03
G50.488+0.735	19:21:34.86	15:55:08.5	4.80	48.12	1.09	0.08	0.82	48.22	1.89	0.07	0.17	new
G51.683+0.717	19:23:59.94	16:57:52.1	0.31	6.55	0.98	0.05	0.45	7.04	0.54	0.05	-8.2	new
G189.030+0.783	06:08:40.65	21:31:07.0	0.49	3.27	1.48	0.05	0.3	3.36	1.61	0.05	-0.2	new
G240.316+0.071	07:44:51.97	-24:07:42.3	2.64	63.62	2.41	0.07	0.95	63.62	1.84	0.06	-	C97
G284.016-0.856	10:20:16.32	-58:03:50.1	0.60	14.25	3.46	0.08	1.62	14.05	1.61	0.08	-3.2	new
G284.351-0.418	10:24:10.68	-57:52:34.0	1.97	5.86	3.51	0.10	2.44	5.76	3.62	0.09	-0.2	C03
G294.511-1.621	11:35:32.21	-63:14:43.0	5.44	-11.99	0.75	0.07	4.71	-11.99	0.78	0.07	0	C03

Table 4.2: Properties of the 6035 MHz ex-OH masers from the Parkes MX's and accurate positions.CO3: Caswell (2003), C98: Caswell (1998), CV95: Caswell & Vaile (1995).

	Right Hand Circular Polarisation						Left Hand Circular Polarisation					
Source Name	RA (J2000)	DEC (J2000)	Peak Flux Density (Jy)	Vel Peak (km s^{-1})	Vel Range (km s^{-1})	RMS (Jy)	Peak Flux Density (Jy)	Vel Peak (km s^{-1})	Vel Range (km s^{-1})	RMS (Jy)	Magnetic Field (mG)	Status
G298.723-0.086	12:14:39.50	-62:39:25.9	0.28	25.12	0.94	0.05	0.20	24.06	0.89	0.05	-	new
G300.969+1.148	12:34:53.27	-61:39:39.9	17.10	-37.39	2.31	0.11	12.08	-37.58	3.93	0.12	3.17	C03
G305.200+0.019	13:11:16.88	-62:45:54.7	1.70	-31.37	2.78	0.11	3.31	-31.56	6.77	0.08	-3.2	C03
G305.208+0.206	13:11:13.78	-62:34:41.1	0.98	-34.90	4.02	0.08	1.25	-35.39	0.64	0.07	-8.2	C98
G305.362+0.150	13:12:35.86	-62:37:17.9	0.41	-36.05	1.66	0.07	0.36	-35.76	1.37	0.05	4.83	new
G308.056-0.396	13:36:32.34	-62:49:05.6	15.93	-14.11	1.95	0.08	25.46	-13.62	4.08	0.09	8.2	new
G308.657-0.493	13:41:51.74	-62:48:11.3	0.35	2.27	2.42	0.05	0.42	2.17	1.65	0.06	-	new
G309.384-0.135	13:47:24.20	-62:18:11.8	0.51	-51.37	6.97	0.08	2.25	-52.05	0.96	0.08	0.2	new
G309.901+0.231	13:51:00.97	-61:49:54.5	0.56	-55.16	0.78	0.07	0.73	-55.16	1.04	0.08	-	new
G309.921+0.479	13:50:41.77	-61:35:10.1	20.20	-59.43	4.92	0.08	18.84	-61.56	5.18	0.08	-	C03
G311.596-0.398	14:06:18.35	-62:00:15.3	1.83	29.70	2.77	0.07	1.56	30.57	2.54	0.06	0.2	C03
G311.643-0.380	14:06:38.74	-61:58:23.1	1.15	33.91	5.13	0.08	0.71	30.61	6.09	0.07	0.3	C03
G312.598+0.045	14:13:14.93	-61:16:53.9	0.51	-66.72	5.38	0.09	0.66	-66.33	0.71	0.07	6.5	new
G318.015+0.071	14:53:31.74	-59:10:40.5	-	-	-	-	0.14	44.96	3.33	0.05	4.2	new
G320.427+0.103	15:09:39.79	-57:59:40.6	0.60	-14.05	1.83	0.05	0.25	-13.66	2.15	0.06	-	new
G323.459-0.079	15:29:19.33	-56:31:21.3	27.14	-70.50	5.42	0.08	44.18	-70.21	5.42	0.07	4.83	C97
G326.448-0.748	15:49:18.63	-55:16:51.6	0.92	-60.88	0.98	0.08	1.82	-60.78	0.76	0.10	0.17	new
G327.944-0.115	15:54:34.00	-53:50:46.7	0.57	-52.05	0.79	0.06	0.65	-51.95	0.52	0.04	-	new
G328.236-0.547	15:57:58.30	-53:59:23.2	1.35	-44.21	2.19	0.09	0.52	-46.05	3.16	0.07	-0.2	C97
G328.307+0.430	15:54:06.44	-53:11:41.1	3.39	-90.52	2.11	0.09	2.96	-90.33	3.10	0.09	0.17	C03
G328.808+0.633	15:55:48.39	-52:43:06.7	22.76	-46.08	4.06	0.10	13.70	-45.79	4.92	0.10	-	C03
G329.031-0.198	16:00:30.32	-53:12:27.8	0.43	-38.75	0.40	0.09	-	-	-	0.09	-	C98
G329.184-0.314	16:01:47.09	-53:11:41.1	0.24	-55.48	1.36	0.04	0.19	-55.68	2.68	0.04	-3.2	new
G329.405-0.459	16:03:32.15	-53:09:29.9	0.33	28.88	2.99	0.05	-	-	-	0.05	0.17	C03
G330.953-0.182	16:09:52.38	-51:54:57.6	6.67	-87.82	2.15	0.07	1.35	-88.01	3.37	0.09	-3.2	C03

Table 4.3: Properties of the 6035 MHz ex-OH masers from the Parkes MX's and accurate positions.CO3: Caswell (2003), C98: Caswell (1998), CV95: Caswell & Vaile (1995).

			Right Hand Circular Polarisation				Left Hand Circular Polarisation					
Source Name	RA (J2000)	DEC (J2000)	Peak Flux Density (Jy)	Vel Peak (km s^{-1})	Vel Range (km s^{-1})	RMS (Jy)	Peak Flux Density (Jy)	Vel Peak (km s^{-1})	Vel Range (km s^{-1})	RMS (Jy)	Magnetic Field (mG)	Status
G331.442-0.187	16:12:12.49	-51:35:10.1	0.53	-89.80	3.17	0.05	0.49	-89.12	2.83	0.05	-	new
G331.511-0.102	16:12:09.76	-51:28:37.8	2.97	-89.86	7.74	0.12	5.40	-85.98	7.86	0.10	-0.3	C03
G331.542-0.066	16:12:09.01	-51:25:47.7	11.08	-85.98	2.86	0.10	22.58	-85.89	7.81	0.08	0.17	C03
G332.824-0.548	16:20:10.23	-50:53:18.1	1.14	-54.98	2.90	0.09	2.49	-54.69	0.71	0.09	0.3	C03
G333.075-0.436	16:20:47.77	-50:37:55.2	0.74	-56.10	1.45	0.13	0.38	-55.81	0.52	0.13	4.8	new
G333.135-0.431	16:21:02.92	-50:35:10.0	8.66	-51.24	6.52	0.14	8.61	-51.43	6.99	0.13	-3.2	C03
G333.235-0.060	16:19:51.06	-50:15:08.7	0.23	-88.87	2.28	0.05	0.26	-90.13	1.99	0.05	-	new
G333.608-0.215	16:22:11.04	-50:05:56.5	2.17	-51.61	1.61	0.15	1.06	47.63	1.21	0.17	-	C03
G336.822+0.028	16:34:38.29	-47:36:32.9	1.17	-77.13	1.47	0.09	1.13	-77.52	1.07	0.07	-6.5	C03
G336.941-0.156	16:35:55.20	-47:38:45.4	4.19	-65.39	5.03	0.09	1.52	-64.90	5.69	0.09	-	C03
G337.404-0.402	16:38:50.45	-47:28:03.2	1.56	-35.51	7.07	0.06	1.14	-35.22	7.57	0.06	4.8	C03
G337.613-0.060	16:38:09.54	-47:04:59.9	0.36	-42.21	3.09	0.04	0.38	-42.41	1.56	0.04	-	C03
G337.705-0.053	16:38:29.67	-47:00:35.8	1.65	-51.13	7.08	0.08	2.90	-50.65	6.07	0.07	0.17	C03
G337.845-0.374	16:40:26.89	-47:07:07.4	0.93	-37.75	0.68	0.07	2.17	-37.95	0.72	0.08	3.2	new
G338.925+0.557	16:40:33.53	-45:41:37.2	0.47	-62.80	1.41	0.05	0.28	-62.80	2.87	0.05	-	C03
G339.053-0.315	16:44:48.99	-46:10:13.1	0.32	-102.24	12.77	0.07	0.31	-111.41	0.99	0.07	-	C03
G339.282+0.136	16:43:43.12	-45:42:08.0	0.59	-70.87	4.03	0.08	0.76	-71.07	3.93	0.07	-3.2	C03
G339.622-0.121	16:46:05.96	-45:36:44.1	0.96	-30.17	4.69	0.07	1.90	-30.47	4.44	0.07	-4.8	C03
G339.884-1.259	16:52:04.61	-46:08:34.0	68.48	-37.36	1.42	0.22	74.85	-37.36	1.59	0.15	-3.3	C03
G339.980-0.539	16:49:14.94	-45:36:31.1	1.81	-88.68	0.56	0.08	1.12	-88.97	0.53	0.08	-4.8	new
G340.785-0.096	16:50:14.84	-44:42:26.7	5.93	-102.07	6.36	0.09	6.20	-101.88	6.68	0.07	3.2	C03
G341.974+0.225	16:53:05.37	-43:35:09.8	0.74	-6.02	1.80	0.07	0.32	-4.66	2.66	0.08	-	new
G343.354-0.067	16:59:04.45	-42:41:34.5	0.52	-116.89	1.59	0.07	1.09	-117.09	0.60	0.07	-3.2	new
G344.419+0.044	17:02:08.60	-41:47:10.2	0.73	-63.26	0.74	0.07	0.45	-62.97	1.72	0.07	4.8	C03
G344.996+1.782	16:56:47.58	-40:15:25.7	2.00	-21.38	6.00	0.09	1.16	-17.69	9.53	0.09	-	C03

Table 4.4: Properties of the 6035 MHz ex-OH masers from the Parkes MX's and accurate positions.CO3: Caswell (2003), C98: Caswell (1998), CV95: Caswell & Vaile (1995).

			Right Hand Circular Polarisation				Left Hand Circular Polarisation					
Source Name	RA	DEC	Peak Flux	Vel Peak	Vel Range	RMS	Peak Flux	Vel Peak	Vel Range	RMS	Magnetic Field	Status
	(J2000)	(J2000)	Density (Jy)	(km s^{-1})	(km s^{-1})	(Jy)	Density (Jy)	(km s^{-1})	(km s^{-1})	(Jy)	(mG)	
G345.003-0.224	17:05:11.20	-41:29:07.0	6.45	-25.95	5.70	0.10	5.51	-25.75	4.66	0.09	0.3	C03
G345.407-0.952	17:09:35.40	-41:35:57.1	0.82	-26.66	0.89	0.12	0.80	-26.27	0.90	0.11	6.5	C03
G345.487+0.314	17:04:28.12	-40:46:25.3	5.17	-22.05	0.90	0.09	2.57	-22.15	1.07	0.07	0.17	C03
G345.495+1.470	16:59:41.48	-40:03:36.3	0.48	-12.51	1.55	0.05	0.55	-12.31	4.84	0.05	3.2	new
G345.698-0.090	17:06:50.60	-40:50:59.6	8.44	-6.45	2.41	0.08	8.58	-6.45	2.52	0.07	-	C03
G347.628+0.149	17:11:50.89	-39:09:29.0	5.41	-96.87	1.78	0.10	11.92	-96.48	2.47	0.08	6.5	C03
G348.698-1.027	17:19:58.98	-38:58:13.5	2.58	-14.61	2.14	0.10	0.56	-15.87	2.73	0.10	0.12	C03
G350.015+0.433	17:17:45.44	-37:03:12.9	0.29	-35.43	0.92	0.04	0.31	-35.62	3.36	0.05	-3.2	C98
G350.113+0.095	17:19:25.58	-37:10:04.5	0.38	-72.06	2.45	0.07	0.45	-72.25	1.30	0.11	-3.2	C98
G350.686-0.491	17:23:28.63	-37:01:48.5	1.58	-13.64	2.04	0.08	2.11	-13.83	1.94	0.09	-0.5	C03
G351.417+0.645	17:20:53.37	-35:47:01.2	333.07	-10.25	4.23	0.11	253.32	-10.45	4.15	0.13	-3.2	C03
G351.581-0.353	17:25:25.08	-36:12:46.1	7.98	-96.41	3.73	0.08	3.65	-96.31	3.53	0.11	-	C03
G351.775-0.536	17:26:42.56	-36:09:16.0	2.31	-7.44	3.78	0.09	4.40	-7.64	2.02	0.06	-3.2	C03
G353.410-0.360	17:30:26.18	-34:41:46.0	25.48	-20.65	3.16	0.08	16.56	-20.75	3.48	0.08	-0.17	C03
G354.725+0.299	17:31:15.84	-33:14:05.0	0.97	91.76	4.08	0.08	0.89	90.20	5.09	0.09	3.3	new
G355.344+0.147	17:33:29.05	-32:47:58.8	5.08	18.11	2.40	0.09	5.00	17.81	2.22	0.08	4.8	C03
G357.924-0.338	17:41:55.45	-30:52:50.5	0.73	-3.57	0.68	0.09	0.91	-3.57	0.56	0.10	-	new
G359.137+0.031	17:43:25.64	-29:39:18.3	2.93	-1.93	0.59	0.06	2.58	-1.93	0.55	0.11	-	C03

Table 4.5: Properties of the 6035 MHz ex-OH masers from the Parkes MX's and accurate positions.CO3: Caswell (2003), C98: Caswell (1998), CV95: Caswell & Vaile (1995).

Source Name	RA (J2000)	DEC (J2000)	6668 MHz Methanol (arcseconds)	6031 MHz ex-OH (arcseconds)	1665 MHz OH (arcseconds)	1667 MHz OH (arcseconds)
G0.666-0.029	17:47:18.64	-28:22:54.6	6.1	0	0	0
G0.666-0.035	17:47:20.14	-28:23:06.2	0	0	0	0
G4.682+0.278	17:55:18.81	-24:46:24.0	21.5	n/e	-	-
G6.882+0.094	18:00:49.36	-22:57:38.8	5.3	0	-	-
G8.669-0.356	18:06:18.99	-21:37:32.2	0	n/e	n/e	n/e
G8.669-0.356	18:06:19.00	-21:37:32.7	0.5	n/e	0	0
G9.620+0.194	18:06:14.92	-20:31:39.6	4.7	n/e	0	0
G10.322-0.258	18:09:23.30	-20:08:01.8	5.1	n/e	-	-
G10.623-0.384	18:10:28.65	-19:55:49.6	11.7	n/e	0	0
G10.958+0.022	18:09:39.32	-19:26:28.0	0	n/e	-	-
G11.034+0.062	18:09:39.85	-19:21:20.1	0.2	n/e	0.1	0.1
G11.904-0.141	18:12:11.44	-18:41:29.0	0.4	n/e	0	0
G12.681-0.182	18:13:54.75	-18:01:46.6	>60	n/e	0	0
G12.908-0.260	18:14:39.53	-17:52:01.1	1.1	n/e	0	0
G15.035-0.677	18:20:24.81	-16:11:34.1	0.7	0	0	0
G18.460-0.005	18:24:36.40	-12:51:09.6	1.6	n/e	-	-
G18.836-0.300	18:26:23.69	-12:39:30.9	9.5	n/e	-	-
G19.486+0.151	18:26:00.39	-11:52:21.9	0.5	0	0	0
G19.755-0.128	18:27:31.66	-11:45:55.0	0	n/e	-	-
G20.237+0.065	18:27:44.56	-11:14:54.6	0.4	0	0	0
G24.594+0.222	18:35:20.98	-07:18:46.9	10.5	n/e	-	-
G25.650+1.050	18:34:20.91	-05:59:40.4	0	n/e	-	-
G25.715+0.047	18:38:03.18	-06:23:52.9	5.5	n/e	-	-
G28.200-0.049	18:42:58.07	-04:13:57.0	1.1	0	0	0
G28.816+0.359	18:42:38.39	-03:29:55.2	0	n/e	-	-

Table 4.6: Separation (in arcseconds) of other maser species at the 6035 MHz positions. 'n/e': means no detected emission, '-' means no observations have taken place for that transition.

Source Name	RA (J2000)	DEC (J2000)	6668 MHz Methanol (arcseconds)	6031 MHz ex-OH (arcseconds)	1665 MHz OH (arcseconds)	1667 MHz OH (arcseconds)
G32.744-0.076	18:51:21.88	-00:12:05.5	0.6	n/e	0.1	0.1
G34.258+0.153a	18:53:18.68	01:15:00.3	3	n/e	0	-
G34.258+0.153b	18:53:18.68	01:15:00.0	2.7	0	0	-
G34.261-0.214	18:54:37.35	01:05:07.2	23.3	n/e	-	-
G35.025+0.350	18:54:00.66	02:01:19.3	9.4	n/e	0	0
G35.133-0.750	18:58:07.48	01:36:59.5	0	n/e	-	-
G35.198-0.743	18:58:13.06	01:40:37.7	26.2	0	0	-
G35.200-1.736	19:01:45.55	01:13:33.3	11.3	0	0	0
G40.283-0.217	19:05:40.76	06:26:21.9	0	n/e		
G40.426+0.701	19:02:39.62	06:59:12.0	1.5	n/e	0.1	0.1
G43.149+0.013	19:10:11.05	09:05:22.1	2.1	n/e	0	-
G43.165-0.028	19:10:21.68	09:05:04.0	>60	n/e	-	-
G43.796-0.127	19:11:53.97	09:35:51.8	1.7	n/e	0	-
G45.123+0.133	19:13:27.80	10:53:39.1	14.54	n/e	0	-
G45.466+0.045	19:14:25.66	11:09:26.5	27.7	0	0	-
G48.988-0.300	19:22:26.05	14:06:30.9	24.43	n/e	-	-
G49.490-0.388	19:23:43.93	14:30:34.9	4.5	n/e	-	-
G49.489-0.388	19:23:43.85	14:30:29.9	0.8	n/e	-	-
G50.488+0.735	19:21:34.86	15:55:08.5	>60	n/e	n/e	n/e
G51.683+0.717	19:23:59.94	16:57:52.1	0	n/e		
G240.316+0.071	07:44:51.97	-24:07:42.	>60	n/e	0	0
G284.016-0.856	10:20:16.32	-58:03:50.	>60	n/e	-	-
G284.351-0.418	10:24:10.68	-57:52:34.	5.1	0	0	0
G294.511-1.621	11:35:32.21	-63:14:43.	0.3	n/e	0	0
G298.723-0.086	12:14:39.50	-62:39:25.	0.1	n/e	-	-

Table 4.7: Separation (in arcseconds) of other maser species at the 6035 MHz positions. 'n/e': means no detected emission, '-' means no observations have taken place for that transition.

Source Name	RA (J2000)	DEC (J2000)	6668 MHz Methanol (arcseconds)	6031 MHz ex-OH (arcseconds)	1665 MHz OH (arcseconds)	1667 MHz OH (arcseconds)
G300.969+1.148	12:34:53.27	-61:39:39.	0.2	0	0	0
G305.200+0.019	13:11:16.88	-62:45:54.	0.5	n/e	0	0
G305.208+0.206	13:11:13.78	-62:34:41.	0.6	n/e	0	0
G305.362+0.150	13:12:35.86	-62:37:17.	9.6	n/e	0	0
G308.056-0.396	13:36:32.34	-62:49:05.	1.3	n/e	-	-
G308.657-0.493	13:41:51.74	-62:48:11.	>60	n/e	-	-
G309.384-0.135	13:47:24.20	-62:18:11.	1.53	n/e	1	1
G309.901+0.231	13:51:00.97	-61:49:54.	1.1	n/e	-	-
G309.921+0.479	13:50:41.77	-61:35:10.	0.1	0	0	0
G311.596-0.398	14:06:18.35	-62:00:15.	>60	n/e	-	-
G311.643-0.380	14:06:38.74	-61:58:23.	0.2	n/e	0.2	0.2
G312.598+0.045	14:13:14.93	-61:16:53.9	0.8	n/e	0.2	0.2
G318.015+0.071	14:53:31.74	-59:10:40.5	0.2	n/e	0	0
G320.427+0.103	15:09:39.79	-57:59:40.6	1.3	n/e	-	-
G323.459-0.079	15:29:19.33	-56:31:21.3	1.5	0	0	0
G326.448-0.748	15:49:18.63	-55:16:51.6	2.2	0	-	-
G327.944-0.115	15:54:34.00	-53:50:46.7	2.6	0	-	-
G328.236-0.547	15:57:58.30	-53:59:23.2	3	n/e	0	0
G328.307+0.430	15:54:06.44	-53:11:41.1	0.6	n/e	0	0
G328.808+0.633	15:55:48.39	-52:43:06.7	0.1	n/e	0	n/e
G329.031-0.198	16:00:30.32	-53:12:27.8	0.5	n/e	0	n/e
G329.184-0.314	16:01:47.09	-53:11:41.1	2.3	n/e	0	0
G329.405-0.459	16:03:32.15	-53:09:29.9	0.6	n/e	0	0
G330.953-0.182	16:09:52.38	-51:54:57.6	0.2	n/e	0	0
G331.442-0.187	16:12:12.49	-51:35:10.1	0	n/e	-	-

Table 4.8: Separation (in arcseconds) of other maser species at the 6035 MHz positions. 'n/e': means no detected emission, '-' means no observations have taken place for that transition.

Source Name	RA (J2000)	DEC (J2000)	6668 MHz Methanol (arcseconds)	6031 MHz ex-OH (arcseconds)	1665 MHz OH (arcseconds)	1667 MHz OH (arcseconds)
G331.511-0.102	16:12:09.76	-51:28:37.8	0.1	n/e	0.2	0.2
G331.542-0.066	16:12:09.01	-51:25:47.7	0.21	n/e	0	0
G332.824-0.548	16:20:10.23	-50:53:18.1	>60	n/e	0	0
G333.075-0.436	16:20:47.77	-50:37:55.2	0.3	n/e	-	-
G333.135-0.431	16:21:02.92	-50:35:10.0	39.7	0	0	0
G333.235-0.060	16:19:51.06	-50:15:08.7	2.6	n/e	0	0
G333.608-0.215	16:22:11.04	-50:05:56.5	>60	n/e	0	0
G336.822+0.028	16:34:38.29	-47:36:32.9	0.7	n/e	0	0
G336.941-0.156	16:35:55.20	-47:38:45.4	0.1	0	0	0
G337.280-0.514	16:38:50.45	-47:38:03.2	2.96	n/e	0	0
G337.613-0.060	16:38:09.54	-47:04:59.9	0	n/e	0.1	0.1
G337.705-0.053	16:38:29.67	-47:00:35.8	0.5	n/e	0	0
G337.845-0.374	16:40:26.89	-47:07:07.4	6.4	n/e	-	-
G338.925+0.557	16:40:33.53	-45:41:37.2	0.1	n/e	0.1	0.1
G339.053-0.315	16:44:48.99	-46:10:13.1	0.1	n/e	0.1	0.1
G339.282+0.136	16:43:43.12	-45:42:08.0	0.1	n/e	0	0
G339.622-0.121	16:46:05.96	-45:36:44.1	0.9	n/e	0	0
G339.884-1.259	16:52:04.61	-46:08:34.0	0.6	0	0	0
G339.980-0.539	16:49:14.94	-45:36:31.1	2.4	n/e	-	-
G340.785-0.096	16:50:14.84	-44:42:26.7	0.4	n/e	0	0
G341.974+0.225	16:53:05.37	-43:35:09.8	30	n/e	-	-
G343.354-0.067	16:59:04.45	-42:41:34.5	2.3	n/e	-	-
G344.419+0.044	17:02:08.60	-41:47:10.0	0.2	n/e	0	0
G344.996+1.782	16:56:47.58	-40:15:25.7	2.98	0	0	0
G345.003-0.224	17:05:11.20	-41:29:07.0	0.1	0	0	0

Table 4.9: Separation (in arcseconds) of other maser species at the 6035 MHz positions. 'n/e': means no detected emission, '-' means no observations have taken place for that transition.

Source Name	RA (J2000)	DEC (J2000)	6668 MHz Methanol (arcseconds)	6031 MHz ex-OH (arcseconds)	1665 MHz OH (arcseconds)	1667 MHz OH (arcseconds)
G345.487+0.314	17:04:28.12	-40:46:25.3	3.7	0	0	0
G345.495+1.470	16:59:41.48	-40:03:36.3	15.6	n/e	0	0
G345.698-0.090	17:06:50.60	-40:50:59.6	>60	0	0	0
G347.628+0.149	17:11:50.89	-39:09:29.0	0.4	0	0	0
G348.698-1.027	17:19:58.98	-38:58:13.5	>60	n/e	0	0
G350.015+0.433	17:17:45.44	-37:03:12.9	1	n/e	0	0
G350.113+0.095	17:19:25.58	-37:10:04.5	51.8	n/e	0	0
G350.686-0.491	17:23:28.63	-37:01:48.5	0.3	n/e	0	0
G351.417+0.645	17:20:53.37	-35:47:01.2	0	0	0	0
G351.581-0.353	17:25:25.08	-36:12:46.1	0.5	0	0	0
G351.775-0.536	17:26:42.56	-36:09:16.0	1.6	n/e	0	0
G353.410-0.360	17:30:26.18	-34:41:46.0	0.4	0	0	-
G354.725+0.299	17:31:15.84	-33:14:05.0	3.7	n/e	0	0
G355.344+0.147	17:33:29.05	-32:47:58.8	0.2	0	0	0
G357.924-0.338	17:41:55.45	-30:52:50.5	3	n/e	-	-
G359.137+0.031	17:43:25.64	-29:39:18.3	1.1	n/e	yes	yes

Table 4.10: Separation (in arcseconds) of other maser species at the 6035 MHz positions. 'n/e': means no detected emission, '-' means no observations have taken place for that transition.

Source Name	RA	DEC	Major Axis (arcsec)	Minor Axis (arcsec)	Positional Angle (deg)
G4.682+0.278	17:55:18.82	-24:46:24.77	6.11	2.21	7.6
G6.882+0.094	18:00:49.38	-22:57:37.30	6.43	2.21	6.2
G9.620+0.194	18:06:14.94	-20:31:39.57	6.87	2.23	6.3
G10.322-0.258	18:09:23.30	-20:08:01.75	6.6	2.4	-2
G12.681-0.182	18:13:54.75	-18:01:46.60	7.02	2.2	-1.4
G18.460-0.005	18:24:36.40	-12:51:09.89	9.05	2.35	-1.5
G18.836-0.300	18:26:23.86	-12:39:29.00	9.24	2.36	-1.4
G24.150-0.008	18:35:20.98	-07:48:46.98	13.84	2.2	-0.78
G25.711+0.045	18:38:03.15	-06:24:09.26	13.98	2.81	2.2
G30.771-0.804	18:50:21.63	-02:17:24.55	27.63	2.58	0.8
G34.261-0.214	18:54:37.35	01:05:07.20	88.1	2	0.16
G48.988-0.300	19:22:26.05	14:06:30.86	10.7	1.84	-3.56
G50.488+0.735	19:21:34.86	15:55:08.46	9.68	1.89	-4.3
G284.016-0.856	10:20:16.32	-58:03:50.07	4.58	1.9	72.5
G298.748-0.110	12:14:50.98	-62:41:01.74	5.38	1.81	45.04
G305.360+0.148	13:12:35.02	-62:37:25.50	2.99	2.27	13
G308.056-0.396	13:36:32.34	-62:49:05.25	3.03	2.3	7.96
G308.657-0.493	13:41:51.74	-62:48:11.33	5.03	1.86	26.07
G309.381-0.151	13:47:24.20	-62:19:12.99	3.05	2.29	7

Table 4.11: The results of the 6035 MHz ex-OH maser ATCA observations

Source Name	RA	DEC	Major Axis (arcsec)	Minor Axis (arcsec)	Positional Angle (deg)
G309.901+0.231	13:51:01.02	-61:49:54.88	3.09	2.35	73.8
G312.598+0.045	14:13:14.93	-61:16:53.83	3.07	2.36	69.9
G318.015+0.071	14:53:31.74	-59:10:40.54	3.09	2.28	51.9
G320.427+0.103	15:09:39.79	-57:59:40.64	3.09	2.23	-2.9
G326.448-0.749	15:49:18.75	-55:16:53.58	4.34	1.96	20.8
G327.944-0.115	15:54:34.00	-53:50:46.74	3.25	2.26	-6.4
G328.236-0.548	15:57:58.39	-53:59:25.50	3.23	2.25	-6.3
G329.184-0.314	16:01:47.09	-53:11:41.07	3.26	2.22	33.8
G331.532-0.119	16:12:20.12	-51:28:31.58	3.33	2.22	31.2
G332.964-0.679	16:21:23.02	-50:52:56.99	3.76	2.14	40.3
G333.075-0.436	16:20:47.77	-50:37:55.23	3.35	2.22	29
G333.235-0.060	16:19:51.06	-50:15:08.70	3.44	2.28	-4.91
G337.845-0.374	16:40:26.89	-47:07:07.42	5.64	2.1	77.9
G339.981-0.539	16:49:14.94	-45:36:30.73	3.68	2.28	-7.7
G340.806+1.609	16:43:05.37	-43:35:09.75	3.75	2.3	21.7
G341.974+0.225	16:53:05.37	-43:35:09.8	3.8	2.32	20.4
G343.354-0.067	16:59:04.45	-42:41:34.48	3.8	2.32	-5.9
G344.956-0.265	17:05:12.32	-41:32:49.88	3.38	2.83	-61
G345.495+1.470	16:59:41.48	-40:03:36.31	3.7	2.67	-5.9
G354.725+0.299	17:31:15.84	-33:14:05.02	3.82	3.12	-10
G357.924-0.338	17:41:55.40	-30:52:50.17	3.75	3.27	5.25

Table 4.12: The results of the 6035 MHz ex-OH maser ATCA observations

4.2 6031 MHz Excited Hydroxyl Results

The 6031 MHz spectra are displayed in Figure 4.20 to Figure 4.22 and the 6031 MHz maser parameters are listed in Tables 4.13 and 4.14.

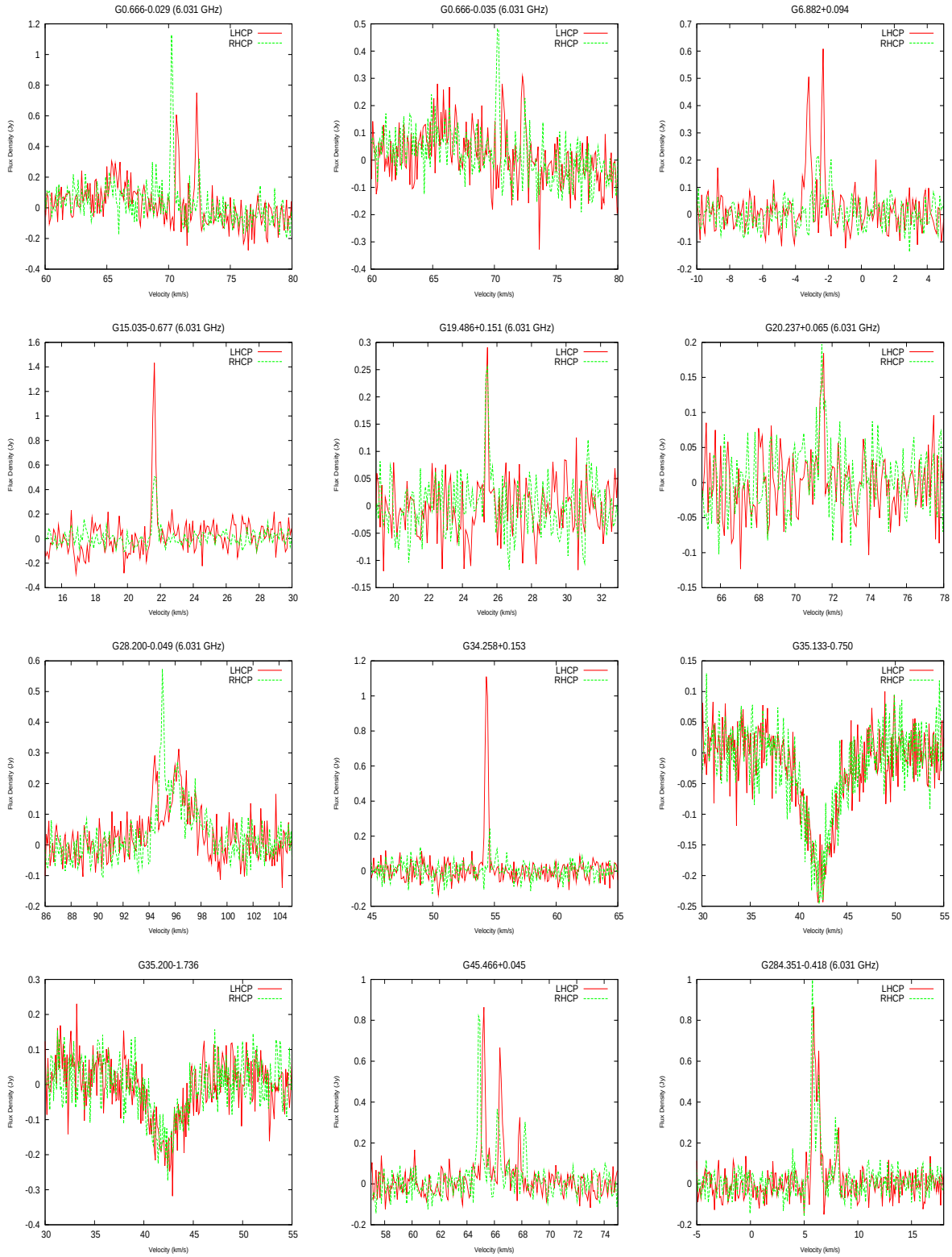

Figure 4.20: Spectra of 6031 MHz ex-OH masers.

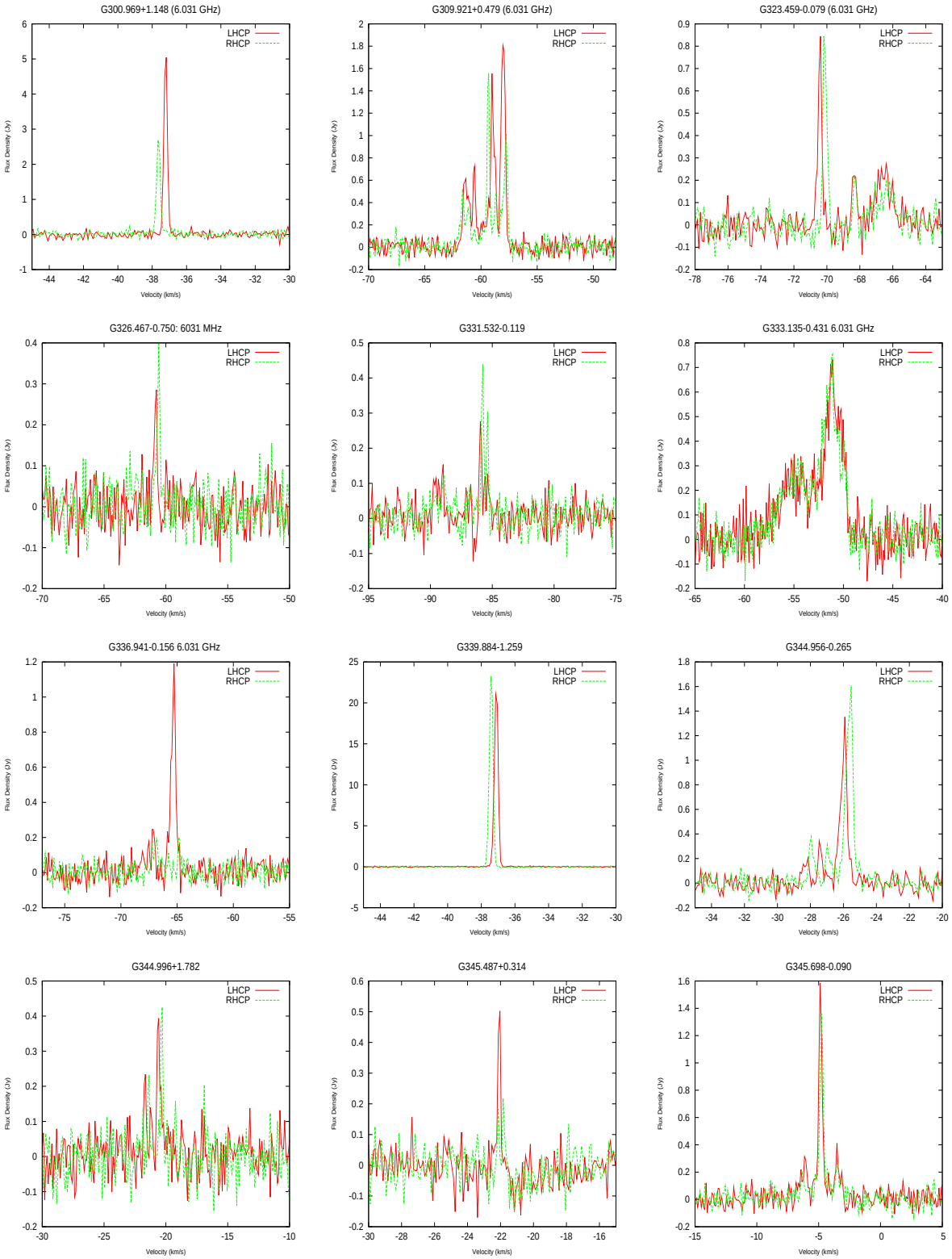

Figure 4.21: Spectra of 6031 MHz ex-OH masers.

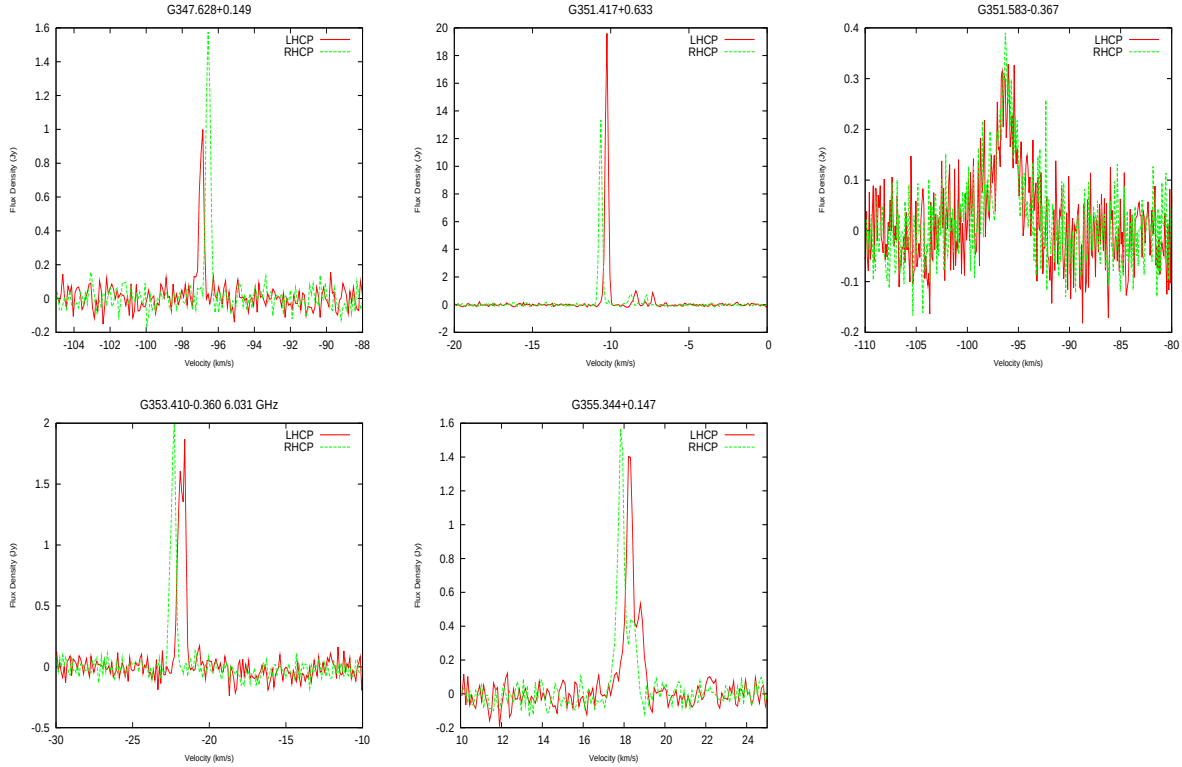

Figure 4.22: Spectra of 6031 MHz ex-OH masers.

			Right Hand Circular Polarization				Left Hand Circular Polarization			
Source Name	RA (J2000)	DEC (J2000)	Peak Flux Density (Jy)	Vel Peak (km s^{-1})	Vel Width (km s^{-1})	RMS (Jy)	Peak Flux Density (Jy)	Vel Peak (km s^{-1})	Vel Width (km s^{-1})	RMS (Jy)
G0.667-0.029	17:47:18.64	-28:22:54.6	1.5	72.28	5.31	0.17	2.26	70.24	4.35	0.2
G0.666-0.035	17:47:20.14	-28:23:06.2	0.61	72.28	9.66	0.15	0.96	70.24	8.48	0.15
G6.882+0.094	18:00:49.36	-22:57:38.8	1.22	-2.32	2	0.13	0.43	23.69	5.75	0.1
G15.035-0.677	18:20:24.81	-16:11:34.1	6.53	21.53	2.83	0.38	3.23	21.53	7.99	0.36
G19.486+0.151	18:26:00.39	-11:52:21.9	0.58	25.45	6.72	0.1	0.51	25.45	7.45	0.09
G20.237+0.065	18:27:44.56	-11:14:54.6	-	-	-	0.1	0.39	-17.86	13.49	0.09
G28.200-0.049	18:42:58.07	-04:13:57.0	0.63	96.29	14.47	0.09	1.15	95.02	10.1	0.08
G34.258+0.153	18:53:18.68	01:15:00.0	2.22	54.34	3.18	0.07	0.48	54.64	10.57	0.08
G35.200-1.736	19:01:45.55	01:13:33.3	0.25	33.19	14.58	0.12	0.27	105.13	17.35	0.11
G35.198-0.743	18:58:13.06	01:40:37.7	0.11	-55.73	3.56	0.08	0.05	141.43	7.72	0.08
G45.466+0.045	19:14:25.66	11:09:26.5	1.73	65.23	3.18	0.09	1.64	64.84	4.3	0.09
G284.351-0.418	10:24:10.68	-57:52:34.0	1.64	5.9	4.57	0.12	2.18	5.8	10.21	0.12
G300.969+1.148	12:34:53.27	-61:39:39.9	10.09	-37.18	11.33	0.14	5.39	-37.66	5.78	0.14
G309.921+0.479	13:50:41.77	-61:35:10.1	3.61	-58.05	3.86	0.11	3.11	-59.32	3.69	0.09
G323.459-0.079	15:29:19.33	-56:31:21.3	1.39	-70.34	6.43	0.1	1.6	-70.05	10.53	0.08
G326.448-0.748	15:49:18.63	-55:16:51.6	0.57	-60.77	4.63	0.1	0.8	-60.57	2.17	0.1
G331.511-0.102	16:12:09.76	-51:28:37.8	0.55	-85.96	11.37	0.07	0.88	-85.77	2.75	0.08
G333.135-0.431	16:21:02.92	-50:35:10.0	1.47	-51.1	4.41	0.12	1.51	-51.1	52.55	0.13
G336.941-0.156	16:35:55.20	-47:38:45.4	2.38	-65.27	11.85	0.11	0.4	-64.89	19.27	0.1

Table 4.13: 6031 MHz masers detected in the MMB survey with the Parkes telescope

			Right Hand Circular Polarization				Left Hand Circular Polarization			
Source Name	RA	DEC	Peak Flux	Vel Peak	Vel Width	RMS	Peak Flux	Vel Peak	Vel Width	RMS
	(J2000)	(J2000)	Density (Jy)	(km s^{-1})	(km s^{-1})	(Jy)	Density (Jy)	(km s^{-1})	(km s^{-1})	(Jy)
G339.884-1.259	16:52:04.61	-46:08:34.0	42.14	-37.15	4.61	0.09	46.51	-37.44	3.98	0.09
G344.996+1.782	16:56:47.58	-40:15:25.7	0.79	-20.58	3.08	0.12	0.85	-20.29	8.3	0.1
G345.003-0.224	17:05:11.20	-41:29:07.0	2.70	-25.91	4.11	0.12	3.21	-25.52	5.04	0.11
G345.487+0.314	17:04:28.12	-40:46:25.3	1.00	-22.03	5.9	0.09	0.44	-21.84	20.02	0.11
G345.698-0.090	17:06:50.60	-40:50:59.6	3.17	-4.88	6.15	0.11	2.72	-4.78	3.93	0.1
G347.628+0.149	17:11:50.89	-39:09:29.0	2.00	-96.86	4.51	0.12	3.15	-96.57	2.71	0.11
G351.417+0.645	17:20:53.37	-35:47:01.2	39.21	-10.24	2.45	0.13	26.66	-10.63	2.3	0.11
G351.581-0.353	17:25:25.08	-36:12:46.1	0.66	-96	3.54	0.13	0.78	-96.3	7.4	0.11
G353.410-0.360	17:30:26.18	-34:41:46.0	3.74	-21.61	1.31	0.16	4	-22.28	1.25	0.08
G355.344+0.147	17:33:29.05	-32:47:58.8	2.81	18.22	10.18	0.1	3.13	17.83	5.42	0.1

Table 4.14: 6031 MHz masers detected in the MMB survey with the Parkes telescope

4.3 6035 MHz Ex-OH Maser Properties

There are several properties of the 6035 MHz ex-OH masers that may be explored, such as their flux density distribution, velocity range, variation and Zeeman splitting. The flux density distribution of the 6035 MHz ex-OH masers is displayed in Figure 4.23. It peaks between 0.5, 1.0 Jy, with 28 masers in this range. In comparison, the methanol maser flux density distribution, peaks in the higher 1.5 to 2.0 Jy range. There are only two 6035 MHz ex-OH masers with flux densities above 100 Jy in comparison with the 6668 MHz methanol maser which has 62 masers over 100 Jy.

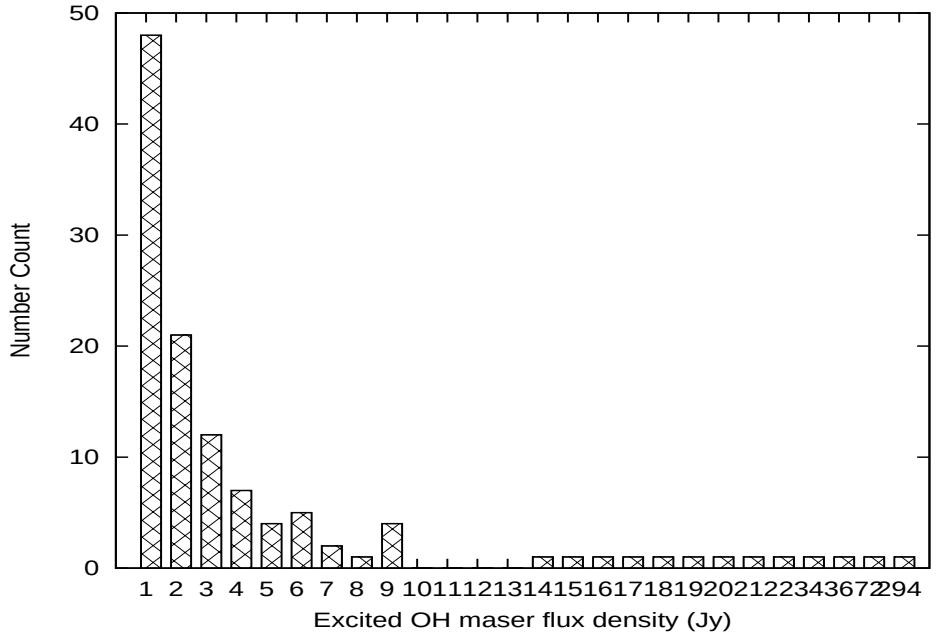

Figure 4.23: The flux density distributions of the 6035 MHz ex-OH masers from the MMB survey.

4.3.1 Zeeman Splitting

As discussed in Chapter 1 the ex-OH maser undergoes Zeeman splitting in the presence of a magnetic field. The separation between the maser peaks in the right and left polarization spectra being proportional to the magnetic field strength (Figure 4.24). A magnetic field strength of 1 mG will cause a separation of 0.060 km s^{-1} in the 6035 MHz ex-OH maser (Caswell 1998). It was possible to calculate the magnetic fields for a large portion of the 6035 MHz masers, which are listed in Tables 4.1 to 4.5. A 6035 MHz ex-OH maser is judged to have a Zeeman pair if there is a small and consistent separation between the peaks. If the left hand circular polarisation spectra has a more negative velocity than the right hand circular peak, it is denoted as a positive magnetic field (Caswell 1998). The calculated magnetic fields are especially useful for the theoretical modelling of the regions.

4.3.2 Absorption

The 6035 MHz transition is sometimes observed in absorption as well as a maser. Figure 4.25 displays two cases of such absorption. The first case, G291.274-0.709 is shown in the 6668 MHz methanol transition and the 6035 MHz transition. The absorption is visible in the 6035 MHz transition whilst a maser, without absorption is seen in the 6668 MHz spectrum. The peak of the ex-OH absorption is at -25km s^{-1} and the methanol maser peak is at -31 km s^{-1}, the velocity range of the ex-OH absorption covers part of the methanol maser range. Towards G32.802+0.193, absorption is visible in both the 6035 MHz ex-OH and 6668 MHz methanol transitions.

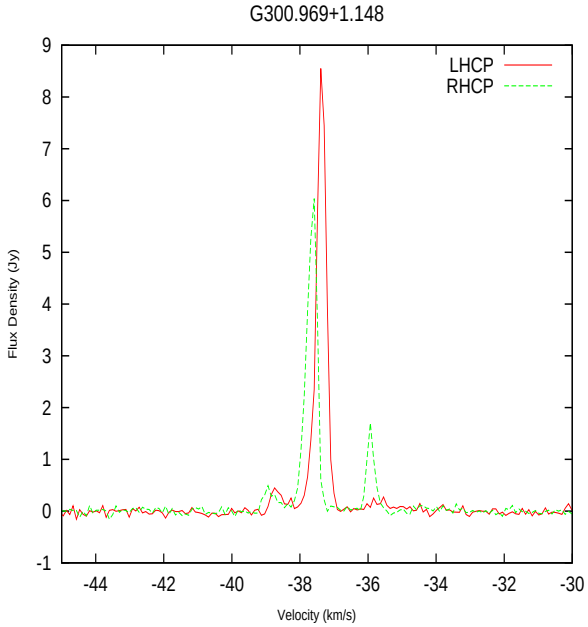

Figure 4.24: G300.969+1.148, an ex-OH 6035 MHz maser, the left hand circular polarization is shown in the red solid line and the right hand circular polarization is shown in the green dashed line. This source exhibits Zeeman splitting due to its presence in a magnetic field of +3.8 mG.

4.4 6035 MHz Excited OH Maser Flux Density Variation

Fifty 6035 MHz masers were observed twice over a Parkes observing run in March 2009, the first time to obtain observations of the 6668 MHz masers and the second time to observe the 6035 & 6031 MHz masers. Significant changes in the flux density and profile structure of the masers occurred in only seven, 14%, of the 6035 MHz masers. The remaining thirty-three 6035 MHz ex-OH masers did not display any variation over these days. In G12.681-0.182 and G34.258+0.153 the intensity has changed rather dramatically (Figures 4.26 and 4.27). In the space of six days the 6035 MHz ex-OH maser at G12.681-0.182 had disappeared from view below the 0.1 Jy noise level, from its previous 0.34 Jy, I intensity, (Figure 4.26). G34.258+0.153 underwent a re-

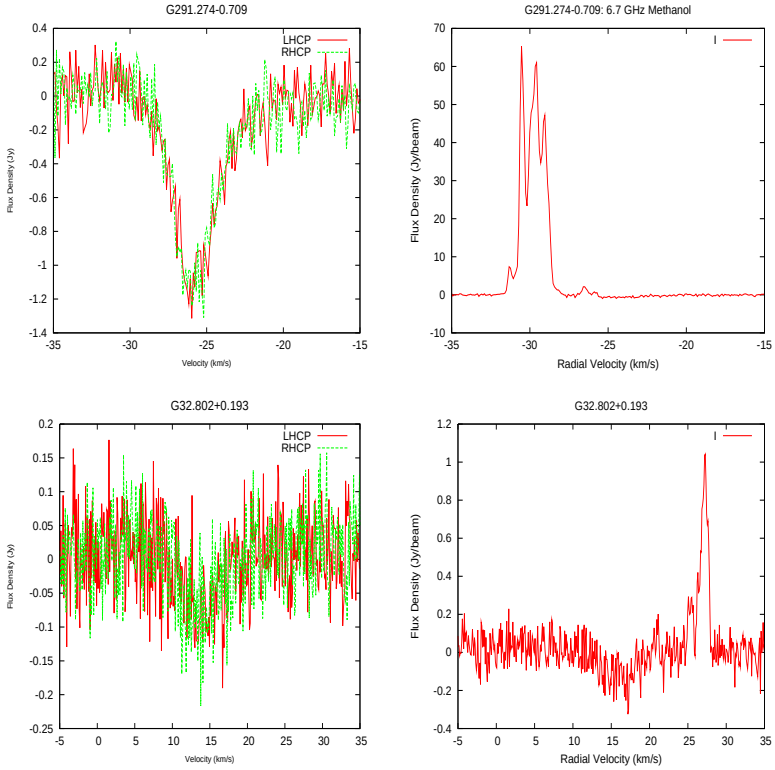

Figure 4.25: Absorption in 6668 MHz methanol and the corresponding 6035 ex-OH masers. The methanol masers are displayed in I flux density, whilst the ex-OH are displayed in the right and left circular polarisation, green and red respectively. On top: G291.274-0.709, the 6035 MHz transition is observed in absorption whilst no absorption is visible in the methanol transition, but a maser is. On bottom: G32.802+0.193, absorption is visible in both the ex-OH and methanol transitions, along with a maser in the methanol transition.

markable shift from 2.0 Jy on the March 26 2009 to below the 0.1 Jy noise level eight days later, (Figure 4.27).

The intensity was not the only variable, G40.426+0.701 and G318.015+0.701, changed their spectral profile, again in a number of days. In G40.426+0.701, Figure 4.28, the peak visible at 14 km s^{-1} in the right and left polarizations on March 23 2009 are only barely visible in the spectrum taken on April 4 2009, whilst the peak at 16.7 km s^{-1}

increased in intensity.

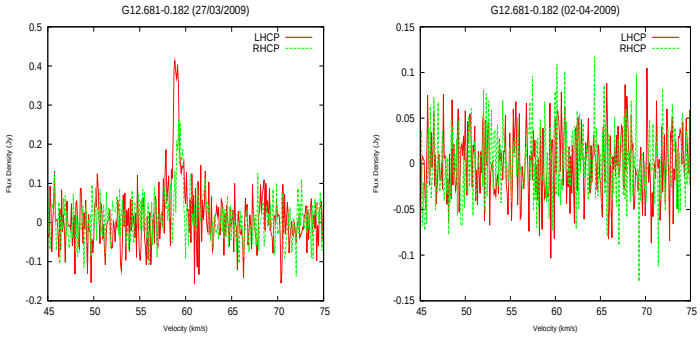

Figure 4.26: The spectra of 6035 MHz G12.681-0.182 from 27/03/09 (left) and the 02/04/09 (right), it is clearly seen that a large variation in its intensity has occurred and the maser is no longer visible on the second date.

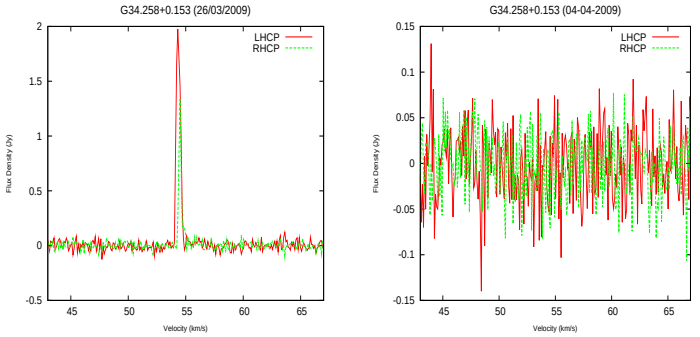

Figure 4.27: The spectra of the 6035 MHz G34.258+0.153 from 26/03/09 (left) and 04/04/09 (right). The maser has decreased from 2 Jy to below the noise level of 0.1 Jy in under 10 days.

4.4.1 Long Term Variation

To investigate the differences in the intensity of the 6035 MHz ex-OH masers, between the 2009 MX observations and Caswell and Vaile (1995), the flux densities are plotted in Figure 4.30. Forty-nine 6035 MHz ex-OH masers in the MMB survey were observed by Caswell (1998), 16 of these 49 masers were not detected in 1998, where the typical noise level was 0.2 Jy. There is no pattern to the intensity variations, (Figure 4.30), with the median difference in the intensity of the sources over the ~10 years is 1.39 Jy.

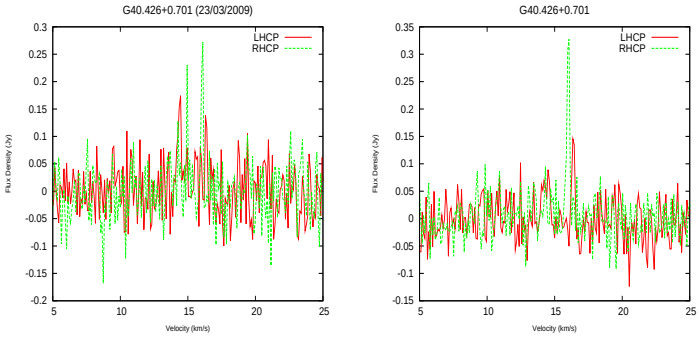

Figure 4.28: The spectra of the 6035 MHz G40.426+0.701 from 23/03/09 on the left on 04/04/09 on the right. The spectral feature at 14 km s^{-1} from 23/03/09, is barely visible in the spectrum on the 04/04/09, whilst the feature at 16.8 km s^{-1} increases in intensity.

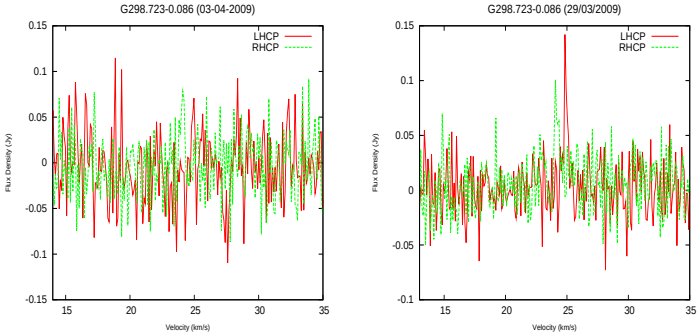

Figure 4.29: The G298.748-0.110 6035 MHz maser. Spectral feature at 25 km s^{-1} on 03/04/09 is barley visible above the noise, several days later the features are more pronounced and the ratio between the peaks of the right and left circular polarisation is dramatic different.

The largest increase was 158.2 Jy in the source G351.417+0.633.

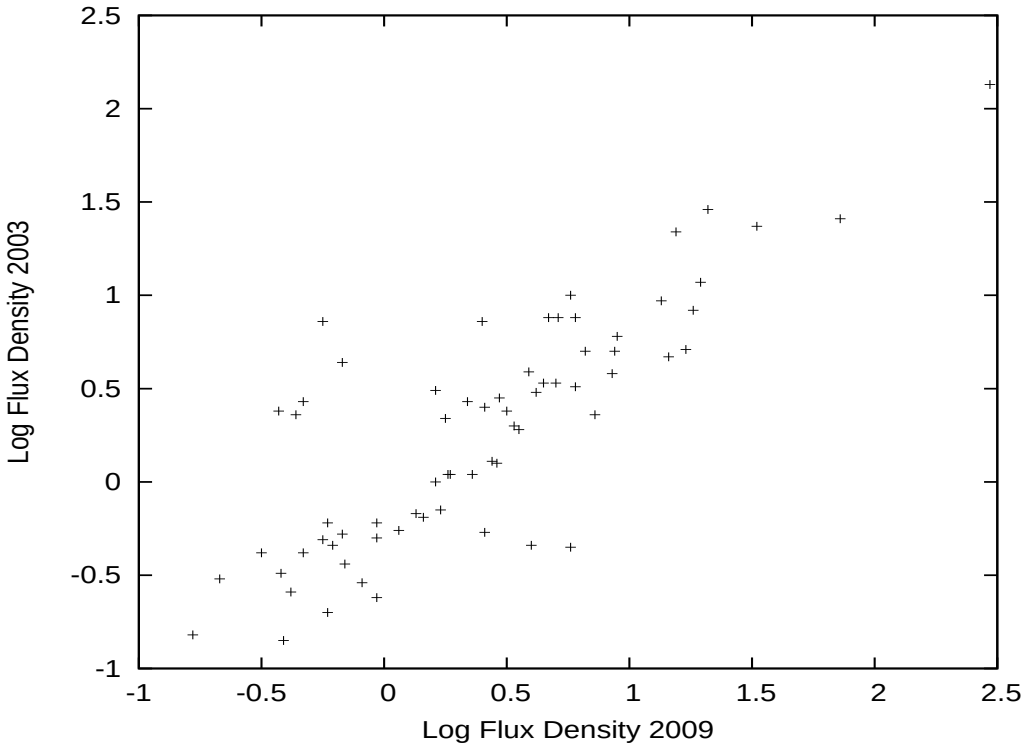

Figure 4.30: Comparison of the flux density of 6035 MHz masers observed in Caswell (1998) and the MMB Survey.

4.4.2 6035 & 6031 MHz Excited OH Masers

Twenty-nine 6035 MHz masers have a 6031 MHz ex-OH companion. Generally the 6035 MHz ex-OH maser is several times greater in flux density than the 6031 MHz transition (Caswell 1998). It is rare that the 6031 MHz maser is greater than the 6035 MHz transition, although cases have been reported (Caswell 1998). In this survey the 6035 MHz masers were found to have a median flux density 4.3 times stronger than the 6031 MHz companion. Figure 4.31 shows the flux density ratio of the 6035 MHz to 6031 MHz ex-OH masers. It is clearly visible that the 6035 MHz maser intensity is generally larger than the 6031 MHz emission, it peaks in the 6035/6031 MHz flux density ratio in the 0-3 range. The smallest ratio, which is the most comparable flux density for the 6035 MHz and 6031 MHz maser, is at G284.350-0.416, (Figure 4.32),

with the 6035 MHz at 2.44 Jy and the 6031 MHz at 2.18 Jy.

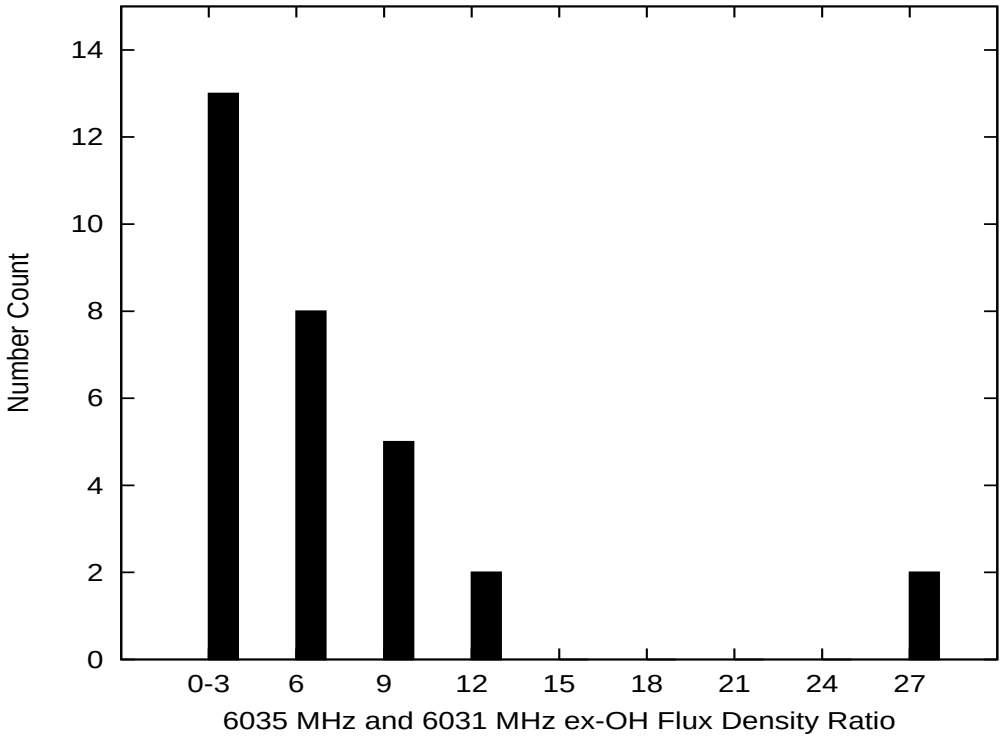

Figure 4.31: The logarithmic flux ratio of the 6035 MHz ex-OH and 6031 MHz ex-OH masers

In all but one case, the peak velocities of the 6035 & 6031 MHz masers match very closely. Figure 4.33 shows the 6035 MHz peak velocity versus the 6031 MHz peak velocity, it may be clearly seen that the peak velocities match. However, the exception, G353.410-0.360, (Figure 4.34), shows the strongest peak of the 6031 MHz maser lines up with a feature in the 6035 MHz maser, but not the strongest one, as in all other cases. The emission range and features of the 6035 & 6031 MHz masers match, with the 6031-MHz transition mirroring the 6035 MHz spectral profile.

The models of Cragg et al. (2002) show that the 6031 MHz maser closely accompanies the 6035 MHz transition and is weaker than the 6035 MHz emission, which matches the observations. The 6031 MHz maser is also useful for comparing the Zeeman splitting with, as it can confirm the magnetic field derived from the 6035 MHz

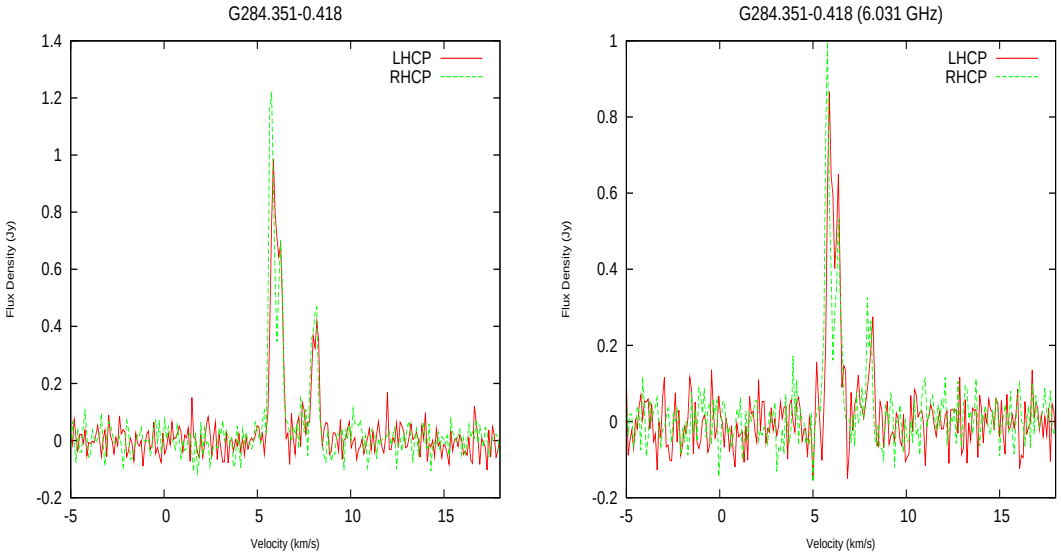

Figure 4.32: The 6035 MHz transition is usually ~3-5 times stronger than the 6031 MHz transition. However, G284.351-0.418, unusually has the most comparable 6035 & 6031 MHz flux density in the survey.

transition.

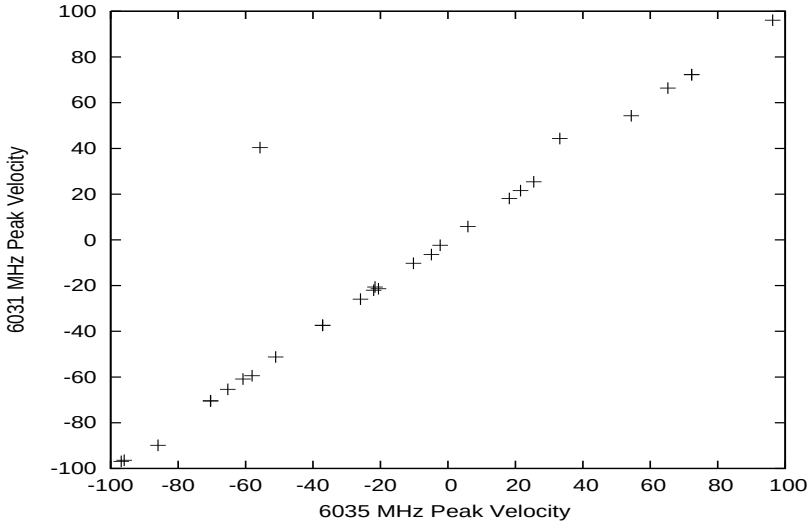

Figure 4.33: Comparison of the 6035 & 6031 MHz ex-OH masers peak velocities

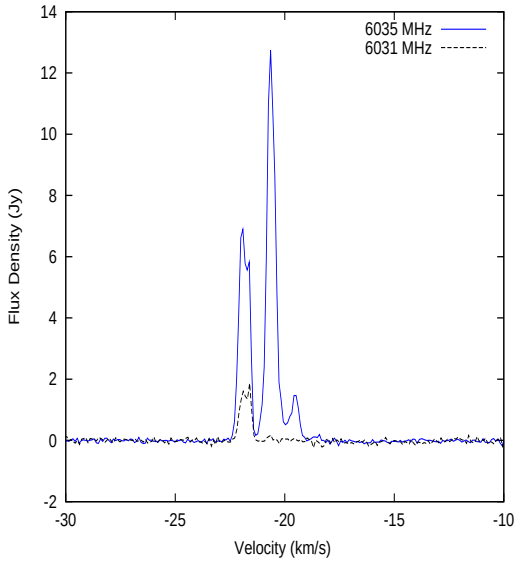

Figure 4.34: The 6035 & 6031 MHz ex-OH masers at G353.410-0.360. The 6035 MHz I flux density is displayed in blue, the 6031 MHz I flux is displayed in the black. The strongest feature of the 6031 MHz maser unusually lines up with the second strongest peak of the 6035 MHz maser, it is the only one in this survey to do so.

4.4.3 6035, 1665 & 1667 MHz OH Masers

The 6035 MHz ex-OH maser is often observed to be associated with 1665 and 1667 MHz OH masers. Caswell (2001) reports that ~30% of 1665 MHz masers have 6035 MHz ex-OH masers detected at their sites. Caswell (1998) observed over 200 1665/7 MHz OH masers using the ATCA, determining their positions. There are 77 1665/7 MHz masers in Caswell (1998) which are coincident with a 6035 MHz ex-OH maser to within ~1″. The remaining 123 1665/7 MHz masers are not associated with the 6035 MHz masers. There is only 1 maser in the MMB, G8.266+0.483, which was observed with the ATCA to determine if there were 1665/7 MHz OH masers present, as it did not have an accompanying 6668 MHz maser detected in the Parkes data, which is very rare. It was found that this source, G8.266+0.483 does not have an accompanying 1665/7 MHz OH maser. A remaining 33 ex-OH maser sites need to be searched for 1665/7 MHz OH masers.

4.5 6035 MHz Excited OH Masers and 6668 MHz Methanol Masers

Out of the 118 6035 MHz ex-OH masers detected in the MMB survey 99 have a methanol maser associated within 20″, 6 between 20-40″, 1 between 40-60″ and 12 are greater than 60″ from a methanol maser (Figure 4.35). The majority of the 6035 MHz masers, 55, are within 1″ of a methanol maser. There are 957 6668 MHz methanol masers detected in the MMB survey, 11% of them are associated with a 6035 MHz (association is defined by a separation less than 20″). On the other hand, 60% of 6035 MHz masers are associated with a 6668 MHz maser (within 2″). Caswell (1997,2004) studied 29 sites with both 6035 MHz ex-OH and 6668 MHz methanol maser emission and found that the masers were both associated at subarcsecond accuracy and that the emission is within comparable velocity range, which suggests they could be co-propagating. The results have demonstrated that this is not always the case.

4.5.1 Flux Density Comparison

Figure 4.36 shows the ratio of the 6668 MHz methanol and the 6035 MHz ex-OH flux density. We find that the flux density of the 6035 MHz ex-OH masers is generally lower than the 6668 MHz methanol masers. There are only nine objects that the ratio is less than 1. The most extreme example is source G308.056-0.396, where the 6035 MHz flux density is 20.7 Jy whilst the 6668 MHz methanol flux density is 1.3 Jy. This result agrees with the work of (Caswell 1998) which finds methanol masers are mostly brighter than the 6035 MHz ex-OH masers and it is rare to find a 6035 MHz ex-OH maser brighter than a 6668 MHz methanol maser.

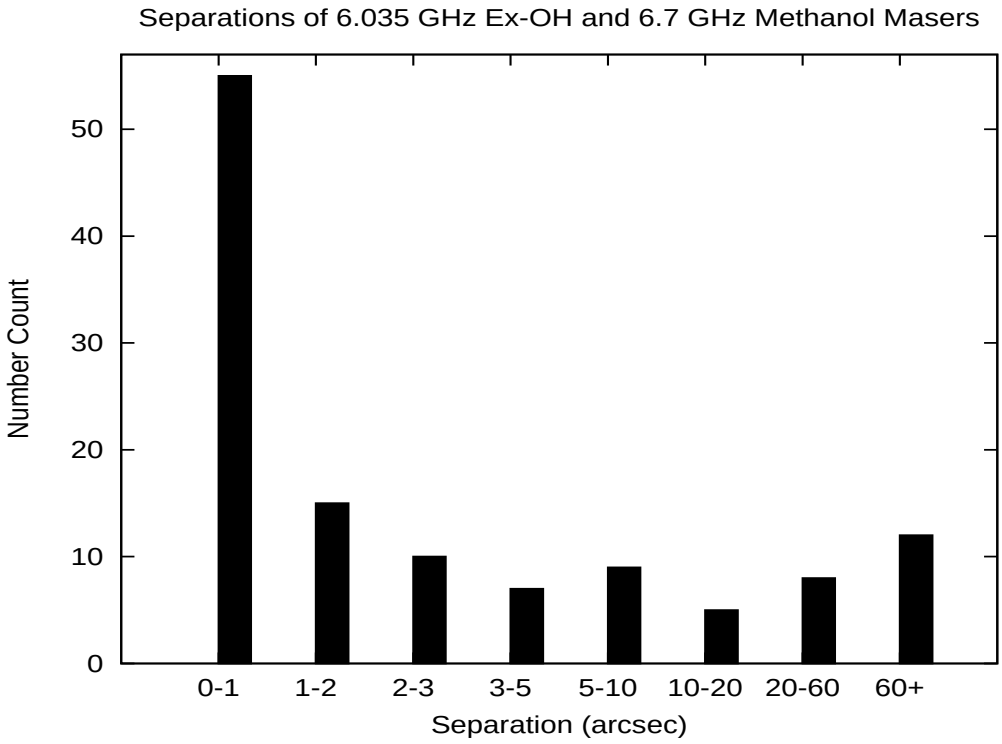

Figure 4.35: The separation of the 6035 MHz ex-OH masers and the 6668 MHz methanol masers in the MMB survey.

4.5.2 Profile and Velocity Comparison

The spectral profiles of the 6035 MHz ex-OH masers and the 6668 MHz methanol masers are usually rather similar, with both displaying a cluster of narrow peaks. The peak velocity of the 6035 MHz ex-OH maser and the methanol maser do not always agree. The peak velocities of the two masers may be separated by up to 7 km s^{-1}. Nonetheless, the peak velocity of the 6035 MHz ex-OH masers are always within the velocity range of the methanol maser. There is a notable difference in the velocity range of the masers. In the 6035 MHz masers the average velocity range is found to be 3.25 km s^{-1} whereas the 6668 MHz methanol maser average velocity range is 6.53 km s^{-1}. The methanol masers mostly have a wider velocity range than the 6035 MHz masers, this can easily be demonstrated by comparing 6668 MHz methanol and 6035 MHz ex-OH maser spectra (Appendix 2).

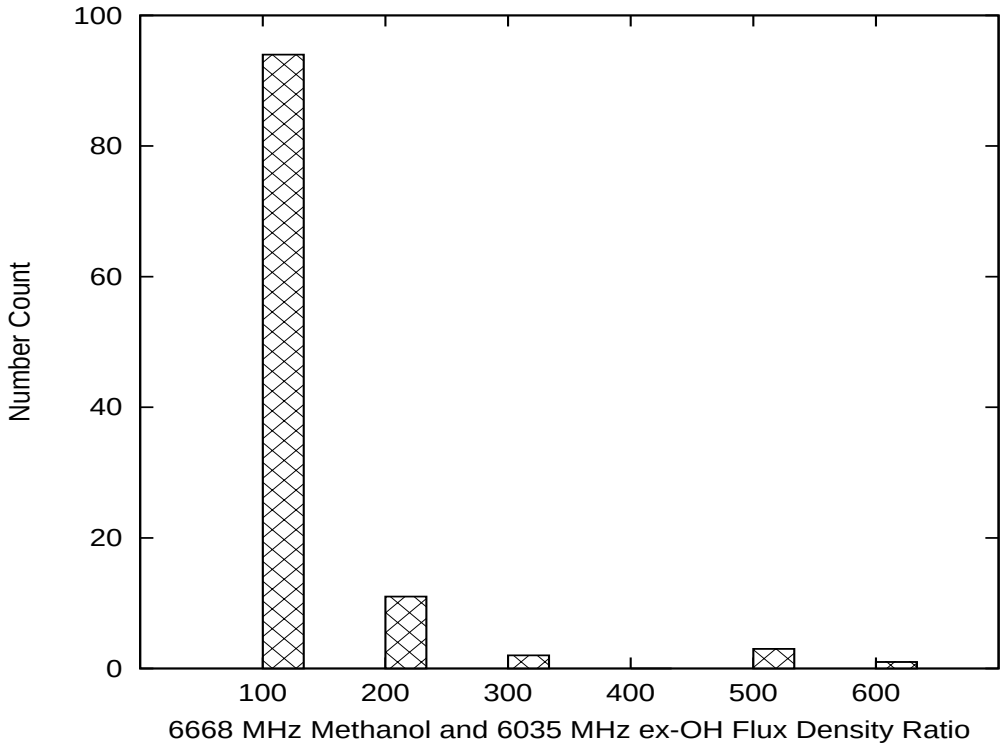

Figure 4.36: The ratio of the 6035 MHz ex-OH to 6668 MHz methanol flux densities.

4.6 GLIMPSE comparison

GLIMPSE is a legacy program of the Spitzer Space Telescope, that surveyed 10°<l<60°, |≤2° of the Galactic plane at 3.6, 4.5, 5.0 & 8.0 μm at a resolution of 1.4-1.9″ (Benjamin et al. 2003). Comparison of the ex-OH masers with GLIMPSE potentially allows us to identify the sources or types of sources exciting the masers. Also, a comparison of the colours of the sources with a 6035 MHz ex-OH maser and a 6668 MHz methanol maser versus sources with a 6668 MHz methanol maser only may potentially reveal if these two sets of sources are different. Sources are frequently targeted for masers based on their GLIMPSE colours, for example Ellingsen (2007).

There are 80 6035 MHz ex-OH masers in the GLIMPSE region. The first step is to determine what 3.6, 4.5, 5.0 & 8.0 μm magnitudes are associated with the masers and look for trends in the colours, such as extreme red colours, with the hope that a

GLIMPSE colour trend may be identified for sources with 6035 MHz ex-OH masers. To investigate this, two colour magnitude plots of the 3.6, 4.5, 5.0 & 8.0 μm colour magnitudes were constructed using an association range of 2″ between the masers and GLIMPSE sources. Figure 4.37 shows the two plots constructed, on the left the [3.6]-[4.5] vs [8.0] and [5.8]-[8.0] vs.[3.6]-[4.5].

It can be seen that the green squares, representing the sources with 6035 MHz ex-OH, the blue crosses representing the 6031 MHz ex-OH masers and the red crosses representing 6668 MHz methanol masers are both randomly dispersed through the plots. There is no obvious difference between the sources with and without the ex-OH masers present.

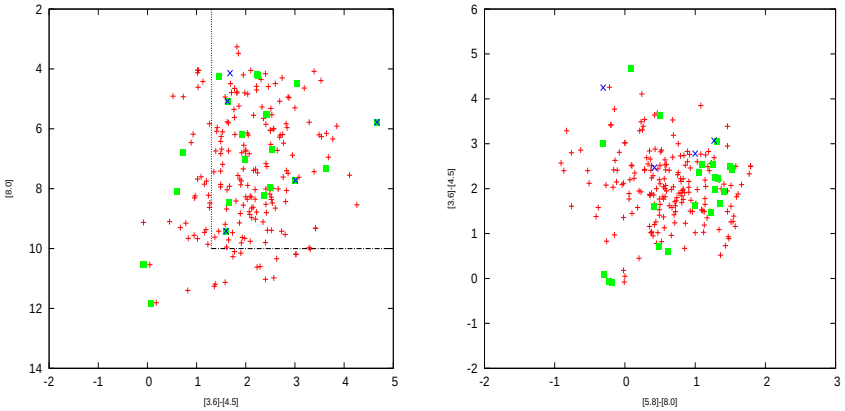

Figure 4.37: -

[4.5] vs [8.0] and [5.8]-[8.0] vs.[3.6]-[4.5] colour magnitude plots]On the left: the [3.6]-[4.5] vs [8.0], The red crosses are the 6668 MHz methanol masers, the green squares are the 6035 MHz ex-OH masers and the blue crosses are the 6031 MHz ex-OH masers. It can be seen that the sources with 6035 MHz ex-OH masers are mixed with the methanol maser sources. On the right: [5.8]-[8.0] vs.[3.6]-[4.5], the annotations are as described, again the sources which host the 6035 MHz maser sources do not have distinguishing colours from the 6668 MHz mehtanol masers.

4.6.1 GLIMPSE Images

It is possible to construct GLIMPSE images using the 3.6, 4.5 & 8.0 μm bands. The three (false) colour images use the standard colours of 3.6 μm is blue, 4.5 μm is green and 8.0 μm is red, the three images are combined using the viewing package Kvis. As GLIMPSE does not cover the same region as the MMB, it was only possible to construct GLIMSPE images for 80 of ex-OH masers (Figure 4.38). The images are centred on the ex-OH maser positions and are 60″ in size, so any possible extended emission may be viewed. Annotations of the 6035, 6031 MHz ex-OH masers, 1665/7 OH masers and 6668 MHz methanol masers were overlaid on the images. All the images were analysed for possible trends, such as whether the 6035 MHz masers are mostly associated with IRDCs or bright sources, are the ex-OH masers coincident or offset with bright sources. As discussed in Chapter 1, there has been a plethora of recent work on Extended Green Objects (EGOs), which are believed to be associated with outflows in regions of high mass star formation (Cyganowski et al. 2009). Hence, any sources with visible EGOs will also be of interest as they may help establish if ex-OH masers are located in outflows (coincident with EGO emission) or closer to the central object. The results are summarised in Table 4.15

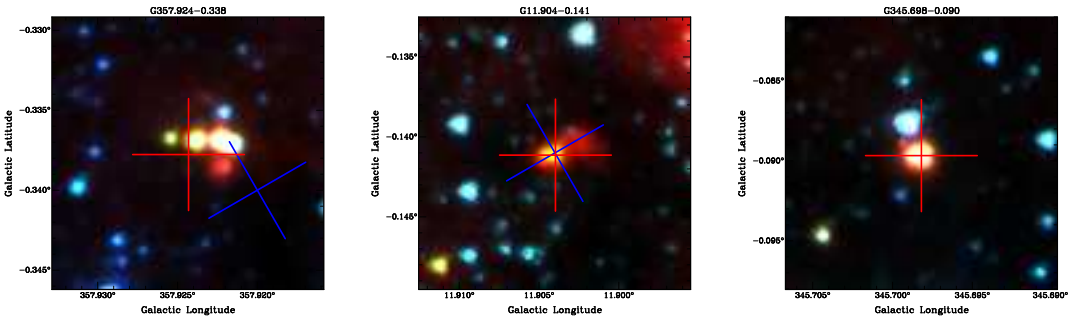

Figure 4.38: Example three colour 3.6, 4.5 & 8.0 micron GLIMPSE images. red crosses represent the 6035 MHz ex-OH masers and blue crosses represent the 6668 MHz methanol masers.

Statistically, the 6035 MHz ex-OH maser is more commonly associated with a

GLIMPSE Source Association	
Coincident with a bright source	39
Offset from a bright source (~4″)	14
Infrared dark region	11
Infrared dark region with EGO emission	9
No GLIMPSE source association	7

Table 4.15: 6035 MHz ex-OH masers and their GLIMPSE associations

bright GLIMPSE source than an IRDC. We find 79% of the images with bright GLIMPSE sources have a coincident or closely associated ex-OH maser, compared to 20% which are associated with an IRDC. This is discussed further in section 4.10.4. To show the nature of the association, example images are shown in Figure 4.38. Figure 4.39 shows three GLIMPSE images, G8.669-0.356, G338.925+0.557 and G351.581-0.353, which display extended green objects (EGO), which are hypothesised to represent outflows in star forming regions (Cyganowski et al. 2009). G8.669-0.356 has 6035 and 6031 MHz ex-OH and 6668 MHz methanol masers at the center of the image and clumps of EGO emission to the East and West. It appears as though the masers may be associated with a cnetral object whilst the EGOs may be marking bipolar outflows on either side. G338.925+0.557, shows 6035 and 6031 MHz masers at the centre and EGO emission to the South-East, it appears as though the ex-OH masers are associated with the central source, whilst the EGO emission marks the outflow. G351.581-0.353 again shows the 6035 and 6031 MHz ex-OH and 6668 MHz methanol maser at the center and EGO emission to the North-East and the South-West. In the remaining images which display EGO emission, it does not appear to be as collimated at the above sources.

During the analysis of the masers in relation to the GLIMPSE images, three sources stood out, G24.594+0.222, G49.489-0.388 & G337.280-0.514, (Figure 4.40). They are all without a methanol or 1665/7 MHz maser, they are also without any visible

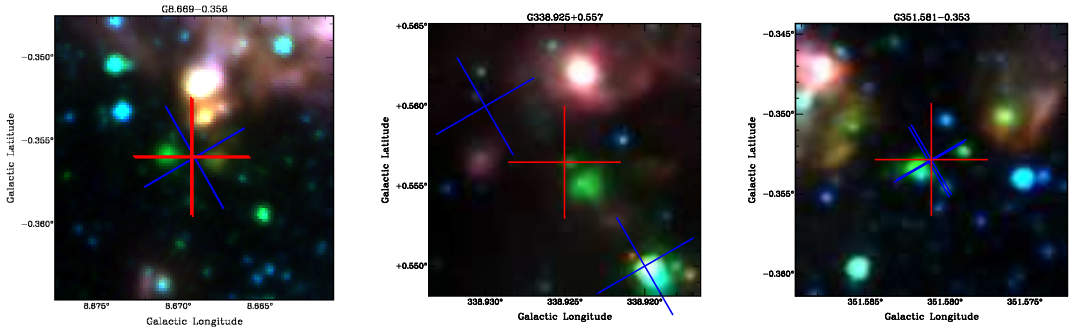

Figure 4.39: Three colour 3.6, 4.5 & 8.0 micron GLIMPSE image, yellow cross indicates the 6035 MHz ex-OH maser. G8.669-0.356, G338.925+0.557 and G351.581-0.353 all display EGO emission which appears from outflows from a central object, with the masers tracing the central object.

GLIMPSE source. G24.594+0.222 appears to be associated with weak EGO emission, it is possibly pinpointing an early stage of MSF evolution. G337.280-0.514 appears to be possibly associated with an IRDC, a sign of MSF. Finally, there is G49.489-0.388, it does not have any tell-tale signs of star formation, let alone MSF. There, of course, are several possibilities, 6035 MHz masers have always been associated with high mass star formation, but is it possible that these three sources are from low mass stars? There was a tentative detection of a 6035 MHz maser in a supernova remnant (priv. comm, J.L.Caswell), although it has never been observed with an interferometer or confirmed. All three sources require further observations to determine the nature of the objects with which they are associated.

4.6.2 CORNISH Comparison

CORNISH is a 5 GHz radio continuum survey of the north GLIMPSE region, as described in Chapter 1. In the CORNISH region there are 36 6035 MHz ex-OH masers and 335 6668 MHz methanol masers. Imposing a 5″ distance limit on the masers to

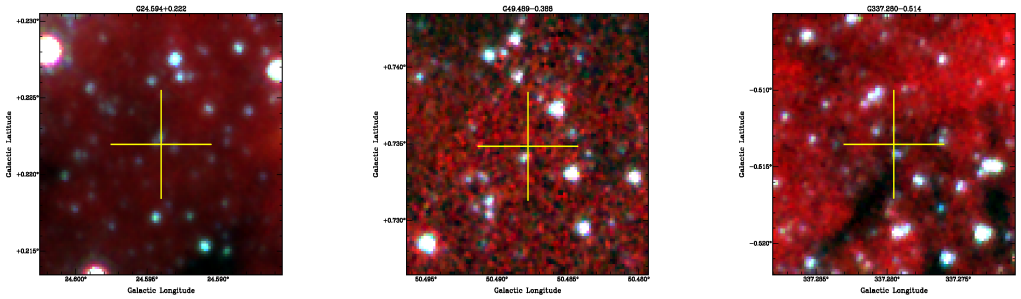

Figure 4.40: Three colour 3.6, 4.5 & 8.0 micron GLIMPSE image, yellow cross indicates the 6035 MHz ex-OH maser. These three images show some of the most interesting sources as they are not associated with a methanol or OH maser, or any visible GLIMPSE source either. They definitely require further investigation to determine the source exciting them.

the peak of the UC HII's we find 16 6035 MHz ex-OH masers and 34 6668 MHz methanol masers are associated with UC HIIs, that's 44% of the ex-OH masers and 10% of the methanol masers are associated with a UC HII region. The observational work by Walsh et al. (1998); Minier et al. (2003); Purcell et al. (2006b), shows that 6668 MHz methanol masers are not associated with the later UC HII stage, but with an earlier hot core stage. Nevertheless the 10% of the methanol masers in the region that are associated with a UC HII region are probably in a crossover stage and will soon be extinguished.

4.7 GLIMPSE and CORNISH Comparison

There are 15 CORNISH sources which are associated with 16 6035 MHz ex-OH masers, one CORNISH source is associated with two ex-OH masers. These images are displayed in Figure 4.41 to Figure 4.55, along with the GLIMPSE counterpart image. Out of the 15 sources 4 have a 6668 MHz methanol maser coincident, 6 have a

6668 MHz maser ∼5″ offset and five do not have a 6668 MHz methanol maser. In all but one region the masers (6035, 6031 MHz ex-OH, 1665/7 MHz OH and 6668 MHz methanol) are not coincident with the peak of the UC HII region. It is only in G10.623-0.384 that the 6035 MHz ex-OH maser and the 1665 MHz OH maser are at the peak of the UC HII. In all other images the masers are offset from the peak.

Interestingly, G11.904-0.141, Figure 4.44, displays excess red emission to the north-east of the central source in GLIMPSE. There is matching emission, at the same positional angle, visible in the CORNISH image. This emission could possibly be an outflow cavity, created by the central source.

G43.149+0.013, (Figure 4.51), shows the 6035 MHz ex-OH and 6668 MHz methanol masers coincident with the central source. There are also two bright peaks to the right and left of the central peak in both the CORNISH and GLIMPSE images. These peaks could possible be bipolar outflows, further observations are required.

G10.623-0.384, G32.744-0.076 and G35.205+0.350 all show EGO emission in the GLIMPSE images. In the corresponding CORNISH images, the EGO emission lies offset from the central source, in keeping with the hypothesis that EGO emission traces outflows, (Figures 4.41, 4.47 & 4.49). G35.205+0.350 appears to show an edge on disk in the GLIMPSE image, with EGO outflows on either side, Figure 4.49.

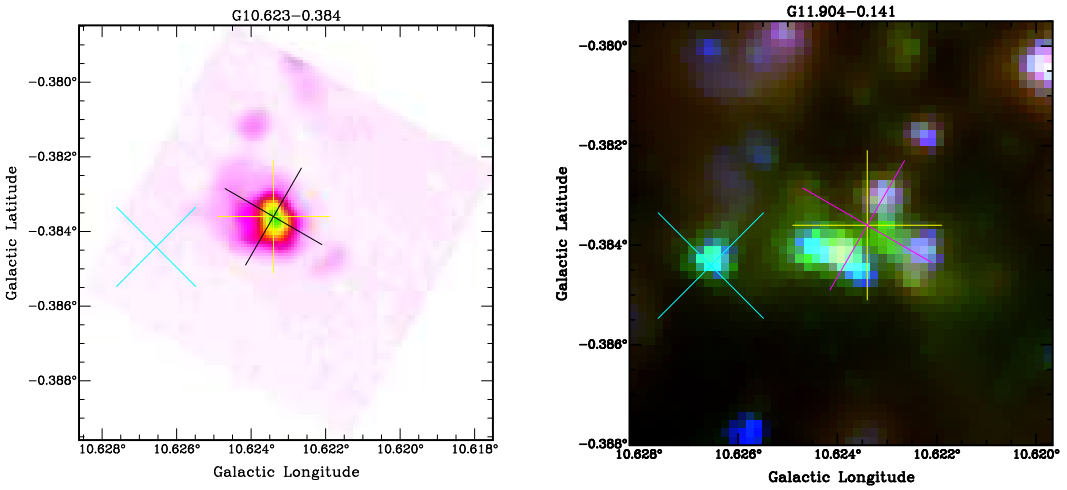

Figure 4.41: In the CORNISH image (left), yellow crosses indicate 6035 MHz ex-OH masers, blue crosses indicate 6668 MHz methanol masers, black crosses indicate 1665/7 MHz OH masers and the red crosses indicate the 6031 MHz ex-OH masers. In GLIMPSE, all the annotations are the same except the 1665/7 MHz masers are now represented by white crosses. This is the only source which has a 6035 MHz ex-OH and 1665 MHz OH maser coincident with its peak. The OH masers are coincident with a UC HII region whilst the methanol maser is offset.

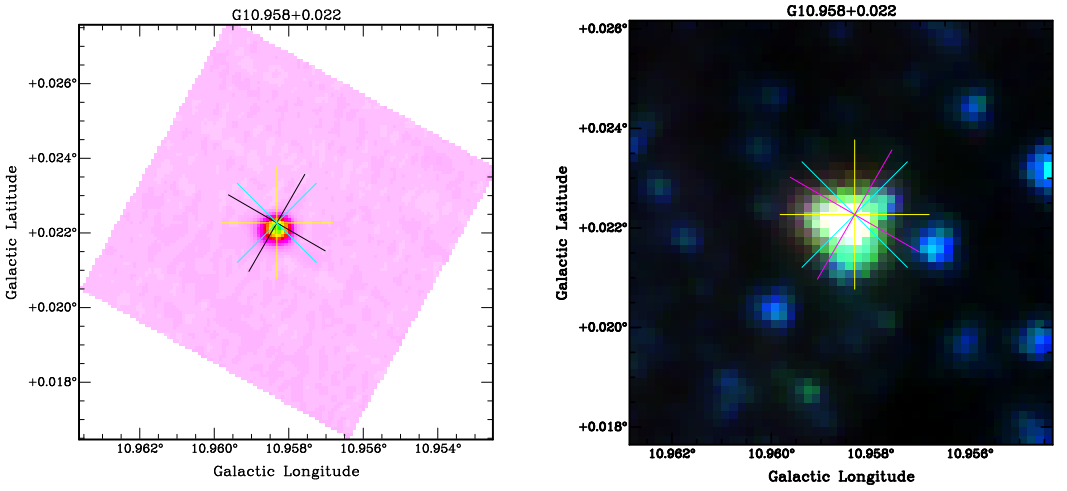

Figure 4.42: Annotations are the same as Figure 4.41. The 6035 MHz ex-OH masers and the 6668 MHz methanol maser are located on the edge of the UC HII region.

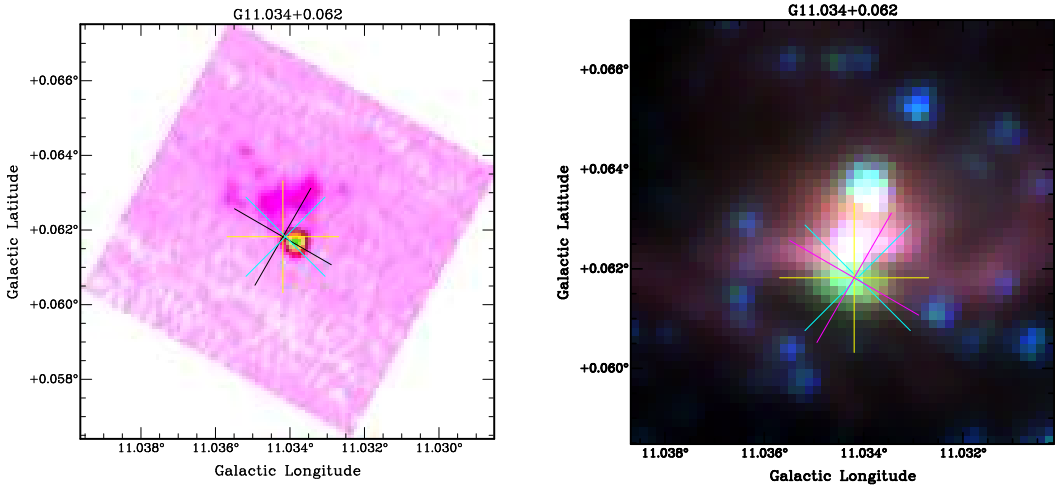

Figure 4.43: Annotations are the same as Figure 4.41. All the masers are coincident and at the edge of the source, there appears to be emission to the north of the source in the CORNISH and GLIMPSE image, with corresponding EGO emission to the South of the source in the GLIMPSE image.

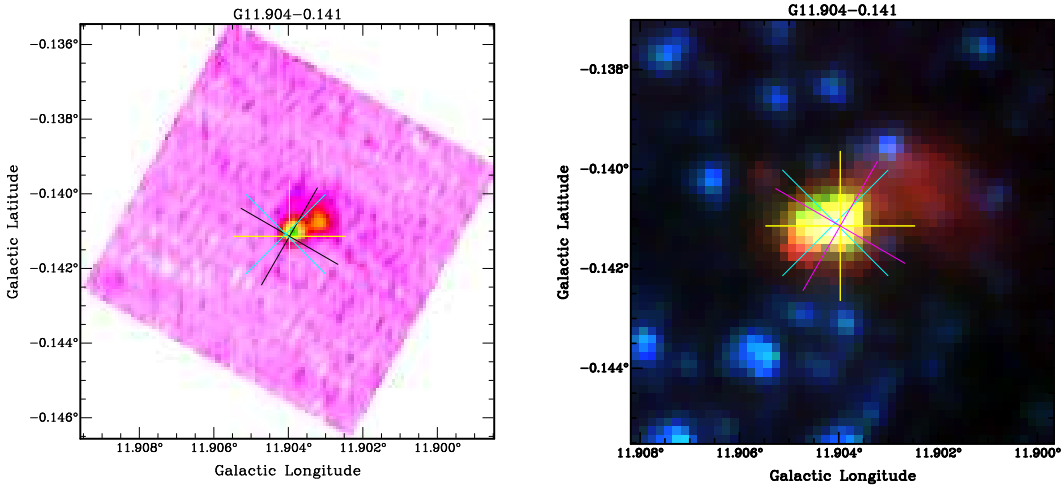

Figure 4.44: Annotations are the same as Figure 4.41. All the masers are coincident at the edge of the UC HII region. An outflow is visible to the west of the central object, with corresponding emission in the GLIMPSE image.

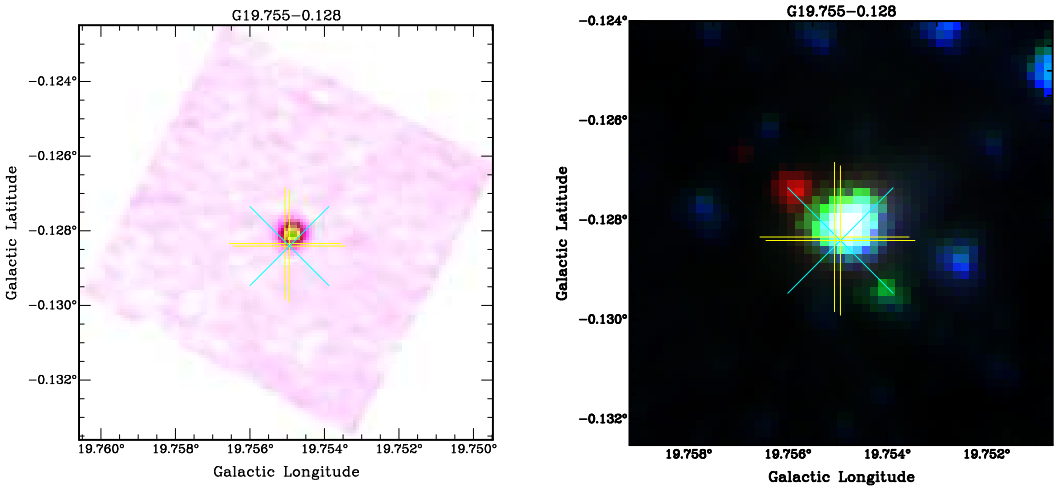

Figure 4.45: Annotations are the same as Figure 4.41. The 6035 MHz ex-OH masers and 6668 MHz methanol maser are located on the edge of a compact CORNISH source, it appears to have some weak EGO emission in the GLIMPSE image.

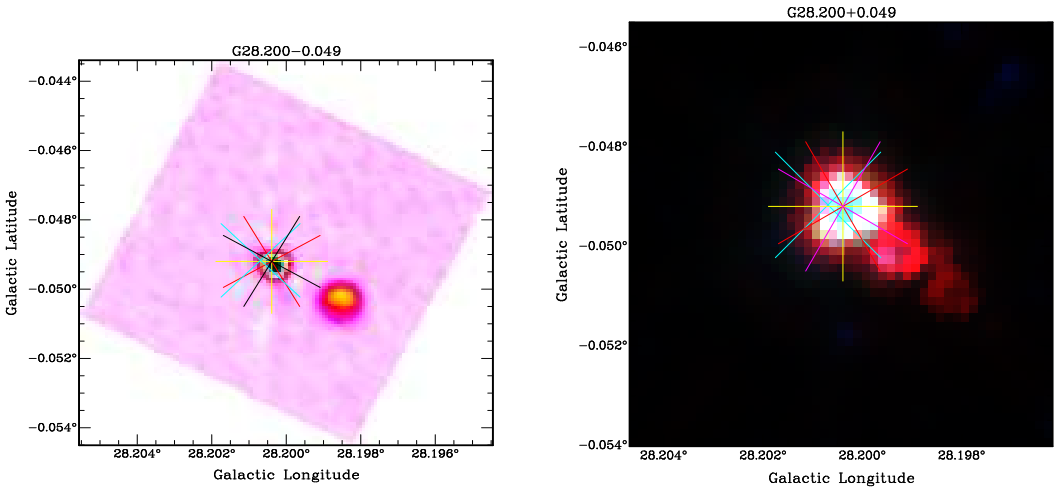

Figure 4.46: Annotations are the same as Figure 4.41. This source contains all four ex-OH, OH and methanol masers in a bright compact source with a bright clump of emission to South-West of the source which appears to be an outflow when compared to the GLIMPSE image.

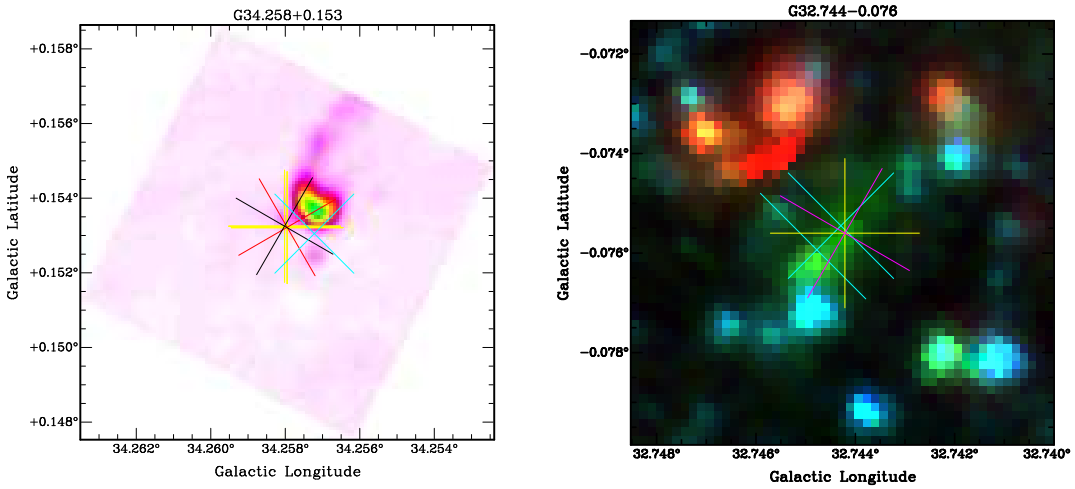

Figure 4.47: Annotations are the same as Figure 4.41. The OH masers are to the left of the source whilst the methanol maser is underneath it. In the CORNISH image there appears to be emission to the top of the source, in GLIMPSE, there is a notable EGO coming out the opposite end.

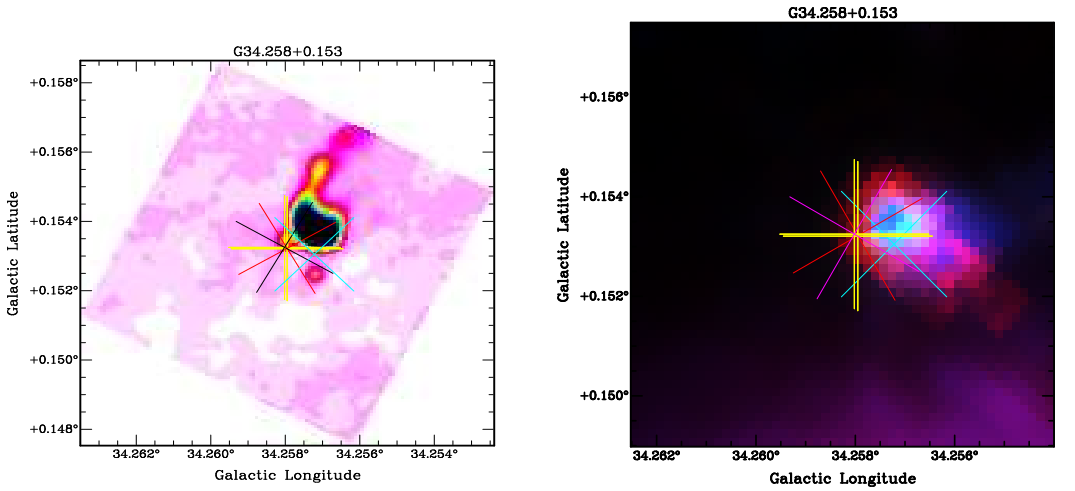

Figure 4.48: Annotations are the same as Figure 4.41.

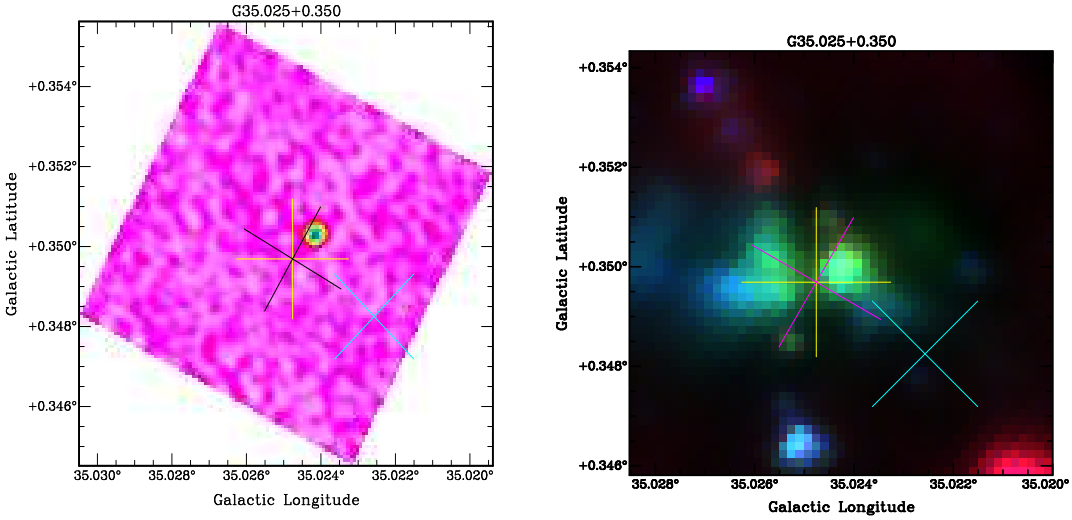

Figure 4.49: Annotations are the same as Figure 4.41. The OH masers are offset from the compact UC HII source, the GLIMPSE image appears to show an edge on disk with EGO outflows.

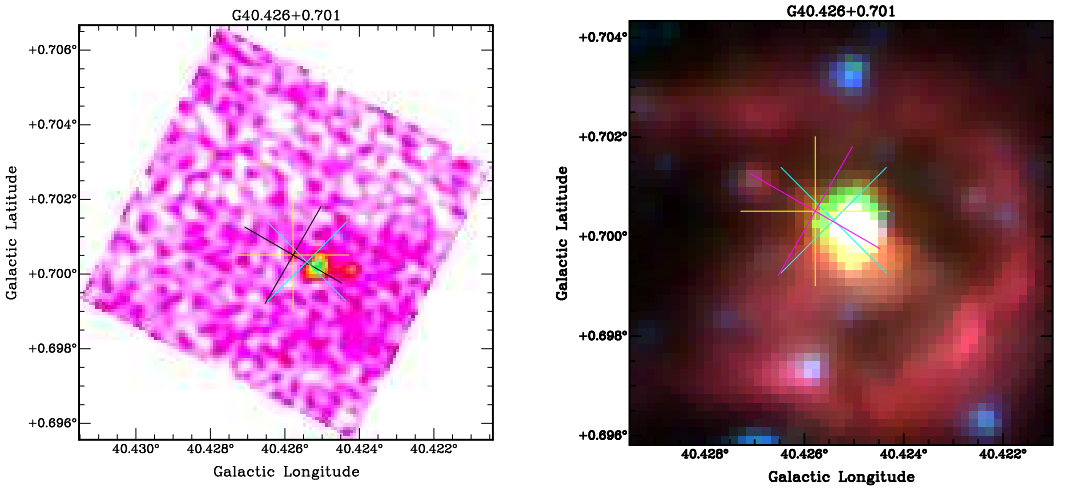

Figure 4.50: Annotations are the same as Figure 4.41. The OH masers are coincident, with the methanol slightly offset, both maser groups are offset from the UC HII region. The CORNISH image appears to show some weak emission to the left of the source on the opposite side to the masers indicating a possible outflow.

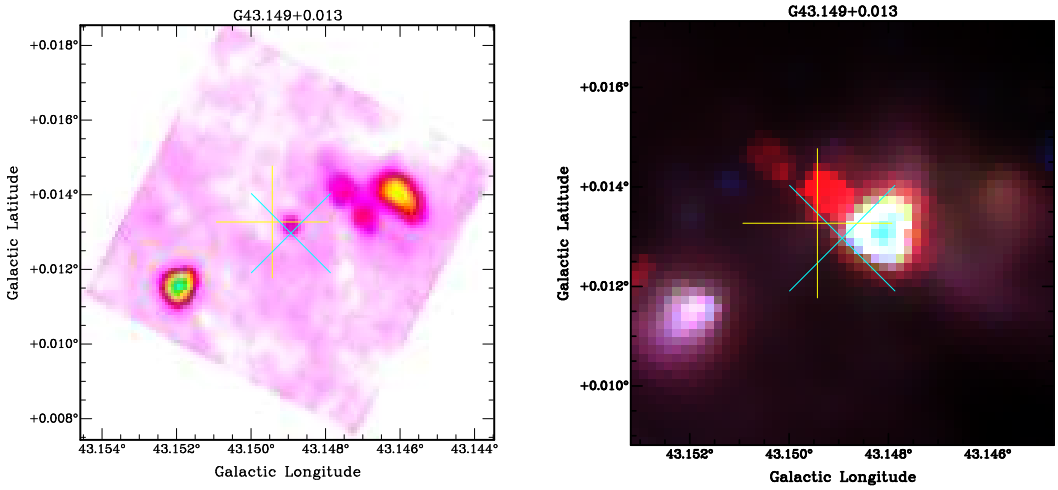

Figure 4.51: Annotations are the same as Figure 4.41. This is one of the most interesting CORNISH sources, it shows emission either side of the masers and the central source. These two clumps of emission either side of the central object are also visible in the GLIMPSE image and could possibly be marking bipolar outflows.

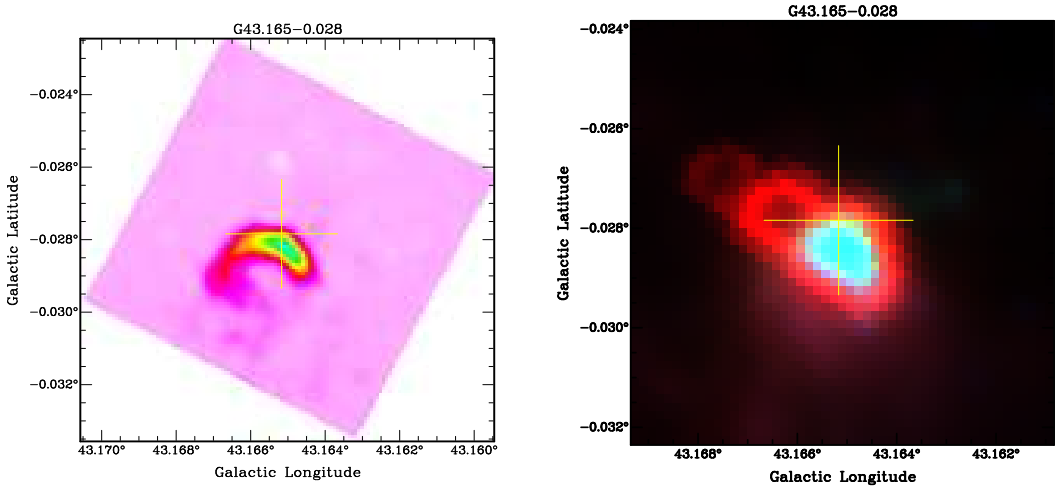

Figure 4.52: Annotations are the same as Figure 4.41. This CORNISH image shows a cometary shaped UC HII region, with only a 6035 MHz ex-OH maser. The GLIMPSE image is equally interesting, with 'bubble' structure coming from the central source.

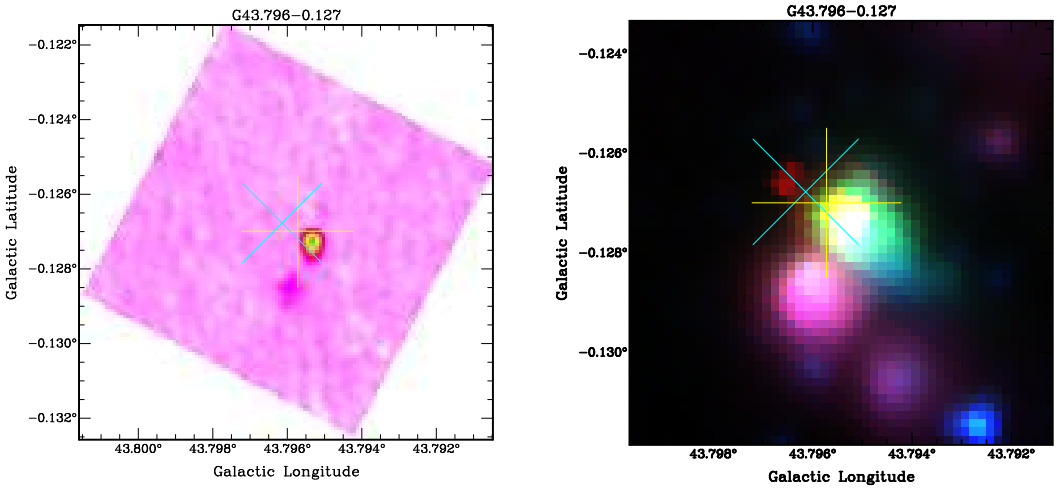

Figure 4.53: Annotations are the same as Figure 4.41. The ex-OH and methanol maser are offset from the central source in the CORNISH image and from each other.

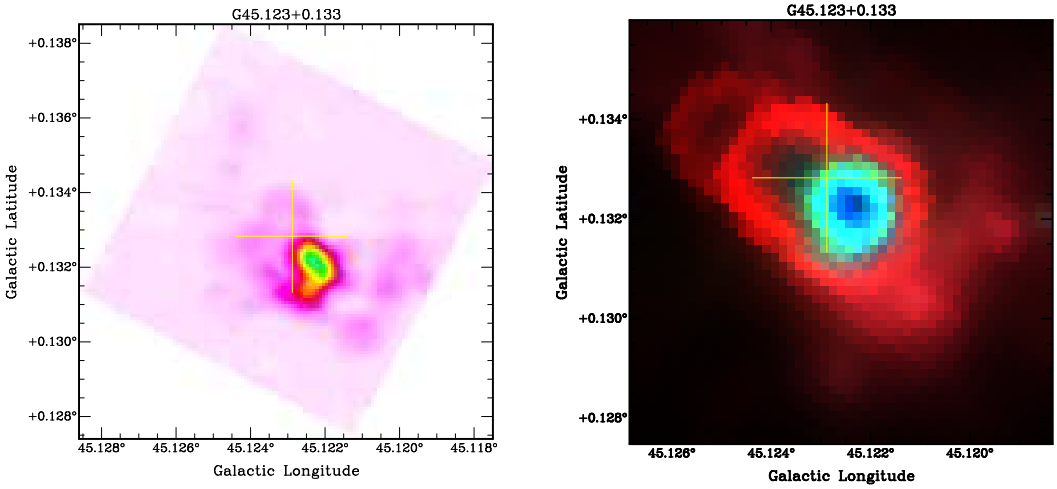

Figure 4.54: Annotations are the same as Figure 4.41. This is a 6035 MHz ex-OH only source, the GLIMPSE structure is remarkably similar to G43.165-0.028, with the 'bubble' morphology. The 6035 MHz ex-OH maser is offset from the UC HII region.

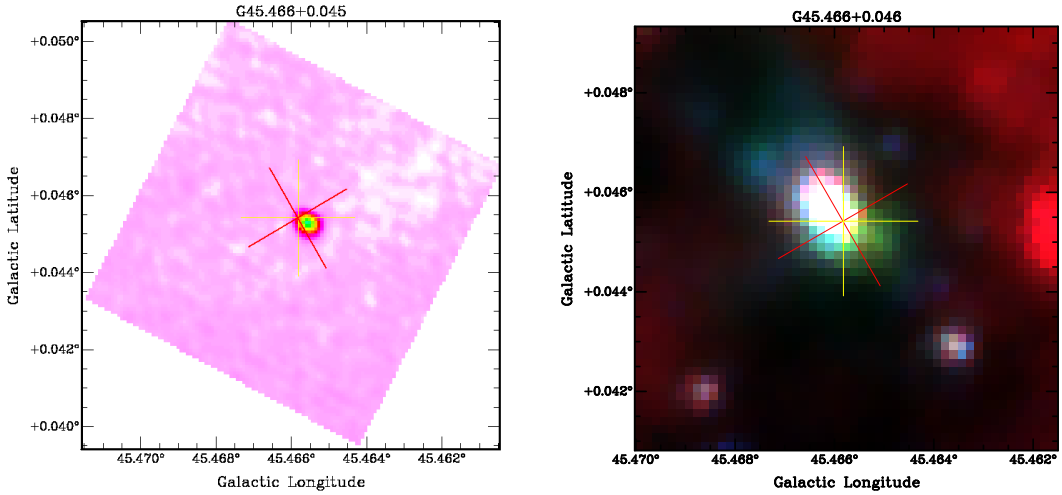

Figure 4.55: Annotations are the same as Figure 4.41. The ex-OH masers are located on the edge of a UC HII region.

4.8 The Evolution of Massive Star Formation using GLIMPSE

As discussed in Chapter 1, it is the holy grail of MSF to find an absolute evolutionary indicator for massive star formation. It is possible to suggest an evolutionary sequence from the GLIMPSE images constructed for this thesis. Simply put, the first stage is when we cannot see the a GLIMPSE source, but the location of the protostar is pinpointed by a IRDC with a 6668 MHz methanol maser (Figure 4.56), followed by an ex-OH/OH maser (Figure 4.57). The next possible stage is marked by EGO emission from the outflows of the protostar (Figure 4.58), although the precise evolutionary position of the EGO stage is not truly known. Following this a GLIMPSE source; evolving massive stellar object which is now large/powerful enough to ionise its surrounding accompanied by the methanol and ex-OH/OH masers, (Figure 4.59). As the central object increases in size and UV output, the methanol could possibly be dissociated and stop masing. Leaving the ex-OH and OH masers with the bright GLIMPSE source (Figure 4.60). It may be seen in Figure 4.60 that there are 6668 MHz methanol masers offset from the GLIMPSE sources, in a darker region, possibly pin pointing an earlier evolutionary stage.

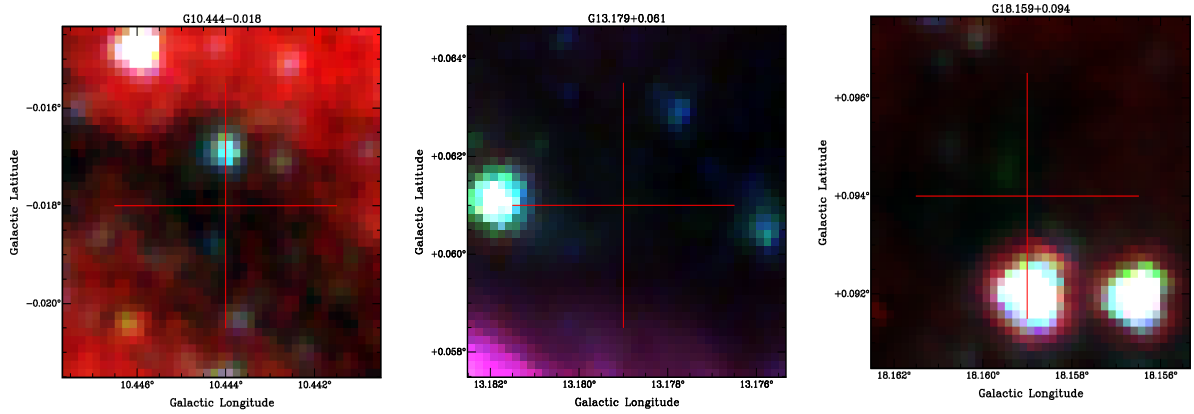

Figure 4.56: Three colour 3.6, 4.5 & 8.0 micron GLIMPSE image, red cross shows 6668 MHz methanol maser. The early stages of a massive star forming in an IRDC is pin pointed by a 6668 MHz methanol maser.

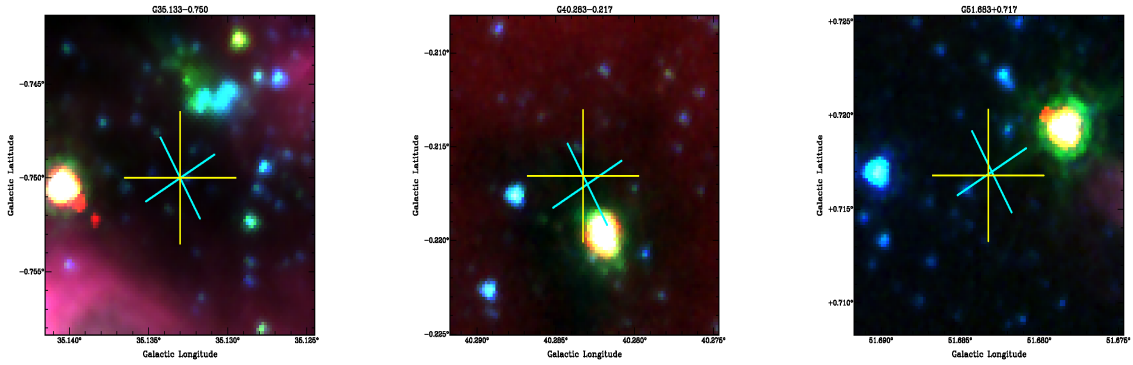

Figure 4.57: Three colour 3.6, 4.5 & 8.0 micron GLIMPSE image, blue cross shows 6668 MHz methanol maser, yellow cross indicates the 6035 MHz ex-OH maser, white cross indicate 1665/7 MHz OH masers, red cross indicates the 6031 MHz ex-OH maser. The 6035 MHz ex-OH masers is next to appear in the IRDC with the 6668 MHz maser.

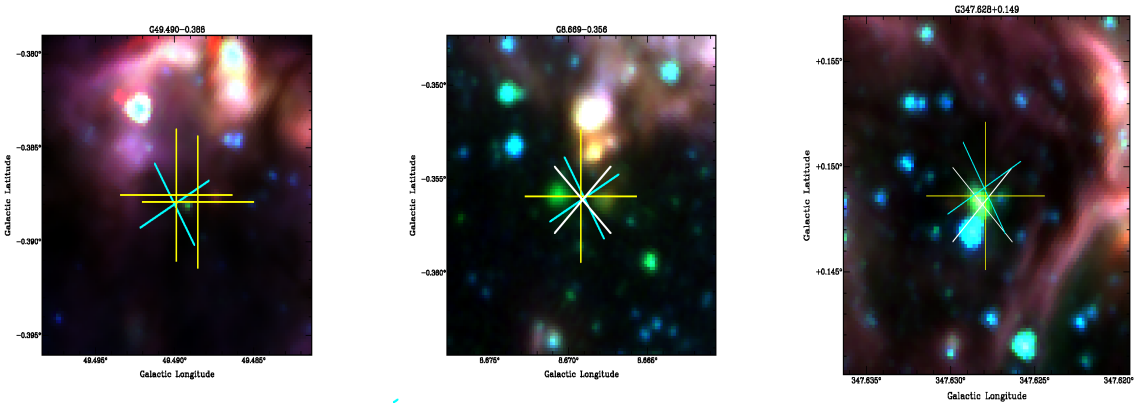

Figure 4.58: Three colour 3.6, 4.5 & 8.0 micron GLIMPSE image, blue cross indicates 6668 MHz methanol maser, yellow cross indicates the 6035 MHz ex-OH maser, white cross indicate 1665/7 MHz OH masers, red cross indicates the 6031 MHz ex-OH maser. As the massive star increases mass it is believed that it has poorly collimated molecular outflows, identified by extended green emission (EGO).

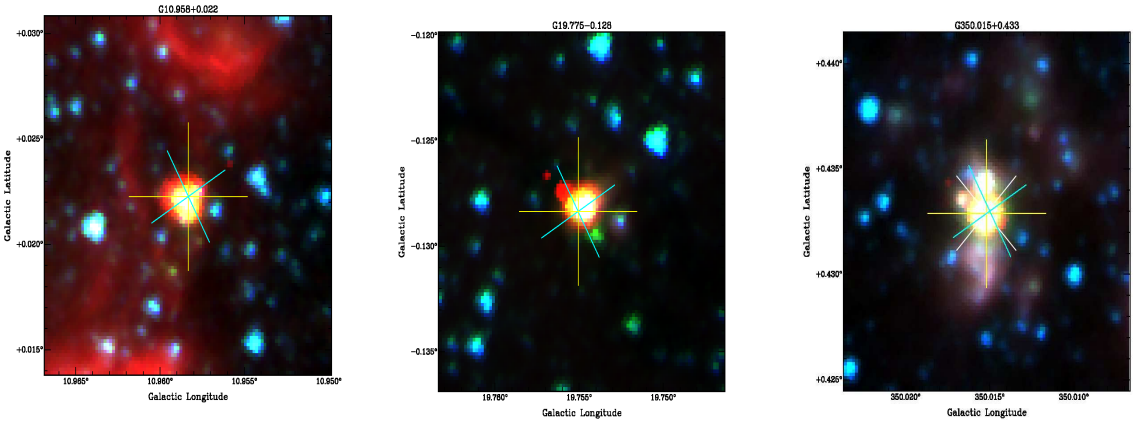

Figure 4.59: Three colour 3.6, 4.5 & 8.0 micron GLIMPSE image, red cross indicates 6668 MHz methanol maser, yellow cross indicates the 6035 MHz ex-OH maser, white cross indicate 1665/7 MHz OH masers, red cross indicates the 6031 MHz ex-OH maser. As the source evolves it ionizes its surroundings and the UC HII region becomes visible in the GLIMPSE tree colour image.

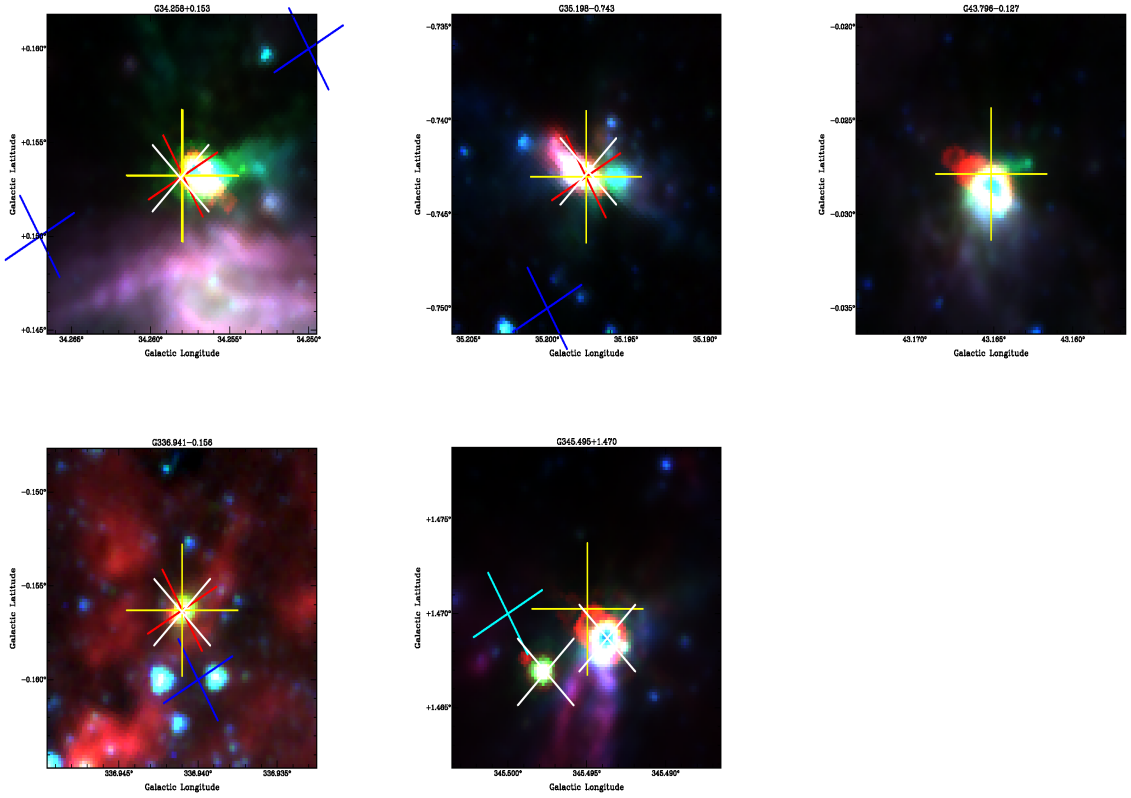

Figure 4.60: Three colour 3.6, 4.5 & 8.0 micron GLIMPSE image, red cross indicates 6668 MHz methanol maser, yellow cross indicates the 6035 MHz ex-OH maser, white cross indicate 1665/7 MHz OH masers, red cross indicates the 6031 MHz ex-OH maser. As the evolution continues the 6668 MHz methanol maser is extinguished, but the ex-OH/OH masers remain masing.

4.9 Discussion

The ex-OH maser survey of the MMB has been a huge success, detecting 118 masers, 43 of which are new detections. An additional 29 6031 MHz ex-OH masers were also detected at sites of the 6035 MHz masers. The magnetic fields have been calculated from the Zeeman splitting of the left and right circular polarization, where possible, and backed up by the 6031 MHz masers in several instances. Comparisons have been made with 6668 MHz methanol and 1665/7 MHz OH masers and the GLIMPSE and CORNISH surveys.

When considering the completeness of the ex-OH MMB survey, it must be considered in two parts. The first being the scanned single dish data which detected 66 masers. The second is the pointed MX observations on all 937 6668 MHz methanol masers. The MXs were conducted to provide higher quality spectra. The unexpected advantage of these 3 minute pointed observations was the detection of 52, out of the total 118, ex-OH maser detections. Most of these masers have flux densities below the three sigma detection threshold of the scanned survey.

Hence the survey may be split into the scanned survey and the pointed survey. The scanned survey is complete down to a three sigma rms of 0.8 Jy. It is clear we are missing 6035 MHz masers below this cutoff from the 52 masers detected with the MX observations. The MX observations have a noise level of ~ 0.05 Jy. It is worth noting that 84% of the 6035 MHz masers are associated with a 6668 MHz methanol maser and all 937 methanol masers were subject to MX observations, which observe 6668 MHz and 6035 MHz simultaneously.

The scanned survey detected 66 masers, 16 of which are new detections. While the pointed observations detected 52 masers, 27 of which are new. This gives an average of one 6035 MHz ex-OH maser every 7.20 sq-deg. As to be expected, 35 of the pointed

MX observations have an I flux density below the three simga scanned survey limit of <0.8 Jy. Every time an ex-OH maser was detected by an MX observation, the Parkes scanned data cube was checked to see if it was visible. None of the MX detections were visible in the scanned data cubes. There are 17 masers which are above the 0.8 Jy three sigma detection threshold, the most striking of which has a flux density of 2.91 Jy. These masers were not missed by eye in the data cube or by the source detection algorithm, neither were the data particularly noisy, leaving one answer: they varied.

4.9.1 Variation

The ex-OH masers are known to vary on monthly to yearly timescales (Caswell 1998), this is also shown in this work with the comparison of the Caswell and Vaile (1995) data set and the MMB data set (Figure 4.30). The largest variation occured in G43.165-0.028, which increased to 2.91 Jy from below the three σ detection threshold of 0.8 Jy in 1.5 years.

This work has shown the ex-OH masers vary on even shorter timescales of days. Over a ~10 day period 50 masers were observed twice, once alongside the 6668 MHz methanol masers, the second time with the 6031 MHz masers. It was found that 14% of the masers have varied in intensity and profile (Figures 4.26 to 4.29). The remaining 33 masers retained their initial intensity and profile. Masers by nature are variable objects, slight changes in the populations of the energy levels or turbulence may lead to massive differences in the maser gain. Variations in H_2O masers are rather common as they are known to be located in the turbulent regions of outflows and may change their velocity structure and spectral profile dramatically in days (Breen et al. 2010). However, just what the (less dramatic) 6035 MHz variations are telling us about the maser and its environment remains to be clearly understood.

4.9.2 Location, Location, Location

The location of the 6035 MHz ex-OH maser in relation to the central source is an important and still disputed point. The theoretical models of Elitzur and de Jong (1978) argue that the OH masers form in the compressed shell between the shock and the ionisation front around the HII region, however, the observational work of Caswell and Haynes (1983b) report that OH masers are not associated with HII regions. The ex-OH and OH masers appear at an earlier evolutionary stage than the HII region. Caswell (1997) observed ex-OH masers with 6668 MHz methanol masers, Cohen et al. (2003) observed OH masers in a young bipolar outflow and Edris et al. (2005) observed OH masers associated with the disk around the central source, proving the ex-OH and OH masers appear at much earlier stage than the HII region .

Caswell et al. (2010), a MMB paper, uses an association radius of 2″, in keeping with this, Table 4.16 shows the separation between the 6035 MHz ex-OH and 6668 MHz using that separation limit. The majority, 60%, of the 6035 MHz masers are $\leq 2''$ from a 6668 MHz methanol maser. However, there are also a significant number of 6035 MHz ex-OH masers $>5''$ from a 6668 MHz methanol maser. These two groupings may correspond to two different environments which contain the 6035 MHz ex-OH masers, such as in an accretion disk or in/near an outflow.

Using the GLIMPSE and CORNISH images the ex-OH masers' location has been investigated (the evolutionary aspect of this is discussed in section 4.10.4) . Eighty masers lie in the GLIMPSE region, resulting in seventy-nine GLIMPSE images (one image contains two close by ex-OH masers). In 79% of the 80 GLIMPSE images the ex-OH maser is associated with a bright GLIMPSE source, a bright source occurs when the area surrounding it is ionised, demonstrating that the ex-OH maser is associated close to the central object.

In the region covered by the CORNISH survey, there are 16 ex-OH masers associated with 15 UC HIIs (there are two ex-OH masers associated with one UC HII region) (Figures 4.41 to 4.55). In all but one instance the ex-OH (and methanol and OH) masers are offset from the peak of the UC HII. This one instance, G10.623-0.384, (Figure 4.41), where the 6035 MHz ex-OH and 1665 MHz OH masers are coincident with the peak of the central source may be due to a chance allignment.

Our findings support the work of Edris et al. (2005); Caswell (1997), that ex-OH masers are closely associated with UC HII regions, but generally not the UC HII peak. There are also three GLIMPSE images, (Figures 4.61), which appear to support the findings of Edris et al. (2005) that the OH masers are located in the disk surrounding the central source, with outflows marked by the EGO emission.

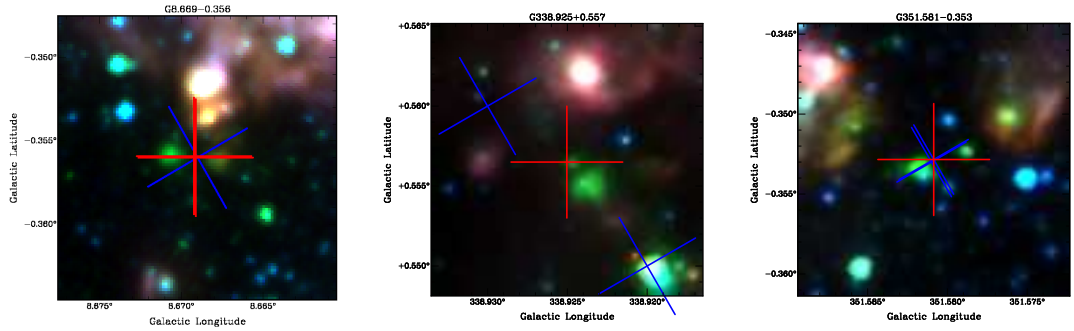

Figure 4.61: Three colour 3.6, 4.5 & 8.0 micron GLIMPSE image, yellow cross indicates the 6035 MHz ex-OH maser. G8.669-0.356, G338.925+0.557 and G351.581-0.353 all display EGO emission which appears from outflows from a central object, with the masers tracing the central object.

4.9.3 6035 MHz Ex-OH and 6668 MHz Methanol Masers

The 6035 MHz ex-OH maser is firmly associated with the 6668 MHz methanol maser, with an 60% association rate in this work (using a 2″ association radius), with the majority matching to subarcsecond accuracy. When analysing the velocity structure

of the matching ex-OH and methanol masers we find the average velocity range for the ex-OH masers to be 3.25km s^{-1} whilst the methanol median velocity range is 6.53 km s^{-1}. It is also interesting that the velocity peak of the ex-OH maser does not always agree with the peak of its matching methanol maser, but it is always in the methanol velocity range.

Distance (arcseconds)	number
0-2″	70
5″	16
10″	8
20″	5
40″	6
60″	1
>60″	12

Table 4.16: The separation distance, in arcesconds, between the 6035 MHz ex-OH and 6668 MHz methanol masers

When considering the ex-OH and methanol association from the methanol masers point of view, we find that 11% of the methanol masers have a 6035 MHz companion. This leads to the question: are the two sets of sources, with and without an ex-OH maser, somehow different? Different in the physical and chemical sense, such as column density of OH and temperature. This work provides these two samples which can be investigated further to address this issue.

As discussed in Chapter 1, the models of Cragg et al. (2002) predict the 6035 MHz ex-OH maser and the 6668 MHz methanol maser will both appear in a low density, high temperature regime (Figure 4.62). The 6035 MHz maser extends to higher densities than the 6668 MHz methanol masers, so sources in which the 6035 MHz ex-OH maser is present and the 6668 MHz methanol maser is weaker or absent, may trace

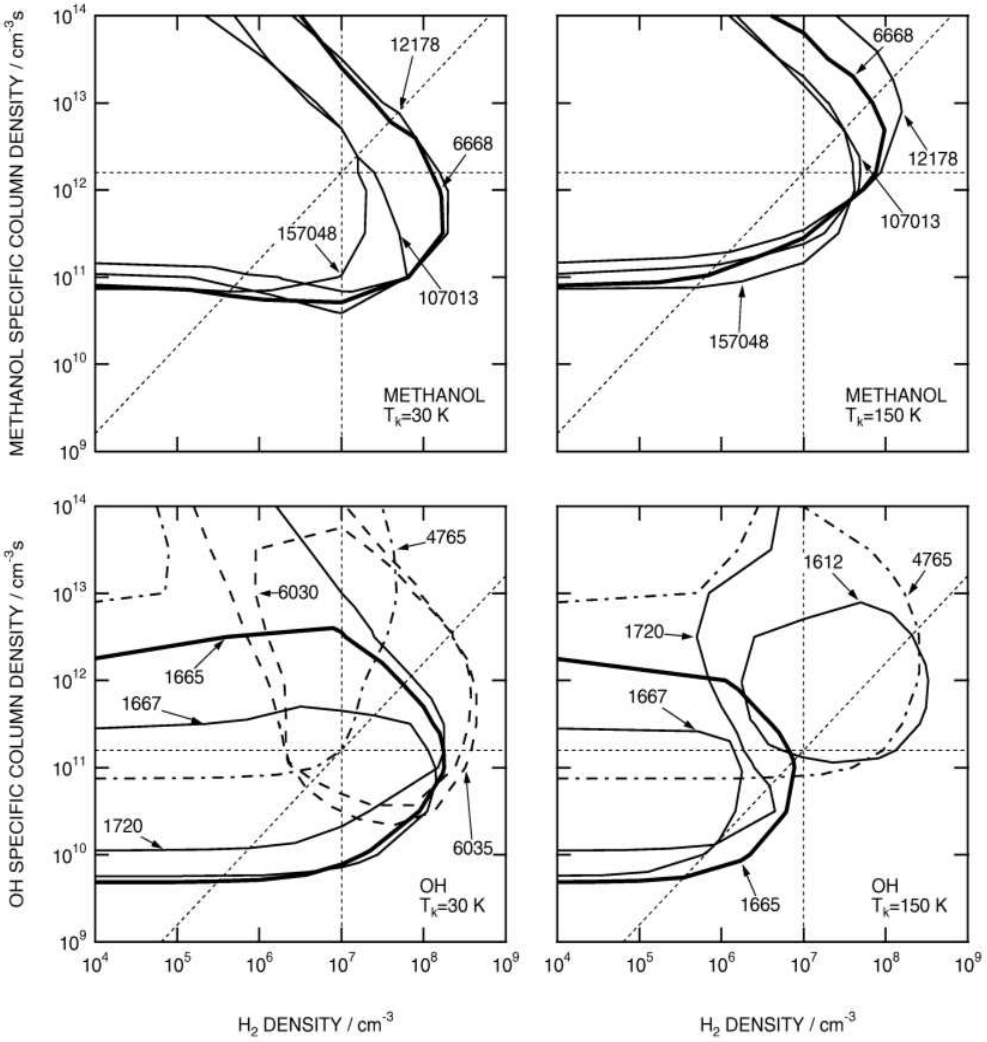

Figure 4.62: (Figure 1 from Cragg et al. (2002)). Contour diagram showing regions where selected masers of methanol and OH become active, as a function of hydrogen density n_H and specific column density of the maser molecule N/ΔV, for T_k =30 K (left-hand panels) and T_k =150 K (right-hand panels). Contours are labelled with the line frequency in MHz. For each maser a single contour representing a brightness temperature of 10^4 K is drawn, with no masers appearing above this threshold in the bottom right regions of the plots.

densities of $10^{8.0}$ cm^{-3}. The 6035 MHz masers may be tracing sources that are still relatively cool but very dense. Density and temperature observations of both samples, with and without ex-OH masers, are required to investigate this further.

4.9.4 A Possible Evolutionary Scheme

As discussed in Chapter 1, finding an absolute evolutionary indicator for a massive forming star through maser emission is the ultimate Holy Grail. There exist several evolutionary models. The most recent is from Breen et al. (2010) (Figure 4.63). It is understood that 6668 MHz methanol masers pinpoint extremely young regions of massive star formation (Walsh et al. 2003; Purcell et al. 2006b). Where exactly the ex-OH and OH masers fit in is in itself evolving. Garay and Lizano (1999) argued that OH masers are associated with an advanced stage of formation of a UC HII region, with models of these regions by Elitzur and de Jong (1978) theorising that the OH masers form in the compressed shell between the shock and the ionization fronts around the HII region. However, whilst OH masers may be found around a more advanced stage of a UC HII region, most OH masers are found to be not associated with UC HII regions (Caswell and Haynes 1983a). More recently, OH masers have been observed in much earlier evolutionary stages with 6668 MHz methanol maser (Edris et al. 2005, 2007; Hutawarakorn et al. 2002; Hutawarakorn and Cohen 1999), confirming that the OH masers are indeed found at early stages of massive stellar evolution.

We know that 6668 MHz methanol masers are associated with the hot core phase, the predecessor to the UC HII region, and the ex-OH maser is associated with 60% of the methanol masers (within 2″), so how does the ex-OH maser fit into this scenario? Is the ex-OH maser a transient phase in all massive star forming regions? Or, is the presence of an ex-OH maser from an enhancement in a physical property?

From the GLIMPSE three colour images, we see that similar numbers of ex-OH masers

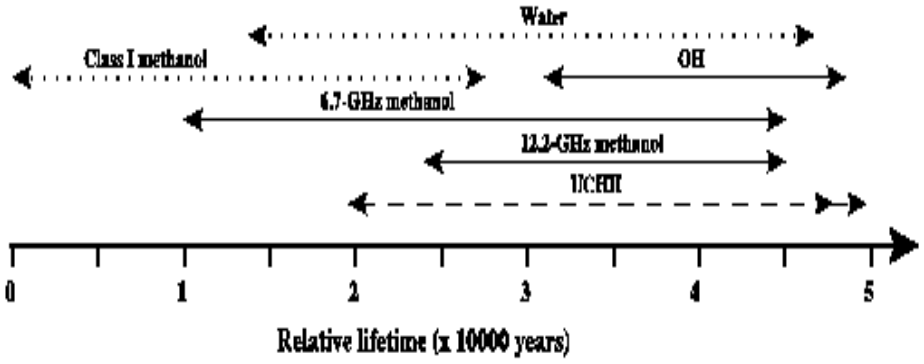

Figure 4.63: Figure from Breen et al. (2010), showing the relative lifetime of Class I and II methanol, OH and water masers along with a UC HII appearance.

are associated with the very early evolutionary stages of MSF (the IRDC stage where the star has not yet ioinised its surrounding region), as there are associated with a bright GLIMPSE source without a methanol maser. These two groups number 20 and 21 respectively, whilst there are 32 objects that have a bright GLIMPSE source with a methanol and ex-OH maser present. So, we have observed 6035 MHz ex-OH masers in the very early, mid and later evolutionary stages of the formation of a massive star, marked not only by the increasing brightness of the GLIMPSE source, but by the presence of the methanol maser at the IRDC and mid stage and its absence due to it being quenched by the growing ionization field.

Classification	Number
IRDC with ex-OH and/or methanol maser	20
Bright GLIMPSE source with ex-OH and methanol masers	32
Very bright GLIMPSE source OH masers only, methanol maser offset	21
Unclassified	7
Total	80

Table 4.17: The 6035 MHz ex-OH maser associations with different stages of protostellar evolution.

This conclusively proves that the ex-OH maser is not a transient phase in all massive star forming regions, but limited to a select few and outliving the 6668 MHz methanol maser as the central source evolves. This result infers there may be a physical or chemical significance to the sources which have both ex-OH and methanol masers, and this work provides the two samples of sources, those with and without ex-OH masers to investigate this theory.

5

The Class I Survey

We have performed the first unbiased survey of Class I methanol masers. This survey allows identification of the objects without any targetting bias applied by previous surveys, which have used IRAS sources, UC HII regions, and other maser species as targets. An unbiased survey for Class I masers will allow us to determine the relationships between these astrophysical objects and Class I masers. The relationship between Class I and Class II methanol masers is of particular interest as recent observational work has shown that the initial class grouping may not be entirely correct.

For these reasons the first unbiased survey for Class I methanol masers was undertaken. A region of 0.92 sq degrees was mapped for the 44 GHz Class I methanol maser, around the l = 30° and b = 0° region in the Galactic Plane, and a smaller region of 0.20 sq degrees was mapped for the 36 GHz Class I methanol maser. The survey was carried out using the 7 mm receiver on the Mopra Telescope in Australia. There were 25 detections of 44 GHz masers, 21 are new detections and 7 36 GHz maser detection, all new.

5.1 Class I and Class II Methanol Masers

As discussed in Chapter 1, the methanol masers are grouped into two emperical classes. The Class I masers, including the 36, 44 and 95 GHz transisitions are offset from centres of star formation (UC HIIs, H_2O masers). The Class II masers, the 6.7 and 12 GHz transisions are associated with known centres of star formation, close to OH and H_2O maser emission and FIR emission. The difference in the classes is explained by the way the masers are pumped. Class I masers are collisionally pumped (Voronkov et al. 2006; Kurtz et al. 2004) and Class II masers are radiatively pumped, hence close to the central source (Cragg et al. 2002).

5.2 Previous Class I Methanol Maser Surveys

Only a small number of surveys for Class I methanol masers have been conducted. An interesting survey performed by Ellingsen (2006) targeted Class II 6.7 GHz methanol masers for Class I 95 GHz masers. The GLIMPSE colours of the exciting sources of the Class II masers were compared to those which had Class I and Class II methanol masers. It was found that those sources with Class I masers present had redder GLIMPSE colours than those with just Class II masers. The redder colours imply the source is more deeply embedded, hence at an earlier evolutionary stage. From this Ellingsen (2006) inferred that sources that have Class I and Class II methanol masers present are younger than those with just Class II masers. However the result is based on a small trial sample.

The best way to investigate the relation between Class I and II methanol masers and their relationship with star formation are unbiased surveys. Many unbiased surveys of Class II 6.7 GHz masers have been and are currently underway, such as the Tourun survey (Szymczak et al. 2002), Arecibo survey (Pandian et al. 2007), Parkes and

ATCA surveys (Caswell 1996) and the ultimate: Methanol Multibeam survey which is surveying the entire Galactic plane in $0° < l < 360°$, $|b| \leq 2°$ (See Chapters 3 & 4; (Green et al. 2009a)). To date only a few unbiased surveys of small regions for Class I masers have taken place (Slysh et al. 1994; Kurtz et al. 2004; Pratap et al. 2008).

A recent unbiased survey of molecular clouds for Class I masers has been carried out by Pratap et al. (2008), at the Haystack Observatory. Several molecular clouds believed to contain regions of massive star formation were surveyed for 36 and 44 GHz Class I maser emission. This resulted in new areas of high mass star formation being identified within the clouds. Class I masers indeed appear to be tracing the youngest sources. In addition, evidence suggested that the ratio of the strength of the 36 GHz line to that of the 44 GHz line decreases as a source evolves. This trend fits with current models for the excitation of Class I masers. As a source forms the 36 GHz maser appears first, as it is excited in regions with temperatures < 100 K. As evolution continues the 44 GHz transition switches on, which is excited over a broader range of temperatures, 80-200 K (Voronkov et al. 2005). As the temperature increases and the source evolves, the 36 GHz maser is quenched leaving the 44 GHz maser still masing.

Pratap et al. (2008) found that sources where the 36 GHz maser line intensity was significantly (>5 times) greater than the 44 GHz maser, the source does not have any near IR or cm radio continuum emission indicative of massive star formation. In sources where the 44 GHz line emission is significantly stronger than the 36 GHz this emission is observed, suggesting that these sources are more evolved. This supports the theoretical work of Voronkov et al. (2006) which states that the 36 GHz methanol maser appears below 100 K and the 44 GHz appears between 80-100 K, so the 36 GHz appears at earlier stages and the 44 GHz continues masing upwards to 200K even when the 36 GHZ is quenched.

A recent survey of 44 and 36 GHz methanol masers towards bipolar outflows by Kalen-

skii et al. (2010) has detected three 44 GHz masers. These detections are all towards low mass star forming regions, the first detections of these masers in low mass star forming regions.

Unbiased surveys are necessary to fully explore the relationship between the methanol maser transitions and star formation. Hence, we have preformed the first complete unbiased survey for 44 GHz Class I methanol masers in the Galactic plane.

Figure 5.1: The spatial distribution of the 44 and 36 GHz masers. The red box shows the area surveyed for the 44 GHz masers and the dotted green boxes show the areas surveyed for 36 GHz masers

5.3 The Class I Survey: Telescope Characteristics

The Class I survey was carried out using the 22 m Mopra telescope, which is operated remotely from Narrabri at the ATCA site. For the Class I observations the 7 mm band

covering 30-50 GHz was used. Table 5.1 shows its parameters. The mm receivers transmit the 8 GHz broadband signal by broadband analogue fibre optic links to the MOPS spectrometer. The 8 GHz IF is split into 2.2 GHz channels (maximum of 4 2.2 GHz channels) and down converted to the base band. Each 2.2 baseband IF signal is digitised by a 2-bit 4.4 Gsample/sec Iridium Phosphide digitiser. MOPS provides a choice of wideband or zoom mode configuration (Figure 5.2). Each 2.2 GHz broadband channel can be broken up into a maximum of 4 zoom bands. A single zoom band has a 137.5 MHz bandwidth and 2 x 4096 channels (for the right and left polarisations). For the Class I observations the zoom modes were used. Using the zoom mode it was possible to observe 16 zoom bands for the 44 GHz observations and 15 for the 36 GHz observations.

For the 44 GHz observations it was possible to observe CS(J=1-0) at 48.99 GHz, simultaneously using the zoom bands. CS is a dense gas tracer associated with star formation. The CS observations provided a very useful comparison with the 44 and 36 GHz masers and will be subject to its own dedicated publication in 2010. For the 36 GHz observations, 15 zoom bands were observed.

Due to system limitations, it is not possible to observe the 36 and 44 GHz frequencies simultaneously. As the 44 GHz methanol maser is more prevalent than the 36 GHz methanol maser, it was decided that the full region would be observed for the 44 GHz maser first; this resulted in a limited number of mapping observations for the 36 GHz.

5.3.1 The Survey Region

The region selected for this survey is centred around $l = 30^\circ$ and $b = 0^\circ$. This region was previously observed with the Tourun telescope (Szymczak et al. 2002) to search for 6.7 GHz Class II methanol masers. It was more recently resurveyed by the Methanol

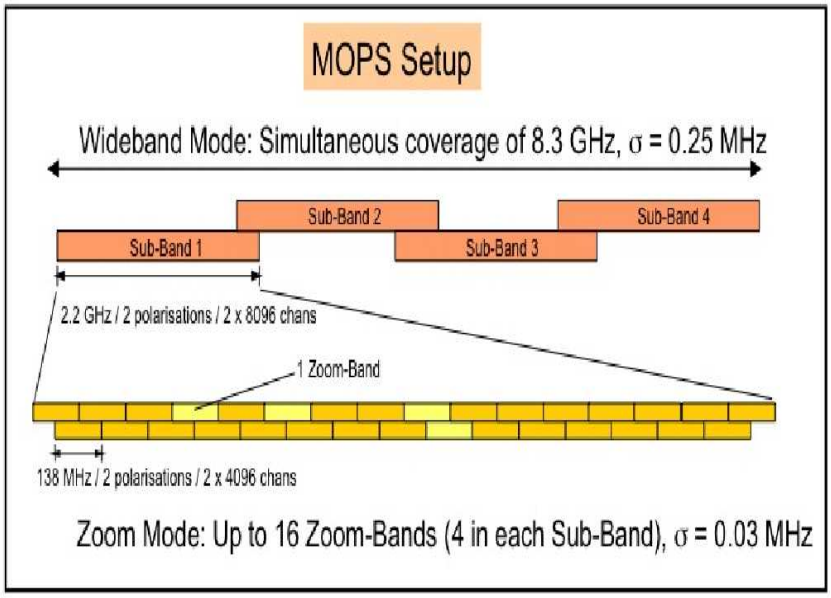

Figure 5.2: Description of the MOPS spectrometer capabilities

Frequency band	30 - 50 GHz
Central Observing frequency	42 GHz
Beamwidth (FWHM)	82″
Average T_{sys}	~200 K
Antenna Efficiency	~0.5

Table 5.1: Average Parameters for the Mopra Receiver

MultiBeam Survey (MMB) (See Chapters 3 & 4; Green et al. (2009a)). The observed region was picked due to the large concentration of Class II 6.7 GHz methanol masers observered from the above surveys, of which there are thirty-five. A large number of Infrared Dark Clouds (IRDC), 217, have been identified in the observed region by Peretto and Fuller (2009). The area encompasses the well studied massive star forming region W43, at a distance of 5.5 kpc from the Sun (Motte et al. 2003).

On-the-fly mapping observations of the 44 GHz methanol maser were conducted with the Mopra 22 m telescope on October 1 to 11, 2008 and again in January 11 to 15,

2009. The MOPS backend was configured to simultaneously observe 16 spectral lines in the frequency range from 42 GHz to 50 GHz including the 44.069476-GHz $7_0 \rightarrow 6_6$ A^+ transition of methanol, the CS J=1-0 transition at 48.990957 GHz and the SiO J=1-0 transition at 43.423864 GHz. Each line was covered by a section of the backend with a witdh of 138 MHz and a channel width of 33.7 kHz, giving a velocity coverage $\sim \pm 200$ km s^{-1} with a channel width of ~ 0.25 km s^{-1} for each of the lines. At these frequencies the beamsize of the telescope is $\sim 1'$.

The survey region was mapped in thirty-three $10' \times 10'$ sized blocks of Galactic longitude and latitude covering the region $29.75^\circ \leq l \leq 31.75^\circ$ and $0.27^\circ \leq b \leq 0.27^\circ$, giving a total area of 0.92 sq. deg. These were initially scanned in longitude and those with the poorest noise were also subsequently scanned in latitude. Each of the mapped blocks consists of a series of rows, at the end of each row a single pointed 'off' position was observed several arcminutes away. The 'off' positions were initially determined to be devoid of any target emission.

Similar mapping observations of the 36.169240 GHz $4_{-1} \rightarrow 3_0$ E transition of methanol were carried out between January 11 to 13, 2009. Due to limited observing time these covered two contiguous regions mapping a total of only 7 of the $10' \times 10'$ blocks observed at 44 GHz. These blocks were chosen to have the highest concentration of 44 GHz masers. The first 36 GHz region mapped at 36 GHz covered $29.58^\circ \leq l \leq 29.75^\circ$, $-0.27^\circ \leq b \leq 0.06^\circ$. and the second $30.45^\circ \leq l \leq 30.98^\circ$, $|b| \leq 0.10^\circ$ (Figure 5.1).

A second epoch of data was taken on March 23^{rd} 2010 using the Mopra telescope. Pointed observations of twenty-three 44 GHz masers (out of the 25 detected) were carried out with the same setup as above.

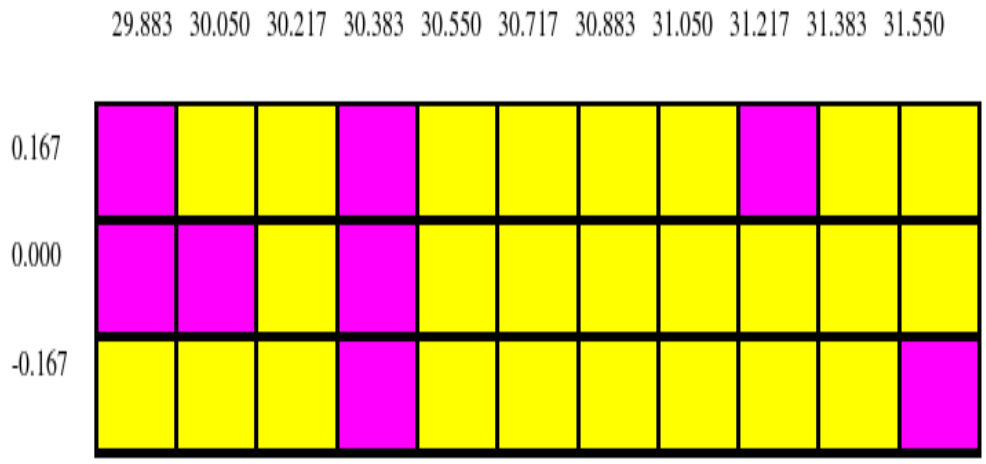

Figure 5.3: The region of the Galactic Plane scanned for the Class I survey. The yellow blocks were observed in a longitudinal scanning direction, the pink blocks were observed in a longitudinal and latitudinal direction.

5.3.2 Data Reduction and Source Detection

As the Class I data was processed using the same packages as the Parkes MMB data (see Chapter 2). The Class I data is at a higher frequency than the MMB data, it is in the 7 mm range which is notoriously difficult to flux density calibrate due to a lack of calibration sources at this frequency.

Several adjustments were made to the Livedata and Gridzilla inputs, namely the frequencies, channels, velocity coverage and beamwidth. Tables 5.2 and 5.3 below summarise the Livedata and Gridzilla inputs.

The data was gridded into two large cubes and a third small cube covering the center of the divide, to ensure no masers are lost due to the edge. As with the data reduction, the same source detection program was also utilised for the spectral line data.

Livedata Settings	Mopra - Class I
IFs	7, 16
Channels	0 - 4096
Mask	0-100; 3996-4096
Flux density calib.	No

Table 5.2: Livedata Parameters for the Class I Survey

Gridzilla Settings	Mopra - Class I
Velocity range	-200 - 200 Km/s
IF 7 (methanol)	44069.476 MHz
IF 16 (CS)	48990.957 MHz
Beamwidth	1 arcmin
FWHM	0.7 arcmin
Cutoff radius	0.7 arcmin

Table 5.3: Gridzilla Parameters for the Class I Survey

Adjustments were made to the input of the program in line with the properties of the Class I data. As the Class I methanol masers are generally of a narrower width than the Class II 6668 MHz methanol masers and the 6035 MHz ex-OH masers, the detection parameters were adjusted after testing. The final inputs used represent a balance between detecting the weakest masers and returing too many false-positives. Two input parameters of the source detection program were adjusted. The first was the number of consecutive channels above the threshold to be considered a detection; this parameter was set as 2 channels. The second parameter changed was the detection threshold, in units of RMS in the spectra, which was lowered to 4.5. The adjustments were made by running the detection program on one piece of the data and changing the parameters to ‘detect’ the known and visually detected masers in the data. Table 5.4 shows the source detection inputs.

-a = 2	Averaging: The number of consecutive spectral channels that will be averaged to check for broad emission
-c= 2	The number of spectral channels that should be above the threshold to be considered a detection
-t = 4.5	A detection threshold in terms of RMS in the spectra
-p = 1	Minimum number of pixels in an image
-d =1	Minimum distance in pixels between peaks of different line ranges to split the source in two.
-r	All velocity ranges will be present in the programs output (default)
-s	Produces spectra of the detections (default)

Table 5.4: Source Detection Program Parameters for the Class I data

5.4 Results

A region of 0.92 sq degrees was mapped at 44 GHz in which 25 sources where detected. In the case of the 36 GHz observations, a combined area 0.20 sq. degrees was observed, resulting in the detection of 7 sources. The parameters of the sources, named by their Galactic coordinates, are listed in Tables 5.5 and 5.6. In addition to the peak positions of the sources, the tables include the peak line intensity, the velocity of the peak emission, the RMS noise level in the spectrum and the velocity range of the emission in the data cubes. In addition the table indicates whether the source corresponds

Source (l,b)	RA (J2000)	Dec (J2000)	Flux Density (Jy)	Peak Vel (km/s)	Start Vel (km/s)	End Vel (km/s)	Line Range (km/s)	RMS (Jy)	Known/New	Distance (kpc)	6.7 GHz Methanol Present
G29.86+0.07	18:45:35.55	-02.42.02.8	3.81	-26.33	-26.89	-24.65	2.24	0.9	New	-	N
G29.87-0.03	18:45:57.87	-02.44.20.5	5.84	99.73	99.24	101.46	2.22	0.96	New	5.56	Y
G29.91-0.04	18:46:05.08	-02.42.27.5	363.64	98.58	98.09	99.8	1.71	0.96	Known[1]	5.5	N
G29.93-0.07	18:46:11.38	-02.42.09.0	12.03	98.58	97.62	100.08	2.47	1.01	New	5.48	N
G29.93-0.20	18:46:40.76	-02.45.54.3	6.81	-95.32	-96.2	-94.84	1.36	1.36	New	-	N
G29.96-0.02	18:46:03.87	-02.39.12.8	5.69	96.52	95.55	100.2	4.64	0.90	Known[2]	5.4	Y
G30.22-0.20	18:47:11.39	-02.30.26.5	9.62	104.77	103.87	106.02	2.15	1.62	New	5.98	N
G30.32+0.07	18:46:25.35	-02.17.48.1	6.49	45.41	44.31	46.6	2.29	1.35	New	2.98	Y
G30.42-0.24	18:47:41.78	-02.20.34.0	10.79	105.02	102.54	108.34	5.79	1.33	New	5.92	Y
G30.57-0.03	18:47:14.58	-02.06.58.2	9.19	87.58	86.5	89.58	3.07	1.36	New	4.98	N
G30.60+0.17	18:46:35.04	-01.59.56.2	8.19	105.69	104.39	108.78	4.39	1.31	New	6.00	N
G30.70-0.07	18:47:36.89	-02.01.15.3	22.03	89.87	88.26	96.24	7.98	0.86	Known[3]	5.1	Y
G30.71-0.08	18:47:39.15	-02.00.42.1	25.59	91.93	88.04	99.00	10.96	0.79	New	5.31	Y
G30.72-0.08	18:47:41.81	-02.00.29.1	53.21	91.93	90.57	97.48	6.90	0.94	New	5.2	N
G30.79+0.20	18:46:48.57	-01.49.10.1	56.25	82.54	80.56	85.48	4.92	1.92	New	4.74	Y
G30.81-0.05	18:47:44.52	-01.54.47.8	19.38	95.14	92.86	103.03	10.17	0.78	New	5.39	Y
G30.81-0.06	18:47:46.97	-01.54.40.9	36.82	97.21	94.11	104.39	10.27	1.26	Known[4]	5.49	N
G30.84-0.08	18:47:55.05	-01.54.01.9	5.86	98.58	96.53	100.99	4.46	0.91	New	5.58	N
G30.87+0.16	18:47:06.17	-01.45.31.4	7.84	35.09	32.53	38.69	6.16	1.36	New	2.43	N
G30.92+0.09	18:47:26.33	-01.45.00.9	32.73	94.23	92.5	95.33	2.83	1.14	New	5.34	N
G31.12+0.02	18:48:04.26	-01.36.23.4	10.25	36.72	35.52	37.43	1.91	1.31	New	2.51	N
G31.28+0.06	18:48:13.15	-01.26.34.4	10.69	107.06	105.45	114.5	9.05	2.15	New	6.23	Y
G31.49+0.17	18:48:12.39	-01.12.08.8	10.31	103.85	103.08	106.43	3.35	1.94	New	6.01	N
G31.58+0.07	18:48:42.44	-01.10.05.8	10.95	95.83	92.52	100.26	7.75	1.61	New	5.48	Y
G31.59-0.13	18:49:25.19	-01.15.00.7	9.42	33.95	32.92	35.32	2.41	1.11	New	2.35	N

Table 5.5: 44 GHz methanol masers detected in the Class I survey.

[a]Val'Tts and Larionov (2007)
[b]Molinari et al. (1998)
[c]Walsh et al. (1997)
[d]Val'Tts and Larionov (2007)

Source (l,b)	RA (J2000)	Dec (J2000)	Flux Density (Jy)	Peak Vel (km/s)	Line Range (km/s)	RMS (Jy)	New/Known
G29.88-0.04	18:45:59.9	-02:44:02.8	12.63	99.38	1.77	0.89	New
G29.92-0.05	18:46:05.8	-02:42:16.4	21.85	98.26	2.93	1.03	New
G29.94-0.07	18:46:12.6	-02:41:43.9	4.43	99.10	2.12	0.58	New
G30.61+0.04	18:47:03.9	-02:03:04.5	5.61	146.29	2.33	0.92	New
G30.70-0.08	18:47:37.8	-02:01:16.9	11.23	92.96	18.46	1.1	New
G30.72-0.08	18:47:42.0	-02:00:21.3	30.71	91.56	12.07	1.3	New
G30.82-0.06	18:47:47.2	-01:54:33.2	42.02	98.26	13.01	1.27	New

Table 5.6: 36 GHz methanol masers detected.

to a previously known Class I methanol maser, within 30″ (Walsh et al. 1997; Molinari et al. 1998; Val'Tts and Larionov 2007). Spectra of the 44 GHz and 36 GHz methanol lines towards the sources are shown in Figures 5.4 and 5.6. All of the 36 GHz and 20 (out of 25) of the 44 GHz sources have corresponding CS emission. Figure 5.7 shows the histogram of the velocity difference between the CS and methanol. The velocities are very similar with a median difference of -0.4 km $s^{-1}$and the largest difference being -2.7 km s^{-1}(Figure 5.8).

Comparing the CH_3OH and CS emission, shows the CS lines to be relatively Gaussian in profile and presumably, due to its high dipole moment, tracing the dense gas along the line of sight. On the other hand, the CH_3OH spectra are often dominated by very narrow spikes with widths comparable to, or less than, the resolution of the observations. In some sources, e.g. G30.22-00.20, the CH_3OH emission is confined to a single such spike, while towards other sources, e.g. G31.26+0.06, there is CH_3OH emission over a velocity range comparable to the CS, the CH_3OH emission has spikes that are not present in the CS. The presence of bright narrow spectral features is diagnostic of maser emission (Menten 1991). Interestingly the ratio of the intensity of spike feature

to the broader emission varies significantly between sources, although all the sources, with the possible exception of the 36 GHz emission towards G030.82-0.06, show some evidence of spiky (maser emission). In total three of the sources detected at 44 GHz (G30.81-0.06, G30.81-0.05, G30.69-0.07) and two detected at 36 GHz (G30.72-0.08, G30.82-0.06) have line widths greater than the $\sim$ 1km s^{-1} is typically observed in Class I masers (Menten 1991). However, interferometric observations of Class I masers by Kurtz et al (2004) and Cyganowski et al. (2009) show that the Class I masers comprise multiple clustered spots and it is possible that at higher spatial resolution observations of G30.82-0.06 (and the broader velocity components towards the other sources) many decompose into multiple, spatially distinct, narrow, maser spots.

Out of the twenty-five 44 GHz masers detected, 23 were re-observed with pointed observations 17 months later. We found that a significant number of the masers varied, 15 (65%) of the masers showed variation in the shape of the profile and also in some cases variation in intensity (Table 5.7). The biggest variation occurred in G30.72-0.08, which has gone from a several peaked source with a peak flux density of 30 Jy to a four peaked source with peak flux density over 70 Jy. The peak velocity remains consistent in both observations. The variations in the masers consist of emerging and disappearing maser peaks. A similar variation occurred in G30.70-0.08, initially it has an almost thermal appearance, with a cluster of $\sim$13 maser peaks, when re-observed, the peak at 90 km s^{-1} has now tripled in intensity and several of the peaks have since vanished, the peak velocity remains constant. In G30.43-0.24, the intensity of two strongest peaks have switched, hence the peak velocity has switched. There are 8 masers which has remained stable in profile and intensity when they were re-observed.

A selection of the maser spectra are displayed in Figure 5.9, the rest are in Appendix 3.

Source (l,b)	Flux Density (Jy)	Peak Vel (km/s)	Line Range (km/s)	RMS (Jy)
G29.87-0.03	9.03	99.7	3.88	0.43
G29.91-0.04	332.57	98.47	2.61	0.58
G29.93-0.07	12.09	99.46	5.11	0.48
G29.96-0.02	6.27	97.34	4.35	0.44
G30.22-0.20	5.75	104.86	2.95	0.44
G30.32+0.07	9.04	45.52	2.02	0.63
G30.42-0.24	11	106.65	5.85	0.46
G30.57-0.03	8.83	87.63	1.79	0.65
G30.60+0.17	8.89	105.75	1.61	0.53
G30.70-0.07	28.87	89.92	7.48	0.45
G30.71-0.08	41.19	91.97	4.89	0.3
G30.72-0.08	72.79	91.9	5.56	0.58
G30.79+0.20	66.36	82.56	4.43	0.4
G30.81-0.05	27.39	97.32	10.45	0.71
G30.81-0.06	36.6	97.23	10.33	0.28
G30.84-0.08	8.47	97.62	1.99	0.35
G30.87+0.16	5.19	34.83	3.55	0.46
G30.92+0.09	32.62	94.18	2	0.22
G31.12+0.02	8.82	36.62	1.54	0.69
G31.28+0.06	8.87	109.52	5.83	0.41
G31.49+0.17	9.8	103.73	2.18	0.54
G31.58+0.07	14.27	95.66	5.28	0.47
G31.59-0.13	5.31	34.02	2.88	0.55

Table 5.7: The second epoch of the 44 GHz methanol masers.

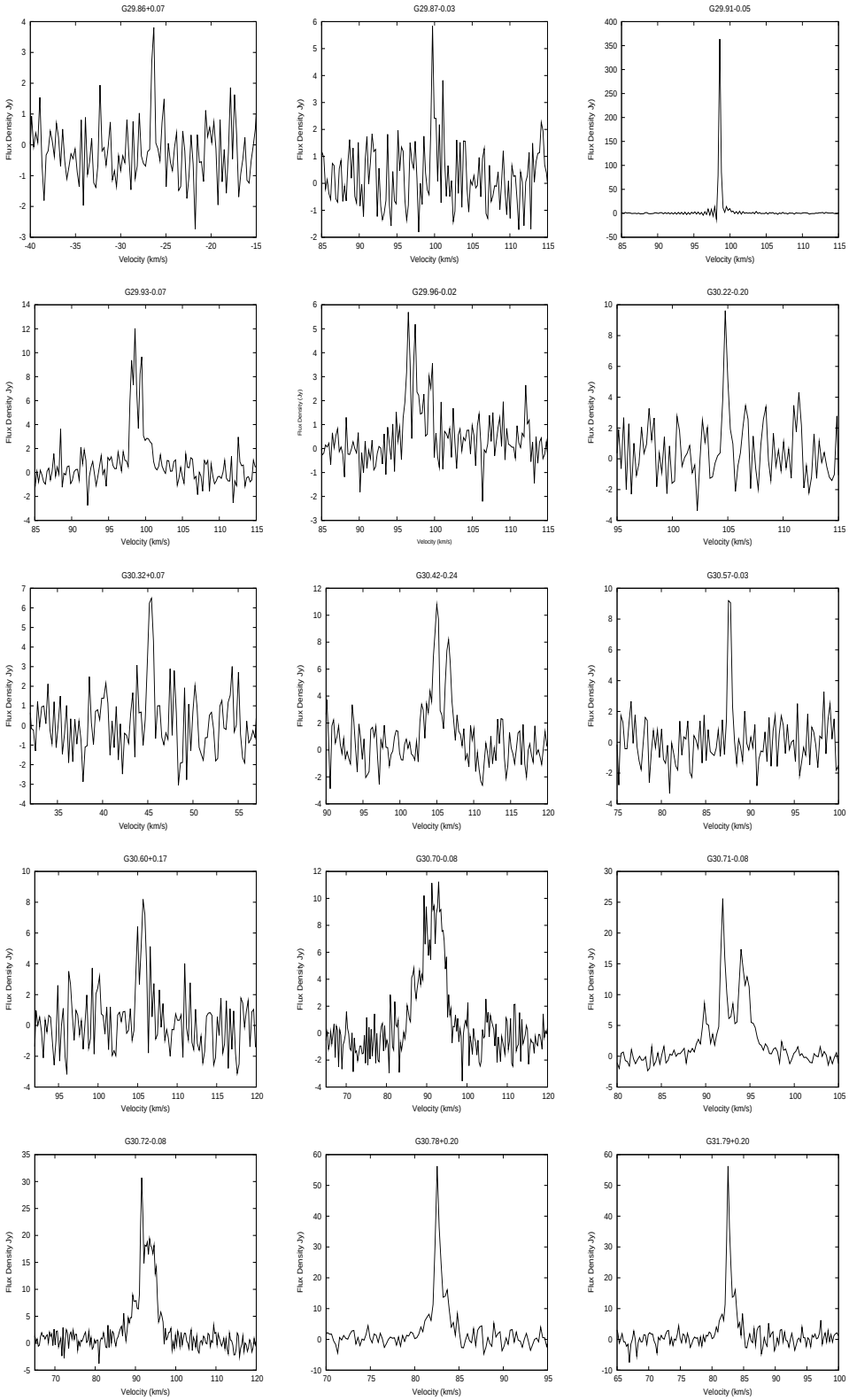

Figure 5.4: The spectra of the 44 GHz methanol masers detected.

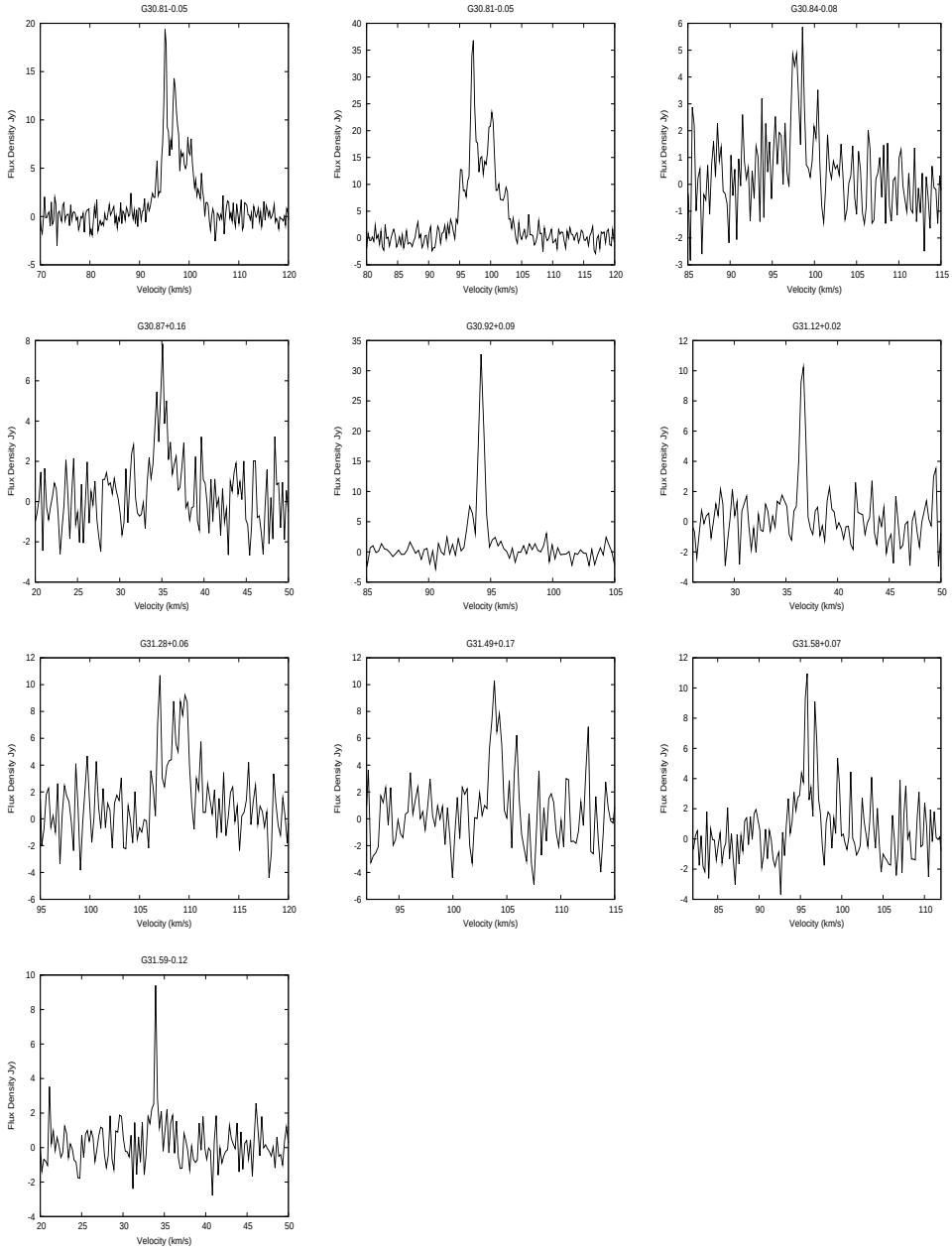

Figure 5.5: The spectra of the 44 GHz methanol masers detected (continued)

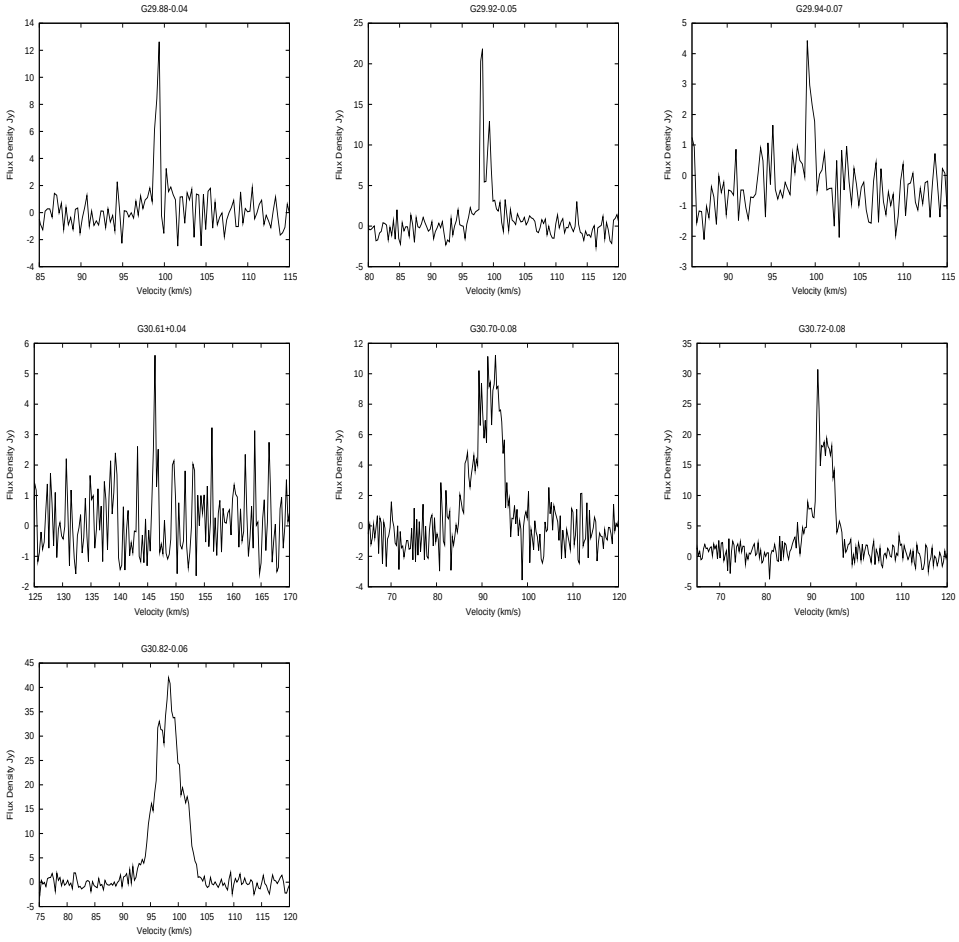

Figure 5.6: The spectra of the 36 GHz methanol masers detected.

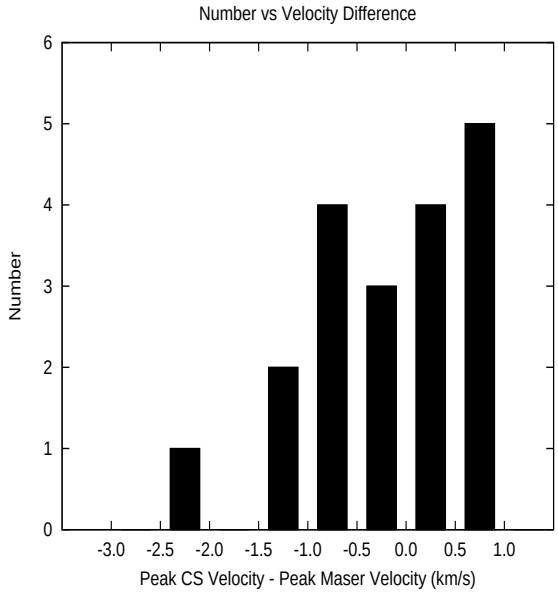

Figure 5.7: Histogram of the difference in the velocity peaks of the 44 GHz methanol and the CS gas.

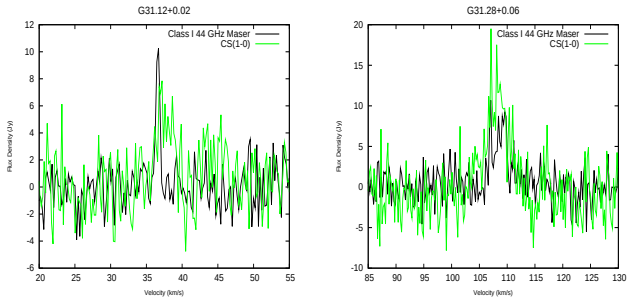

Figure 5.8: Two 44 GHz methanol masers (in black), overlayed with the CS(1-0) emission at the same location (in green). Note the close alignment of the peak velocities.

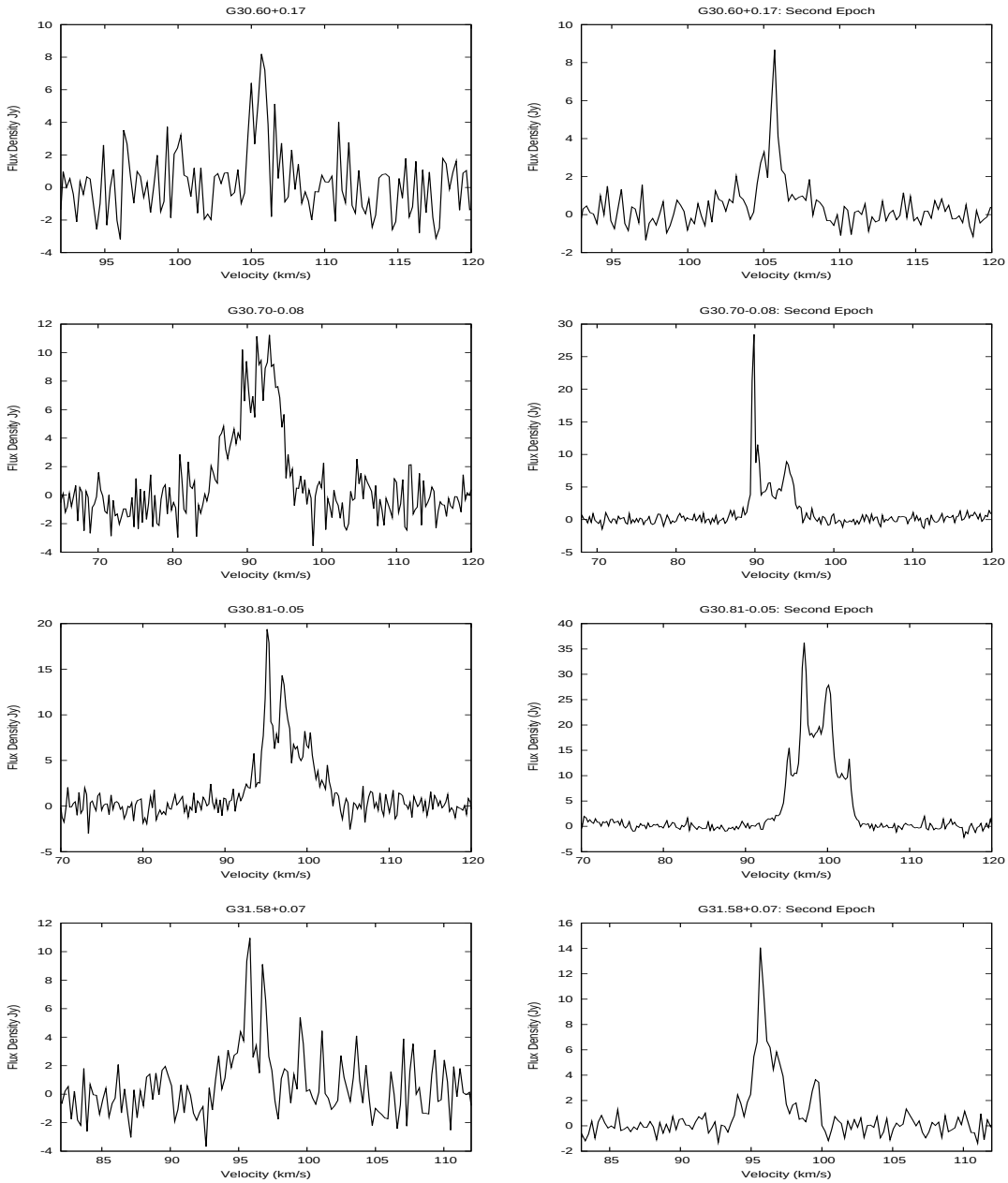

Figure 5.9: The spectra of the 44 GHz methanol masers from the Class I survey. On the left are the spectra from Oct 2008, on the right from March 2010. The top maser, G30.60+0.17, shows variation in its profile shape. G30.70-0.08 shows magnificaent variation in spectral profile and flux density, it initially looked like thermal emission, but it may be seen from the reobservation, that it is a large cluster of 44 GHz maser spikes. Third down, G30.81-0.05 displays an increse in flux desnsity and its profile shape, not as many peaks are visible in the March 2010 observations, giving it an almost thermal appearance. On the bottom, G31.58+0.07 displays a flus density increase in its stongest peak, the second strongest peak has almost disappeared.

5.5 The Nature of the Sources

Below we compare the Class I masers to various other tracers to help establish the nature of the masers and the sources exciting them.

This section includes a full investigation of the 44 & 36 GHz masers within the limiting resolution of the single dish observations. A comparison of the peak maser velocity will be made with the peak of the CS gas velocity (observed simultaneously, see section 2). The Class I maser positions will be compared to the IRAS sources, Class II 6.7 GHz methanol masers and the Infrared Dark Clouds (IRDCs) (Peretto and Fuller 2009) in the region.

5.5.1 44 & 36 GHz Class I Methanol Masers

An initial question is whether the 44 GHz and 36 GHz emission are associated with each other. The estimated uncertainty in the peak positions of the emission is 15″, based on 2-D Gaussian fits to the integrated intensity images of each source detected. Six of the seven 36 GHz masers are within 36″ of a 44 GHz source. Of course at the likely multiple-kpc distance to these sources a separation of several tens of arcseconds could indicate that the masers are tracing (are excited by) different embedded sources, and a full and detailed comparison must await higher angular resolution observations. Nevertheless, we conservatively, class these six 36 GHz sources as associated with corresponding 44 GHz emission. In the model proposed by Pratap et al. (2008) the presence of maser emission in only the 36 GHz methanol transition indicates an extremely young protostellar object, and so a potentially very young and very interesting source.

5.5.2 Class I and Class II Methanol Masers

There are 35 Class II 6.7 GHz masers in the surveyed region (priv. comm. G. Fuller; Green et al. (2009a)). There are ten 44 GHz methanol masers are within 60″ of a Class II 6.7 GHz methanol maser, which corresponds to 40% of the Class I masers being associated with Class II maser sources. Restricting the separation range to 20″ only 5 of the 44 GHz masers are associated with Class II masers. Val'Tts and Larionov (2007) find that 72% of their sample of Class I masers are associated with a Class II 6.7 GHz methanol maser (using a maximum separation of 120″). This significant difference may be explained by the fact that previous searches for Class I masers have targeted selected sources, often Class II methanol masers. Our survey shows that such targeted surveys towards known Class II masers misses a significant population of Class I masers. This is similar to the situation for surveys of Class II masers (Green et al. 2009a).

Conversely, we find that 14% of the Class II masers in the survey region are associated (within 20″) with Class I masers. This compares with Ellingsen (2005) who found a 38% detection rate for 95 GHz Class I masers towards Class II methanol masers. Ellingsen (2007) suggested an evolutionary sequence where the younger protostellar objects are traced by Class I masers, followed by Class II. If this is the case then the present survey is detecting a high number of very young protostellar objects.

5.5.3 IRAS Comparison

The InfraRed Astronomical Satellite (IRAS) carried out an unbiased all sky survey at 12, 25, 60 & 100um. There are 115 IRAS point sources in the surveyed region. A statistical analysis performed on a catalogue of known Class I masers by Val'Tts and Larionov (2007) resulted in 76% of the Class I masers having an association with an IRAS source where they defined association as a 2′ separation. Using a more realistic separation value of 45″ we find that only 24% of the 44 GHz Class I masers detected

here are associated with an IRAS source. This difference is likely due to our small association radius.

There are 217 infrared dark clouds in the Spitzer derived catalogue of Peretto and Fuller (2009) within the survey region. These cold, dense regions are thought to be the sites of the formation of stellar clusters and massive stars. There is no clear one-to-one correlation between the clouds and the masers: some of the methanol masers are clearly associated with dark clouds, while others are not. More detail can be seen in the three colour images in Figure 5.10.

5.5.4 GLIMPSE Comparison

GLIMPSE is a legacy program of the Spitzer Space Telescope, that surveyed much of the Galactic plane at 3.6, 4.5, 5.0 & 8.0 μm at a resolution of 1.4-1.9″ (Benjamin et al. 2003). Comparison of these methanol observations with GLIMPSE potentially allows us to identify the sources or types of sources exciting the maser, however the resolution difference between GLIMPSE and the observations presented here needs to be kept in mind.

There are 18,915 GLIMPSE sources in the surveyed region, using the 2007 release of the GLIMPSE point source catalogue. The [3.6]-[4.5] vs. [8.0] colour-colour distribution and the [3.6]-[8.0] vs. [3.6]-[5.8] distribution of these sources are shown in Figure 5.11. The sources within 15″ of the 44 GHz masers are also shown. The [3.6]-[4.5] vs.[8.0] plot does not display any distinguishing colours for 44 GHz masers as they mostly lie in the main body of sources. Interestingly, in the [3.6]-[8.0] vs. [3.6]-[5.8] colour-colour plot, where the 44 GHz masers are represented by the green squares, we can see that there are four 44 GHz sources with extreme colours well above the other sources. As we now know the 44 GHz masers are variable, the other extreme sources in this region may harbour other 44 GHz masers that were not detected in the main survey due to variation.

Three colour GLIMPSE images centred on the maser peak position and 60″ in size (equal to the Mopra primary beam size) were constructed using the 3.6 m, 4.5 m and 8.0 m bands. These were inspected to try to identify the possible sources exciting the masers. A sample of these images are displayed in Figure 5.12.

As can be seen in Figure 5.12 a and b, and also in several other fields, there are multiple sources to which the 44 GHz Class I maser could be associated, pressing the need for higher resolution observations. On the other hand, Figure 5.12 c, d and e show that a targeted search for Class I masers based on GLIMPSE point source colours would miss a significant amount of masers, as discussed above, as these images show very little possible objects for the Class I masers to be associated with.

Figure 5.12f shows a 36 GHz maser position, this image shows no sign of bright mid-infrared emission. This particular maser, G29.88-0.37, does not have any 44 GHz maser or 6.7 GHz Class II methanol maser present. All of the other 36 GHz masers have a 44 GHz maser within 36 arcseconds. In Figure 5.12b an Extended Green Object (EGO) is visible. A recent survey by Cyganowski et al. (2009) targeted 19 EGOs, selected from the catalogue of Cyganowski et al. (2008b), for Class I 44 GHz and Class II 6.7 GHz methanol masers using the VLA. Outflow tracers HCO^+(3-2) and SiO(5-4) were also observed towards the selected objects. From the sample, 90% (17/19) of the 44 GHz Class I masers are associated with the selected EGOs. They find the 6.7 GHz Class II methanol masers line up with the centers of EGOs and 44 GHz Class I masers tend to surround the edges of the EGO emission. These observations support the theory that 44 GHz masers are located at the interface of the outflow and the surrounding ambient medium. It is to early to tell if we find the same results in the majority, but the GLIMPSE images show that targeting EGOs for 44 GHz masers would miss a significant population of these masers.

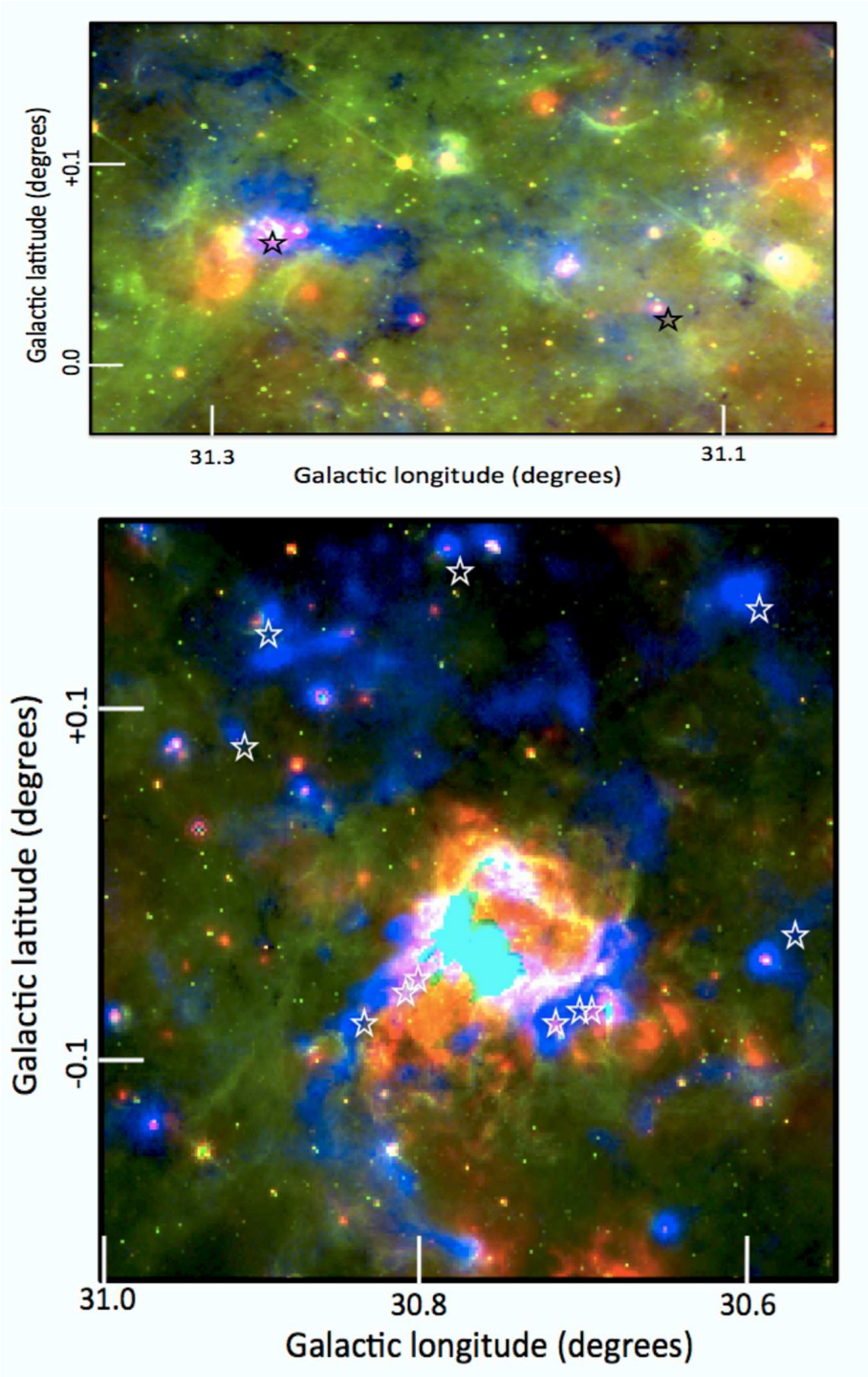

Figure 5.10: The three colour images of two regions containing the majority of the 44 GHz sources. The 8μm and 24μm Spitzer GLIMPSE and MIPSGAL are shown as red and blue respectively and the 1.1mm BOLOCAM continuum emission in blue. The stars mark the position of the 44 GHz methanol sources.

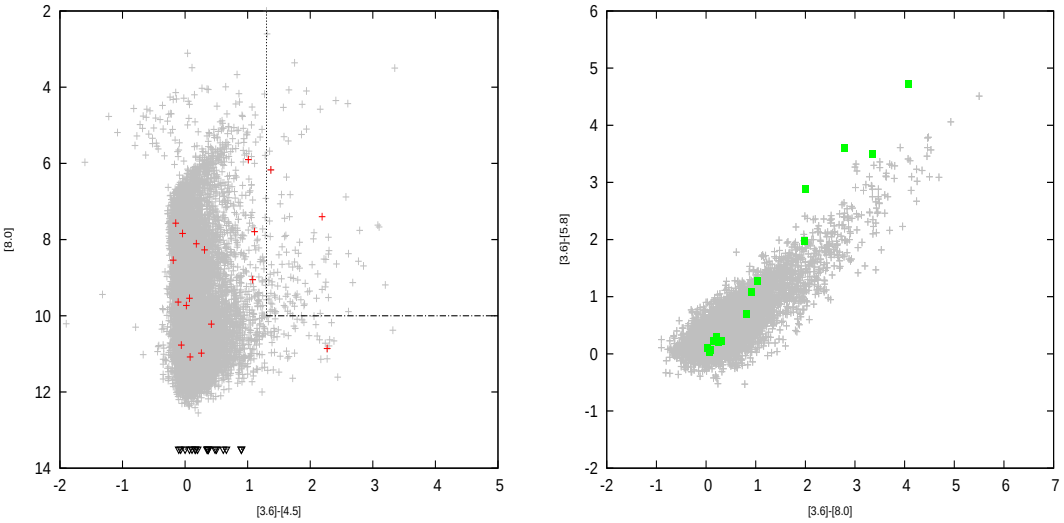

Figure 5.11: -

[4.5] vs.[8.0] & [3.6]-[8.0] vs. [3.6]-[5.8] colour-colour plots for the Class I region.]On the left:Colour-colour diagram [3.6]-[4.5] vs.[8.0] of all the GLIMPSE point sources in survey region (grey crosses) and of the GLIMPSE sources within 15 arcseconds (red crosses) of a 44 GHz maser detected in the survey, the black triangles represent the lower [3.6]-[4.5] limits. The black lines represent the colour-colour constraints devised by Ellingsen (2006), to target massive star forming regions with 6.7 GHz methanol masers. On the right: [3.6]-[5.8] vs.[3.6]-[8.0] of all the GLIMPSE point sources in survey region (grey crosses) and of the GLIMPSE sources within 15 arcseconds (green squares) of a 44 GHz maser detected in the survey. The four most extreme colours in this plot are associated with 44 GHz methanol masers.

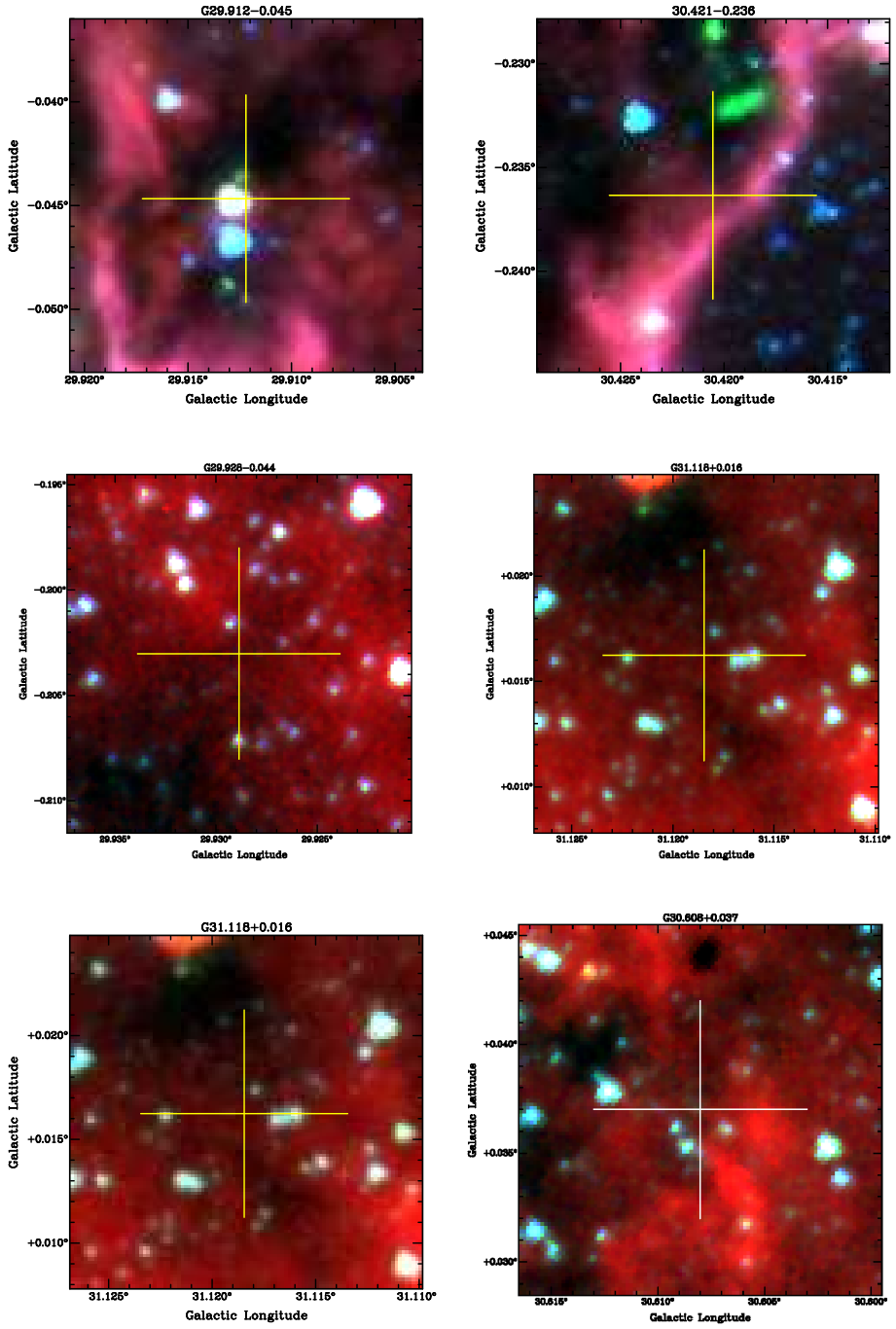

Figure 5.12: The three colour 3.6, 4.5 and 8.0 micron GLIMPSE images with the yellow crosses marking the 44 GHz methanol masers and white marking the 36 GHz maser, from top right to left: a, b, c, d, e, f.

5.5.5 The Exciting Sources SEDs

The spectral energy distributions (SEDs) were constructed for 12 of the twenty-five 44 GHz masers in the survey. If a maser could be identified as associated with a nearby (up to 15″) Bolocam 1.2mm source then an SED was constructed for that source. The bolocam camera is situated on the Caltech Submillimeter Observatory (CSO) in Hawaii. However, if the maser position was close to several Bolocam sources, making a probable identification impossible, an SED was not constructed - which was the case for 13 of the twenty-five 44 GHz masers. There were three flux densities used: 24 micron MIPS Band 1, 70 micron MIPS Band 2 and 1.2 mm Bolocam. It was not possible to use the 8 micron data as the fields were too confused, especically as it has the highest resolution. An aperture ranging from 40-50 arcseconds was used to calculate each of the flux densities, with the same aperture used for each source. The distances were calculated from the rotation curve of Reid et al. (2009) derived from maser parallaxes. The online SED fitter of (Robitaille et al. 2007) was used to calculate the SEDs using the flux densities, aperture, distances and an interstellar A_v range of 10 - 1000. The measured fluxes for the sources, together with their derived luminosities are given in Table 5.8. The luminosities are the average of the top ten model fits.

Figures 5.13 and 5.14 show the measured fluxes together with the best fit SEDs. All of the SEDs are well fit by the (Robitaille et al. 2007) models. The models return several values for the source, the luminosity being the most useful. From the luminosities the SEDs provide we can clearly see a divide, those of high and low luminosity. We believe the source with the lowest luminosity, G31.59-0.13, to be a low mass star forming region.

44 GHz Maser	8 micron	24 micron	70 micron	1.2 mm	Distance	Luminosity	6.7 GHz Methanol Maser
	IRAC Band 4	MIPS Band 1	MIPS Band 2	Bolocam	kpc	$L_\odot$	Present
G30.32+0.07	0.01*	0.1	4.12	0.25	2.98	268	Y
G30.42-0.24	0.01*	0.29	31.61	0.31	5.92	6588	Y
G30.57-0.03	1.65	1.54	80.23	0.37	4.98	7456	N
G30.60+0.17	0.09	0.37	16.9	0.90	6.00	2106	N
G30.72-0.08	0.63	1.35	32.82	2.04	5.20	3987	Y
G30.79+0.20	0.06	1.62	22.7	0.91	4.74	1476	Y
G30.92+0.09	0.26	0.2	2.1	0.18	5.34	509	N
G31.12+0.02	0.37	0.7	6.27	0.41	2.51	207	N
G31.28+0.06	2.76	2.14	133.61	2.82	6.23	12380	Y
G31.49+0.17	0.55	0.61	2.24	0.15	6.01	456	N
G31.58+0.07	0.62	2.18	52.91	1.15	5.48	4628	Y
G31.59-0.13	0.14	0.05	5.39	0.16	2.35	203	N

Table 5.8: The 8, 24, 70 micron and 1.2 mm flux densities for the 12 possible masers, all in mJy. The $*$ denotes an upper limit.

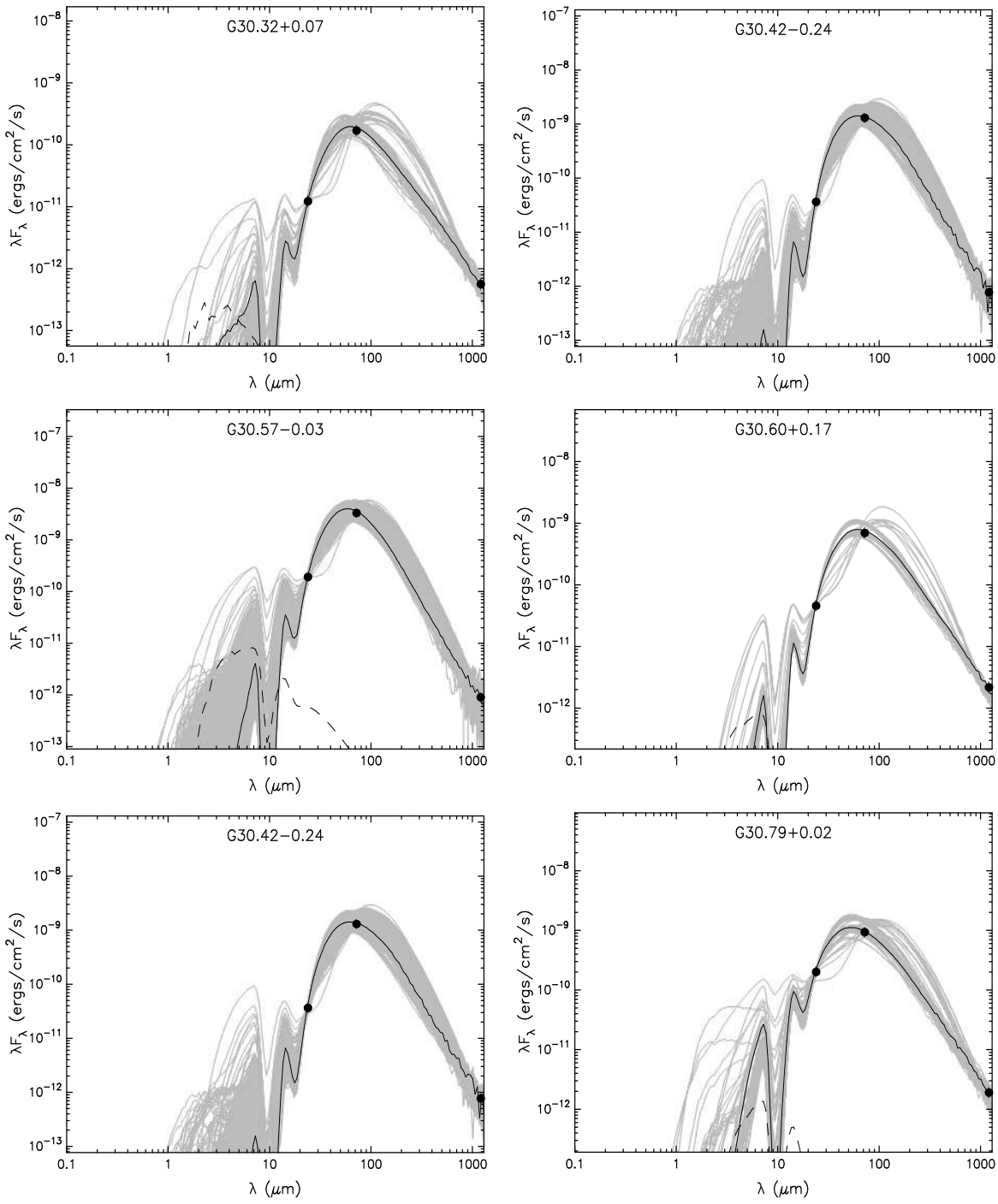

Figure 5.13: Spectral energy distribution of 6 of the sources. The filled circles show the measured fluxes. The black line shows the best fit, and the gray lines show subsequent good fits. The dashed line shows the stellar photosphere corresponding to the central source of the best fitting model, as it would look in the absence of circumstellar dust (but including interstellar extinction).

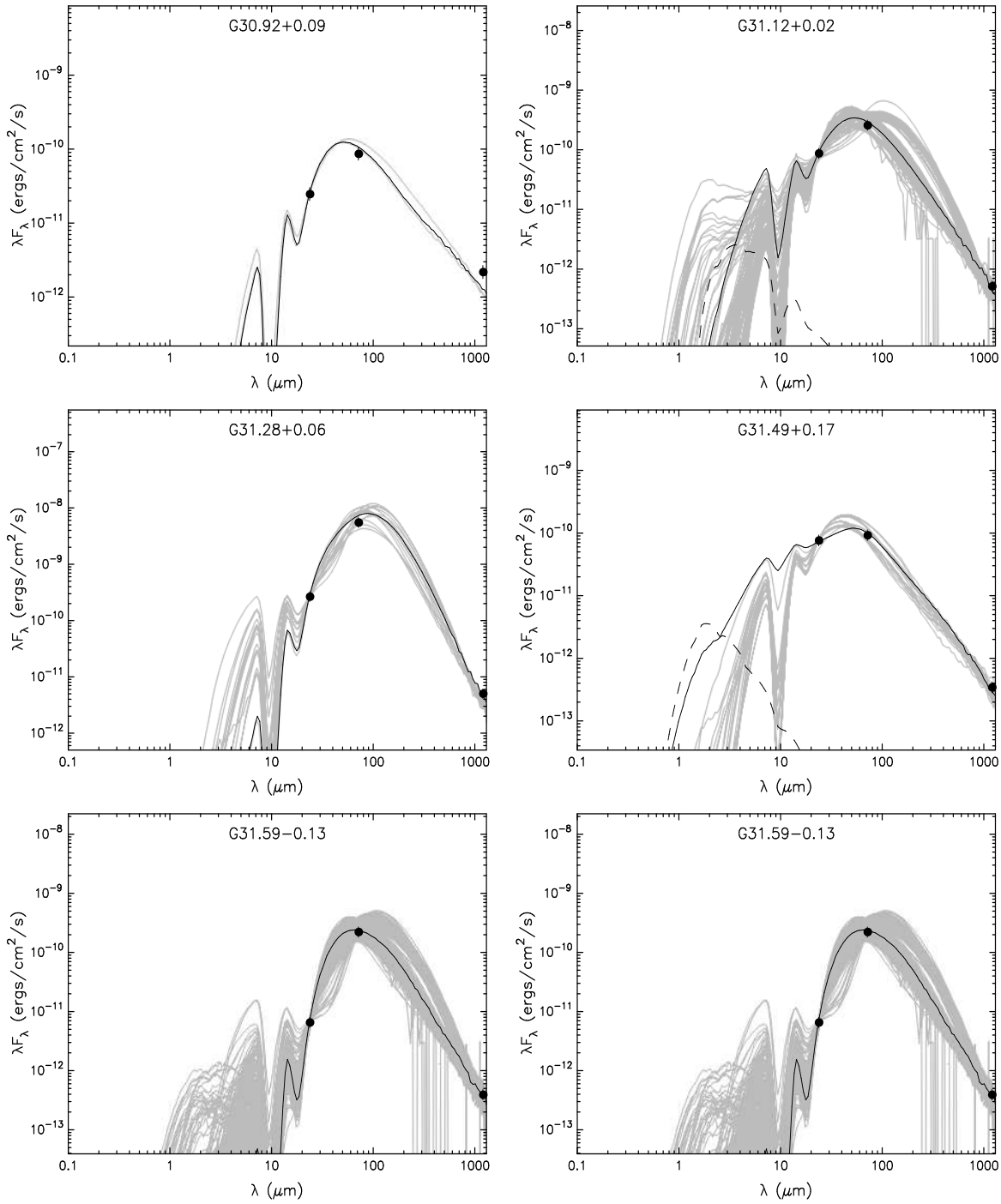

Figure 5.14: SEDs of the remaining 6 sources. The filled circles show the measured fluxes. The black line shows the best fit, and the gray lines show subsequent good fits. The dashed line shows the stellar photosphere corresponding to the central source of the best fitting model, as it would look in the absence of circumstellar dust (but including interstellar extinction).

5.5.6 44 GHz Masers in High and Low Mass Star Formation

Kalenskiĭ et al. (2006) searched known low mass star formation sites for 44 GHz masers . They detected 44 GHz methanol maser emission in three of the six low mass sources, with flux densities not exceeding 10.7 Jy. This may explain the non detections in the previous surveys by Bachiller et al. (1990); Kalenskii et al. (1992), since the previous searches had sensitivities of ∼10 Jy, which may have been insufficient to detect the masers.

Kalenskii (2010) targeted young bipolar outflows of low to intermediate mass star formation for 44 GHz and 36 GHz Class I methanol masers. Their observations detected four 44 GHz masers and 1 separate 36 GHz maser with flux densities no higher than 11 Jy.

In this survey, we have identified four masers which we believe to be in low mass star forming regions. The four masers identified are G30.92+0.09, G31.12+0.02, G31.49+0.17 & G31.59-0.13. All of these sources have luminosities $\leq$ 500 $L_{\odot}$, calculated from the SEDs and these Class I masers are not associated with a 6.7 GHz methanol maser. Three of the four GLIMSPE images constructed (see GLIMPSE comparison section 5.5.4) for these sources also lack any obvious signs of star formation. It should also be noted that there may be more 44 GHz masers associated with low mass star forming regions in the group for which an SED was not possible to construct.

5.5.7 Relation of Masers to Outflows

Class I masers are hypothesised to be collisionally pumped. Plambeck and Menten (1990) first suggested, followed by Johnston et al. (1992), Kurtz et al. (2004) and Voronkov et al. (2006), that the Class I methanol masers (95, 25 & 44 GHz) were associated with outflows, from the alignment of the maser spots with shock tracers H_2 and SiO. And recently, Kalenskii et al. (2010) detected 3 44 GHz and 1 36 GHz

methanol masers towards young bipolar outflows. From observational and theoretical studies, the 44 GHz maser occurs at the edges of the interaction of the outflow and the surrounding medium.

The maser spots of Voronkov et al. (2006) correlated well with the H_2 shocked gas. The velocity of these maser spots were compared to the ambient medium and found to be a close match. The masers in this complete Class I survey are compared to the CS(1-0) gas which is a tracer of the ambient gas, observed simultaneously (see section 2). Figure 5.7 shows CS peak velocity minus the 44 GHz maser peak velocity, the maximum difference is -2.7 and the median is -0.3 km/s. Obviously this result determines the masers location, observations and comparisons with shock tracers would be necessary for this. However, it is worth nothing that an object thought to be at the edge of an outflow would have a comparable velocity to the ambient medium.

5.6 Summary

The first unbiased survey for 44 GHz Class I methanol masers has detected 25 sources, 21 of which are new detections. A smaller survey for 36 GHz Class I methanol masers was carried out in the regions of the highest density of 44 GHz masers, resulting in 7 new 36 GHz methanol masers being detected.

A second epoch of data was obtained for 23 of the 25 44 GHz maser detections 17 months after their initial detection. Whilst 35% of the masers remained stable in profile and intensity, 65% of the masers had profile and intensity variations, with some intensities doubling and some maser peaks emerging and disappearing.

One of the new 36 GHz masers, G29.88-0.37, does not have any 44 GHz maser or 6.7 GHz Class II methanol maser present. Pratap et al. (2008) postulate that the 36 GHz Class I maser is associated with a younger, less evolved protostar than an object

with both 36 & 44 GHz masers, making this object a potentially an extremely young stellar object, requiring significant follow-up observations.

There are thirty-five 6.7 GHz Class II methanol masers in the same region covered by the 44 GHz survey. 20% of the 44 GHz masers are associated with a 6.7 GHz methanol maser within 20″. Conversely, only 14% of the 6.7 GHz Class II methanol masers were associated with the 44 GHz Class I methanol masers within 20″.

Figure 5.11 shows the sources within 15″ of the 44 GHz masers are also shown. The [3.6]-[4.5] vs.[8.0] plot does not display any distinguishing colours for 44 GHz masers, as they mostly lie in the main body of sources. Interestingly, in the [3.6]-[8.0] vs. [3.6]-[5.8] colour-colour plot, where the 44 GHz masers are represented by the green squares, we can see that there are four 44 GHz sources with extreme colours are well above the other sources. As we now know, the 44 GHz masers are variable, the other extreme sources in this region may harbour 44 GHz masers too that were not detected in the main survey due to variability.

However, using IRAS sources, 6.7 GHz Class II methanol masers, GLIMPSE colours or EGOs as targets for the 44 GHz methanol masers will miss a significant population, making clear that unbiased surveys are necessary.

The 44 & 36 GHz masers have been detected in high and low mass star forming regions. From this unbiased survey we have identified four masers which we believe to be associated with low mass star forming regions based on their low luminosities (>509 L) derived from SEDs, their non-association with 6.7 GHz Class I methanol masers and their 3 colour GLIMPSE images.

6

ATLASGAL & The Clump Finding Algorithms

The process by which clouds are identified, in vatious datasets, is extremely important as the size of a cloud will be used to determine its mass and other physical parameters important to studying star formation. Not every algorithm is suitable for all data types. Hence, the four clump finding algorithms in the Starlink package have been tested to find the best one for identifying the clumps in ATLASGAL data.

This chapter consists of two parts. The first, the testing of the four clump finding algorithms: Clumpfind, Reinhold, Clumpfind and Fellwalker, in the Starlink package, on the APEX Telescope Large Area Survey (ATLASGAL) data. The second, the comparisons of the ATLASGAL data with the 6668 MHz methanol and 6035 MHz ex-OH masers around ±6° of the galactic plane.

6.1 ATLASGAL

ATLASGAL: APEX Telescope Large Area Survey: the GALaxy, first began observations in 2006 with the 12 m APEX telescope in Chile, providing an unbiased view

of star formation at submillimeter wavelengths. The survey aims to map the inner 100 square degree of the Galactic disk; +/-1° in latitude and -80° to +20° in longitude, with a uniform sensitivity of 50mJy/beam. The Atacama Pathfinder EXperiment (APEX) telescope is located on the Chajnantor plateau in Chile, high above sea level in a dry environment suitable for submillimeter observations. The APEX telescope and its receivers are a collaboration between the MPIfR Bonn, Onsala Space Observatory (OSO) and the European Southern Observatory (ESO). ATLASGAL uses the Large Apex BOLometer CAmera (LABOCA), consisting of 295 element bolometers observing at a wavelength of 870μm and a field of view of 11 arcmin. It was constructed by the Bolometer Development group at the MPIfR.

An initial shallow survey at 870μm is currently underway with plans for complementary observations at 350μm, 1.4 & 2 mm. Submillimeter continuum emission traces dust in the region of high molecular column densities such as dense star forming molecular clouds. As well as providing the first unbiased sample of massive cold dusty clumps in the Galaxy (in the submillimeter range), it also aims to derive column densities and spectral indices, compute the prestellar initial mass function and explore large scale structure of cold dust (Schuller et al. 2009).

To investigate how to best identify the molecular clouds in the ATLASGAL data we need to find the best clump finding algorithm, so the survey may be properly compared to other surveys and galactic sources. Hence, the four clump finding algorithms in the Starlink packages are analysed (http://www.starlink.ac.uk/).

6.2 Starlink Clump Finding Algorithms

Findclumps is a Starlink package which identifies clumps of emission within 1, 2 & 3-D (NDF) data files. The program contains four clump finding algorithms: Clumpfind, Gaussclumps, Reinhold, Fellwalker and has several outputs including: an output cata-

logue of the parameters of the clumps along with a log file detailing the progress of the algorithm and a pixel mask identifying pixels as background, clump or edge pixels.

The algorithms were tested on three areas of ATLASGAL as they represent different populations of emission:
G7.0+0.0: Galactic longitude 6.75 → 7.25 and latitude ±1,
G331.5+0.0: Galactic longitude -27.75 → -28.25 and latitude ±1.
G359.5+0.0: Galactic longitude -0.25 → -0.75 and latitude ±1,

6.2.1 Clumpfind

The Clumpfind algorithm was developed by Jonathan Williams and is described fully in Williams et al. (1994).
The main points of the algorithm are:
• The algorithm contours the data and separates it into clumps based on these contours.
• The program does not assume any clump profile
• Clumps never overlap.
• Clumps which touch the edge of the data array can be identified and removed.

Clumpfind contours the data starting at a level close to the peak value in the array and moving down to lower levels to a specified minimum. At each contour level all adjacent level-pixels above the contour level are detected and considered. If this set contains pixels which have not been identified at a higher contour level then they are deemed to be in a new clump. If the set contains pixels which have been assigned to another clump, it is extended to include them. If the set includes pixels that have been assigned to two different clumps, these pixels are divided between the clumps based on the distance to the closest pixel already identified by another clump, not the distance to a peak pixel. This is refereed to as the 'friends-of-friends' method. This method continues down to the lowest contour level although the clumps found at the lowest contour levels are ignored.

6.2.2 Reinhold

In this algorithm, developed by Kim Reinhold at Joint Astronomy Centre in Hilo.
The main points of the algorithm are:
• Mask of clump edges is produced.
• Edges are cleaned up using cellular automata.
• Clumps are filled.
• A second round of cellular automata is applied to reduce improved the edges.

The edges of the clumps are found by finding the peaks within a 1-d profile and following them down to the noise level or a local minimum set by the user. Once the initial identification of the clumps is made they then need to be cleaned as there may be holes in the edges or spurious pixels marked as edge pixels. The process of Cellular Automata (CA) is employed for this purpose. Each pixel is considered to be a central pixel in a 3x3 square of neighbouring pixels. First, the edge pixels are dilated using a CA algorithm: if a pixel is marked as an edge pixel then all the immediate neighbours of the edge pixel are also marked as edge pixels.

Secondly, the thickened edges are then eroded using another CA algorithm: if the number of neighbouring pixel edge pixels is greater than a certain threshold then the central pixel would be marked as an edge pixel. If the number of pixels surrounding the central pixel is less or equal to the threshold then it is discarded. This process can be applied repeatedly. Next the clumps are filled with an integer that identifies the associated peak. The use of CA in the first instance reduces the risk of holes in the edges but does not completely alleviate it.

If there are holes in the edges when the filling takes place, the filling may 'leak out' through a hole in the edge. Thus, another CA is used again once the clumps have been filled to reduce the artifacts created by the leaks. This CA replaces each clump identifier by the most commonly occurring clump identifier within a 2x2 square. The results of the cleaning process are the final clump allocations reported by the program in the final catalogue.

6.2.3 Fellwalker

The name of this algorithm was chosen as it provides a good comparison of the program with 'fell walking', due to the parallel between the contours of the 2-d data array

and the contours on a geographical map used by fell walkers.
The main points of the algorithm are:

- The algorithm takes a ‘walk up hill’ along the greatest gradient.
- At each step the algorithm considers its surrounding 3x3 pixels
- Algorithm stops at local maximum
- A round of cellular automata is applied to reduce the noise

The algorithm considers every data pixel in turn to start the ‘walk’ to a neighbouring pixel peak. Pixels which are below the specified background level are ignored, they are skipped over as are pixels which are already assigned to a clump. When a pixel is found above the background level and is not already assigned to a clump, the process begins: at each step the algorithm looks at a 3x3 pixel square around the starting pixel and decides which step would give the steepest gradient. The algorithm then moves to that pixel. The algorithm will eventually reach a local maximum; a point where all routes go downhill. To ensure this is not just a noise spike the algorithm widens its search (a pixel number specified by the user) to see if a pixel with a higher data value can be found. If so the algorithm ’jumps’ to the higher value pixel and continues on the ‘walk’. If a pixel with a higher data value is not found within the extended neighbourhood search the pixel is designated a peak and assigned a unique integer number. All the pixels visited along the walk are also assigned the integer.

If the algorithm is ‘walking up the hill’ and visits a pixel already assigned to a clump then the walk is terminated and all previous pixels are assigned to that clump. Once all the pixels in the data array have been considered another array is created which contains integer identities for the clumps. To reduce the effect of noise at the boundaries of the clump, a round of cellar automata is performed. It replaces each clump integer ID with the most commonly occurring ID in a 3x3 square. The amount of times the process can be repeated is set by the user. If the high data values in the clump form a plateau with slight undulations then the algorithm may create two separate clumps.

This is probably inappropriate, especially if the dips in the undulations are less than the dips in the noise. To avoid this issue the clumps are merged if the dip between them is less than the specified user set value. The results form the output catalogue.

6.2.4 Gaussclumps

This is based on the algorithm by Stutzki and Guesten (1990).
The main points of the algorithm are:
• It fits a Gaussian to the brightest peak and subtracts it.
• continues to fit Gaussians to the data until one of the criteria are met.
• Clumps may overlap so pixels are not assigned to a single clump.

The output data does not assign the pixels a clump index number, like the other three algorithms. Instead, each pixel contains the number of Gaussians fitted to it. The weightings values associated with each pixel are user defined, the most important being the beam FWHM, the velocity resolution and the clump threshold of the data.

6.3 Evolution of the Clumpfinding Process

During the initial testing a global rms of 0.05 Jy was used. This was unrealistic as the noise varies across the data, especially at the edges, where it is extremely noisy. Neither did this technique make use of the accompanying ATLASGAL rms file. We needed to incorporate the RMS file into the data file to take account of the varying noise. This was possible using several of the Starlink functions.

First the ATLASGAL rms file was squared and incorporated into the data file as the variance component. The data with the variance file was turned into a Signal-to-Noise Ratio (SNR) data array, taking the varying noise into consideration. This SNR data

file was used as a mask file. From visual inspection it was decided that anything above two sigma did warrant inclusion and anything below two sigma was probably noise. Such a drastic cut may in fact get rid of pixels which are part of a clump, in the form of extended emission or just having a randomly high noise spike. Hence the data was first smoothed with a symmetrical Gaussian PSF using a FWHM of 2 pixels. Next, all pixels above 2 sigma were given a value of 1 and those below a value of 0. The resulting output of this procedure is the mask file.

The mask file was multiplied by the original ATLASGAL data file, leaving all possible clumps with their real flux density values rather than sigma values. The final 'clipped' data file is used by the clumpfinding algorithms and global RMS of 0.05 is now validly used.

As Gaussclumps algorithm clumps do not have definite edges, a lower threshold is defined as 'bad', this produces a model which can be used as a mask to extract an area from the original data file.

6.4 Testing and Results

Several aspects of the clump finding results are analysed and discussed, the main are the number of clumps detected, the peak and sum intensities of the clumps, the areas covered by the clumps and most importantly, the visual inspections. Tables 6.1, 6.3, & 6.2 display the results, the values for SExtractor, used by MPIR Bonn are included where available.

The four algorithms provide varying results. Clumpfind consistently found the highest number of clumps, Gaussclumps and Reinhold the least and Fellwalker in the middle range. Figures 6.1 to 6.12 show the histograms of the number of clumps for each region from each algorithm, the distribution of the clump area defined by each algorithm

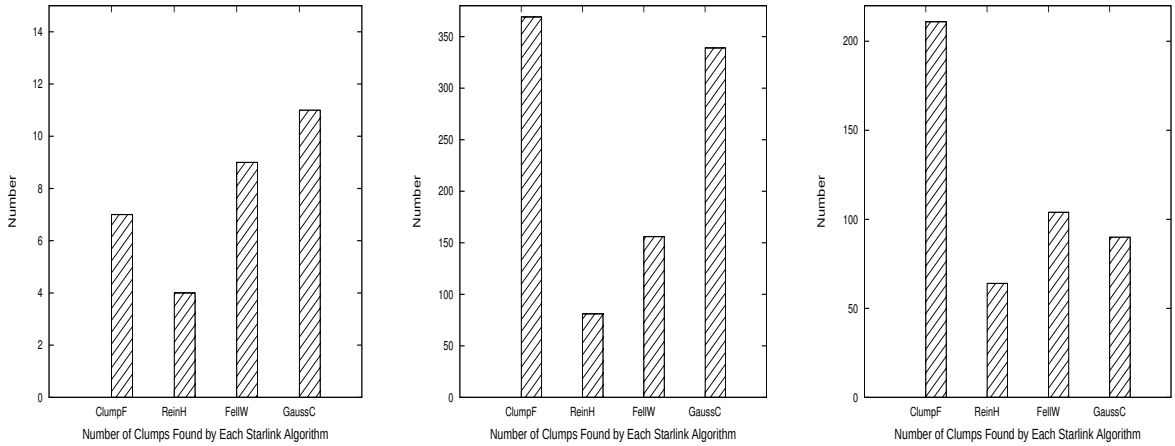

Figure 6.1: The number of clumps found, in G7.0+0.0, G359.5+0.0 and G331.5+0.0, by each Starlink algorithm in each region.

for each region, the number of clumps found by each algorithm for each region.

6.4.1 Region G7.0+0.0

This region does not offer a great deal of insight as there are so few clumps leading to small number statistics. However, the visual inspection of this region is most straightforward, it was also a useful region to see test if all the clumps were being picked up by the algorithms. Figure 6.2 shows the output of the algorithms and the data file

G7.0+0.0	Clumpfind	Reinhold	Fellwalker	Gaussclumps	SExtractor
No. of Clumps	7	4	9	11	20
Peak Pixel (Jy)	11.14	7.3	6.88	7.92	5.47
Peak Clump Sum (Jy)	216.87	208.5	215.72	186.8	
Average Clump Sum (Jy)	67.58	95.71	67.59	43.33	
Average Area (arcsec^2)	2677.44	3191.31	3336.86	3847.03	

Table 6.1: Comparison of results: G7.0+0.0

(Gaussclumps is not shown in the visual inspections due to a bug in the output files). Inspecting the images shows that Reinhold misses several clumps in the given sample and all the extended emission. Clumpfind picks up more clumps than Reinhold but still misses a few clumps. Fellwalker picks up all of the clumps and extended emission in this region. The results of SExtractor are included where possible. SExtractor is the algorithm used by MPIR on the ATLASGAL data.

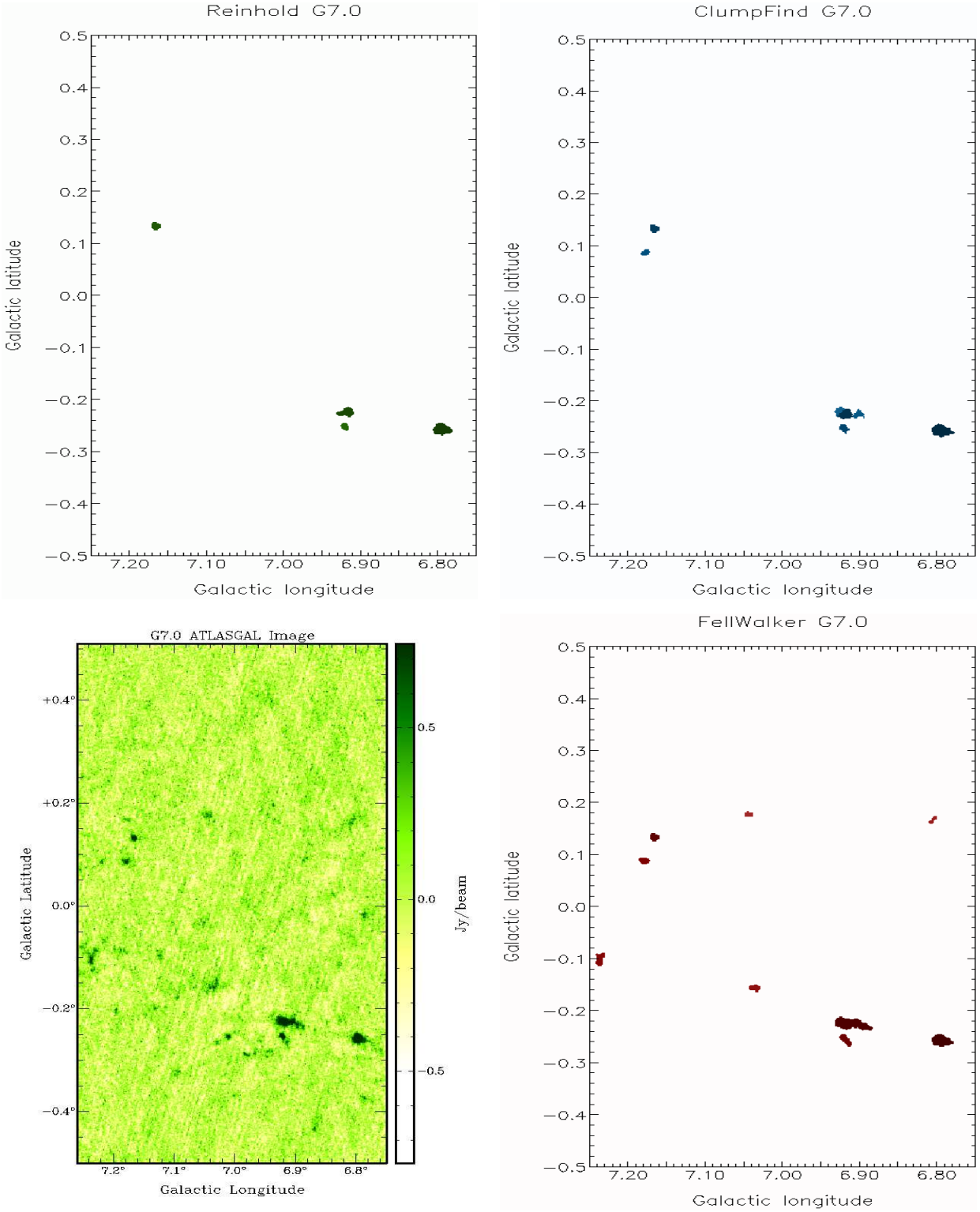

Figure 6.2: The outputs from Reinhold, Clumpfind and Fellwalker for G7.0+0.0, displaying where the clumps and emission was detected. The corresponding ATLASGAL 870μm image is also shown for comparison.

6.4.2 Region G331.5+0.0

This region has the most emission of all three. Here the clump area and flux density distribution are useful, Figures 6.3, 6.4 & 6.5.

Clump Area Distribution

G331.50+0.0	Clumpfind	Reinhold	Fellwalker	Gaussclumps	SExtractor
Clumps	211	64	104	90	169
Peak Pixel (Jy)	23.39	30.78	22.27	18.74	13.54
Peak Clump Sum (Jy)	756.62	607.99	1209.67	667.74	
Average Clump Sum (Jy)	39.99	74.3	90.41	71.23	
Average Area (arcsec^2)	2297.25	2884.72	6172.11	6020.68	

Table 6.2: Comparison of results: G331.50+0.0

Reinhold detects clumps across the range of areas. It peaks in the lower range of 2000 arcsec^2. Clumpfind peaks in the 2000 arcsec^2 range, it fails to detect many large (> 6000 arcsec^2) area clumps. Gaussclumps appears to find the opposite of Clumpfind, it peaks in the higher 4000 arcsec^2 range whilst it is devoid of any clumps in the 1000 and 2000 arcsec^2 bins. Fellwalker peaks in the higher area range at 10,000 arcsec^2, it also detects many clumps across the range including the 2000 arcsec^2 bin.

Flux Density Distribution

Reinhold peaks in the lower flux density scale at 0-25 Jy, also detecting several higher flux density clumps as well. Clumpfind also peaks in the low 0-25 Jy range of the flux density distribution. It detects very few clumps above > 150 Jy. Gaussclumps peaks in the 50 Jy range, but follows the Reinhold and Clumpfind by not finding very many clumps above > 150 Jy. Fellwalker too peaks in the 0-25 Jy range, but it appears well balanced and detects the most clumps at the higher end of the flux density scale.

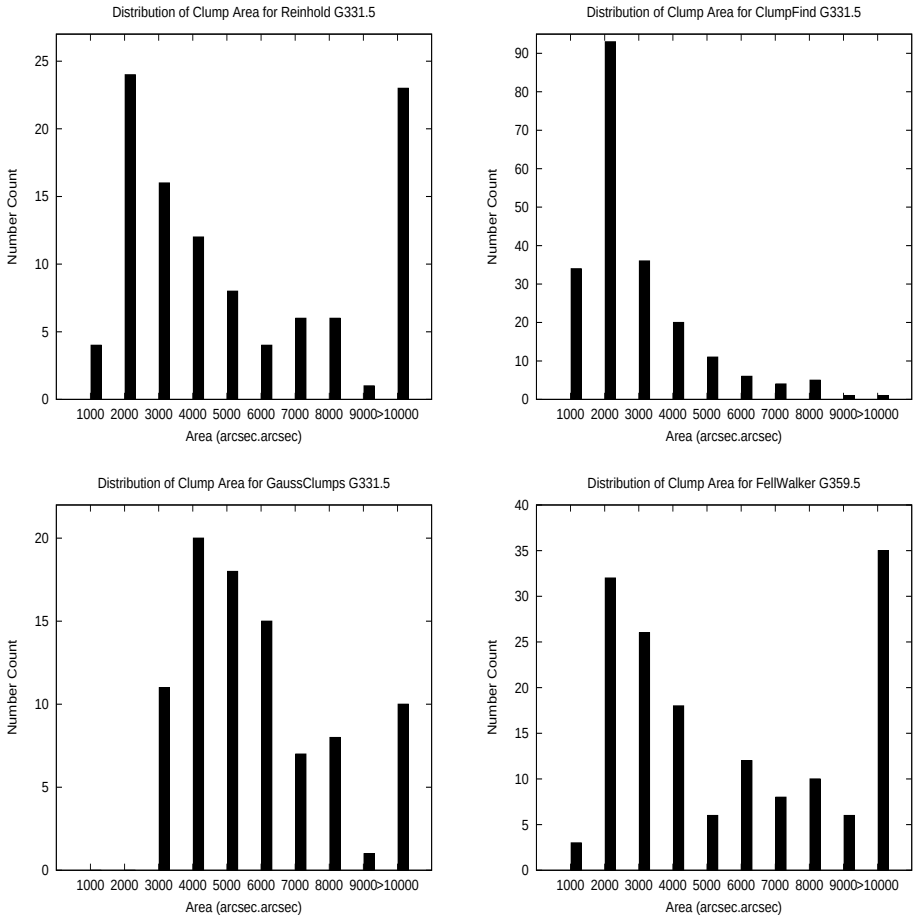

Figure 6.3: The distribution of the clump areas found by each of the algorithms for the G331.5+0.0 region.

The visual inspection, (Figure 6.5), provides the simplest form of comparison. Reinhold detects the majority of the peaks but misses the extended emission. Clumpfind is picking up more of the extended emission but is missing several obvious clumps. Fellwalker detects all of the clumps and extended emission in the region.

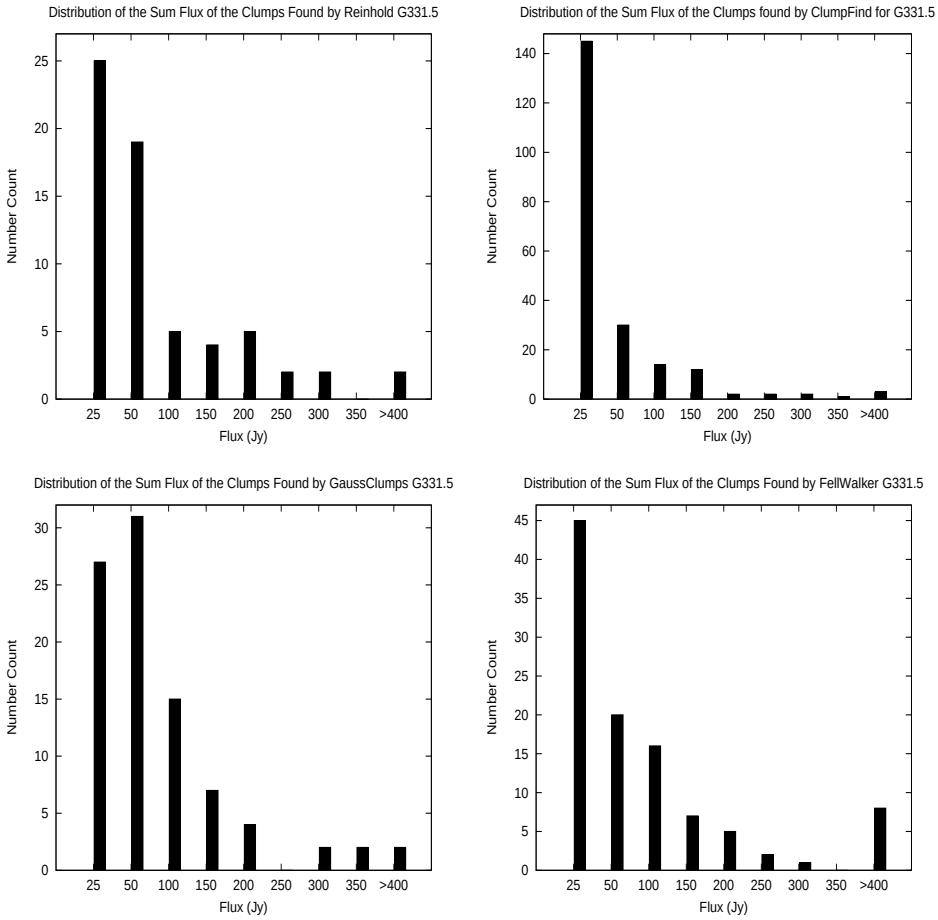

Figure 6.4: The distribution of the total flux density of each clump found by Reinhold, Clumpfind, Gaussclumps and Fellwalker G331.5+0.0

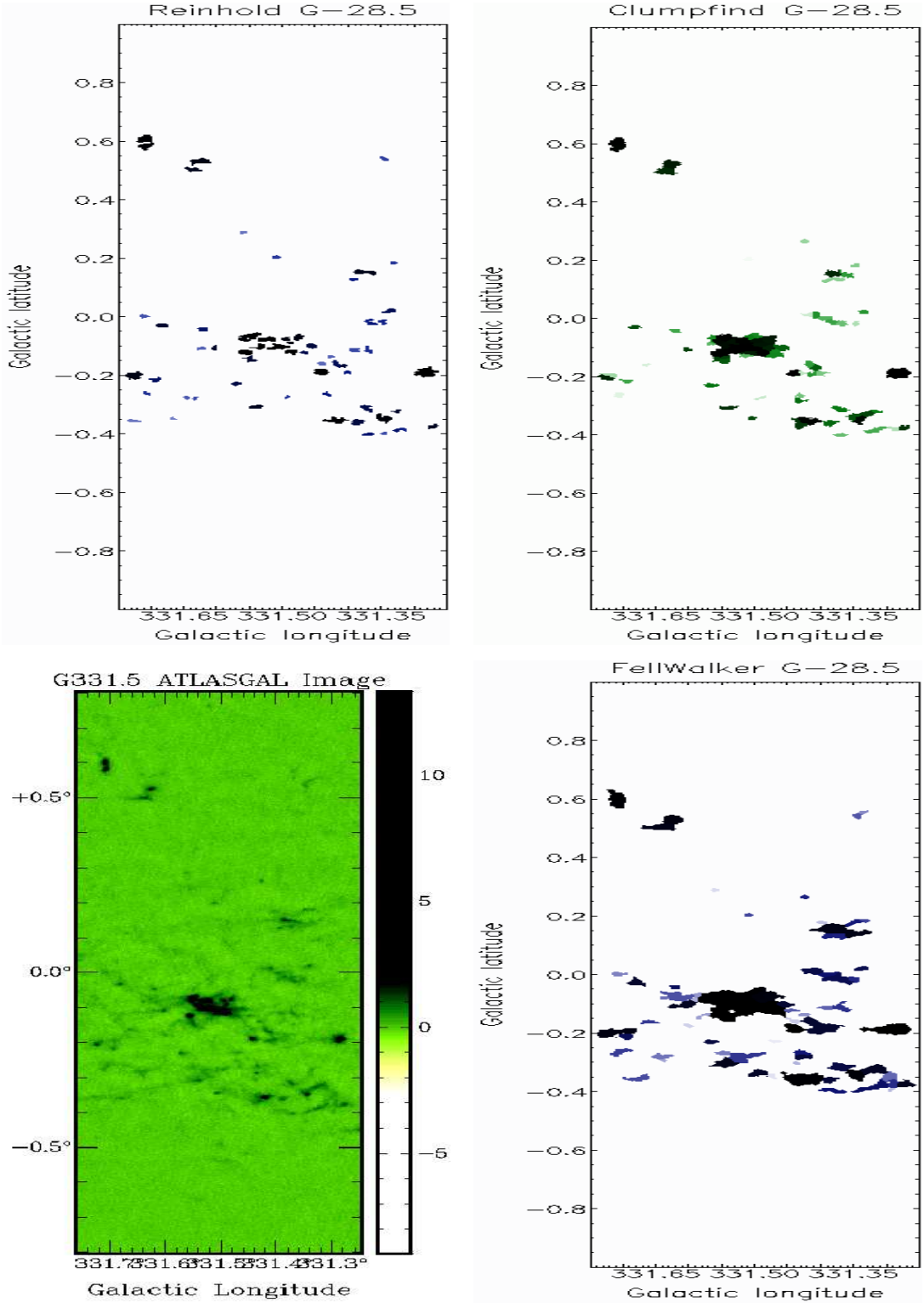

Figure 6.5: The outputs from Reinhold, Clumpfind and Fellwalker for G331.5+0.0, displaying where the clumps and emission was detected. The corresponding ATLASGAL 870μm image is also shown for comparison

6.4.3 Region G359.5+0.0

This region has a large amount of extended emission. Table 6.3 summarises the results of the algorithms below and Figures 6.6, 6.7 & 6.8 display the distributions of the clump area detected, the total flux density of the clumps and the visual outputs.

G359.05+0.0	Clumpfind	Reinhold	Fellwalker	Gaussclumps	SExtractor
Clumps	369	81	156	339	191
Peak Pixel (Jy)	56.02	14.48	12.18	1838.1	12.38
Peak Clump Sum (Jy)	430.24	535.67	907.27	2385.31	
Average Clump Sum (Jy)	38.45	60.85	106.3	41.81	
Average Area (arcsec^2)	2082.89	2335.74	6666.31	4632.49	

Table 6.3: Comparison of results: G359.05+0.0

Clump Area Distribution

Reinhold peaks in the lower end of the clump sizes with few above > 5000 arcsec^2 (Figure 6.6). Clumpfind too peaks in the lower end of the range at 2000 arcsec^2 range. It detects few larger clumps. Gaussclumps appears more balanced, it too peaks in the 2000 arcsec^2 range, but also detects more large area clumps. Fellwalker peaks in the higher 10000 arcsec^2 range, it also detects a large number of peaks at 2000 arcsec^2, like the other three algorithms.

Flux Density Distribution

Reinhold peaks in the low range with few higher flux density clumps. Clumpfind too peaks in the lower 20 Jy end of the range, with few higher value clumps. Gaussclumps repeats as above, peaking in the 20 Jy range and detecting few higher value clumps. Fellwalker is again the most balanced of the lot. It peaks in the 20 Jy range too, but it also detects a large number of clumps of higher flux density.

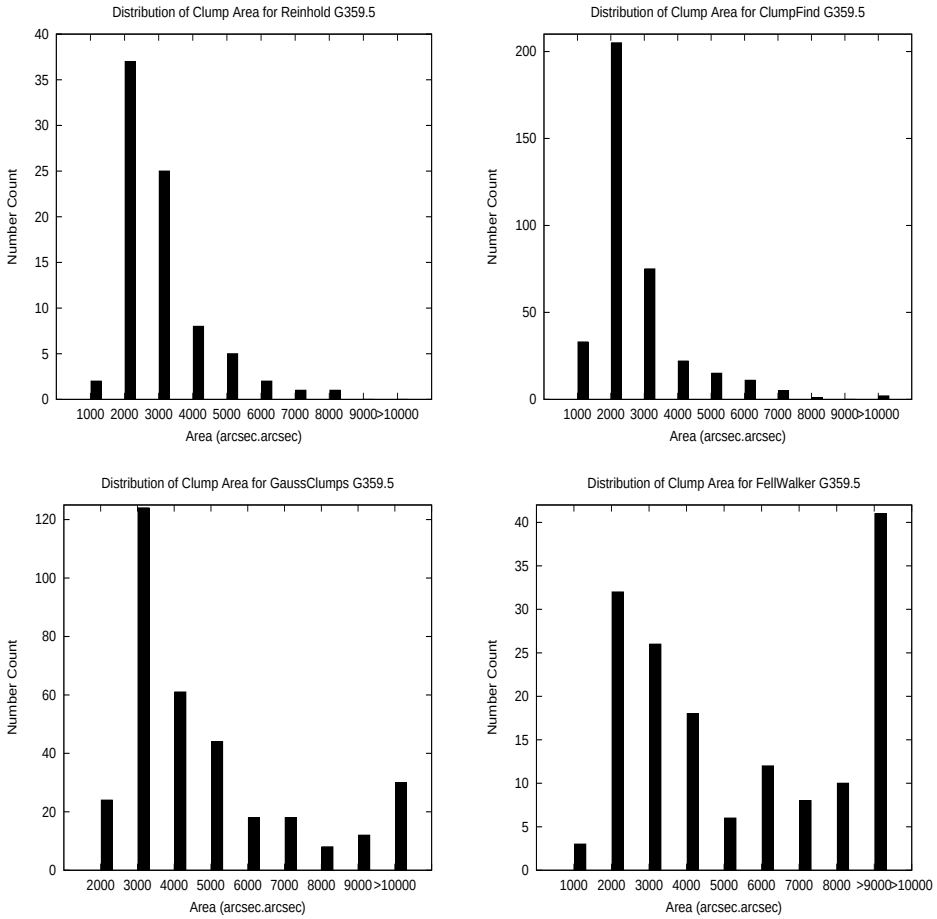

Figure 6.6: The distribution of the clump area found by each of the algorithms for G359.5+0.0.

The visual inspection of this region repeats the findings of before, Reinhold detects the peaks, but not the extended emission, it also misses a large number of clumps. Clumpfind finds the majority of the peaks but too misses out on some extended emission. Fellwalker detects all of the emission clumps along with the extended emission.

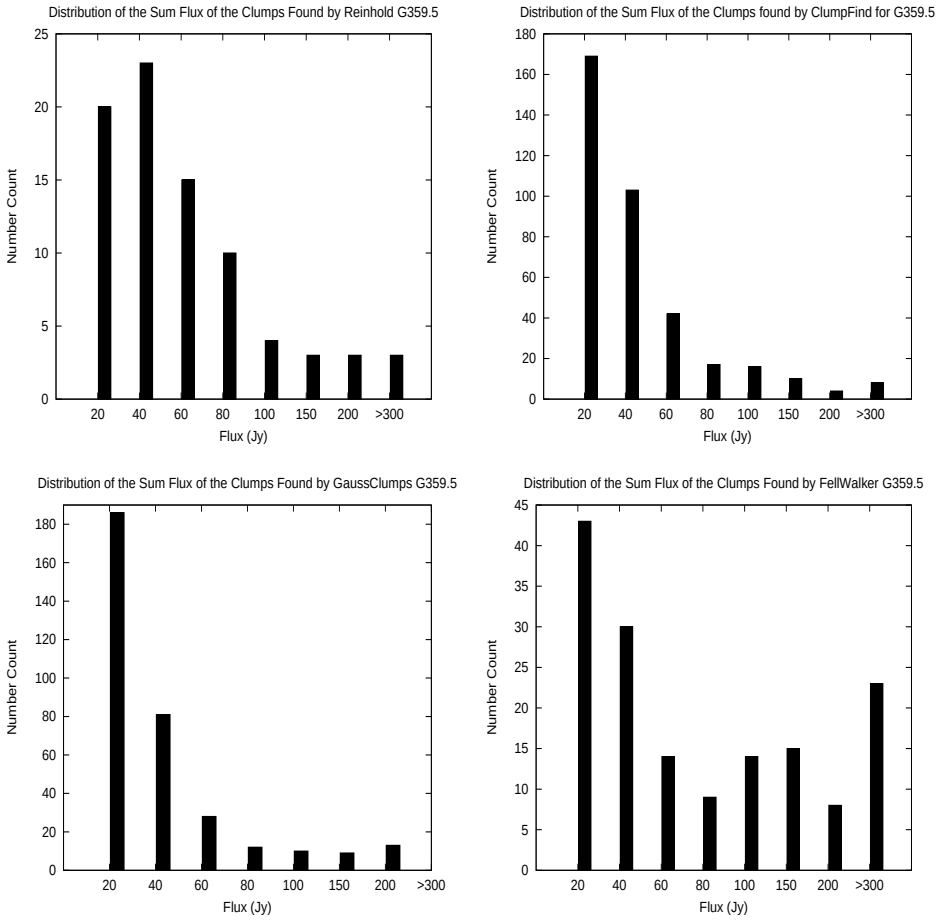

Figure 6.7: The distribution of the total flux density of each clump found by Reinhold, Clumpfind, Gaussclumps and Fellwalker G359.5+0.0

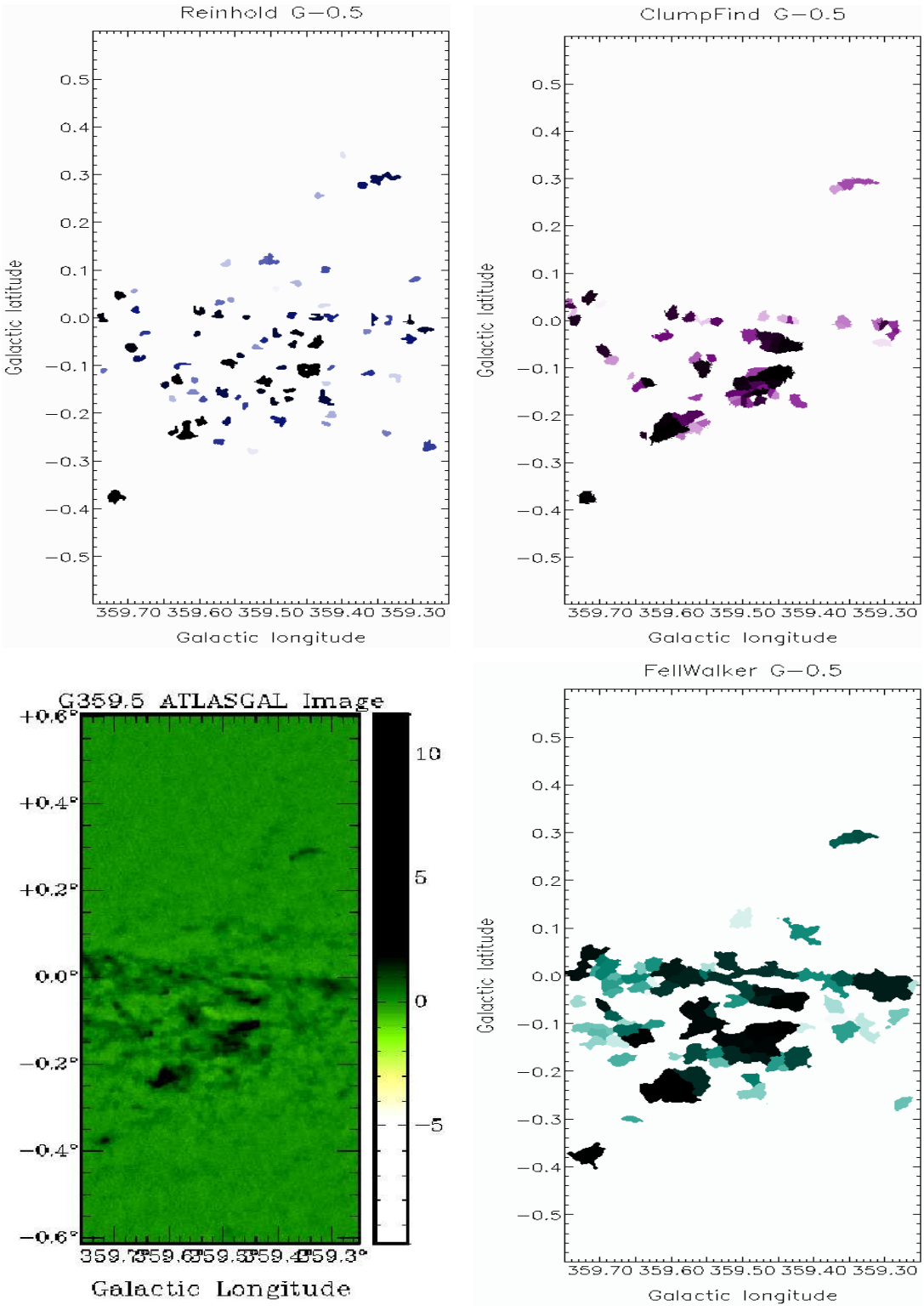

Figure 6.8: The outputs from Reinhold, Clumpfind and Fellwalker for G359.5+0.0, displaying where the clumps and emission was detected. The corresponding ATLASGAL 870μm image is also shown for comparison.

6.5 Discussion

Comparing the results of the three test regions shows a number of common features of the algorithms:

Reinhold

This algorithm appears to work reasonably well. It locates the peaks of the emission clumps in each region. However it completely misses the extended emission from the clumps.

Clumpfind

From the analysis of the G7.0 clump output, the clump flux density and area distributions it is apparent that Clumpfind not only misses clumps of emission, it also divides the clumps into too many smaller clumps. Comparing the clump output images from Clumpfind and Fellwalker for G331.5, Clumpfind outputs 211 clumps while Reinhold outputs 102 for a very comparable area. This is clear evidence that clumpfind is diving larger emission clumps into smaller adjacent clumps.

Gaussclumps

Although it picked up a majority of peaks and emission, it missed some and also has a bug in the output clump file. The flux density peaks it provided were 2-3 orders of magnitude above what was in the data, thus eliminating Gaussclumps.

Fellwalker

Fellwalker has emerges as the favourite and clear winner. It is superior at locating the emission peaks and the surrounding extended emission. From the analysis of the clump area and flux density distribution it is the best at picking up the smaller weak clumps and the larger clumps with extended emission. The comparison of the ATLASGAL image alongside the Fellwalker clump output provides the clearest evidence that

Fellwalker is the best algorithm for finding the emission clumps (Figures 6.8 and 6.5

6.5.1 Understanding the Algorithms

It is good to note that the four algorithms use the same contouring and noise levels throughout. The reason why Reinhold and Clumpfind miss several emission clumps remains unclear. This problem is easily highlighted in Figure 6.9. It is obvious that Fellwalker is picking up all the emission visible by eye (blue annotations) however Clumpfind (red annotations) and Reinhold (green annotations) overlook several large clumps. In an effort to understand why this occurs the noise and contouring levels of Clumpfind and Reinhold were varied to try and pick-up the previously missed emission. By reducing these values to an incredibly low and unrealistic level the clumps were picked up. The reason why they do not pick up the emission clumps at the 'normal' levels remains unclear and adds to Fellwalkers strengths.

6.5.2 Comparison of Fellwalker and SExtractor

Fellwalker and SExtractor both produce a similar number of clumps for each of the three regions, with the biggest difference in the G331.5+0.0 region; Fellwalker finds 104 clumps and SExtractor 169. The peak flux densities for the G7.0+0.0 and G359.5+0.0 region are comparable but differ greatly in G331.5+0.0 as with the clump outputs, table 4 summarises the results. Comparing the positions that Fellwalker and SExtractor find for several clumps also shows some differences. While the peaks identified by Fellwalker are coincident with the flux density peak of the clump (checked with the images), SExtractor is slightly shifted ~2 pixels away. This offset may be due to the outputs that SExtractor provides. Fellwalker outputs both the peak pixel position in the clump and also the centroid position. It appears that the SExtractor position is the centroid position of the clump rather than the peak and because of this the peak

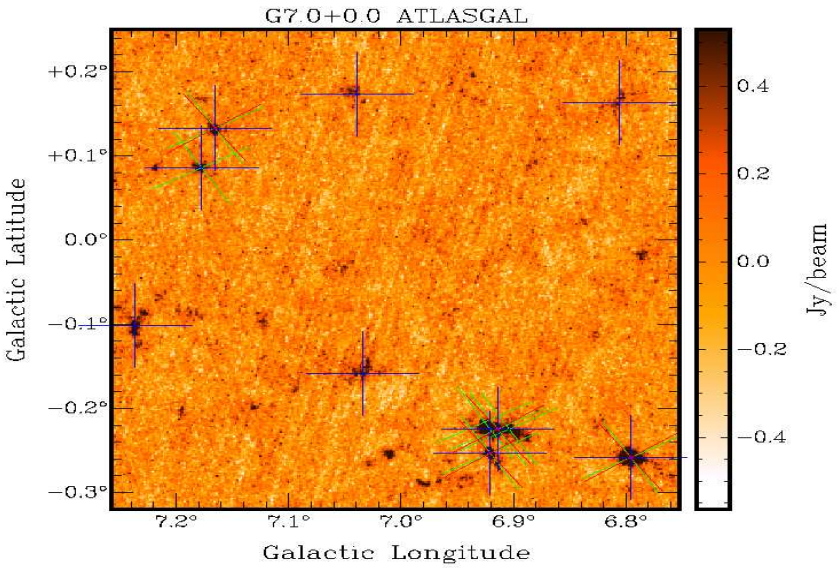

Figure 6.9: ATLASGAL image of G7.0 with Fellwalker in blue annotations, Clumpfind in red, Reinhold in green. Reinhold and Clumpfind miss several clumps picked up by Fellwalker and even visible by eye The visible clumps not marked by any annmotations are noise.

pixel position in the clumped is missed. The difference between the centroid and the peak position depends on the shape of the clump. This also highlights the advantage of Fellwalker (and all the Starlink algorithms), they output both the peak and centroid positions of the clumps found. Three regions are in Figures 6.10, 6.11, & 6.12 which highlight the difference in positions.

6.5.3 Algorithm Improvements

Over the course of the testing several aspects of the algorithms came into question which could be improved. As regards Clumpfind, an input control for merging smaller adjacent clumps together would be useful as the downfall of this algorithm is that it divides real emission clumps into clumps which are too small and unrealistic. With Fellwalker there is a parameter called ‘MinDip’, this allows the user to specify if the minimum dip between two adjacent peaks. If this dip is less than a specified value the peaks are considered part of the same clump. Currently this value is specified as

G7.0	Fellwalker	SExtractor
Clumps	9	20
Peak Pixel (Jy/beam)	6.88	5.47
G359.5		
Clumps	156	191
Peak Pixel (Jy/beam)	12.18	12.38
G331.5		
Clumps	102	169
Peak Pixel (Jy/beam)	56.02	13.54

Table 6.4: Comparison of Fellwalker and SExtractor

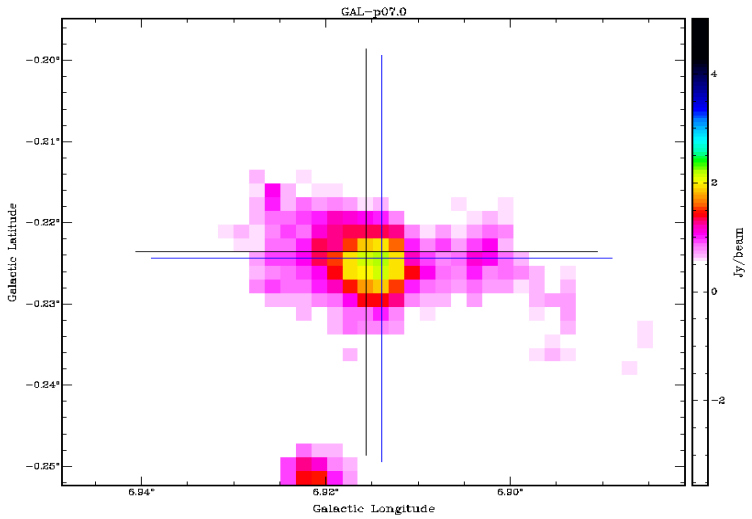

Figure 6.10: The blue cross denotes the Fellwalker position and the black cross denotes the SExtractor position. The Fellwalker is at a position of G6.914-0.224 at a flux density of 2.21 Jy (the peak flux of the clump) and SExtractor is at a position of G6.912-0.222 at a flux density of 1.84 Jy.

a multiple of the RMS value, however it may be more useful if it was expressed as a percentage of the peak value of the highest flux density value. The fact that Clumpfind

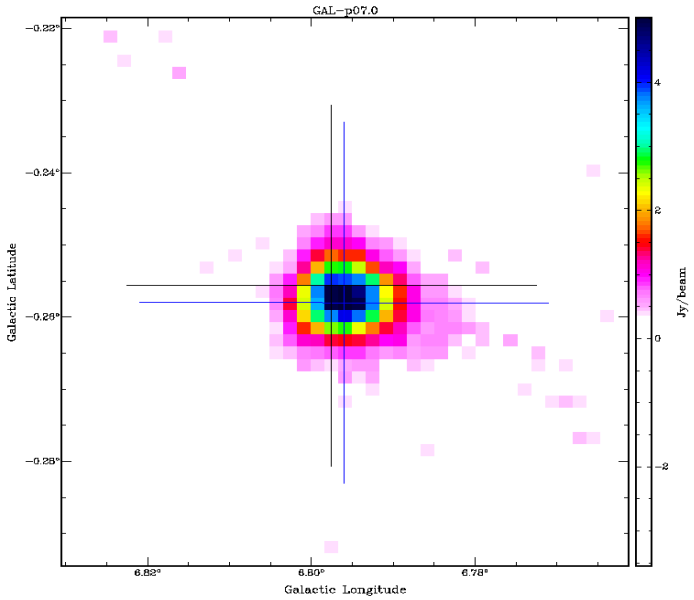

Figure 6.11: The blue cross denotes the Fellwalker position and the black cross denotes the SExtractor position. The Fellwalker is at a position of G6.796-0.258 at a flux density of 5.31 Jy (the peak flux of the clump) and SExtractor is at a position of G6.797-0.254 at a flux density of 3.93 Jy.

divides real clumps into too many sub-clumps has also been also been identified by Pineda et al. (2009).

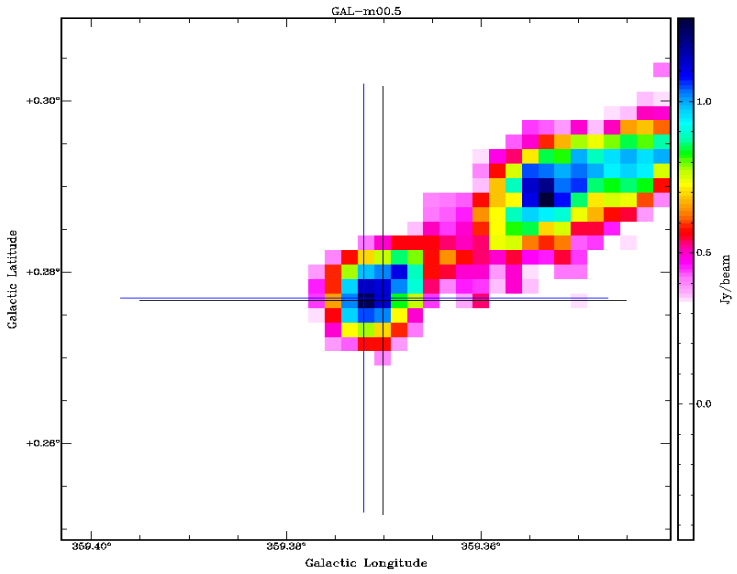

Figure 6.12: The blue cross denotes the Fellwalker position and the black cross denotes the SExtractor position. The Fellwalker is at a position of G359.372+0.277 at a flux density of 1.25 Jy (the peak flux of the clump) and SExtractor is at a position of G359.271+0.277 at a flux density of 1.131 Jy

6.6 Part II: ATLASGAL and MMB Comparison

As Fellwalker proved to be the best algorithm for the ATLASGAL data it was chosen for the final clump identification in this work. A region of 24 sq-degrees, ±6° in longitude around the galactic centre and longitude of -1°≤*b* ≤1° was analysed.

6.6.1 ATLASGAL Clumpfinding Results

A total of 17,200 clumps were detected in the ±6° region around the Galactic centre using Fellwalker, Figures 6.13 & 6.14 show the clumps detected. Figure 6.15 shows the distribution of the molecular cloud areas detected. It peaks in the 4000 arcsec^2 range and only 62 are greater than 20,000 arcsec^2. The flux density distribution is representative of the clump area distribution, it too peaks in the lower 2-3 Jy end and there are far fewer, ~30, in the higher flux density region (Figure 6.18) .

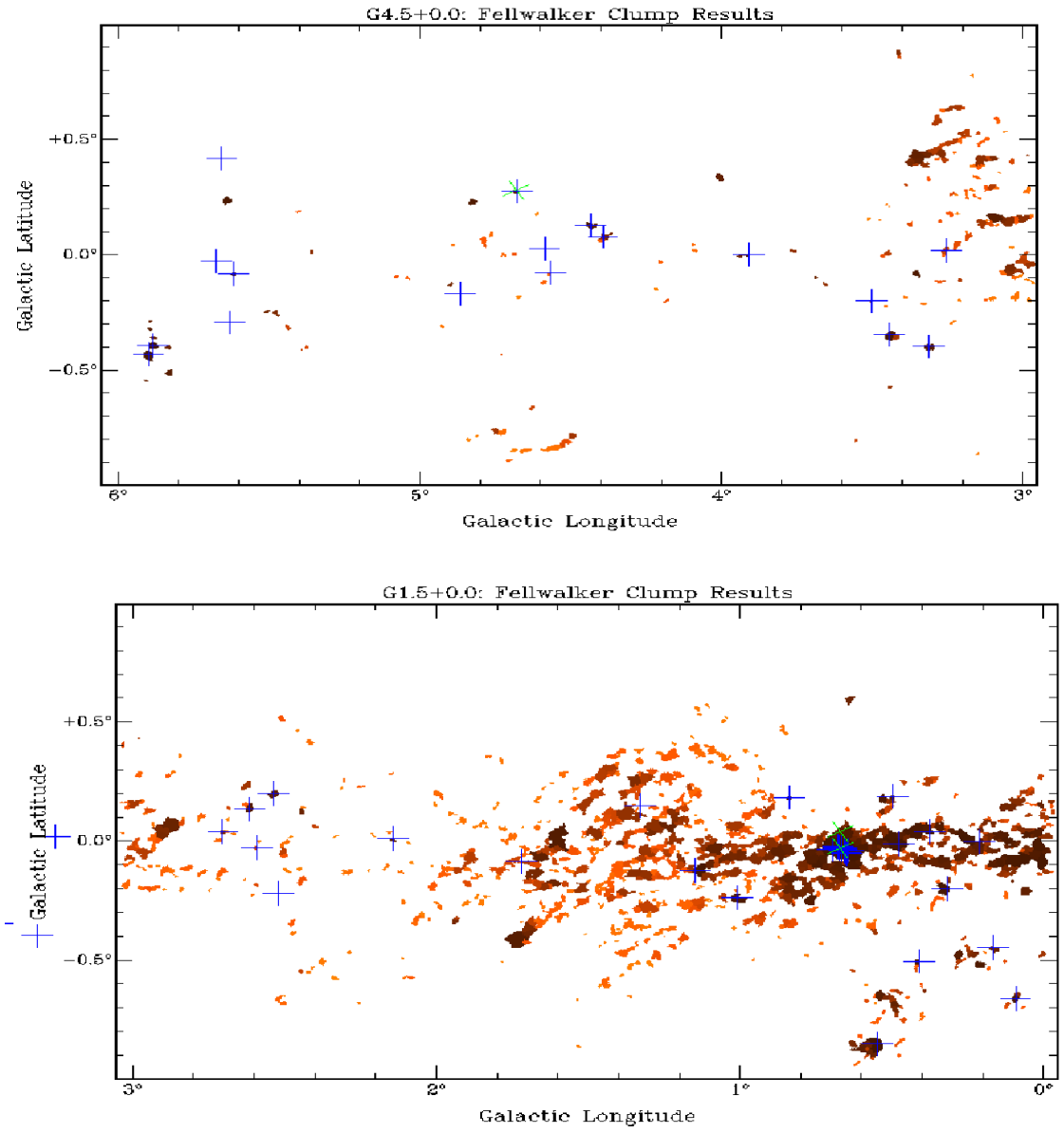

Figure 6.13: The results from the Fellwalker algorithm Clumpfinder on the ATLASGAL data. The black crosses indicate the 6668 MHz methanol maser positions.

6.6.2 Maser Comparison

There are 1720 molecular clouds in the region (Figure 6.16), 85 6668 MHz methanol masers and 7 6035 ex-OH masers. There are 42 methanol masers and 2 ex-OH masers are within 10″ of a clump peak, 63 within 60″, 81 within 300″ and 11 greater than

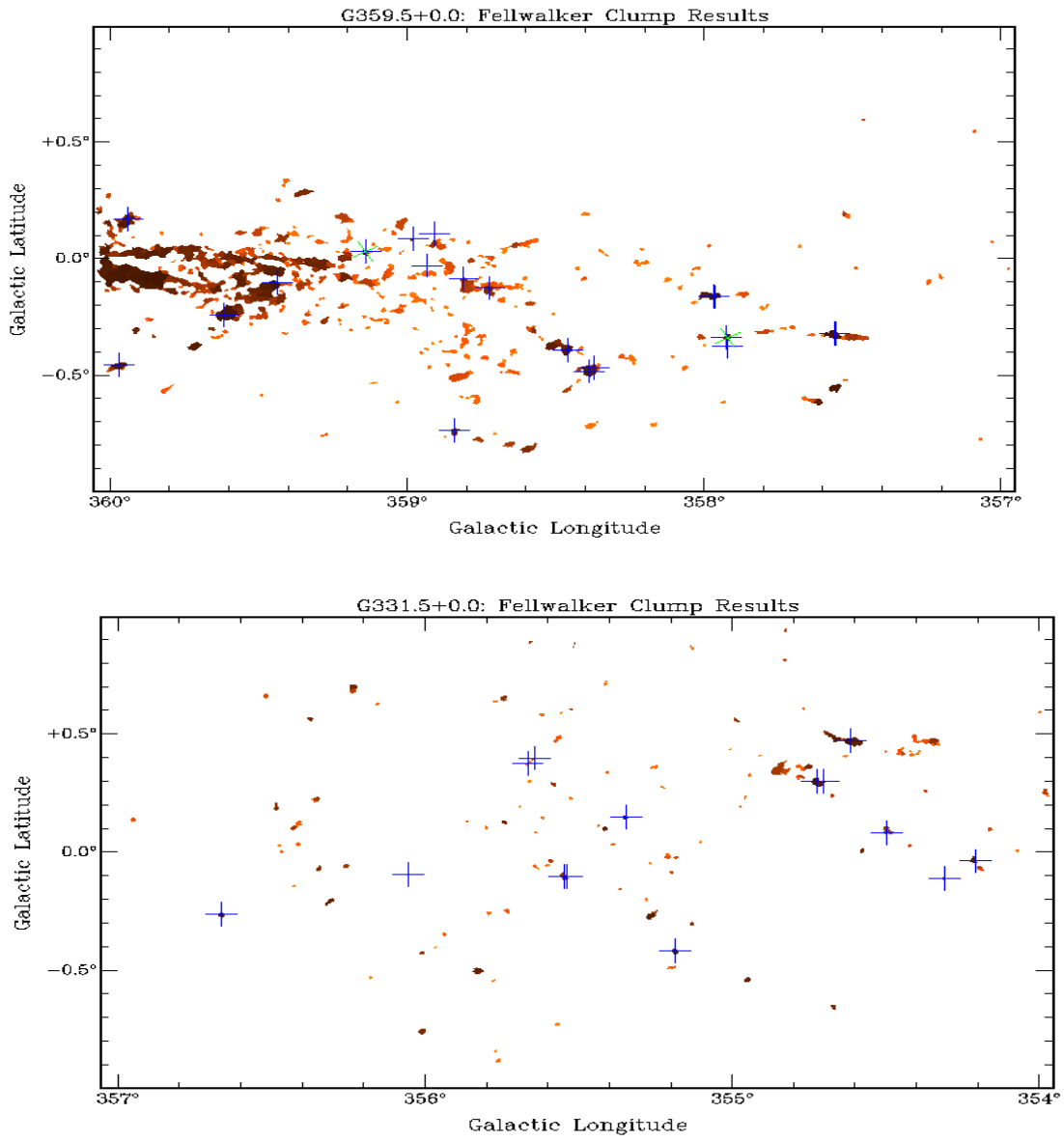

Figure 6.14: The results from the Fellwalker algoithm Clumpfinder on the ATLASGAL data. The black crosses indicate the 6668 MHz methanol maser positions.

300″ from a clump peak (Figure 6.17). All of the masers lie in a molecular cloud, as expected (Figure 6.16).

Figure 6.18 shows the distribution of the flux density of the clump peaks. It peaks in

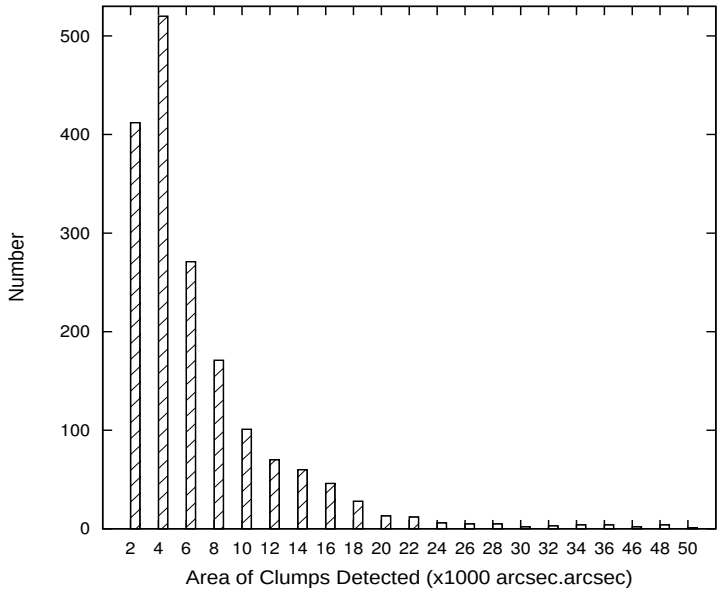

Figure 6.15: The distribution of the molecular cloud area in the central Galactic region.

the 2-3 Jy range with over 700 molecular cloud peaks in the range. Figure 6.18, on the right, displays a zoomed in version of the flux density distribution of the clump peaks to show the distribution of the higher end of the flux density scale. When this is compared with the flux density distribution of the clump peaks associated within 10″ of a maser peak (Figure 6.19), it shows that the masers are preferentially associated with the brightest clumps peaks.

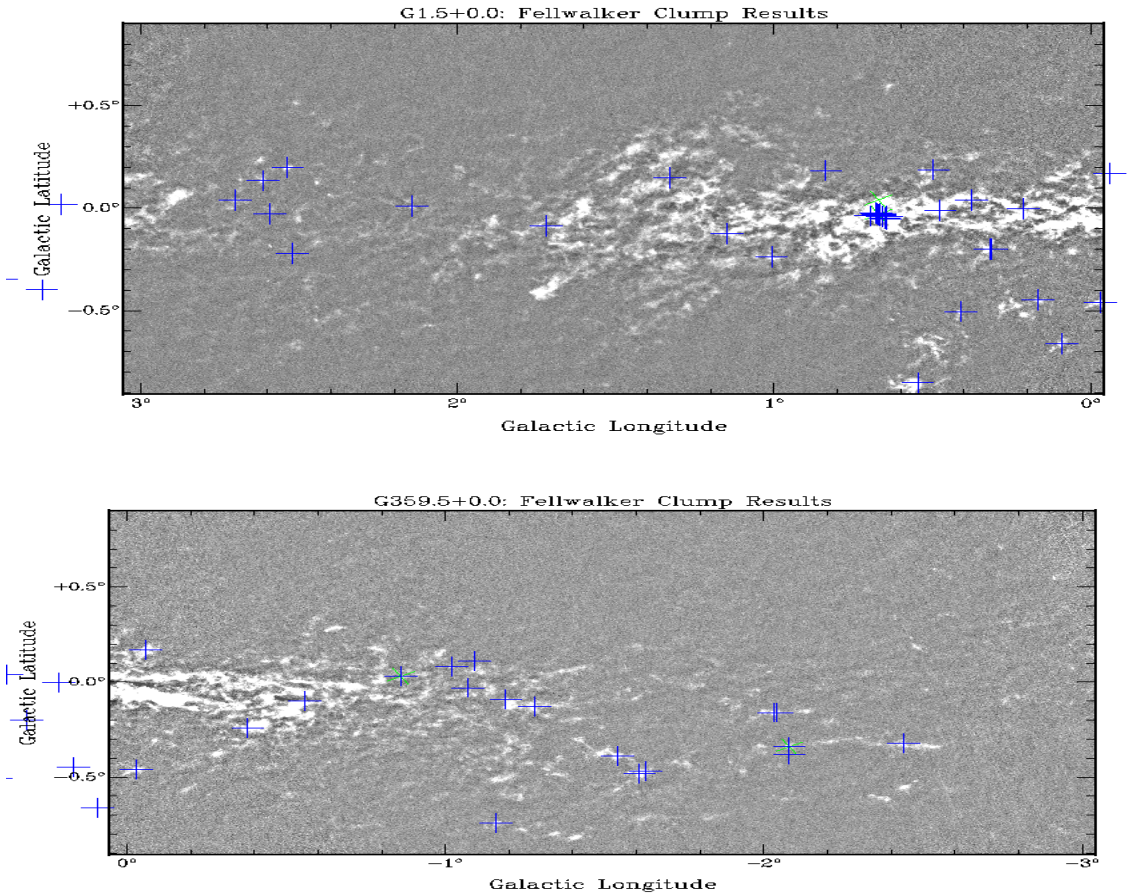

Figure 6.16: The ATLASGAL data overlayed with 6668 MHz methanol maser positions (blue crosses) and 6035 MHz ex-OH masers (green crosses).

6.6.3 Clump Mass

It is possible to calculate a mass for the clumps using their total flux density. From Hildebrand (1983):

$$M = \frac{d^2 F_\nu R}{B_\nu (T_D)\, \kappa_\nu} \tag{6.1}$$

where d is the distance, F_ν is the flux density, R is the dust to gas ratio, B_ν is the plank function for a dust temperature T_D and κ_ν is the opacity coefficent. Assuming a gas temperature of 30 K, κ_ν = 1.85 $cm^{-2}g^{-1}$ and a d = 5 kpc (Schuller et al. 2009 and references therin), the masses of the clumps have been calculated. Figure 6.20 shows the distribution of the clump masses, it peaks in the 0-1000 $M_\odot$ range with over 1400

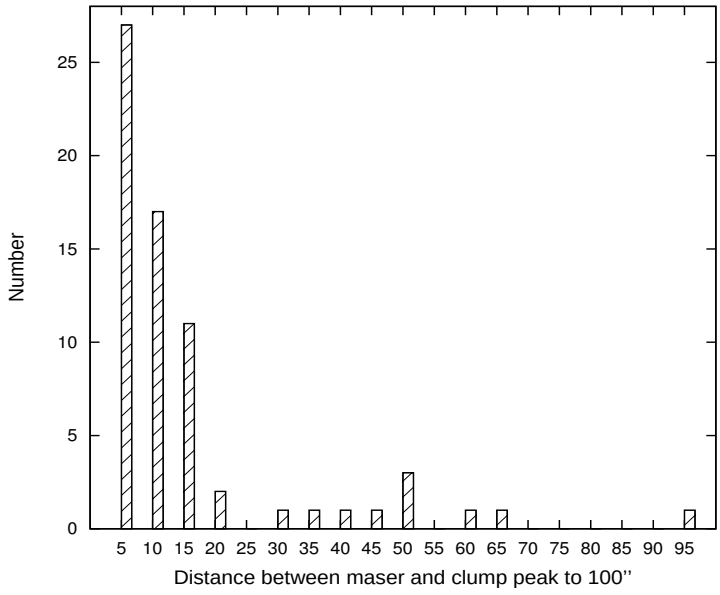

Figure 6.17: The separation between the molecular cloud peaks and the masers, up to 100".

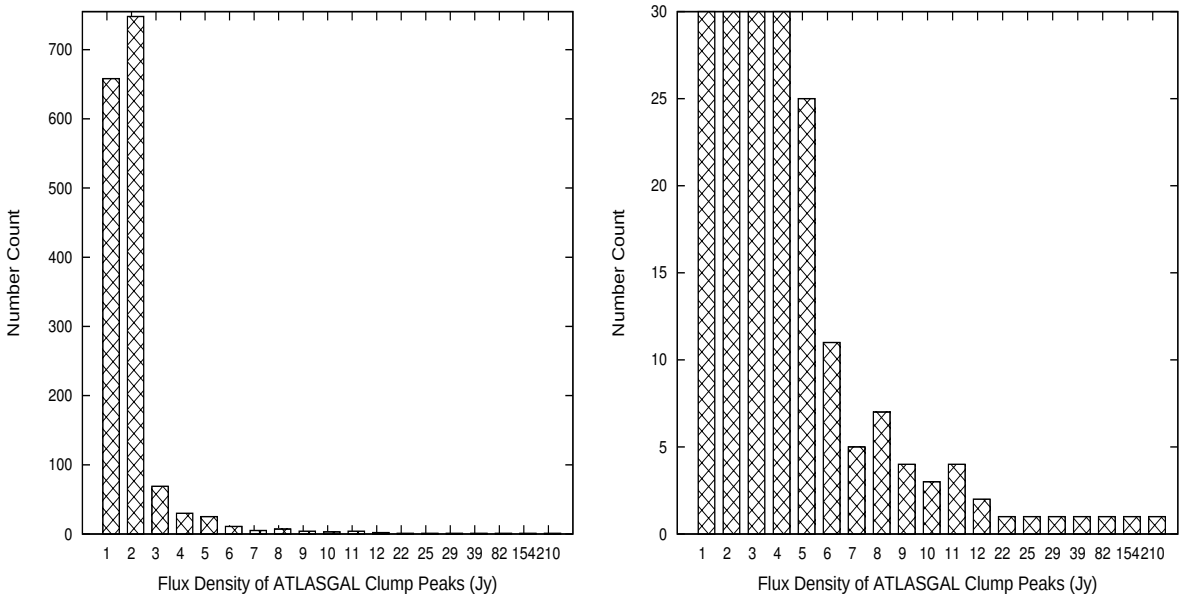

Figure 6.18: The flux density distribution of the peaks of the ATLASGAL sources in the central Galactic region. On the right: zoomed in so the higher ranges may be displayed.

clumps. The largest clump has an estimated mass of 6519568 $M_{\odot}$ and the peak of this clump is associated with a 6668 MHz methanol maser. The fraction of clumps with a 6668 MHz methanol maser within 10″ in terms of mass, is shown in Figure 6.21, it

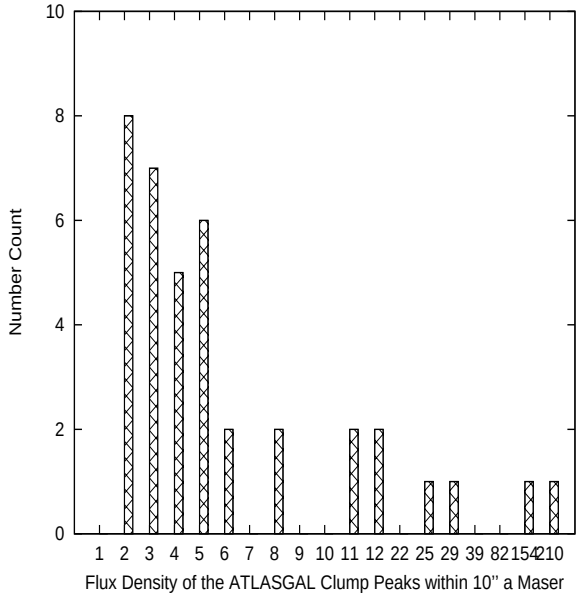

Figure 6.19: The flux density of the molecular cloud peaks that are within 10” of a maser.

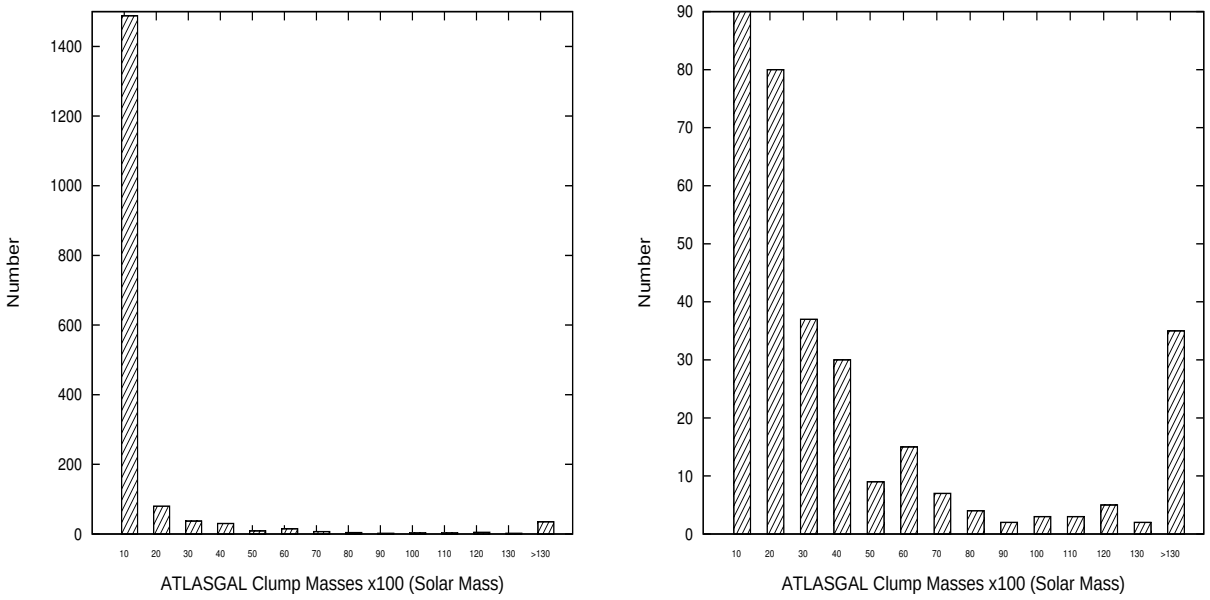

Figure 6.20: The distribution of the ATLASGAL clump masses, on the right a zoomed in version to see the higher ranges more clearly.

can be seen that the masers are associated with the clumps across a mass range, but it peaks toward the higher clump masses.

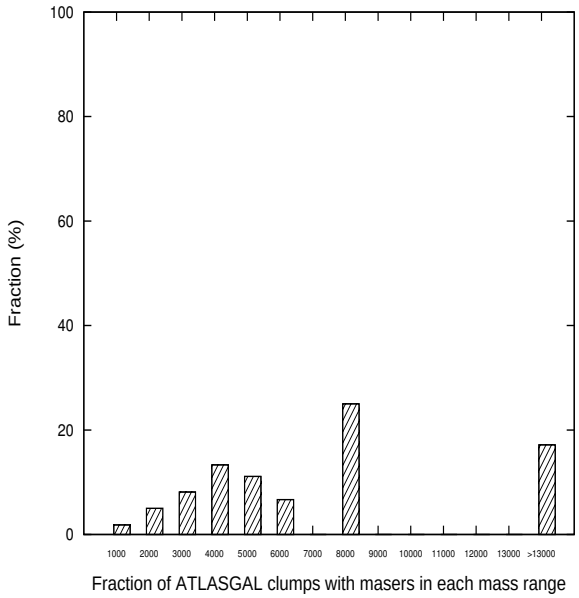

Figure 6.21: The fraction of ATLASGAL clouds that have a methanol maser within 10″, in terms of the clump mass. The distribution peaks toward the higher clump masses.

6.7 Discussion

From the testing of the four Starlink Algorithms, Fellwalker was found to be the best for the ATLASGAL data. Fellwalker was used to analysed on a ±6° around the Galactic centre and detected 1720 clumps. The majority of the clumps are less than 5000 arcsec^2 in area and only 62 are greater than 20,000 arcsec^2 in area (Figure 6.15). The distribution of the peak flux densities peaks in the 2-3 Jy range, there are far fewer, ~30, in the higher flux density region. This leads to the conclusion that the majority of molecular clouds in this region are ~2000-4000 arcsec^2 in area and peak flux density of 2-3 Jy.

When comparing the 6668 MHz methanol and 6035 MHz ex-OH masers with the peaks of the molecular clouds, we find that all of the masers lie within the molecular. Of course, this is to be expected as masers require the higher densities the molecular clouds provide. There are 42 methanol masers and 2 ex-OH masers are within 10″ of a clump peak and 63 within 60″ and 29 are greater than 120″ from the peak of molecular cloud.

Looking at the fraction of ATLASGAL clouds, that are within 10″ from a maser (42 6668 MHz methanol and 2 6035 MHz ex-OH), over the range of flux densitites, we see that the methanol and ex-OH masers are preferentially associated with the clouds with the highest flux densities. From an estimation of the clumps mass, we see that the majority of the clumps are >100 $M_\odot$. Looking at the fractional abundance of clumps with masers within 10″, in terms of mass, it is clear that the masers are preferentially assocaited with the highest mass objects as well as with the highest flux density objects (Figure 6.22).

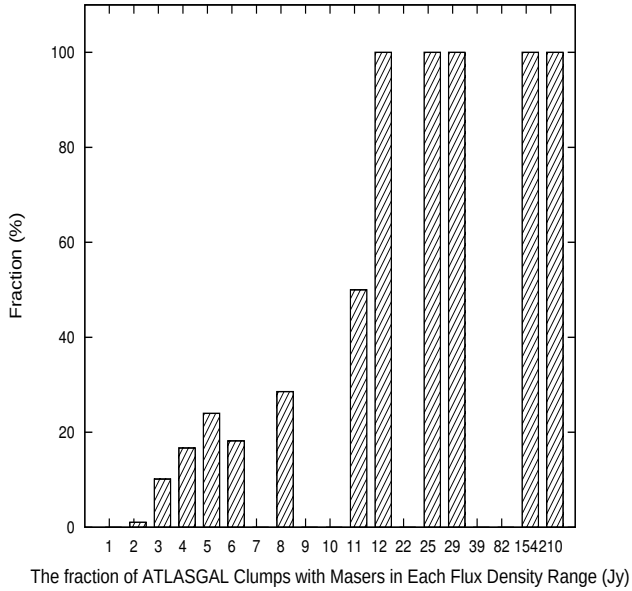

Figure 6.22: This graph shows the fraction of masers within 10″from the peak of an ATLASGAL cloud, over the range of flux densities of the cloud peaks. It is clearly seen that the methanol and ex-OH masers are preferentially associated with the clouds with the highest peak flux densitites.

7

Summary and Future Work

During the course of this work, over one thousand 6668 MHz Class II methanol, 6035 MHz ex-OH and 44 GHz Class I methanol masers have been detected. This thesis presents the first results of the MMB survey (Chapter 3), the first unbiased survey of 6035 MHz ex-OH masers (Chapter 4), the first unbiased survey for 44 GHz Class I methanol masers (Chapter 5) and a comparison of Starlink clump finding algorithms and a comparison of the clumps in ATLASGAL with the MMB masers (Chapter 6). Below I summarise the results and highlight areas for future work.

7.1 MMB First Results

The southern part of the single dish Parkes MMB survey, from l=0°-60° and l = 180°-360°, is now complete and follow up observations are currently taking place. Over nine-hundred 6668 MHz Class II methanol masers have been detected (Appendix 1). The first results from l=345° to 6° and |b|≤2° are presented in Caswell et al. (2010). Using the rotation curve of Reid et al. (2009) the distance of each of the masers can be determined. It was found that there are 42 6668 MHz methanol masers which are located in the near and far 3 kpc arms (Green et al. 2009d). Until these detections, it was believed that these spiral arms were devoid of high mass star formation. As 6668 MHz methanol masers are known tracers of high mass star formation (Minier et al.

2003), we now know that this is not correct, a fact which will impact on the modelling of our Galaxy's structure.

The MMB has also completed a survey of the LMC and the SMC for 6668 MHz methanol and 6035 MHz ex-OH masers. The survey consisted of mapping and targeted searches towards 11 known regions of star formation (Chapter 3). The scanned survey detected two known 6668 MHz methanol and one known 6035 MHz ex-OH maser, in the LMC (Figure 3.5). From the targeted observations, the third known methanol maser was detected, and a new 6668 MHz methanol maser was detected towards the known 6035 MHz ex-OH survey in the LMC. A new 6035 MHz ex-OH maser was also detected towards a pointing of N157a, in the LMC. There were no detections made towards the SMC.

From the analysis of the star formation rates, metalicities and masses of the LMC, SMC and our own Galaxy, it is estimated that the 6668 MHz methanol masers are ~ 5 times under abundant in the LMC. Although, Beasley et al. (1996) argue that the lower rates of carbon and oxygen in the LMC are responsible for this, further investigation is needed for to confirm this.

7.2 The 6035 MHz Ex-OH Maser survey

The 6035 MHz ex-OH maser survey, part of the MMB survey, is the first unbiased survey for masers in this transition. One hundred and eighteen 6035 MHz ex-OH masers have been detected, 43 of which are new sources. The flux density distribution of the 6035 MHz ex-OH masers peaks in the 0-1 Jy range, and there are only two masers >100 Jy, compared with the methanol masers which have 65 masers over 100 Jy. Where possible the Zeeman splitting has been calculated and is listed in Tables 4.1 to 4.10. The average magnetic field detected is |B| = 3.14 mG, for the 74 6035 MHz ex-OH masers with Zeeman splitting. Twenty-nine 6035 MHz ex-OH masers were

found to have a 6031 MHz ex-OH maser comparison. As the 6031 MHz ex-OH maser also undergoes Zeeman splitting in the presence of a magnetic field, it provided a very useful check for the magnetic field measurements, and matched every time.

This work has shown that the 6035 MHz ex-OH masers are variable on a timescale of days, not just years, as previously shown and confirmed here. A comparison of the intensity of 49 6035 MHz ex-OH masers in the MMB and were also detected by Caswell (1998) showed that all the intensities had varied (Figure 4.30), the median difference over the ∼10 years is 1.39 Jy. The largest flux density increase was in the source G351.417+0.633, which increased 158.2 Jy in flux density.

7.2.1 6035 MHz ex-OH and 6668 MHz Methanol Masers

There is a 60% assocation rate between the 6035 MHz ex-OH and 6668 MHz methanol masers, using an association radius of 2″ (Table 4.16). This is a lower and certainly more realistic association rate than those derived from targeted surveys. There are a significant number of 6035 MHz ex-OH masers >5″ from a 6668 MHz methanol maser. There are two hypothesis for this, the first is that these are more evolved sources and the 6668 MHz methanol maser has been extinguished by the growing ionised field. The second is that these association groupings may correspond to two different environments which host the 6035 MHz ex-OH masers. For example, they could be located in an accretion disk or in/near an outflow. From the models of Cragg et al. (2002), we know that sources where the 6035 MHz ex-OH maser is present without a 6668 MHz methanol maser, may trace densities of $10^{8.0}$ cm^{-3}. The sources with the 6035 MHz ex-OH maser only, are a very interesting subset to investigate further.

A question posed at the start of this thesis is whether the 6035 MHz ex-OH maser is a transient phase in all sources with 6668 MHz methanol masers, or, if there is something physically different about the sources which host both the 6035 MHz ex-OH and

6668 MHz methanol maser. This question has been answered using GLIMPSE images and associations. The earliest stages of protostellar formation are defined by an IRDC, EGO emission and the presence of a 6668 MHz methanol maser. Later stages of protostellar formation are characterised by a bright GLIMPSE source, possibly the presence of ionised gas, and 6035 MHz ex-OH masers, 1665/7 MHz OH masers and no 6668 MHz masers. We find very similar numbers of 6035 MHz ex-OH masers associated with the very earliest stages of protostellar evolution, 20 6035 MHz masers, as with the later stages of protostellar evolution, 21 6035 MHz ex-OH masers (Table 4.17). There are 32 6035 MHz ex-OH masers associated with a bright GLIMPSE source and a methanol maser, the mid point of the two stages described above and a further 7 6035 MHz masers which do not have any obvious GLIMPSE source association. The presence of the 6035 MHz ex-OH maser proves that it is not just a transient phase, but it appears at an early time in the evolution of a protostellar source and remains active until after the 6668 MHz maser has been extinguished. Therefore, it must be asked if there is a physical difference in the sources that host both 6035 MHz ex-OH and 6668 MHz methanol masers. This work provides both samples for future investigation.

A comparison of the GLIMPSE and CORNISH images identified several interesting sources. G43.149+0.013, (Figure 4.51), shows the 6035 MHz ex-OH and the 6668 MHz methanol maser are associated with the central object and there are two regions of emission either side of the central object, visible in both the GLIMPSE and CORNISH images. These regions of emission could be marking two bipolar outflows. Further observations, using an outflow tracer, such as SiO, are required to determine if they are bipolar outflows. Figure 4.49 shows the CORNISH and GLIMPSE image centred on the G35.025+0.350 6035 MHz ex-OH maser. The GLIMPSE image appears to show the 6035 MHz ex-OH and 6668 MHz methanol masers associated with the central source, in what appears to be an edge on disk. The CORNISH images shows that the masers are offset from the central object. There are two very interesting objects for further investigation as disks and bipolar outflows around high mass stars.

From the GLIMPSE images we have identified 7 6035 MHz ex-OH masers without any obvious GLIMPSE sources (Figure 4.40), these sources require further investigation to see what is pumping these masers.

We have found that the 6035 MHz ex-OH maser is not as closely associated with the 6668 MHz methanol maser as was previously believed. Sources which host 6035 MHz ex-OH masers only could possibly be extremely dense objects. The 6035 MHz ex-OH has been observed in this survey to be associated with methanol masers through a variety of protostellar evolutionary stages. Thus, the 11% of 6668 MHz masers with a 6035 MHz ex-OH maser association must represent a subset of sources with different physical properties. This work provided the two samples, with and without 6035 MHz ex-OH masers, for further investigation.

7.3 The Class I Methanol Survey

The first unbiased Class I survey has detected twenty-five 44 GHz methanol (21 are new) and six 36 GHz methanol (all new) masers. A second epoch of the 44 GHz methanol masers revealed they are variable on relatively short timescales of $\sim$ 17 months (Figure 5.9).

We have constructed 12 SEDs of the sources exciting the 44 GHz masers. The rest were not possible to construct due to confusion in the fields. Table 5.8 shows the flux densities of the 24 micron MIPS Band 1, 70 micron MIPS Band 2, 1.2 mm Bolocam the distance estimates and the derived luminosities. From this, we have identified four sources, G30.92+0.09, G31.12+0.02, G31.49+0.17 & G31.59-0.13 which have luminosities $\leq$ 500 $L_{\odot}$ and are not associated with a 6.7 GHz methanol maser. We believe these sources to be low mass star forming regions.

Looking at the GLIMPSE colour magnitude plots, (Figure 5.11), the [3.6]-[4.5] vs.[8.0] plot does not display any distinguishing colours for 44 GHz masers as they mostly lie in the main body of sources. In the [3.6]-[8.0] vs. [3.6]-[5.8] colour magnitude plot, the four most extreme points on the plot are associated with 44 GHz masers. Therefore, the other extreme objects may host 44 GHz masers too, that were not detected due to variation.

Previous surveys for the Class I masers have targeted IRAS sources and 6.7 GHz masers (e.g., Ellingsen 2007). Our unbiased Class I survey shows that only 24% of the 44 GHz Class I methanol masers have an IRAS association and only 20% of of the 44 GHz masers had a 6.7 GHz methanol maser association. This proves that targeted surveys of 44 GHz masers towards these sources will miss a high fraction of the population.

Breen et al. (2010) present the most recent evolutionary scheme using masers (Figure 4.63). The Class I masers are argued to be the earliest maser signposts of massive protostellar evolution, appearing before the 6.7 GHz methanol masers. Out of the twenty-five 44 GHz masers we have detected 80% do not have a 6.7 GHz methanol maser association, therefore these 44 GHz maser sites are candidates for very early stages of high mass star formation. We have also compared the 44 GHz Class I methanol maser positions with the CORNISH survey of UCHII regions. Only two, out of twenty-five 44 GHz masers are associated with a UCHII region, this further suggests that the 44 GHz methanol masers appear at very early evolutionary stages of protostellar evolution, before the surrounding regions become ionised. Pratap et al. (2008) add to the evolutionary scenario by arguing the 36 GHz Class I maser appears before the 44 GHz Class I maser. We have detected six 36 GHz Class I masers in this survey, five of which are associated with a 44 GHz methanol maser, but one 36 GHz does not have an associated 44 GHz maser, or a 6.7 GHz maser, or even a GLIMPSE source associated with it. Hence, this source could possibly be in the extremely early stages of protostellar evolution.

7.4 ATLASGAL Comparison

The first part of the ATLASGAL comparison was the analysis of the four Starlink clump finding algorithms. The number of clumps, the peak and the total flux densities and a visual inspection of the outputs from each of the four algorithms was analysed. We found that Gausclumps and Reinhold select the clump peaks, but miss a significant amount of the extended emission. Clumpfind divided the emission into an unrealistically high number of clumps, leaving Fellwalker, which performed excellently on the ATLASGAL data. It picked up all the clumps and the extended emission and the number of clumps were realistic, when compared with the real data. Fellwalker also faired better than SExtractor, on the ATLASGAL data. Whilst Sextractor picked up the clumps, it often did not identify the peak, giving a position 2-3 pixels away from it

(Figure 6.12).

During the analysis, we developed a new technique to take into account the varying noise and also the extended emission of the clouds. This technique may be used for future continuum surveys, such as SCUBA 2.

Twelve degrees of the Galactic plane, $|l| \leq 6°$, were analysed for 870 μm emission in the ATLASGAL data. Fellwalker identified 1720 clumps of emission (Figure 6.15). These clumps were compared with the forty-two 6668 MHz methanol masers and two 6035 MHz ex-OH masers from the MMB. The analysis showed that the methanol masers are associated with the strongest flux density clump peaks (Figure 6.22) and the largest in mass (Figure 6.21). This work provides two groups of source, those clumps with and without a methanol maser for further analysis.

7.5 Future Work

The work carried out in this thesis has produced many very interesting sources for further investigation. The 6035 MHz survey has produced a list of sources with and without a 6035 MHz ex-OH or 6667 MHz Class I methanol maser. A sample of each sources, those with and without a 6035 MHz ex-OH maser will be observed, using NH_3 to determine the temperatures in the sources. Several interesting sources with a 6035 MHz ex-OH maser have been found using the GLIMPSE images, these sources appear to trace a central disk around a massive protostar (Figure 4.39). Figure 4.40 shows the GLIMPSE images where the 6035 MHz maers do not have any obvious exciting sources. These 6035 MHz ex-OH masers may be pin-pointing sources of low mass star formation.

The Class I survey has identified three possible sources that may be low mass star formation. These sources will require further investigation to determine if they are in

fact low mass stars. The precise location of the Class I masers will also be determined using the VLA in the next 6 months.

The work on the ATLASGAL data has provided two groups of sources, those with and without a 6668 MHz methanol maser. Further observations will be carried out on these two groups to determine if there are physicsal or chemical differences between them.

Part I

Appendices

.1 The Catalogue of 6668 MHz Class II Methanol Masers from the MMB

Source Name	Parkes Gal L	Parkes Gal B	Parkes:RA(2000)	Parkes:DEC(2000)	Parkes Sp	Parkes Vp	Vstart	Vstop	Vrange	Status
G305.634+1.645	305.633	1.650	13:13:48.95	-61:06:14.7	7.30	-54.8	-55.8	-54.2	1.6	New
G305.646+1.589	305.650	1.584	13:14:00.10	-61:10:08.7	3.05	-58.1	-58.8	-56.7	2.1	New
G305.799-0.245	305.799	-0.242	13:16:42.97	-62:58:22.6	0.63	-39.3	-39.9	-36.3	3.6	Known
G305.822-0.115	305.817	-0.117	13:16:45.72	-62:50:47.3	2.92	-42.2	-47.0	-41.2	5.8	New
G305.887+0.017	305.883	0.017	13:17:13.60	-62:42:25.9	7.93	-34.2	-35.6	-32.8	2.8	Known
G305.940-0.164	305.917	-0.167	13:17:40.71	-62:53:10.5	0.88	-50.9	-51.2	-50.6	0.6	New
G306.322-0.334	306.333	-0.342	13:21:29.03	-63:00:53.4	0.50	-24.7	-24.8	-22.3	2.5	Known
G307.133-0.477	307.133	-0.483	13:28:38.89	-63:03:04.1	1.82	-38.7	-39.6	-33.5	6.2	New
G308.056-0.396	308.050	-0.383	13:36:27.83	-62:48:24.5	1.26	-11.8	-13.1	-11.4	1.7	New
G308.651-0.507	308.648	-0.508	13:41:48.49	-62:49:11.0	3.99	3.2	0.4	3.8	3.3	New
G308.686+0.530	308.681	0.525	13:40:23.30	-61:47:56.7	1.81	-53.1	-53.6	-51.7	1.9	New
G308.715-0.216	308.700	-0.200	13:41:44.09	-62:30:25.6	1.07	-12.5	-13.5	-12.1	1.3	New
G308.754+0.549	308.750	0.550	13:40:55.28	-61:45:41.3	11.63	-45.3	-55.6	-35.8	19.8	Known
G308.918+0.123	308.917	0.133	13:43:00.09	-62:08:15.9	45.24	-54.8	-60.2	-48.2	11.9	Known
G309.384-0.135	309.383	-0.133	13:47:23.58	-62:18:07.7	1.35	-49.6	-50.7	-49.1	1.6	Known
G309.901+0.231	309.900	0.233	13:51:00.03	-61:49:47.9	16.70	-54.6	-62.7	-53.7	9.0	New
G309.92+10.479	309.917	0.483	13:50:39.34	-61:34:57.8	885.30	-59.7	-67.9	-50.5	17.4	Known
G310.144+0.760	310.133	0.767	13:51:52.48	-61:15:25.8	93.87	-55.7	-62.5	-50.3	12.1	Known
G310.180-0.122	310.183	-0.117	13:54:02.55	-62:06:13.6	1.13	3.6	2.7	4.8	2.1	Known
G311.230-0.032	311.217	-0.033	14:02:21.25	-61:45:32.6	1.92	24.8	24.1	26.7	2.6	New
G311.551-0.055	311.550	-0.050	14:05:05.89	-61:40:58.9	1.13	-56.3	-56.9	-55.9	1.1	New
G311.628+0.266	311.617	0.267	14:04:53.34	-61:21:37.4	4.31	-57.6	-58.3	-54.8	3.5	Known
G311.643-0.380	311.633	-0.383	14:06:34.62	-61:58:44.4	11.13	32.6	27.4	36.5	9.1	Known
G311.729-0.735	311.700	-0.733	14:07:59.36	-62:17:41.3	0.76	30.9	30.5	31.4	0.9	New
G311.947+0.142	311.947	0.142	14:07:49.80	-61:23:07.6	0.25	-38.7	-38.8	-38.5	0.4	Known

Table 20: The Catalogue of 6668 MHz Class II methanol masers detected by the Parkes telescope in the MMB Survey. The Parkes source name, Galactic longitude and latitude, the Parkes RA and Dec, the Peak Flux Density, Peak velocity, start velocity, stop velocity, velocity range and its status are listed above.

Source Name	Parkes Gal L	Parkes Gal B	Parkes:RA(2000)	Parkes:DEC(2000)	Parkes Sp	Parkes Vp	Vstart	Vstop	Vrange	Status
G0.092-0.663	0.083	-0.667	17:48:25.57	-29:12:38.1	24.80	23.5	10.0	25.0	15.0	New
G0.167-0.446	0.167	-0.450	17:47:46.43	-29:01:38.3	4.44	13.8	9.5	17.0	7.5	New
G0.212-0.001	0.217	0.000	17:46:08.07	-28:45:04.2	3.47	49.3	41.0	50.5	9.5	Known
G0.315-0.201	0.317	-0.217	17:47:12.98	-28:46:41.4	72.16	19.4	14.0	27.0	13.0	Known
G0.316-0.201	0.317	-0.200	17:47:09.16::	-28:46:09.4	0.60	21.0	20.0	22.0	2.0	Known
G0.376+0.040	0.367	0.033	17:46:21.61	-28:36:20.5	2.32	37.0	35.0	40.0	5.0	Known
G0.409-0.504	0.400	-0.517	17:48:35.13	-28:51:42.9	2.77	25.3	24.5	27.0	2.5	New
G0.475-0.010	0.467	-0.017	17:46:47.48	-28:32:46.3	3.43	28.8	23.0	31.0	8.0	Known
G0.496+0.188	0.500	0.183	17:46:05.55	-28:24:49.7	32.14	0.8	-12.0	2.0	14.0	Known
G0.546-0.852	0.550	-0.850	17:50:14.65	-28:54:16.7	62.83	11.8	8.0	20.0	12.0	Known
G0.645-0.042	0.650	-0.067	17:47:25.11	-28:24:55.2	76.08	49.5	46.0	53.0	7.0	Known
G0.666-0.029	0.666	-0.050	17:47:24.07	-28:23:22.6	32.90	70.0	68.0	73.0	5.0	Known
G0.695-0.038	0.700	-0.050	17:47:28.31	-28:21:50.2	36.41	68.6	64.0	75.0	11.0	Known
G0.836+0.184	0.833	0.167	17:46:56.62	-28:08:15.4	8.99	3.6	2.0	5.0	3.0	Known
G1.008-0.237	1.000	-0.250	17:48:57.17	-28:12:37.4	15.23	1.6	1.0	7.0	6.0	New
G1.147-0.124	1.133	-0.133	17:48:48.66	-28:02:09.5	2.97	-15.3	-20.5	-14.0	6.5	Known
G1.329+0.150	1.317	0.133	17:48:12.32	-27:44:28.8	1.56	-12.0	-13.5	-11.0	2.5	New
G1.719-0.088	1.717	-0.100	17:50:02.29	-27:31:06.7	9.81	-8.0	-9.0	-4.5	4.5	New
G2.143+0.009	2.150	0.017	17:50:35.25	-27:05:12.0	6.70	62.7	54.0	65.0	11.0	Known
G2.521-0.220	2.520	-0.233	17:52:23.59	-26:53:56.9	0.70	4.2	-7.5	5.0	12.5	New
G2.536+0.198	2.533	0.200	17:50:45.71	-26:39:48.7	36.41	3.2	2.0	20.5	18.5	Known
G2.591-0.029	2.600	-0.033	17:51:48.74	-26:43:31.8	1.69	-8.2	-9.5	-4.0	5.5	New
G2.615+0.134	2.617	0.133	17:51:12.54	-26:37:33.7	1.10	94.5	93.5	104.0	10.5	New
G2.703+0.040	2.700	0.050	17:51:43.20	-26:35:49.1	9.00	93.6	91.5	98.0	6.5	New
G3.253+0.018	3.250	0.017	17:53:05.90	-26:08:26.2	3.70	2.2	-1.5	3.5	5.0	New

Table 1: The Catalogue of 6668 MHz Class II methanol masers detected by the Parkes telescope in the MMB Survey. The Parkes source name, Galactic longitude and latitude, the Parkes RA and Dec, the Peak Flux Density, Peak velocity, start velocity, stop velocity, velocity range and its status are listed above.

Source Name	Parkes Gal L	Parkes Gal B	Parkes:RA(2000)	Parkes:DEC(2000)	Parkes Sp	Parkes Vp	Vstart	Vstop	Vrange	Status
G3.312-0.399	3.300	-0.383	17:54:44.94	-26:18:00.8	0.88	0.5	0.0	10.0	10.0	New
G3.442-0.348	3.450	-0.367	17:55:01.36	-26:09:44.4	0.66	-35.0	-35.5	-34.5	1.0	New
G3.502-0.200	3.500	-0.200	17:54:29.68	-26:02:05.8	2.02	43.9	43.0	45.5	2.5	New
G3.910+0.001	3.917	0.000	17:54:39.85	-25:34:27.6	5.10	17.9	15.0	24.5	9.5	Known
G4.393+0.079	4.400	0.083	17:55:25.55	-25:06:54.2	7.67	2.0	0.0	9.0	9.0	New
G4.434+0.129	4.430	0.133	17:55:18.91	-25:03:56.3	4.59	-0.9	-1.5	8.0	9.5	New
G4.569-0.079	4.583	-0.091	17:56:29.91	-25:02:40.9	0.61	9.5	9.0	10.0	1.0	New
G4.586+0.028	4.583	0.033	17:56:01.46	-24:58:54.8	0.96	26.3	15.0	27.0	12.0	New
G4.676+0.276	4.683	0.283	17:55:17.67	-24:46:10.3	2.48	4.4	-5.5	6.0	11.5	New
G4.866-0.171	4.867	-0.183	17:57:28.70	-24:50:44.3	0.64	5.4	5.0	6.0	1.0	New
G5.618-0.082	5.617	-0.083	17:58:44.76	-24:08:46.2	3.42	-27.0	-28.0	-18.5	9.5	New
G5.630-0.294	5.633	-0.300	17:59:36.37	-24:14:22.9	1.31	10.6	9.0	22.0	13.0	New
G5.657+0.416	5.667	0.417	17:56:57.61	-23:51:09.6	1.90	20.1	13.0	22.0	9.0	New
G5.677-0.027	5.683	-0.033	17:58:42.12	-24:03:48.4	0.99	-11.5	-14.5	-11.0	3.5	New
G5.885-0.393	5.883	-0.391	18:00:29.82	-24:04:05.9	1.30	6.7	6.0	7.5	1.5	New
G5.900-0.430	5.900	-0.424	18:00:39.56	-24:04:11.7	6.20	10.4	0.0	10.6	10.6	Known
G6.189-0.358	6.183	-0.367	18:01:03.34	-23:47:43.6	221.60	-30.2	-37.5	-27.1	10.4	New
G6.368-0.052	6.367	-0.067	18:00:18.93	-23:29:14.7	1.49	144.1	141.0	147.8	6.8	New
G6.539-0.108	6.539	-0.108	18:00:50.72	-23:21:29.9	0.50	13.4	12.7	13.8	1.1	Known
G6.588-0.192	6.600	-0.183	18:01:15.65	-23:20:33.0	7.70	5.0	3.5	7.0	3.5	New
G6.610-0.082	6.617	-0.083	18:00:55.15	-23:16:43.1	21.20	0.8	-6.6	7.5	14.1	Known
G6.795-0.257	6.800	-0.250	18:01:56.68	-23:12:06.6	55.08	16.3	12.1	31.4	19.3	Known
G6.881+0.093	6.883	0.083	18:00:51.88	-22:57:51.9	3.25	-2.1	-3.8	-1.5	2.3	New
G7.166+0.131	7.167	0.117	18:01:20.89	-22:42:06.6	2.47	85.7	74.5	91.0	16.5	New
G7.601-0.139	7.600	-0.150	18:03:16.78	-22:27:23.9	8.12	154.7	151.0	156.5	5.5	New

Table 2: The Catalogue of 6668 MHz Class II methanol masers detected by the Parkes telescope in the MMB Survey. The Parkes source name, Galactic longitude and latitude, the Parkes RA and Dec, the Peak Flux Density, Peak velocity, start velocity, stop velocity, velocity range and its status are listed above.

Source Name	Parkes Gal L	Parkes Gal B	Parkes:RA(2000)	Parkes:DEC(2000)	Parkes Sp	Parkes Vp	Vstart	Vstop	Vrange	Status
G7.632-0.109	7.633	-0.117	18:03:13.51	-22:24:40.4	6.26	157.0	146.5	158.9	12.4	New
G8.139+0.226	8.133	0.217	18:03:02.16	-21:48:42.8	5.24	19.9	18.8	21.8	3.0	Known
G8.317-0.096	8.317	-0.100	18:04:36.74	-21:48:28.4	3.03	47.1	44.0	49.2	5.2	New
G8.669-0.356	8.669	-0.336	18:06:14.47	-21:36:57.9	10.46	39.0	35.8	39.7	3.9	Known
G8.683-0.368	8.683	-0.367	18:06:23.16	-21:37:06.7	141.70	43.2	35.8	45.6	9.8	Known
G8.832-0.028	8.833	-0.033	18:05:27.06	-21:19:29.2	126.80	-3.8	-6.0	5.9	11.9	Known
G8.872-0.493	8.867	-0.500	18:07:16.27	-21:31:24.2	27.37	23.3	22.5	27.5	5.0	Known
G9.215-0.202	9.217	-0.200	18:06:52.67	-21:04:18.0	9.16	45.6	36.0	50.0	14.0	New
G9.6190.193	9.617	0.200	18:06:13.12	-20:31:38.5	5196.00	1.3	-4.8	8.9	13.7	Known
G9.6210.196	9.617	0.183	18:06:17.00::	-20:32:07.3	65.00	5.4	5.0	7.0	2.0	Known
G9.986-0.028	9.983	-0.033	18:07:51.05	-20:19:14.9	70.24	42.2	40.6	51.8	11.2	Known
G10.205-0.345	10.200	-0.333	18:09:25.07	-20:16:36.5	1.28	7.2	5.6	11.0	5.4	New
G10.287-0.125	10.283	-0.133	18:08:49.53	-20:06:30.0	8.29	4.5	1.5	6.0	4.5	Known
G10.299-0.146	10.299	-0.146	18:08:55.46	-20:05:58.1	1.51	20.0	19.0	21.0	2.0	Known
G10.323-0.160	10.317	-0.150	18:08:58.51	-20:05:09.5	94.62	11.6	4.0	16.0	12.0	Known
G10.320-0.259	10.320	-0.260	18:09:23.55	-20:08:10.7	8.87	39.0	35.0	39.6	4.6	Known
G10.342-0.142	10.342	-0.142	18:08:59.89	-20:03:35.7	14.00	14.8	6.0	18.0	12.0	Known
G10.444-0.018	10.456	0.000	18:08:42.78	-19:53:16.4	24.92	73.4	67.6	79.0	11.4	Known
G10.472+0.027	10.467	0.033	18:08:36.13	-19:51:57.2	35.07	75.1	57.5	77.6	20.1	Known
G10.480+0.033	10.480	0.033	18:08:37.89	-19:51:15.8	24.07	59.5	57.0	66.0	9.0	Known
G10.627-0.384	10.617	-0.383	18:10:27.73	-19:56:10.3	3.78	4.6	-6.0	7.7	13.7	Known
G10.629-0.333	10.633	-0.333	18:10:18.61	-19:53:50.9	4.20	-0.4	-13.5	1.0	14.5	Known
G10.735-0.320	10.735	-0.320	18:10:28.18	-19:48:07.2	1.51	-2.1	-2.5	-1.6	0.9	New
G10.792-0.094	10.817	-0.100	18:09:49.10	-19:37:27.1	0.90	72.1	68.0	74.0	6.0	New
G10.886+0.123	10.883	0.117	18:09:07.90	-19:27:44.4	12.24	17.2	14.0	22.5	8.5	Known

Table 3: The Catalogue of 6668 MHz Class II methanol masers detected by the Parkes telescope in the MMB Survey. The Parkes source name, Galactic longitude and latitude, the Parkes RA and Dec, the Peak Flux Density, Peak velocity, start velocity, stop velocity, velocity range and its status are listed above.

Source Name	Parkes Gal L	Parkes Gal B	Parkes:RA(2000)	Parkes:DEC(2000)	Parkes Sp	Parkes Vp	Vstart	Vstop	Vrange	Status
G10.958+0.022	10.950	0.017	18:09:39.51	-19:27:03.9	16.63	24.5	23.0	25.5	2.5	Known
G11.034+0.062	11.034	0.062	18:09:39.79	-19:21:20.4	0.89	20.6	15.2	21.0	5.8	Known
G11.109-0.114	11.117	-0.117	18:10:29.70	-19:22:10.7	14.81	24.1	22.0	34.5	12.5	Known
G11.497-1.485	11.500	-1.484	18:16:21.98	-19:41:16.4	61.75	6.7	4.8	17.0	12.2	Known
G11.903-0.102	11.900	-0.133	18:12:09.19	-18:41:28.1	66.53	42.8	39.5	45.0	5.5	Known
G11.904-0.141	11.916	-0.091	18:12:01.77	-18:39:50.9	11.60	33.8	32.0	36.7	4.7	Known
G11.936-0.616	11.933	-0.174	18:12:22.28	-18:40:54.2	2.30	48.4	46.0	50.0	4.0	Known
G11.936-0.150	11.933	-0.617	18:14:00.77	-18:53:37.0	49.32	32.2	30.1	44.6	14.5	Known
G11.992-0.272	11.999	-0.258	18:12:48.97	-18:39:50.9	1.60	59.8	56.0	60.5	4.5	Known
G12.025-0.025	12.017	-0.033	18:12:01.18	-18:32:26.7	103.10	108.3	105.0	113.1	8.1	Known
G12.112-0.126	12.116	-0.116	18:12:33.02	-18:29:30.4	2.80	39.9	38.0	52.0	14.0	New
G12.181-0.123	12.181	-0.123	18:12:41.10	-18:26:22.9	1.40	29.7	29.0	31.0	2.0	Known
G12.199-0.033	12.199	-0.034	18:12:23.44	-18:22:50.9	16.91	49.3	48.2	57.1	8.9	Known
G12.202-0.120	12.202	-0.120	18:12:42.98	-18:25:11.4	0.60	26.4	26.0	27.0	1.0	Known
G12.203-0.107	12.203	-0.107	18:12:40.22	-18:24:45.8	1.83	20.5	20.0	32.0	12.0	Known
G12.209-0.102	12.217	-0.100	18:12:40.29	-18:23:50.5	10.16	19.8	16.0	22.0	6.0	Known
G12.265-0.051	12.260	-0.051	18:12:34.49	-18:20:07.3	2.56	68.3	58.0	70.9	12.9	Known
G12.526+0.016	12.533	0.025	18:12:50.90	-18:03:34.0	3.30	42.5	38.8	44.0	5.2	New
G12.625-0.017	12.616	-0.016	18:13:11.46	-18:00:18.3	23.61	21.6	21.2	28.0	6.8	Known
G12.681-0.182	12.683	-0.183	18:13:55.27	-18:01:39.7	350.50	57.5	50.0	62.0	12.0	Known
G12.776+0.128	12.783	0.126	18:12:58.90	-17:47:31.0	0.90	32.9	30.4	33.0	2.6	New
G12.889+0.489	12.883	0.483	18:11:52.02	-17:31:56.5	78.93	39.2	28.0	43.0	15.0	Known
G12.904-0.031	12.900	-0.033	18:13:48.21	-17:45:56.3	40.34	59.1	55.8	61.0	5.2	Known
G12.909-0.260	12.909	-0.250	18:14:37.29	-17:51:41.0	245.48	39.9	34.7	47.0	12.3	Known
G13.179+0.061	13.183	0.067	18:14:00.23	-17:28:08.6	2.57	46.5	45.6	50.0	4.4	Known

Table 4: The Catalogue of 6668 MHz Class II methanol masers detected by the Parkes telescope in the MMB Survey. The Parkes source name, Galactic longitude and latitude, the Parkes RA and Dec, the Peak Flux Density, Peak velocity, start velocity, stop velocity, velocity range and its status are listed above.

Source Name	Parkes Gal L	Parkes Gal B	Parkes:RA(2000)	Parkes:DEC(2000)	Parkes Sp	Parkes Vp	Vstart	Vstop	Vrange	Status
G13.657-0.599	13.667	-0.583	18:17:21.90	-17:21:13.8	33.71	51.3	45.0	52.7	7.7	Known
G13.696-0.156	13.700	-0.150	18:15:50.08	-17:07:06.5	1.86	99.4	98.3	108.5	10.2	New
G13.713-0.083	13.717	-0.083	18:15:37.36	-17:04:19.4	12.63	43.6	43.0	53.2	10.2	Known
G14.101+0.087	14.100	0.083	18:15:46.42	-16:39:20.2	86.55	15.4	4.4	16.6	12.2	Known
G14.230-0.509	14.233	-0.500	18:18:10.94	-16:48:55.5	3.62	25.3	24.6	26.7	2.1	New
G14.390-0.020	14.383	-0.033	18:16:45.87	-16:27:42.9	4.40	26.9	24.5	28.5	4.0	Known
G14.457-0.143	14.450	-0.133	18:17:15.81	-16:27:02.8	1.48	43.1	38.0	44.2	6.2	New
G14.490+0.014	14.483	0.017	18:16:46.75	-16:21:00.6	1.15	20.2	19.8	24.5	4.7	New
G14.521+0.155	14.517	0.167	18:16:17.72	-16:14:58.3	1.31	4.1	-3.0	6.0	9.0	New
G14.604+0.017	14.600	0.017	18:17:00.61	-16:14:51.1	2.30	24.7	22.1	35.8	13.7	Known
G14.631-0.577	14.617	-0.567	18:19:11.09	-16:30:33.3	1.18	25.2	23.9	25.9	2.0	New
G14.991-0.121	14.983	-0.117	18:18:15.37	-15:58:23.8	6.63	46.0	44.6	54.0	9.4	Known
G15.034-0.677	15.033	-0.667	18:20:22.32	-16:11:21.4	51.59	21.3	20.0	24.0	4.0	Known
G15.094+0.192	15.100	0.200	18:17:19.60	-15:43:13.7	18.62	25.8	22.5	26.5	4.0	New
G15.607-2.550	15.600	-0.250	18:19:57.36	-15:29:34.8	0.85	66.0	65.1	66.5	1.4	New
G15.665-0.499	15.667	-0.500	18:21:00.10	-15:33:07.5	47.65	-2.9	-5.0	-2.0	3.0	Known
G16.112-0.303	16.117	-0.300	18:21:08.92	-15:03:39.3	2.22	34.5	33.4	35.6	2.3	New
G16.302-0.196	16.300	-0.183	18:21:04.80	-14:50:39.2	9.91	51.8	46.9	53.6	6.7	Known
G16.403-0.181	16.417	-0.183	18:21:18.43	-14:44:28.7	0.50	39.2	39.1	40.0	0.9	New
G16.585-0.051	16.583	-0.050	18:21:08.71	-14:31:53.3	33.30	62.1	56.5	69.5	13.0	Known
G16.662-0.331	16.667	-0.333	18:22:20.44	-14:35:28.2	2.56	43.0	42.5	44.2	1.8	New
G16.831+0.079	16.833	0.083	18:21:08.74	-14:14:53.3	4.44	58.7	57.2	69.4	12.1	New
G16.855+0.641	16.850	0.650	18:19:07.04	-13:57:57.8	1.49	24.2	23.0	25.0	2.0	New
G16.976-0.005	16.983	0.000	18:21:44.42	-14:09:17.9	0.70	6.6	5.0	9.0	4.0	New
G17.029-0.071	17.033	-0.067	18:22:04.79	-14:08:32.2	1.69	91.4	90.4	96.0	5.6	Known

Table 5: The Catalogue of 6668 MHz Class II methanol masers detected by the Parkes telescope in the MMB Survey. The Parkes source name, Galactic longitude and latitude, the Parkes RA and Dec, the Peak Flux Density, Peak velocity, start velocity, stop velocity, velocity range and its status are listed above.

Source Name	Parkes Gal L	Parkes Gal B	Parkes:RA(2000)	Parkes:DEC(2000)	Parkes Sp	Parkes Vp	Vstart	Vstop	Vrange	Status
G17.638+0.157	17.633	0.167	18:22:23.55	-13:30:10.6	34.17	20.8	20.0	22.0	2.0	Known
G17.862+0.074	17.850	0.083	18:23:06.80	-13:21:02.6	1.42	110.5	107.3	119.6	12.3	New
G18.073+0.077	18.067	0.083	18:23:31.84	-13:09:33.7	6.00	55.8	44.0	57.5	13.5	Known
G18.159+0.094	18.167	0.100	18:23:39.76	-13:03:47.5	10.25	59.0	54.0	60.0	6.0	Known
G18.262-0.244	18.267	-0.233	18:25:03.88	-13:07:50.8	22.98	74.2	72.0	81.0	9.0	Known
G18.341+1.768	18.350	1.767	18:17:59.37	-12:06:59.0	99.28	28.1	26.0	32.0	6.0	Known
G18.440+0.045	18.433	0.050	18:24:21.39	-12:51:03.5	2.45	61.8	57.0	66.0	9.0	New
G18.460-0.004	18.467	0.000	18:24:36.11	-12:50:41.6	25.30	49.4	46.7	50.0	3.3	Known
G18.667+0.025	18.667	0.033	18:24:51.87	-12:39:09.0	8.78	76.6	76.1	81.0	4.9	Known
G18.735-0.227	18.733	-0.233	18:25:57.54	-12:43:05.1	3.59	38.2	36.3	38.5	2.2	New
G18.834-0.300	18.833	-0.300	18:26:23.52	-12:39:38.5	7.47	41.2	37.5	44.0	6.5	Known
G18.874+0.053	18.883	0.050	18:25:13.14	-12:27:11.4	9.80	38.7	37.7	40.6	2.8	Known
G18.888-0.475	18.883	-0.467	18:27:05.53	-12:41:38.7	5.56	56.4	53.0	57.6	4.6	Known
G19.009-0.029	19.017	-0.233	18:26:30.02	-12:28:03.1	0.90	69.4	65.0	69.8	4.8	New
G19.025-0.259	19.017	-0.033	18:25:46.54	-12:22:27.2	20.39	55.4	53.0	63.0	10.0	Known
G19.249+0.267	19.250	0.267	18:25:08.16	-12:01:40.1	3.35	19.8	12.5	21.0	8.5	New
G19.267+0.349	19.267	0.350	18:24:51.99	-11:58:26.8	3.40	16.3	12.5	17.5	5.0	New
G19.365-0.030	19.367	-0.033	18:26:26.63	-12:03:52.6	34.16	25.3	24.0	30.0	6.0	Known
G19.496+0.115	19.483	0.167	18:25:56.58	-11:52:05.3	5.00	20.9	19.0	27.5	8.5	Known
G19.472+0.170	19.483	0.167	18:25:56.58	-11:52:05.3	15.06	21.7	17.0	23.0	6.0	Known
G19.472+0.170	19.483	0.183	18:25:52.96	-11:51:37.3	1.97	13.8	12.7	17.7	5.0	Known
G19.609-0.234	19.609	-0.234	18:27:37.93	-11:56:36.9	1.00	40.2	36.0	42.0	6.0	Known
G19.612-0.134	19.617	-0.133	18:27:16.92	-11:53:23.9	11.74	56.5	49.0	61.0	12.0	Known
G19.614+0.011	19.617	0.017	18:26:44.36	-11:49:12.4	3.80	32.9	30.8	34.8	4.0	New
G19.667+0.117	19.667	0.117	18:26:28.39	-11:43:45.3	1.52	16.3	13.4	17.8	4.4	New

Table 6: The Catalogue of 6668 MHz Class II methanol masers detected by the Parkes telescope in the MMB Survey. The Parkes source name, Galactic longitude and latitude, the Parkes RA and Dec, the Peak Flux Density, Peak velocity, start velocity, stop velocity, velocity range and its status are listed above.

Source Name	Parkes Gal L	Parkes Gal B	Parkes:RA(2000)	Parkes:DEC(2000)	Parkes Sp	Parkes Vp	Vstart	Vstop	Vrange	Status
G19.701-0.267	19.700	-0.267	18:27:55.37	-11:52:41.6	11.72	43.8	41.5	46.5	5.0	Known
G19.755-0.128	19.750	-0.117	18:27:28.52	-11:45:51.1	2.31	123.1	115.5	124.0	8.5	New
G19.884-0.534	19.883	-0.533	18:29:14.17	-11:50:23.1	6.83	46.8	46.0	48.0	2.0	Known
G20.081-0.135	20.083	-0.133	18:28:10.12	-11:28:36.7	1.62	43.6	42.2	45.4	3.2	Known
G20.237+0.065	20.250	0.067	18:27:45.74	-11:14:10.7	86.22	71.9	62.9	80.1	17.2	Known
G20.364-0.013	20.367	0.000	18:28:13.45	-11:09:50.4	3.02	56.0	49.8	59.3	9.5	New
G20.733-0.059	20.750	-0.067	18:29:11.42	-10:51:19.7	1.52	60.8	60.1	63.6	3.5	New
G20.927-0.050	20.933	-0.050	18:29:28.58	-10:41:07.4	2.73	25.9	23.5	29.4	5.9	New
G20.963-0.075	20.967	-0.067	18:29:35.97	-10:39:48.9	2.27	34.6	33.6	34.8	1.2	New
G21.023-0.063	21.033	-0.050	18:29:39.91	-10:35:48.5	2.16	31.2	30.5	32.4	1.9	New
G21.407-0.254	21.417	-0.250	18:31:06.51	-10:20:58.9	13.01	89.0	82.7	92.1	9.4	Known
G21.562-0.033	21.567	-0.033	18:30:36.61	-10:06:59.1		117.2	108.8	120.7	11.9	Known
G21.866-0.233	21.866	-0.233	18:31:53.54	-09:56:36.3	0.93	82.0	81.3	83.8	2.5	New
G21.880+0.014	21.883	0.017	18:31:01.53	-09:48:45.3	5.36	20.4	19.2	22.2	3.0	Known
G22.038+0.222	22.050	0.217	18:30:37.16	-09:34:20.1	4.97	49.5	45.6	55.2	9.7	Known
G22.335-0.155	22.333	-0.150	18:32:28.16	-09:29:26.2	38.88	35.6	23.1	42.1	19.1	Known
G22.356+0.066	22.367	0.067	18:31:45.16	-09:21:39.4	12.92	80.2	75.2	89.6	14.4	Known
G22.435-0.169	22.433	-0.170	18:32:43.68	-09:24:41.01	13.81	29.6	22.0	40.3	18.3	Known
G23.003+0.124	23.000	0.133	18:32:41.92	-08:46:06.3	2.47	110.7	109.0	112.5	3.5	New
G23.010-0.411	23.017	-0.400	18:34:38.73	-08:59:58.9	482.60	74.8	68.0	87.5	19.6	Known
G23.126+0.395	23.117	0.400	18:31:57.65	-08:32:29.4	1.95	22.1	21.5	22.4	0.9	New
G23.133+0.400	23.133	0.400	18:31:38.32	-08:31:38.3	1.36	13.6	11.9	14.6	2.7	New
G23.133+0.417	23.133	0.417	18:31:55.85	-08:31:09.7	0.75	17.9	17.7	18.3	0.6	New
G23.206-0.378	23.216	-0.366	18:34:53.73	-08:48:25.3	41.15	81.7	75.1	85.5	10.4	Known
G23.257-0.241	23.267	-0.233	18:34:30.77	-08:42:03.5	8.53	64.1	58.4	66.5	8.1	Known

Table 7: The Catalogue of 6668 MHz Class II methanol masers detected by the Parkes telescope in the MMB Survey. The Parkes source name, Galactic longitude and latitude, the Parkes RA and Dec, the Peak Flux Density, Peak velocity, start velocity, stop velocity, velocity range and its status are listed above.

Source Name	Parkes Gal L	Parkes Gal B	Parkes:RA(2000)	Parkes:DEC(2000)	Parkes Sp	Parkes Vp	Vstart	Vstop	Vrange	Status
G23.365-0.291	23.367	-0.283	18:34:52.73	-08:38:06.9	1.96	82.6	81.9	83.3	1.4	New
G23.389+0.185	23.400	0.183	18:33:15.95	-08:23:26.0	39.07	74.6	72.0	77.6	5.6	Known
G23.437-0.184	23.433	-0.183	18:34:38.63	-08:31:48.0	75.42	103.0	91.7	111.2	19.6	Known
G23.4840.097	23.483	0.100	18:33:43.21	-08:21:19.2	9.33	87.2	81.4	93.0	11.7	Known
G23.657-0.127	23.667	-0.117	18:34:50.35	-08:17:31.8	14.17	82.4	75.4	88.5	13.1	Known
G23.706-0.198	23.717	-0.200	18:33:47.86	-08:06:05.7	11.74	79.1	72.7	81.0	8.3	Known
G23.8830.067	23.883	0.067	18:34:35.09	-08:00:55.5	1.51	43.9	43.1	45.4	2.3	Known
G23.9170.083	23.917	0.083	18:34:35.23	-07:58:41.3	0.79	31.6	31.0	32.1	1.1	New
G23.966-0.109	23.967	-0.100	18:35:20.25	-08:01:05.5	18.64	70.9	60.1	75.9	15.8	Known
G24.147-0.009	24.133	-0.017	18:35:20.91	-07:49:54.7	27.11	17.5	12.7	22.6	9.8	Known
G24.329+0.144	24.317	0.133	18:35:09.09	-07:36:00.2	0.83	115.5	115.1	115.7	0.6	Known
G24.450+0.200	24.450	0.200	18:35:09.63	-07:27:03.6	3.73	125.1	119.7	126.0	6.3	New
G24.493-0.039	24.483	-0.050	18:36:07.07	-07:32:11.1	11.45	115.2	107.0	121.1	14.1	Known
G24.541+0.312	24.533	0.317	18:34:53.85	-07:19:23.8	35.99	105.6	100.8	114.4	13.6	Known
G24.633-0.333	24.633	-0.333	18:37:24.60	-07:32:00.8	4.20	43.9	34.9	46.4	11.5	Known
G24.667-0.150	24.667	-0.150	18:36:48.97	-07:25:10.4	4.18	116.3	111.8	117.4	5.6	Known
G24.790+0.083	24.783	0.083	18:36:11.87	-07:12:31.3	115.50	113.4	102.6	119.9	17.3	Known
G24.850+0.087	24.917	0.083	18:36:26.63	-07:05:25.0	7.64	53.3	51.4	53.8	2.5	Known
G24.933+0.067	24.933	0.067	18:36:32.06	-07:04:59.3	3.07	46.7	45.0	47.8	2.8	Known
G25.217+0.283	25.217	0.283	18:36:17.02	-06:43:55.1	3.23	42.1	40.9	42.6	1.7	New
G25.267-0.433	25.267	-0.433	18:38:56.48	-07:00:59.8	1.96	65.9	53.9	67.2	13.3	Known
G25.367-0.183	25.367	-0.183	18:38:13.86	-06:48:47.0	2.76	58.2	56.5	58.6	2.1	Known
G25.383-0.183	25.383	-0.183	18:38:15.71	-06:47:53.7	2.66	60.7	60.2	62.3	2.1	Known
G25.400+0.100	25.399	0.100	18:37:16.65	-06:39:15.3	19.63	97.2	93.5	97.9	4.4	Known
G25.483+0.083	25.483	0.083	18:37:29.56	-06:35:14.3	1.21	93.1	92.5	93.5	1.0	New

Table 8: The Catalogue of 6668 MHz Class II methanol masers detected by the Parkes telescope in the MMB Survey. The Parkes source name, Galactic longitude and latitude, the Parkes RA and Dec, the Peak Flux Density, Peak velocity, start velocity, stop velocity, velocity range and its status are listed above.

Source Name	Parkes Gal L	Parkes Gal B	Parkes:RA(2000)	Parkes:DEC(2000)	Parkes Sp	Parkes Vp	Vstart	Vstop	Vrange	Status
G25.617+0.217	25.617	0.217	18:37:15.74	-06:24:26.4	0.78	109.8	109.7	110.8	1.1	New
G25.650+1.050	25.650	1.050	18:34:20.78	-05:59:40.2	72.33	41.9	34.4	46.9	12.5	Known
G25.710+0.044	25.700	0.050	18:38:00.73	-06:24:35.3	607.00	95.6	89.0	103.3	14.3	Known
G25.826-0.178	25.816	-0.183	18:39:03.62	-06:24:49.0	70.82	91.6	89.5	99.9	10.5	Known
G25.833-0.383	25.833	-0.383	18:39:48.51	-06:29:24.1	0.79	-1.8	-2.1	-1.2	1.0	New
G25.917-0.124	25.917	-0.124	18:39:02.14	-06:17:48.5	1.55	113.9	113.2	114.3	1.1	New
G26.417+1.684	26.417	1.684	18:33:30.32	-05:01:19.9	2.84	31.1	27.7	31.8	4.0	New
G26.533+0.417	26.533	0.417	18:38:14.40	-05:30:04.0	1.34	82.3	81.5	83.0	1.6	New
G26.550-0.300	26.550	-0.300	18:40:49.86	-05:48:53.2	3.19	109.6	106.8	110.4	3.7	Known
G26.600-0.217	26.600	-0.217	18:40:37.51	-05:43:55.8	18.65	103.4	102.4	115.9	13.5	Known
G26.600-0.020	26.600	-0.017	18:39:54.63	-05:38:26.0	14.67	24.9	16.7	29.7	13.0	Known
G26.650+0.017	26.650	0.017	18:39:53.01	-05:34:51.1	2.20	107.7	106.4	108.2	1.8	Known
G27.000-0.033	27.000	-0.033	18:40:42.37	-05:17:33.6	2.12	-21.0	-22.1	-17.8	4.3	New
G27.217+0.250	27.217	0.133	18:40:30.58	-05:01:25.4	27.80	118.7	112.7	124.1	11.4	Known
G27.217+0.133	27.217	0.250	18:40:05.59	-04:58:13.1	8.67	9.2	7.4	11.4	4.0	Known
G27.283+0.150	27.283	0.150	18:40:34.36	-04:57:24.6	38.32	34.8	23.4	37.2	13.8	Known
G27.367-0.167	27.367	-0.167	18:41:51.38	-05:01:39.6	46.03	100.2	87.6	106.3	18.7	Known
*** 0.967	18:38:08.99	-04:20:44.0	0.71	67.0	66.6	67.4	0.8	New		
G27.567+0.100	27.567	0.100	18:41:16.31	-04:43:40.1	0.91	87.3	86.2	88.0	1.8	New
G27.783-0.250	27.783	-0.250	18:42:55.13	-04:41:42.8	3.93	98.2	96.2	99.4	3.2	Known
G27.785+0.057	27.783	0.050	18:41:50.89	-04:33:28.9	3.03	108.5	108.3	113.2	4.9	Known
G27.867-0.233	27.867	-0.233	18:43:00.73::	-04:36:46.9	0.40	20.1	19.8	20.4	0.6	Known
G27.917+1.850	27.917	1.850	18:35:40.59	-03:36:51.7	0.64	103.7	103.6	103.9	0.3	New
G28.011-0.426	28.017	-0.433	18:44:00.07	-04:34:17.3	10.07	16.9	11.9	28.6	16.7	Known
G28.117+0.867	28.117	0.867	18:39:32.88	-03:53:15.9	0.63	112.7	112.6	113.1	0.4	New

Table 9: The Catalogue of 6668 MHz Class II methanol masers detected by the Parkes telescope in the MMB Survey. The Parkes source name, Galactic longitude and latitude, the Parkes RA and Dec, the Peak Flux Density, Peak velocity, start velocity, stop velocity, velocity range and its status are listed above.

Source Name	Parkes Gal L	Parkes Gal B	Parkes:RA(2000)	Parkes:DEC(2000)	Parkes Sp	Parkes Vp	Vstart	Vstop	Vrange	Status
G28.148-0.004	28.150	0.000	18:42:41.96	-04:15:17.4	58.09	101.2	93.6	108.0	14.4	Known
G28.201-0.049	28.199	-0.058	18:42:59.69	-04:14:16.0	2.72	97.3	93.8	98.0	4.2	Known
G28.282-0.359	28.282	-0.358	18:44:13.08	-04:18:02.6	2.90	40.9	40.0	43.1	3.1	Known
G28.305-0.387	28.299	-0.391	18:44:22.05	-04:18:04.1	72.80	81.6	74.4	87.4	12.9	Known
G28.321-0.011	28.316	-0.008	18:43:01.83	-04:06:39.9	2.06	103.6	102.4	106.2	3.9	New
G28.399+0.076	28.399	0.076	18:42:53.17	-03:59:55.9	12.98	71.5	68.1	82.3	14.2	Known
G28.500+0.133	28.500	0.133	18:42:51.93	-03:52:57.3	0.95	39.4	39.0	40.0	1.1	New
G28.532+0.126	28.532	0.126	18:42:57.14	-03:51:26.5	2.41	27.4	23.7	28.1	4.4	Known
G28.608+0.018	28.599	0.009	18:43:29.43	-03:51:04.9	3.46	106.4	104.8	106.9	2.1	New
G28.687-0.283	28.699	-0.274	18:44:41.05	-03:53:30.7	1.20	92.4	91.7	92.7	1.1	New
G28.699+0.409	28.699	0.409	18:42:14.87	-03:34:46.5	1.58	94.3	87.8	94.8	7.0	Known
G28.816+0.359	28.816	0.359	18:42:38.39	-03:29:55.2	8.06	90.7	87.4	97.5	10.1	Known
G28.832-0.253	28.832	-0.258	18:44:52.13	-03:45:56.2	83.77	83.5	79.5	92.6	13.1	Known
G28.848-0.228	28.832	0.492	18:42:11.71	-03:25:22.4	3.98	83.2	82.5	86.3	3.8	Known
G28.850-0.233	28.850	-0.233	18:44:48.86	-03:44:19.6	2.35	102.8	102.6	103.6	1.0	Known
G28.883+1.100	28.883	1.100	18:40:07.41	-03:05:59.2	0.80	-34.5	-34.7	-34.2	0.5	New
G29.316-0.174	29.316	-0.174	18:45:27.38	-03:17:51.0	8.50	48.9	40.9	49.7	8.8	Known
G29.603-0.625	29.599	-0.624	18:47:34.72	-03:15:02.7	2.04	81.5	80.2	82.5	2.3	New
G29.865-0.043	29.932	-0.174	18:46:34.94	-02:44:56.6	1.79	95.9	95.7	97.1	1.4	New
G29.956-0.016	29.949	0.007	18:46:01.23	-02:39:28.5	238.15	96.0	93.3	106.5	13.2	Known
G29.979-0.047	29.982	-0.041	18:46:11.99	-02:38:37.9	37.26	103.0	97.6	105.8	8.2	Known
G29.993-0.283	30.000	-0.283	18:47:05.70	-02:44:17.8	2.60	103.0	103.0	103.9	0.9	New
G30.010-0.273	30.010	-0.273	18:47:09.27	-02:43:36.5	2.24	106.1	105.5	106.3	0.8	New
G30.116-0.058	30.116	-0.058	18:46:30.20	-02:31:56.8	0.71	96.0	94.8	97.4	2.6	New
G30.199-0.169	30.199	-0.174	18:47:04.27	-02:30:41.5	35.50	108.6	101.1	117.8	16.7	Known

Table 10: The Catalogue of 6668 MHz Class II methanol masers detected by the Parkes telescope in the MMB Survey. The Parkes source name, Galactic longitude and latitude, the Parkes RA and Dec, the Peak Flux Density, Peak velocity, start velocity, stop velocity, velocity range and its status are listed above.

Source Name	Parkes Gal L	Parkes Gal B	Parkes:RA(2000)	Parkes:DEC(2000)	Parkes Sp	Parkes Vp	Vstart	Vstop	Vrange	Status
G30.206-0.165	30.216	-0.174	18:47:06.07	-02:29:46.9	14.20	113.4	101.1	117.8	16.7	Known
G30.317+0.070	30.316	0.076	18:46:23.62	-02:17:37.0	14.70	36.5	33.7	51.4	17.7	Known
G30.370+0.482	30.366	0.492	18:45:00.07	-02:03:32.1	1.92	19.5	16.3	19.8	3.5	New
G30.419-0.232	30.415	0.458	18:45:12.68	-02:01:46.7	1.98	8.0	5.1	9.1	4.0	New
G30.424+0.466	30.416	-0.241	18:47:42.27	-02:20:56.9	26.55	103.0	95.9	109.7	13.8	Known
G30.532+0.009	30.532	0.009	18:47:01.59	-02:07:54.0	0.95	53.2	52.2	54.8	2.6	Known
G30.583-0.141	30.583	-0.141	18:47:39.16	-02:09:18.7	1.28	115.5	115.0	116.4	1.4	Known
G30.591-0.042	30.583	-0.041	18:47:17.79	-02:06:34.5	7.10	43.1	40.2	49.1	8.9	Known
G30.704-0.068	30.699	-0.074	18:47:37.69	-02:01:15.4	131.40	88.2	85.2	92.6	7.4	Known
G30.760-0.052	30.766	-0.808	18:50:21.75	-02:17:45.6	10.10	74.4	69.6	80.1	10.5	New
G30.770+0.080	30.766	-0.058	18:47:41.55	-01:57:14.4	60.22	91.7	88.0	92.6	4.6	Known
G30.770-0.805	30.782	0.225	18:46:42.72	-01:48:35.7	57.02	49.0	44.8	54.2	9.4	Known
G30.788+0.204	30.783	0.076	18:47:14.78	-01:52:39.9	1.45	98.7	96.9	99.0	2.1	New
G30.781+0.231	30.788	0.204	18:46:46.36	-01:49:01.4	22.02	84.5	75.7	89.8	14.1	Known
G30.818-0.057	30.816	-0.058	18:47:46.91	-01:54:34.3	9.52	108.3	104.0	111.0	7.0	Known
G30.816+1.276	30.816	-0.058	18:47:46.91	-01:54:34.3	5.55	101.4	99.6	110.0	10.4	Known
G30.818-0.057	30.816	-0.058	18:47:46.91	-01:54:34.3	9.16	93.1	92.0	98.0	6.0	Known
G30.819+0.273	30.816	0.292	18:46:32.24	-01:44:59.3	2.90	104.8	99.2	110.6	11.4	Known
G30.822-0.053	30.816	1.276	18:43:02.09	-01:18:02.4	1.57	101.8	101.5	101.9	0.4	New
G30.851+0.123	30.849	0.125	18:47:11.39	-01:47:46.4	1.47	29.0	27.2	29.4	2.2	New
G30.898+0.162	30.899	0.159	18:47:09.75	-01:44:11.9	76.98	101.8	98.6	110.3	11.7	Known
G30.966-0.141	30.966	-0.141	18:48:21.15	-01:48:50.5	25.82	77.9	69.7	82.6	12.9	Known
G30.970+0.080	30.966	0.076	18:47:34.83	-01:42:53.6	1.60	39.8	34.8	44.8	10.1	New
G30.973+0.562	30.967	0.567	18:45:50.03	-01:29:25.8	0.95	19.9	19.0	20.6	1.6	New
G30.980+0.216	30.980	0.216	18:47:04.64	-01:37:52.8	2.38	111.2	110.8	111.3	0.5	New

Table 11: The Catalogue of 6668 MHz Class II methanol masers detected by the Parkes telescope in the MMB Survey. The Parkes source name, Galactic longitude and latitude, the Parkes RA and Dec, the Peak Flux Density, Peak velocity, start velocity, stop velocity, velocity range and its status are listed above.

Source Name	Parkes Gal L	Parkes Gal B	Parkes:RA(2000)	Parkes:DEC(2000)	Parkes Sp	Parkes Vp	Vstart	Vstop	Vrange	Status
G31.049+0.359	31.049	0.359	18:46:43.46	-01:30:42.3	4.40	80.9	78.0	83.2	5.3	Known
G31.061+0.094	31.050	0.083	18:47:42.42	-01:38:12.7	23.83	16.5	11.3	21.2	9.8	Known
G31.076+0.457	31.066	0.459	18:46:23.92	-01:27:04.5	1.15	26.8	24.9	27.4	2.5	New
G31.122+0.063	31.117	0.067	18:47:53.29	-01:35:06.4	2.85	48.1	47.3	48.4	1.1	New
G31.150+0.050	31.150	0.050	18:48:00.50	-01:33:47.0	4.35	41.2	39.2	42.9	3.7	Known
G31.182-0.148	31.183	-0.158	18:48:48.45	-01:37:43.6	3.07	46.3	43.2	49.9	6.7	New
G31.282+0.062	31.283	0.059	18:48:13.11	-01:26:27.4	131.40	110.4	102.0	114.0	12.0	Known
G31.411+0.307	31.416	0.309	18:47:34.31	-01:12:29.5	22.28	95.8	87.6	105.9	18.3	Known
G31.583+0.076	31.583	0.076	18:48:42.41	-01:09:58.7	9.60	98.9	94.5	100.3	5.8	Known
G31.594-0.192	31.583	-0.200	18:49:41.36	-01:17:29.1	1.84	48.2	47.9	49.1	1.1	New
G32.050+0.059	32.050	0.059	18:49:37.08	-00:45:30.2	163.30	92.9	87.7	106.4	18.7	Known
G32.117+0.100	32.117	0.100	18:49:35.73	-00:40:46.8	4.61	97.7	91.4	98.7	7.3	Known
G32.516+0.323	32.517	0.317	18:49:33.16	-00:13:30.6	2.06	52.4	51.9	53.3	1.4	New
G32.744-0.075	32.750	-0.083	18:51:24.13	-00:11:59.6	59.63	38.5	25.5	44.2	18.8	Known
G32.802+0.193	32.800	0.200	18:50:29.09	-00:01:34.3	1.04	27.5	26.2	28.1	1.8	Known
G32.825-0.328	32.817	-0.333	18:52:24.83	-00:15:16.3	1.65	82.3	81.2	83.7	2.5	New
G32.917-0.083	32.917	-0.083	18:51:42.38	00:03:05.5	1.00	103.6	103.2	104.2	1.1	New
G32.983-0.333	32.983	-0.333	18:52:43.07	00:06:22.3	0.83	48.7	48.2	50.0	1.8	New
G32.999+0.033	32.999	0.033	18:51:26.56	00:04:29.1	18.18	91.9	89.4	92.3	2.9	Known
G33.100-0.067	33.100	-0.067	18:51:58.88	00:07:09.3	19.90	103.9	94.4	106.5	12.1	Known
G33.133-0.083	33.133	-0.083	18:52:06.08	00:08:28.4	16.93	73.2	68.7	81.9	13.2	Known
G33.317-0.360	33.317	-0.360	18:53:28.30	00:10:19.8	1.29	29.3	25.7	31.3	5.6	New
G33.400+0.017	33.400	0.017	18:52:13.91	00:25:27.0	23.71	105.3	93.1	111.1	17.9	Known
G33.486+0.040	33.500	0.050	18:52:17.73	00:31:42.7	3.93	122.8	121.8	123.9	2.1	New
G33.634-0.021	33.633	-0.233	18:53:32.77	00:31:03.7	1289.87	59.6	57.9	63.3	5.4	Known

Table 12: The Catalogue of 6668 MHz Class II methanol masers detected by the Parkes telescope in the MMB Survey. The Parkes source name, Galactic longitude and latitude, the Parkes RA and Dec, the Peak Flux Density, Peak velocity, start velocity, stop velocity, velocity range and its status are listed above.

Source Name	Parkes Gal L	Parkes Gal B	Parkes:RA(2000)	Parkes:DEC(2000)	Parkes Sp	Parkes Vp	Vstart	Vstop	Vrange	Status
G33.648-0.224	33.634	-0.021	18:53:18.68	00:38:31.8	0.84	” 103.6 ”	102.7	103.7	1.0	New
G33.733-0.117	33.733	-0.117	18:53:18.94	00:39:34.5	3.28	53.4	52.9	54.8	1.9	Known
G33.867+0.033	33.867	0.033	18:53:01.42	00:50:49.6	3.38	64.1	62.4	65.0	2.6	Known
G33.983-0.017	33.983	-0.017	18:53:24.87	00:55:41.3	5.43	58.9	58.6	59.6	1.1	Known
G34.100+0.017	34.100	0.017	18:53:30.52	01:02:49.8	5.56	56.0	54.0	57.8	3.9	Known
G34.250+0.160	34.250	0.160	18:53:16.36	01:14:45.7	26.00	57.8	57.0	62.0	5.0	Known
G34.267-0.217	34.267	-0.217	18:54:38.62	01:05:20.6	8.14	54.6	49.6	55.1	5.5	New
G34.267+0.150	34.267	0.150	18:53:20.29	01:15:22.7	20.00	55.0	50.7	63.8	13.1	Known
G34.400+0.216	34.400	0.216	18:53:20.81	01:24:18.2	11.00	55.7	55.3	63.3	8.0	Known
G34.767-0.100	34.767	-0.100	18:55:08.45	01:35:14.1	4.74	52.8	48.0	53.8	5.8	Known
G34.767+0.017	34.767	0.017	18:54:43.52	01:38:25.7	1.88	76.5	76.1	77.3	1.2	Known
G34.800-1.384	34.800	-1.384	18:59:46.28	01:01:52.7	24.49	47.0	39.4	53.3	13.9	Known
G34.817+0.350	34.817	0.350	18:53:37.77	01:50:13.3	0.72	59.7	59.4	60.1	0.7	Known
G35.023+0.348	35.030	0.350	18:54:01.49	02:01:47.1	24.80	44.4	38.8	52.0	13.2	Known
G35.200-1.730	35.133	-0.750	18:58:07.48::	01:36:59.5	84.28	35.4	29.5	37.8	8.3	Known
G35.133-0.750	35.200	-1.730	19:01:44.81	01:13:35.4	965.20	42.5	35.8	50.5	14.7	Known
G35.200-0.750	35.200	-0.750	18:58:14.79	01:40:33.7	174.00	28.5	25.8	35.0	9.2	Known
G35.250-0.250	35.250	-0.250	18:56:33.45	01:56:55.8	1.68	72.4	72.0	73.4	1.4	Known
G35.400+0.020	35.400	0.020	18:55:52.91	02:12:14.5	1.48	89.0	88.7	90.1	1.4	Known
G35.583+0.067	35.583	0.067	18:56:02.24	02:23:23.4	0.71	45.2	44.0	47.2	3.2	Known
G35.800-0.180	35.800	-0.180	18:57:19.51	02:28:07.1	23.11	60.8	52.7	67.8	15.1	Known
G36.120+0.550	36.120	0.550	18:55:17.44	03:05:06.3	29.25	73.0	65.7	84.8	19.2	Known
G36.170-0.900	36.170	-0.900	19:00:32.90	02:28:02.6	0.55	90.1	90.0	90.3	0.4	New
G36.650-0.217	36.650	-0.217	18:59:00.02	03:12:34.0	1.03	77.4	77.3	77.6	0.3	Known
G36.700+0.100	36.700	0.100	18:57:57.69	03:23:55.4	7.14	53.1	52.0	63.0	11.1	Known

Table 13: The Catalogue of 6668 MHz Class II methanol masers detected by the Parkes telescope in the MMB Survey. The Parkes source name, Galactic longitude and latitude, the Parkes RA and Dec, the Peak Flux Density, Peak velocity, start velocity, stop velocity, velocity range and its status are listed above.

Source Name	Parkes Gal L	Parkes Gal B	Parkes:RA(2000)	Parkes:DEC(2000)	Parkes Sp	Parkes Vp	Vstart	Vstop	Vrange	Status
G36.850-0.020	36.850	-0.020	18:58:39.12	03:28:44.0	2.55	61.7	60.8	64.6	3.9	Known
G36.930+0.480	36.930	0.480	18:57:01.30	03:46:53.0	1.21	-35.9	-36.4	-35.1	1.2	Known
G37.033-0.033	37.033	-0.033	18:59:02.82	03:38:03.4	9.56	78.5	74.0	86.0	12.0	Known
G37.433+1.517	37.433	1.517	18:54:14.77	04:41:50.4	336.10	41.2	36.3	46.5	10.3	Known
G37.483-0.100	37.483	-0.100	19:00:06.56	04:00:14.7	10.02	54.7	52.0	67.4	15.5	Known
G37.550-0.100	37.550	-0.100	19:00:13.89	04:03:48.2	5.01	50.0	49.3	51.6	2.3	Known
G37.550+0.200	37.550	0.200	18:59:09.69	04:12:01.9	14.71	83.8	78.5	91.7	13.2	Known
G37.600+0.433	37.600	0.433	18:58:25.23	04:21:05.7	19.77	87.0	81.7	92.4	10.7	Known
G37.733-0.100	37.733	-0.100	19:00:34.07	04:13:35.1	1.02	50.3	50.0	50.5	0.4	Known
G37.750-0.183	37.750	-0.183	19:00:53.73	04:12:11.3	1.71	54.8	54.5	56.0	1.5	Known
G37.800-0.217	37.800	-0.217	19:01:06.48::	04:13:55.9	0.50	69.0	68.5	70.0	1.5	Known
G38.033-0.300	38.033	-0.300	19:01:49.91	04:24:06.0	10.45	58.2	51.2	62.9	11.7	Known
G38.117-0.233	38.117	-0.233	19:01:44.82	04:30:22.6	2.65	70.3	67.3	80.1	12.8	Known
G38.200-0.067	38.200	-0.067	19:01:18.32	04:39:23.9	10.13	84.3	74.8	88.0	13.2	Known
G38.267-0.200	38.267	-0.200	19:01:54.22	04:39:17.6	0.98	70.2	68.7	70.5	1.8	Known
G38.267-0.083	38.267	-0.083	19:01:29.24	04:42:29.9	8.01	15.4	6.1	20.0	13.9	Known
G38.5670+.533	38.567	0.533	18:59:50.18	05:15:25.8	1.50	-28.8	-30.0	-27.2	2.8	New
G38.600-0.217	38.600	-0.217	19:02:34.65	04:56:36.4	0.56	62.4	62.3	63.4	1.1	Known
G38.650+0.083	38.650	0.083	19:01:35.80	05:07:31.5	1.63	-31.4	-31.6	-31.1	0.5	Known
G38.917-0.350	38.917	-0.350	19:03:38.07	05:09:50.5	2.78	32.0	30.9	33.9	3.0	Known
G39.100+0.500	39.100	0.500	19:00:56.11	05:42:58.0	22.57	15.9	10.1	23.5	13.4	Known
G39.400-0.133	39.400	-0.133	19:03:45.05	05:41:34.2	1.34	60.4	59.5	61.1	1.6	Known
G40.283-0.217	40.283	-0.217	19:05:40.76	06:26:22.0	22.83	74.0	64.6	84.8	20.2	Known
G40.425+0.700	40.433	0.700	19:02:40.53	06:59:35.5	22.28	15.6	4.7	20.8	16.1	Known
G40.601-0.717	40.601	-0.717	19:08:03.27	06:29:28.4	0.85	72.7	72.2	76.6	4.4	New

Table 14: The Catalogue of 6668 MHz Class II methanol masers detected by the Parkes telescope in the MMB Survey. The Parkes source name, Galactic longitude and latitude, the Parkes RA and Dec, the Peak Flux Density, Peak velocity, start velocity, stop velocity, velocity range and its status are listed above.

Source Name	Parkes Gal L	Parkes Gal B	Parkes:RA(2000)	Parkes:DEC(2000)	Parkes Sp	Parkes Vp	Vstart	Vstop	Vrange	Status
G40.623-0.138	40.617	-0.133	19:05:59.87	06:46:25.7	12.57	31.2	29.3	32.3	3.0	Known
G40.933-0.033	40.933	-0.033	19:06:13.58	07:06:03.7	2.60	36.7	35.8	41.4	5.6	Known
G41.083-0.133	41.083	-0.133	19:06:51.73	07:11:17.5	0.76	57.6	57.4	58.5	1.1	Known
G41.122-0.216	41.122	-0.216	19:07:13.83	07:11:04.4	2.60	63.5	61.4	64.1	2.7	Known
G41.133-0.100	41.133	-0.100	19:06:50.14	07:14:52.6	0.84	36.5	35.8	37.4	1.6	Known
G41.166-0.183	41.166	-0.183	19:07:11.64	07:14:19.7	1.66	61.8	61.6	63.8	2.2	Known
G41.233-0.200	41.233	-0.200	19:07:22.75	07:17:26.63	5.58	55.5	50.7	65.8	15.0	Known
G41.350-0.133	41.350	-0.133	19:07:21.42	07:25:30.0	16.06	11.8	2.8	17.8	15.0	Known
G42.033+0.183	42.033	0.183	19:07:29.49	08:10:38.7	23.87	12.9	7.5	17.8	10.3	Known
G42.133+0.517	42.133	0.517	19:06:28.85	08:25:10.3	0.86	-33.4	-33.6	-32.9	0.6	New
G42.300-0.300	42.300	-0.300	19:09:43.29	08:11:28.9	5.92	28.2	26.2	30.7	4.6	Known
G42.433-0.267	42.433	-0.267	19:09:51.05	08:19:30.1	2.00	66.8	65.8	68.8	3.0	Known
G42.700-0.150	42.700	-0.150	19:09:55.80	08:36:55.6	3.30	-42.9	-47.1	-41.6	5.4	Known
G43.050-0.450	43.050	-0.450	19:11:39.56	08:47:13.6	6.95	54.9	51.3	63.4	12.1	Known
G43.083-0.083	43.083	-0.083	19:10:24.44	08:59:10.4	8.83	10.3	9.9	11.0	1.1	Known
G43.149+0.013	43.133	-0.016	19:10:15.51	09:03:41.0	13.42	13.0	6.5	22.3	15.8	Known
G43.165+0.013	43.167	0.000	19:10:15.81	09:05:55.0	2.59	-1.2	-1.9	-0.2	1.8	Known
G43.167-0.004	43.167	0.017	19:10:12.21	09:06:22.7	31.34	9.3	5.5	22.8	17.3	Known
G43.183-0.533	43.183	-0.533	19:12:12.58	08:52:00.3	2.21	58.9	58.5	65.6	7.1	New
G43.796-0.127	43.800	-0.133	19:11:55.79	09:35:54.9	46.47	39.7	34.9	47.8	12.9	Known
G43.900-0.783	43.900	-0.783	19:14:27.21	09:23:08.8	10.16	47.6	43.0	56.4	13.4	Known
G44.317+0.050	44.317	0.050	19:12:14.47	10:08:29.1	0.91	55.7	55.1	56.4	1.3	Known
G44.633-0.533	44.633	-0.533	19:14:56.29	10:09:04.7	1.10	49.5	48.5	50.4	1.9	Known
G45.120+0.130	45.067	0.133	19:13:21.28	10:50:40.5	46.86	57.8	53.3	63.4	10.1	Known
G45.383-0.600	45.383	-0.600	19:16:35.89	10:47:02.1	2.34	53.3	52.7	54.6	1.9	New

Table 15: The Catalogue of 6668 MHz Class II methanol masers detected by the Parkes telescope in the MMB Survey. The Parkes source name, Galactic longitude and latitude, the Parkes RA and Dec, the Peak Flux Density, Peak velocity, start velocity, stop velocity, velocity range and its status are listed above.

Source Name	Parkes Gal L	Parkes Gal B	Parkes:RA(2000)	Parkes:DEC(2000)	Parkes Sp	Parkes Vp	Vstart	Vstop	Vrange	Status
G45.445+0.069	45.450	0.083	19:14:15.61	11:09:39.4	1.04	49.9	49.2	50.7	1.6	Known
G45.467+0.133	45.467	0.133	19:14:06.67	11:11:56.2	2.68	62.3	62.0	62.9	0.9	New
G45.467+0.053	45.467	0.050	19:14:24.80	11:09:37.9	5.07	56.0	55.6	59.3	3.7	Known
G45.473+0.134	45.483	0.133	19:14:08.57	11:12:49.3	5.80	65.7	64.1	70.7	6.6	Known
G45.493+0.126	45.500	0.117	19:14:14.07	11:13:14.6	7.65	57.2	52.7	59.9	7.2	Known
G45.800-0.350	45.800	-0.350	19:16:29.34	11:16:08.8	15.70	59.1	59.6	70.6	11.0	Known
G46.067+0.217	46.067	0.217	19:14:56.89	11:46:08.2	0.98	23.4	22.6	24.7	2.0	Known
G46.117+0.383	46.117	0.383	19:14:26.40	11:53:26.5	1.21	59.1	57.6	60.0	2.5	Known
G48.900-0.280	48.900	-0.280	19:22:12.20	14:02:19.9	0.89	71.9	71.1	72.7	1.6	Known
G48.990-0.320	49.000	-0.300	19:22:27.51	14:07:09.2	1.03	71.6	71.4	72.0	0.6	Known
G49.049-1.083	49.049	-1.083	19:25:23.88	13:47:31.5	31.28	36.7	35.0	41.1	6.2	Known
G49.266+0.316	49.266	0.316	19:20:43.89	14:38:37.7	7.59	-4.6	-5.7	7.4	13.1	Known
G49.349+0.416	49.349	0.416	19:20:31.66	14:45:50.6	10.06	68.1	66.9	69.0	2.1	Known
G49.416+0.333	49.416	0.333	19:20:57.66	14:47:03.1	9.66	-12.0	-26.7	-9.7	17.0	Known
G49.470-0.371	49.470	-0.370	19:23:37.77	14:30:01.6	6.67	63.9	63.6	65.1	1.6	Known
G49.490-0.388	49.500	-0.383	19:23:44.13	14:31:14.7	753.28	59.3	51.5	61.3	9.8	Known
G49.599-0.250	49.599	-0.250	19:23:26.66	14:40:15.0	48.95	63.0	62.0	66.8	4.8	Known
G49.633-0.367	49.633	-0.367	19:23:56.23	14:38:43.8	0.81	50.2	50.0	50.7	0.7	Known
G50.033+0.583	50.033	0.583	19:21:14.93	15:26:46.6	5.75	-5.1	-10.5	-2.4	8.1	Known
G50.317+0.683	50.317	0.683	19:21:26.08	15:44:37.7	3.22	30.1	25.6	33.2	7.6	Known
G50.783+0.150	50.783	0.150	19:24:18.31	15:54:12.8	4.72	49.1	47.8	50.6	2.8	Known
G51.683+0.717	51.683	0.717	19:23:59.94	16:57:52.1	1.22	7.2	5.5	8.5	3.0	New
G51.833+1.250	51.833	1.250	19:22:19.60	17:20:54.4	2.19	46.5	45.7	47.5	1.8	New
G52.200+0.717	52.200	0.717	19:25:01.40	17:25:10.4	4.82	3.8	1.7	4.5	2.8	New
G52.667-1.100	52.667	-1.100	19:32:38.30	16:57:37.6	2.45	65.2	63.6	67.7	4.0	Known

Table 16: The Catalogue of 6668 MHz Class II methanol masers detected by the Parkes telescope in the MMB Survey. The Parkes source name, Galactic longitude and latitude, the Parkes RA and Dec, the Peak Flux Density, Peak velocity, start velocity, stop velocity, velocity range and its status are listed above.

Source Name	Parkes Gal L	Parkes Gal B	Parkes:RA(2000)	Parkes:DEC(2000)	Parkes Sp	Parkes Vp	Vstart	Vstop	Vrange	Status
G52.933+0.417	52.933	0.417	19:27:35.69	17:55:19.0	4.77	39.1	38.5	45.2	6.7	Known
G53.050+0.100	53.050	0.100	19:28:59.91	17:52:23.5	1.68	10.2	9.2	10.4	1.2	Known
G53.150+0.083	53.150	0.083	19:29:15.68	17:57:10.9	1.04	24.6	23.4	25.2	1.8	Known
G53.633+0.033	53.633	0.033	19:30:25.30	18:21:11.6	11.49	19.0	14.7	24.0	9.4	Known
G56.983-0.233	56.983	-0.233	19:38:19.33	21:09:10.7	1.11	29.9	29.6	30.7	1.1	New
G57.617+0.017	57.617	0.017	19:38:43.33	21:49:39.1	10.23	38.9	27.8	40.2	12.4	New
G58.767+0.650	58.767	0.650	19:38:46.72	23:08:25.4	6.30	33.3	28.8	37.2	8.4	Known
G188.784+1.033	188.784	1.033	06:09:06.28	21:51:18.3	7.82	-5.5	-6.2	-3.4	2.8	Known
G188.946+0.886	188.950	0.883	06:08:53.18	21:38:12.9	517.30	10.8	4.0	16.8	12.7	Known
G189.030+0.783	189.034	0.759	06:08:35.67	21:30:10.9	11.05	8.9	8.7	10.0	1.3	Known
G189.467-1.217	189.467	-1.217	06:02:07.52	20:09:32.3	2.08	18.8	18.3	19.3	1.1	New
G189.778+0.345	189.767	0.350	06:08:35.02	20:39:50.3	7.69	5.7	3.0	6.5	3.5	Known
G192.600-0.048	192.601	-0.058	06:12:51.93	17:59:04.3	67.85	4.6	-1.4	10.3	11.8	Known
G196.454-1.677	196.450	-1.667	06:14:38.84	13:50:06.1	18.13	15.2	9.9	20.1	10.2	Known
G212.067-0.750	212.067	-0.750	06:47:11.34	00:25:40.7	1.03	44.4	43.9	44.9	1.1	Known
G232.620+0.996	232.617	1.000	07:32:10.26	-16:57:53.5	178.20	22.9	16.9	28.6	11.8	Known
G254.880+0.451	254.883	0.450	08:22:25.48	-36:15:12.4	1.76	30.1	29.8	31.1	1.2	New
G259.939-0.041	259.933	-0.033	08:35:31.96	-40:37:49.2	2.15	-1.0	-1.4	-0.4	1.1	Known
G263.250+0.514	263.250	0.500	08:48:44.27	-42:54:58.9	68.93	12.3	6.9	20.0	13.1	Known
G264.140+2.018	264.133	1.984	08:58:01.73	-42:38:31.4	0.90	8.1	8.0	8.9	1.0	New
G264.289+1.469	264.283	1.450	08:56:20.92	-43:06:10.6	0.50	8.7	7.7	9.4	1.7	Known
G269.153-1.128	269.153	-1.128	09:03:33.60	-48:28:03.6	0.65	16.0	8.0	17.0	9.0	Known
G269.456-1.467	269.450	-1.467	09:03:13.34	-48:54:52.6	5.96	56.1	55.0	56.8	1.8	Known
G269.658-1.270	269.650	-1.283	09:04:51.99	-48:56:29.2	4.52	16.2	14.9	17.5	2.6	New
G270.255+0.835	270.255	0.835	09:16:41.40	-47:56:11.7	0.50	4.0	3.0	5.0	2.0	Known

Table 17: The Catalogue of 6668 MHz Class II methanol masers detected by the Parkes telescope in the MMB Survey. The Parkes source name, Galactic longitude and latitude, the Parkes RA and Dec, the Peak Flux Density, Peak velocity, start velocity, stop velocity, velocity range and its status are listed above.

Source Name	Parkes Gal L	Parkes Gal B	Parkes:RA(2000)	Parkes:DEC(2000)	Parkes Sp	Parkes Vp	Vstart	Vstop	Vrange	Status
G281.710-1.104	281.717	-1.100	10:05:08.98	-56:57:29.3	1.32	1.0	0.3	1.6	1.2	New
G284.352-0.419	284.350	-0.417	10:24:10.82	-57:52:28.4	2.71	3.9	3.1	5.0	1.9	Known
G284.694-0.361	284.700	-0.350	10:26:41.03	-58:00:11.9	5.01	13.3	11.8	13.8	1.9	New
G285.337-0.002	285.333	0.017	10:32:12.49	-58:01:00.0	17.95	0.7	-8.3	3.2	11.4	Known
G286.383-1.834	286.384	-1.834	10:31:55.26	-60:08:37.8	17.58	9.6	7.7	10.5	2.8	New
G287.371+0.644	287.367	0.650	10:48:03.74	-58:26:34.8	115.70	-1.9	-7.4	4.0	11.4	Known
G290.374+1.661	290.367	1.650	11:12:12.96	-58:46:46.9	0.85	-24.2	-24.3	-23.5	0.9	Known
G291.270-0.719	291.267	-0.700	11:11:51.45	-61:17:45.1	71.17	-29.7	-35.7	-23.6	12.0	Known
G291.579-0.431	291.583	-0.433	11:15:07.30	-61:09:53.4	2.14	10.4	8.9	11.0	2.1	Known
G291.642-0.546	291.650	-0.533	11:15:20.19	-61:16:55.9	1.46	12.1	11.3	12.2	0.9	New
G291.879-0.810	291.883	-0.817	11:16:18.16	-61:37:50.3	1.34	33.5	32.0	34.3	2.3	New
G292.074-1.131	292.067	-1.133	11:16:47.51	-61:59:31.2	1.76	-19.1	-19.4	-18.7	0.7	New
G292.468+0.168	292.467	0.167	11:23:41.23	-60:54:34.4	6.23	10.9	7.8	24.0	16.2	New
G293.723-1.742	293.717	-1.734	11:28:31.23	-63:06:43.9	0.82	24.2	24.0	25.9	1.9	New
G293.827-0.746	293.833	-0.733	11:32:10.45	-62:11:48.1	2.93	37.0	36.2	39.2	3.0	Known
G293.942-0.874	293.933	-0.867	11:32:38.95	-62:21:14.3	3.66	41.1	40.5	41.3	0.8	Known
G294.337-1.706	294.334	-1.700	11:33:49.11	-63:16:07.8	14.51	-11.7	-16.8	-11.0	5.8	New
G294.511-1.621	294.517	-1.617	11:35:35.61	-63:14:33.9	9.00	-11.9	-17.7	-8.0	9.7	Known
G294.977-1.734	294.966	-1.717	11:39:11.00	-63:27:56.4	1.99	-5.3	-6.7	-4.8	1.9	New
G294.990-1.719	294.984	-1.717	11:39:20.12	-63:28:14.0	9.08	-12.2	-13.3	-11.5	1.8	Known
G296.893-1.305	296.900	-1.300	11:56:54.42	-63:31:53.3	2.32	22.2	20.5	23.3	2.8	Known
G297.406-0.622	297.417	-0.633	12:02:35.05	-62:58:50.8	1.65	27.8	27.5	28.4	0.9	New
G298.177-0.795	298.183	-0.800	12:09:00.23	-63:16:47.6	1.74	23.5	22.7	25.0	2.3	New
G298.213-0.343	298.233	-0.333	12:10:06.33	-62:49:38.7	1.17	37.4	36.2	38.2	2.0	Known
G298.262+0.739	298.267	0.750	12:11:50.76	-61:45:45.3	14.95	-30.1	-35.0	-25.3	9.7	Known

Table 18: The Catalogue of 6668 MHz Class II methanol masers detected by the Parkes telescope in the MMB Survey. The Parkes source name, Galactic longitude and latitude, the Parkes RA and Dec, the Peak Flux Density, Peak velocity, start velocity, stop velocity, velocity range and its status are listed above.

.2 The Three Colour GLIMPSE Images for the 6035 MHz ex-OH Masers

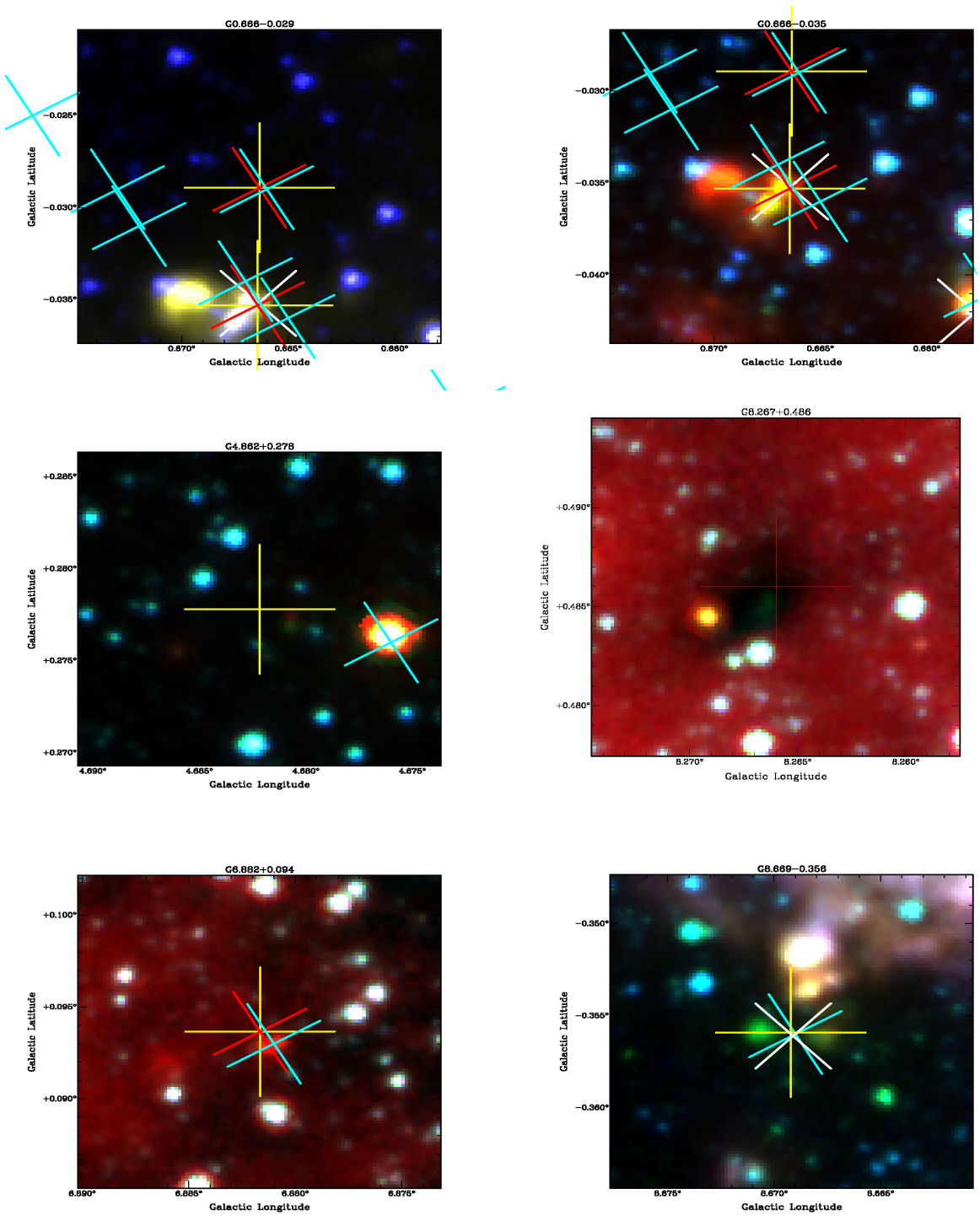

Figure 1: Three color 3.6, 4.5 & 8.0 micron GLIMPSE Images. Centered on the yellow 6.035 GHz ex-OH maser crosses. The blue crosses indicate the 6.7 GHz methanol masers, red crosses represent 6.031 GHz ex-OH masers and white crosses indicate the 1665 & 1667 OH masers.

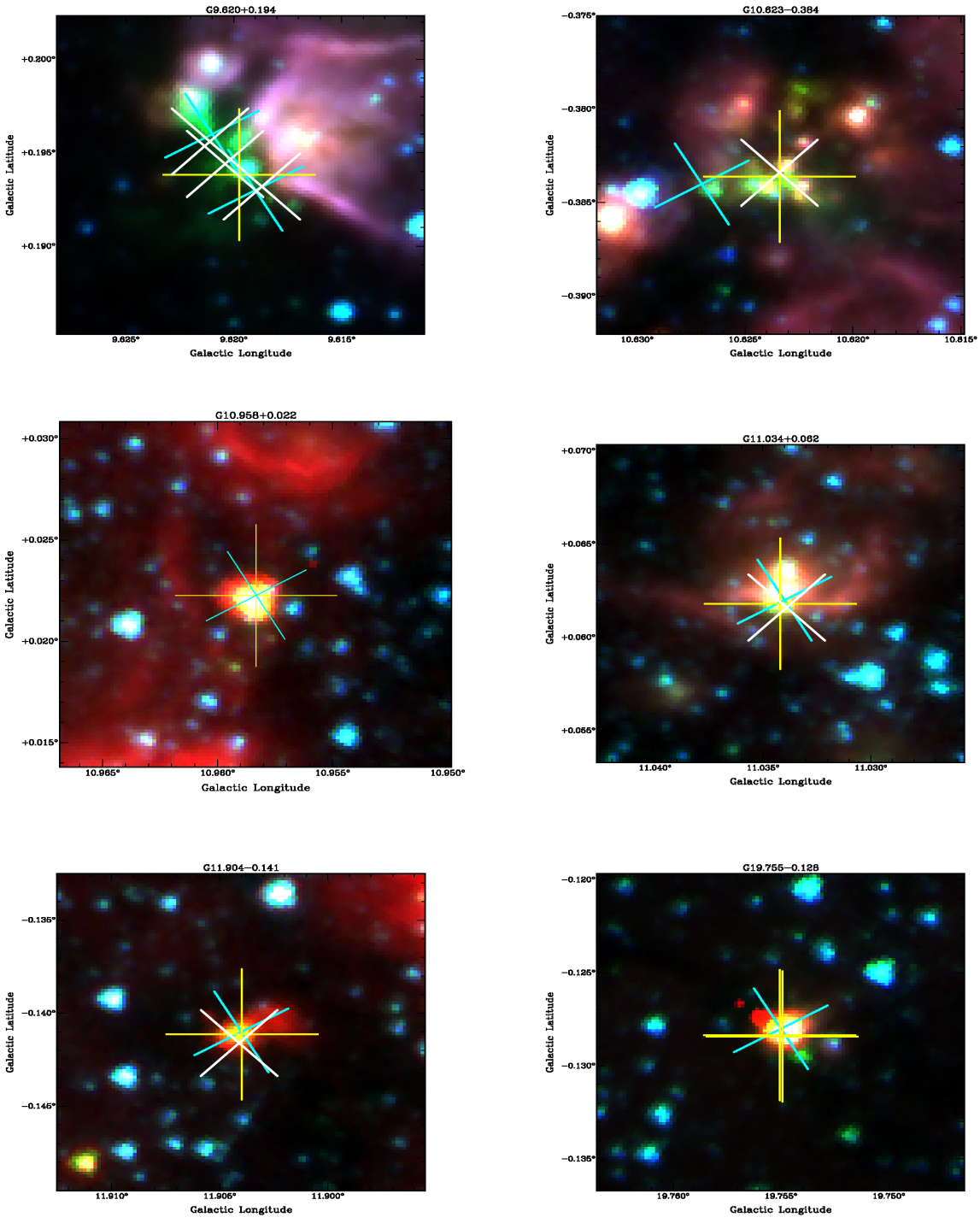

Figure 2: Three color 3.6, 4.5 & 8.0 micron GLIMPSE Images. Centered on the yellow 6.035 GHz ex-OH maser crosses. The blue crosses indicate the 6.7 GHz methanol masers, red crosses represent 6.031 GHz ex-OH masers and white crosses indicate the 1665 & 1667 OH masers.

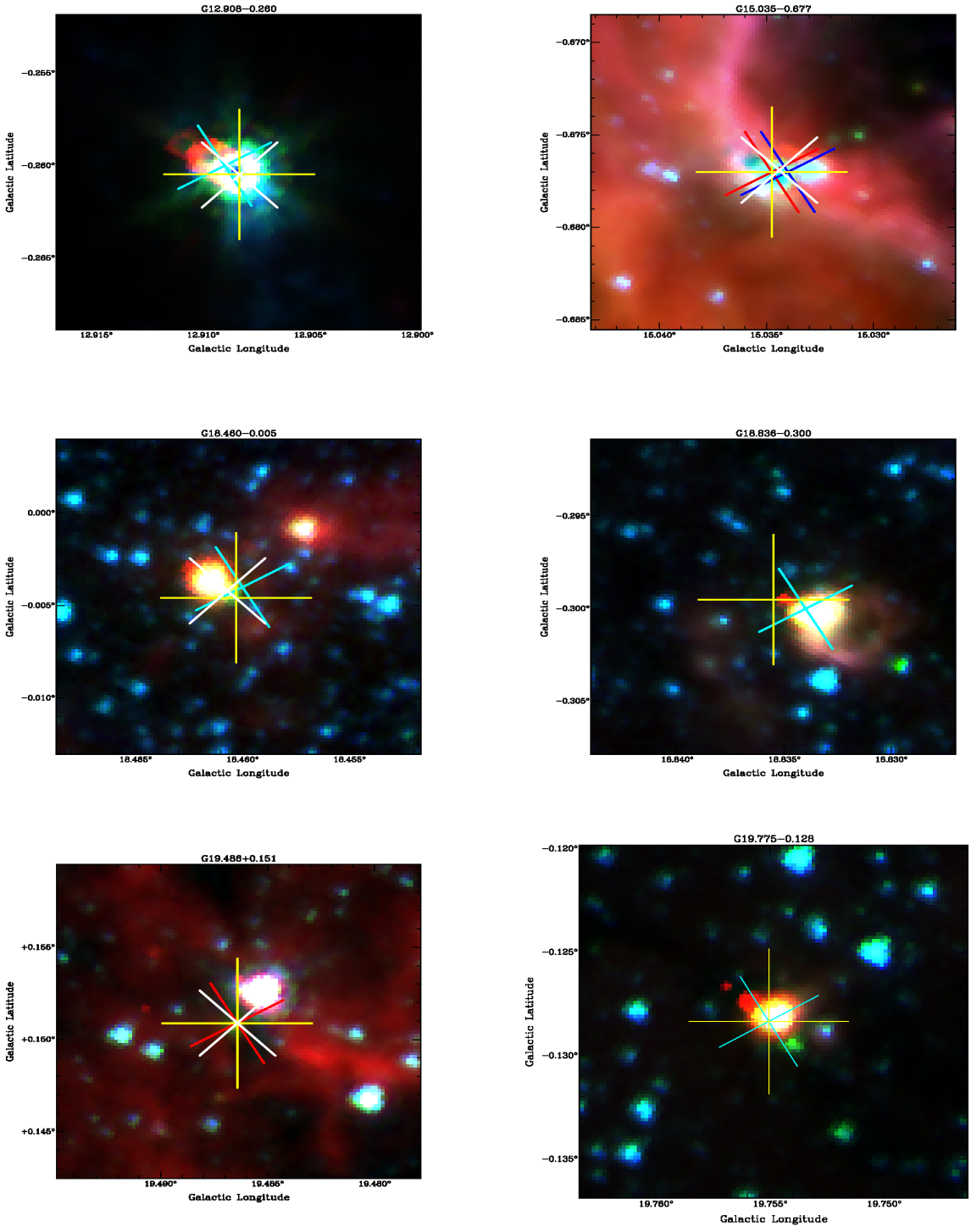

Figure 3: Three color 3.6, 4.5 & 8.0 micron GLIMPSE Images. Centered on the yellow 6.035 GHz ex-OH maser crosses. The blue crosses indicate the 6.7 GHz methanol masers, red crosses represent 6.031 GHz ex-OH masers and white crosses indicate the 1665 & 1667 OH masers.

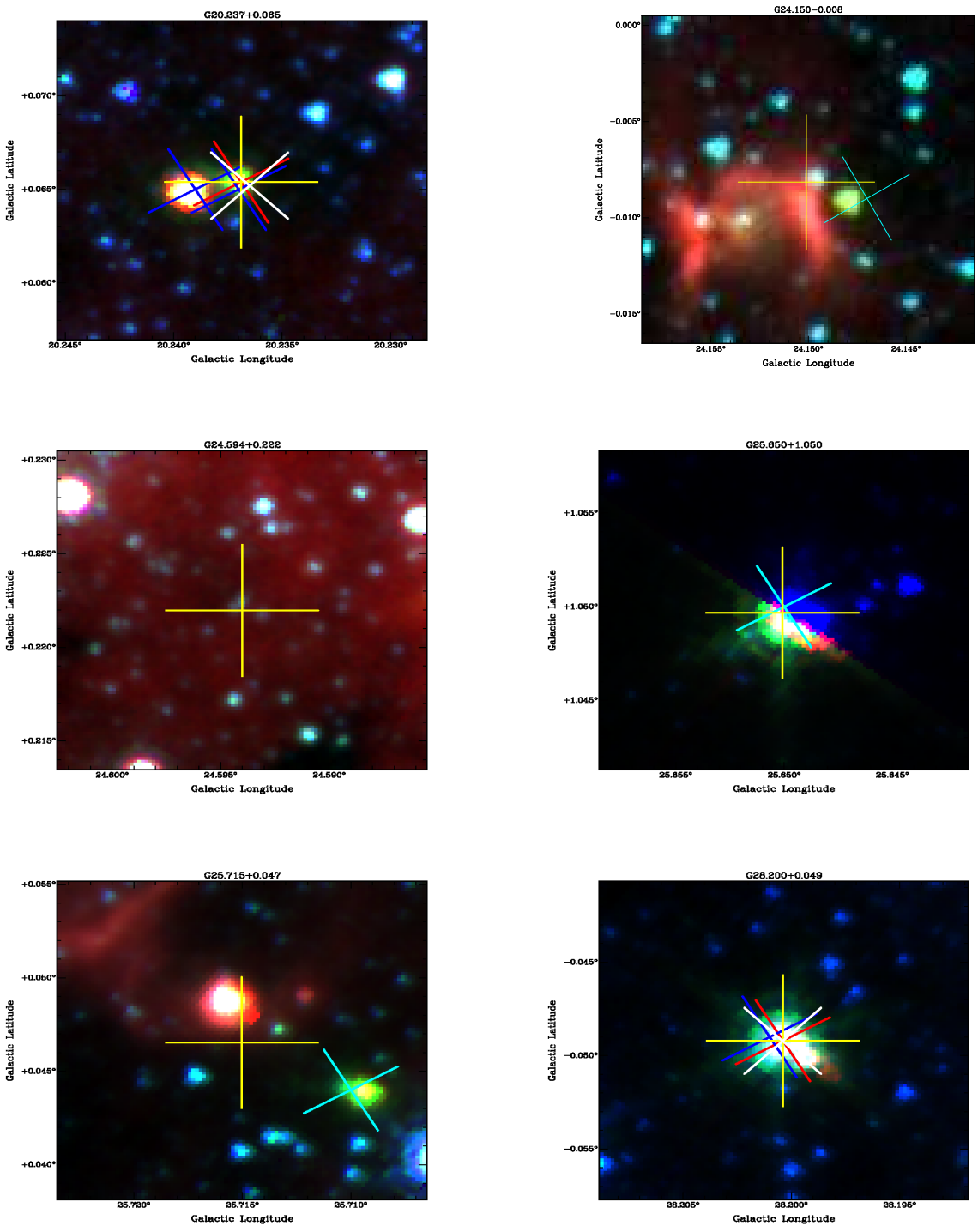

Figure 4: Three color 3.6, 4.5 & 8.0 micron GLIMPSE Images. Centered on the yellow 6.035 GHz ex-OH maser crosses. The blue crosses indicate the 6.7 GHz methanol masers, red crosses represent 6.031 GHz ex-OH masers and white crosses indicate the 1665 & 1667 OH masers.

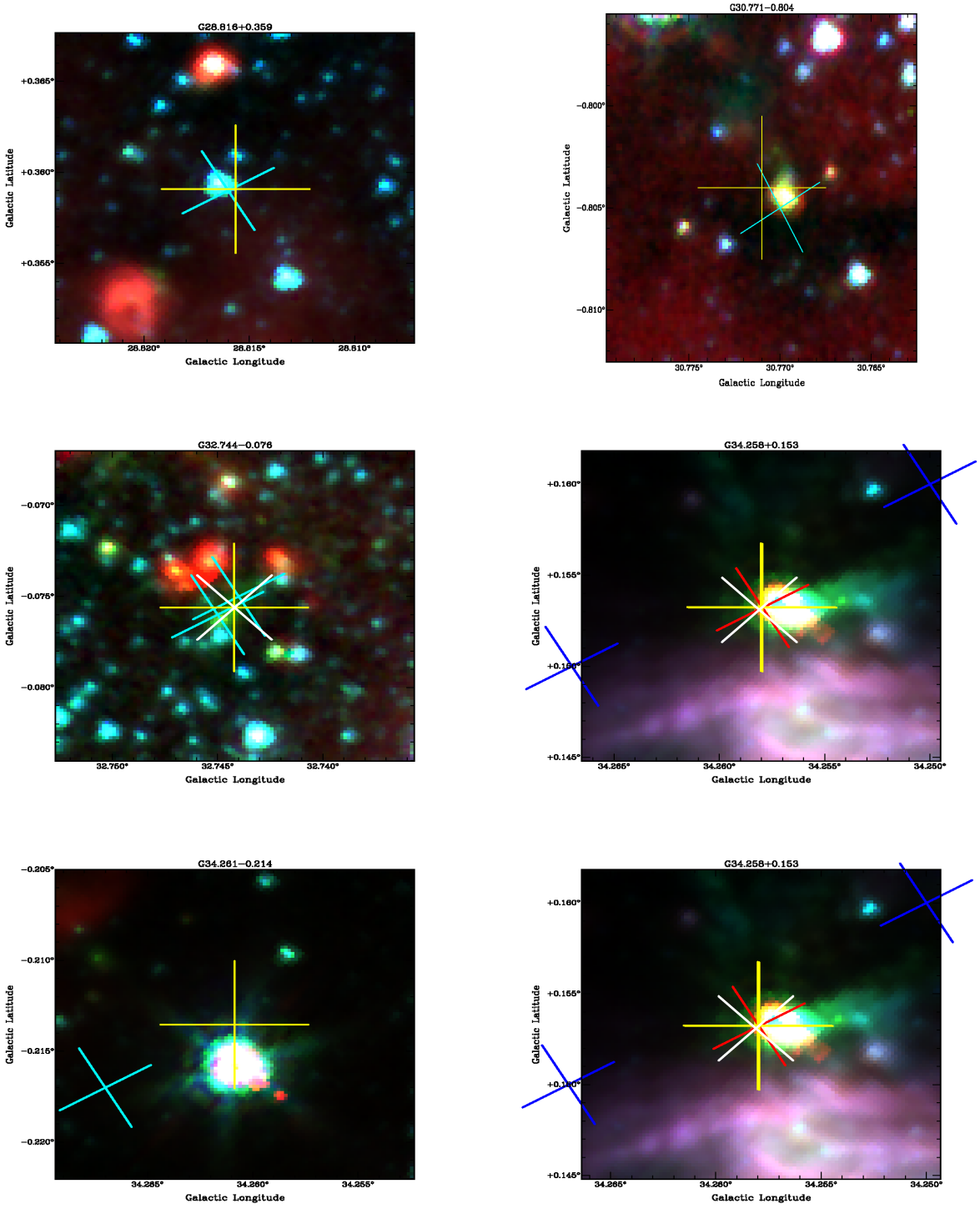

Figure 5: Three color 3.6, 4.5 & 8.0 micron GLIMPSE Images. Centered on the yellow 6.035 GHz ex-OH maser crosses. The blue crosses indicate the 6.7 GHz methanol masers, red crosses represent 6.031 GHz ex-OH masers and white crosses indicate the 1665 & 1667 OH masers.

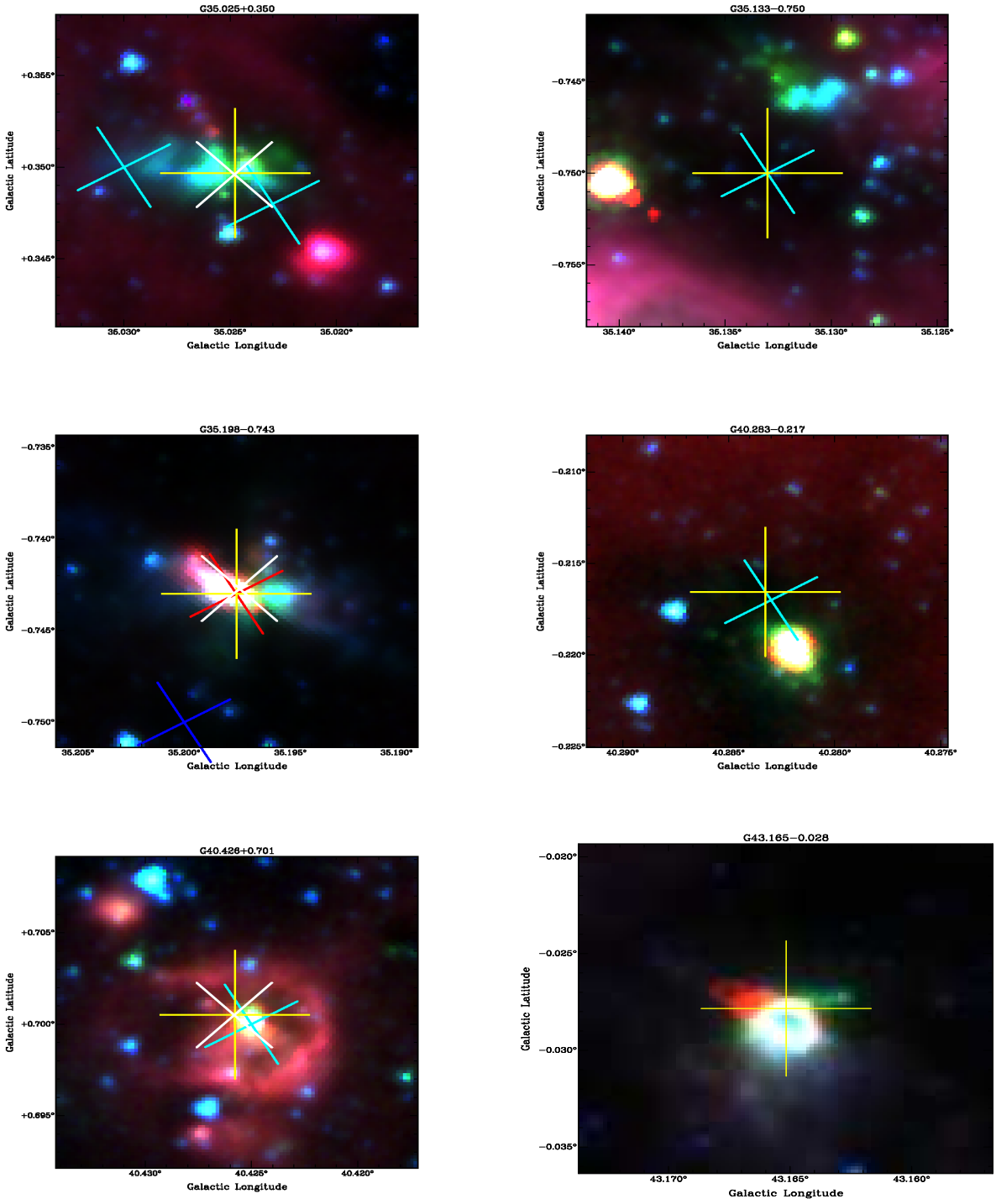

Figure 6: Three color 3.6, 4.5 & 8.0 micron GLIMPSE Images. Centered on the yellow 6.035 GHz ex-OH maser crosses. The blue crosses indicate the 6.7 GHz methanol masers, red crosses represent 6.031 GHz ex-OH masers and white crosses indicate the 1665 & 1667 OH masers.

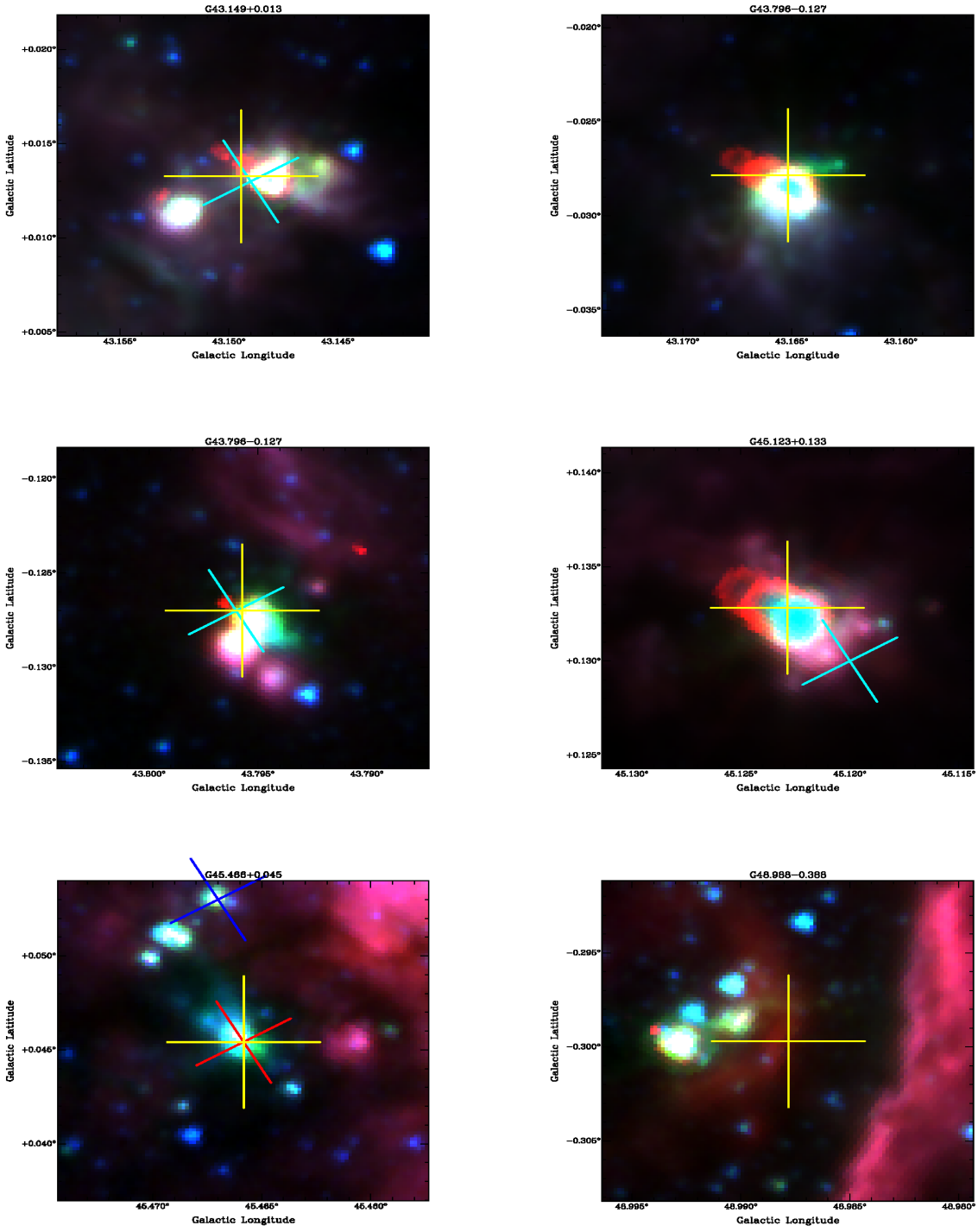

Figure 7: Three color 3.6, 4.5 & 8.0 micron GLIMPSE Images. Centered on the yellow 6.035 GHz ex-OH maser crosses. The blue crosses indicate the 6.7 GHz methanol masers, red crosses represent 6.031 GHz ex-OH masers and white crosses indicate the 1665 & 1667 OH masers.

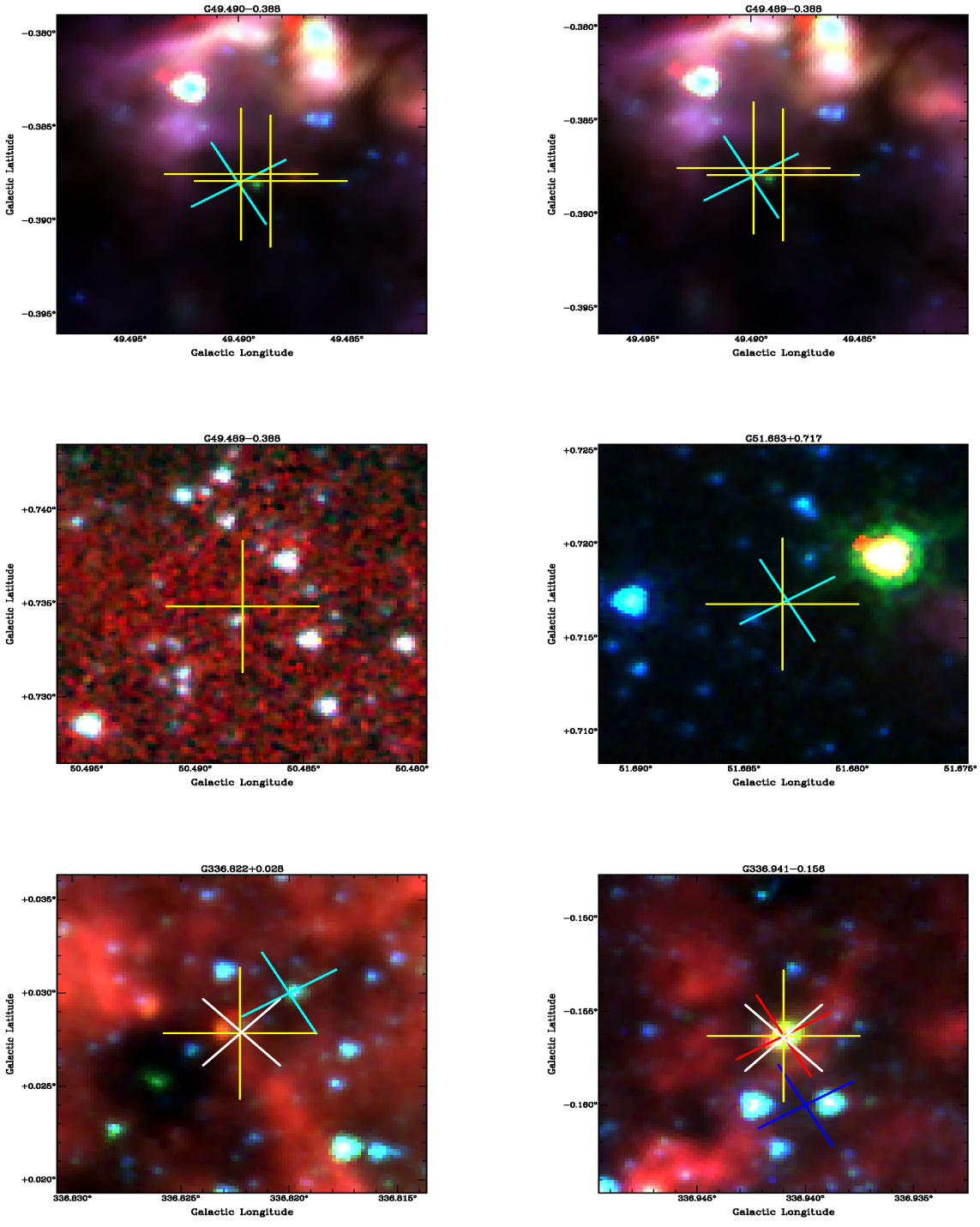

Figure 8: Three color 3.6, 4.5 & 8.0 micron GLIMPSE Images. Centered on the yellow 6.035 GHz ex-OH maser crosses. The blue crosses indicate the 6.7 GHz methanol masers, red crosses represent 6.031 GHz ex-OH masers and white crosses indicate the 1665 & 1667 OH masers.

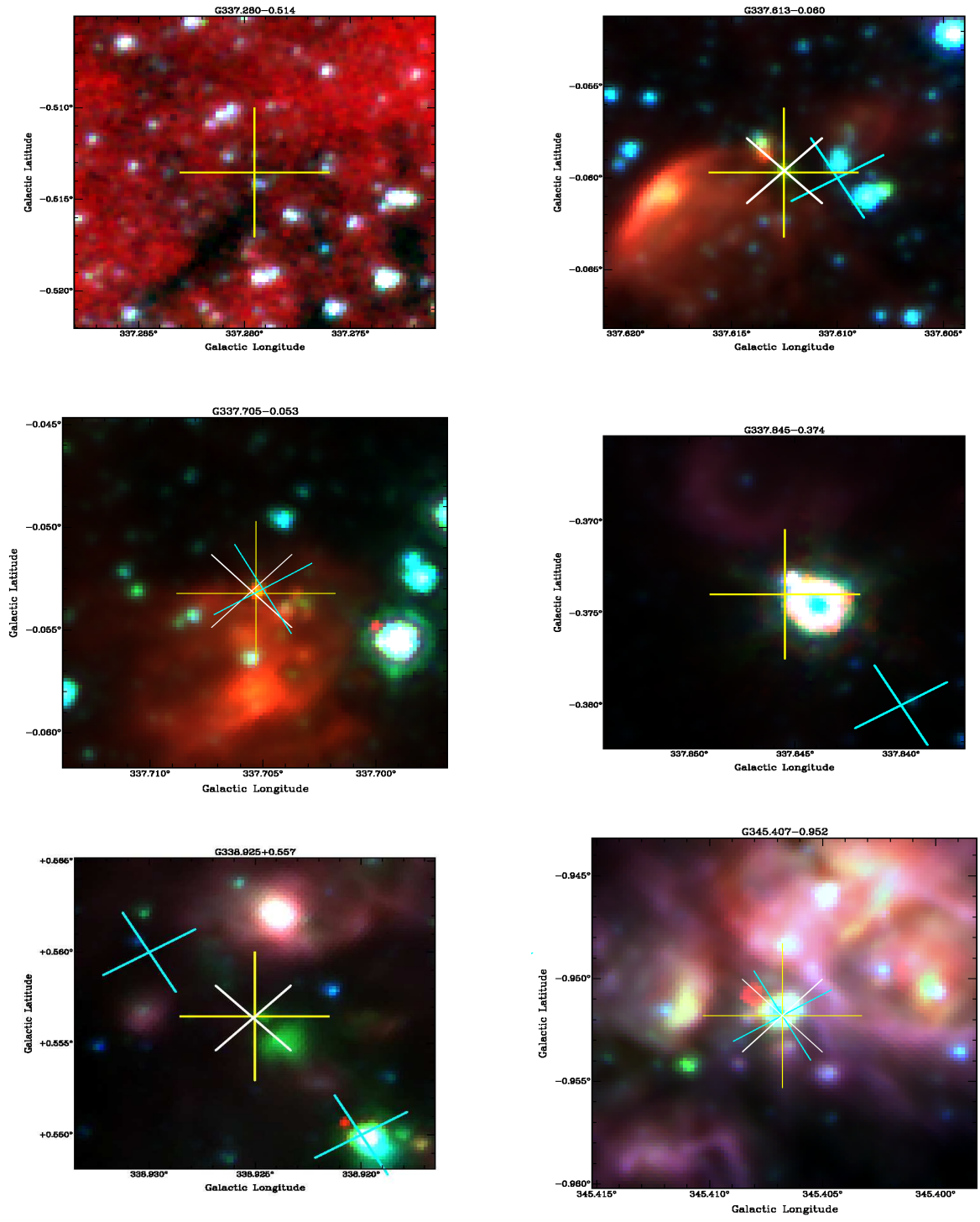

Figure 9: Three color 3.6, 4.5 & 8.0 micron GLIMPSE Images. Centered on the yellow 6.035 GHz ex-OH maser crosses. The blue crosses indicate the 6.7 GHz methanol masers, red crosses represent 6.031 GHz ex-OH masers and white crosses indicate the 1665 & 1667 OH masers.

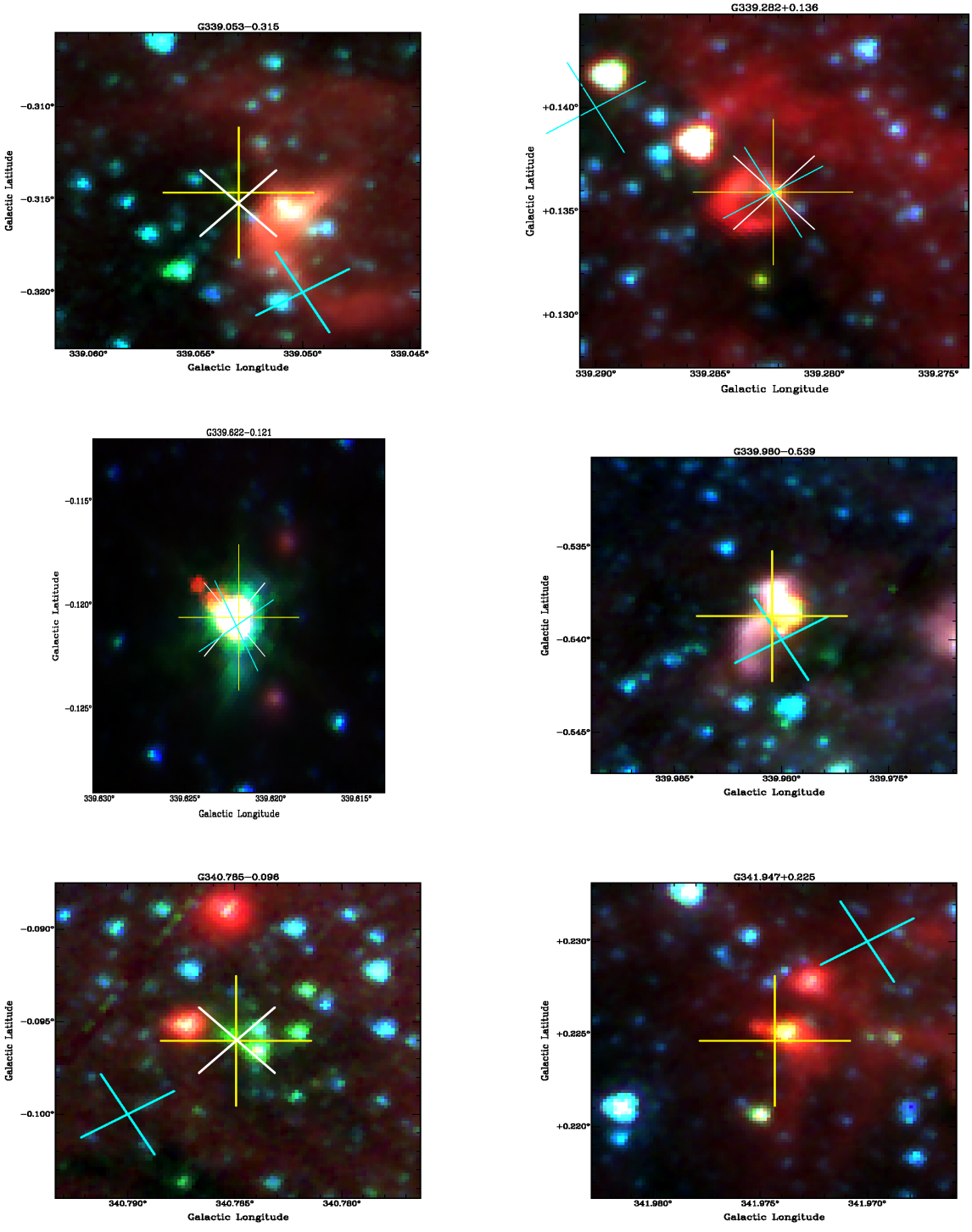

Figure 10: Three color 3.6, 4.5 & 8.0 micron GLIMPSE Images. Centered on the yellow 6.035 GHz ex-OH maser crosses. The blue crosses indicate the 6.7 GHz methanol masers, red crosses represent 6.031 GHz ex-OH masers and white crosses indicate the 1665 & 1667 OH masers.

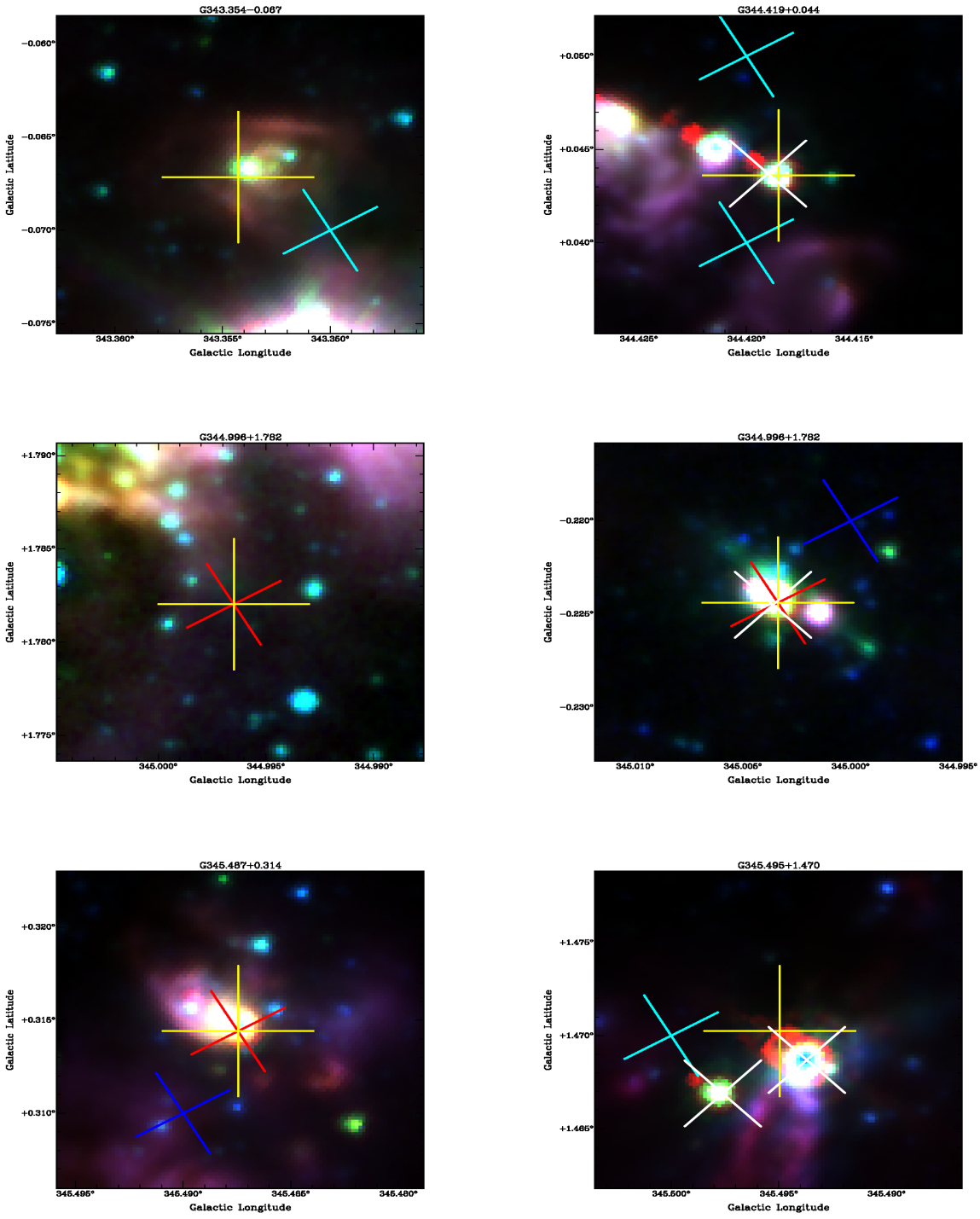

Figure 11: Three color 3.6, 4.5 & 8.0 micron GLIMPSE Images. Centered on the yellow 6.035 GHz ex-OH maser crosses. The blue crosses indicate the 6.7 GHz methanol masers, red crosses represent 6.031 GHz ex-OH masers and white crosses indicate the 1665 & 1667 OH masers.

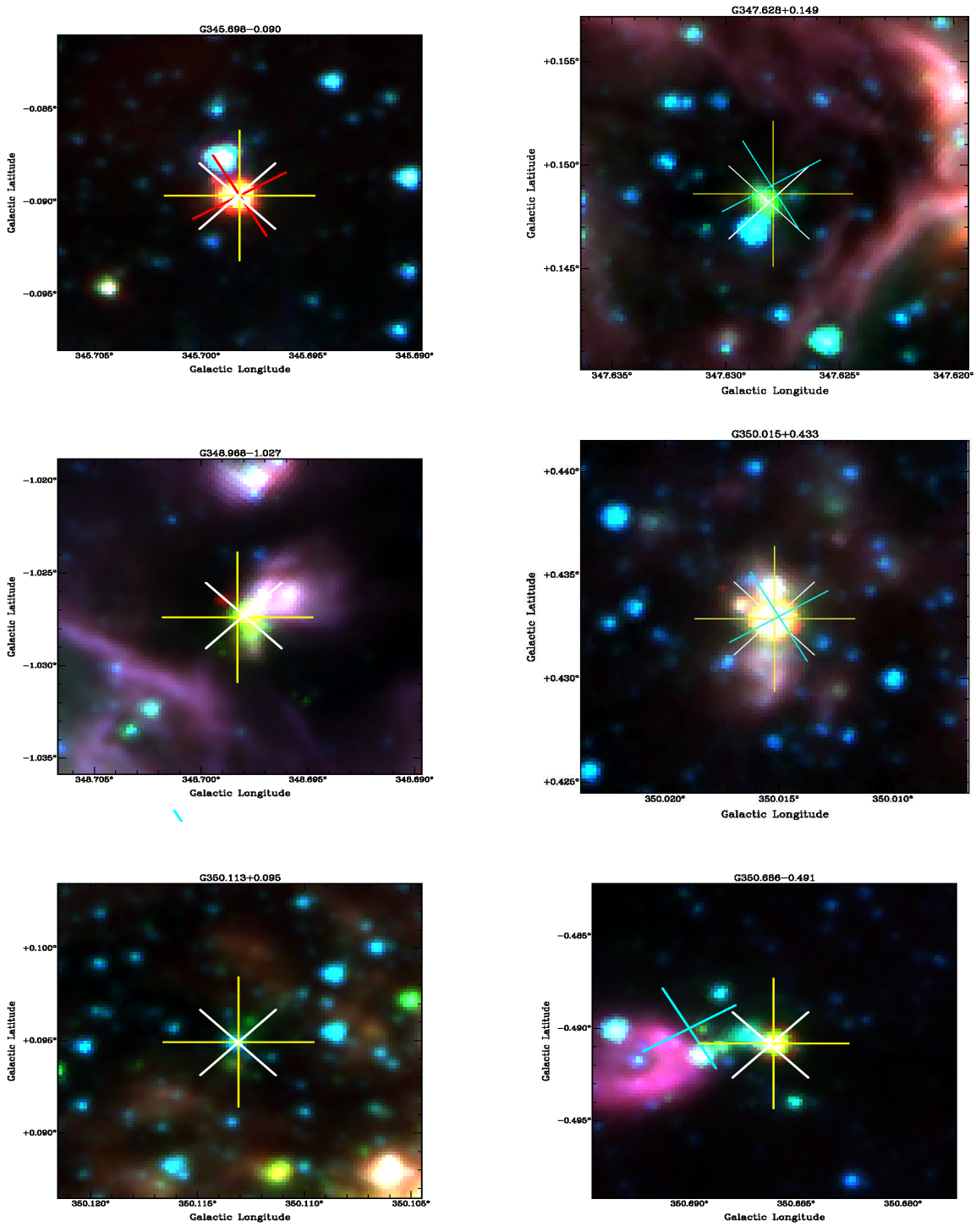

Figure 12: Three color 3.6, 4.5 & 8.0 micron GLIMPSE Images. Centered on the yellow 6.035 GHz ex-OH maser crosses. The blue crosses indicate the 6.7 GHz methanol masers, red crosses represent 6.031 GHz ex-OH masers and white crosses indicate the 1665 & 1667 OH masers.

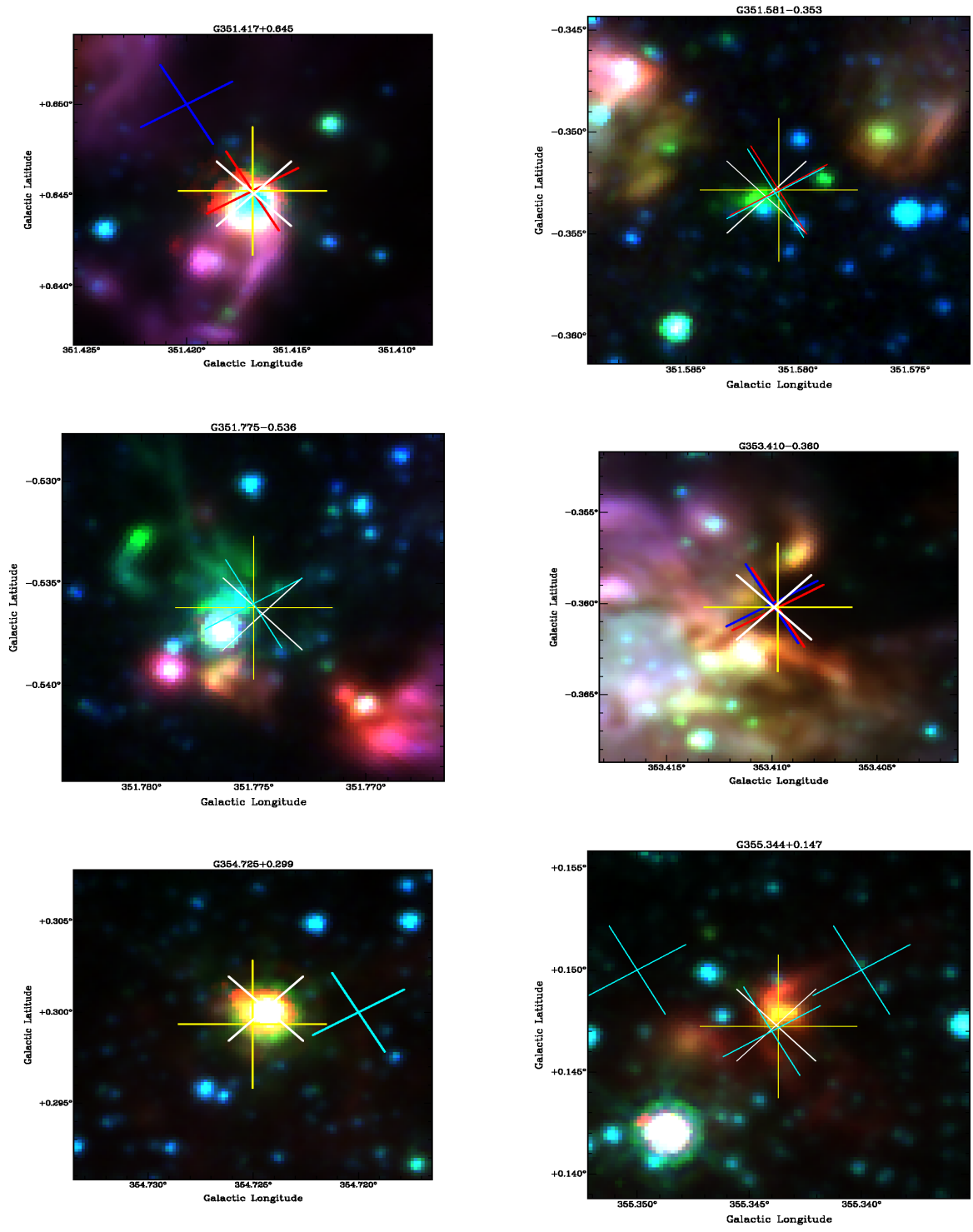

Figure 13: Three color 3.6, 4.5 & 8.0 micron GLIMPSE Images. Centered on the yellow 6.035 GHz ex-OH maser crosses. The blue crosses indicate the 6.7 GHz methanol masers, red crosses represent 6.031 GHz ex-OH masers and white crosses indicate the 1665 & 1667 OH masers.

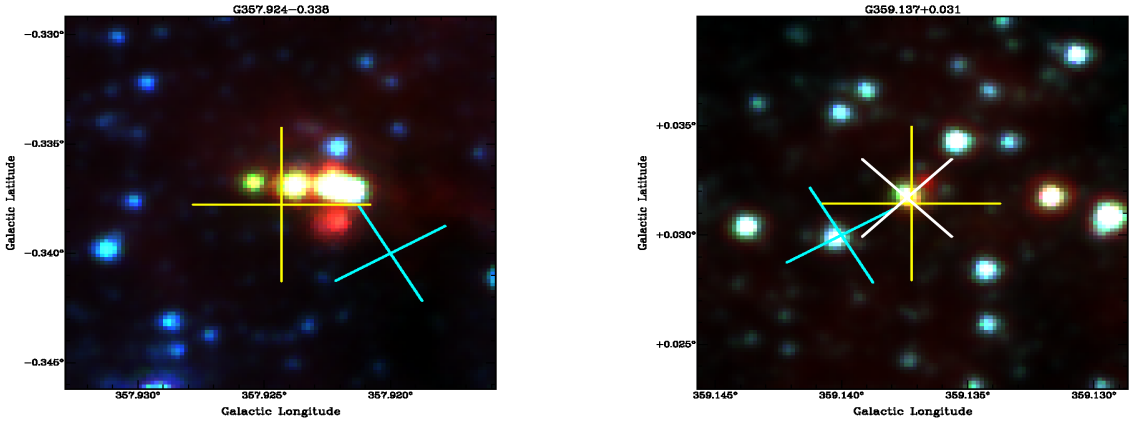

Figure 14: Three color 3.6, 4.5 & 8.0 micron GLIMPSE Images. Centered on the yellow 6.035 GHz ex-OH maser crosses. The blue crosses indicate the 6.7 GHz methanol masers, red crosses represent 6.031 GHz ex-OH masers and white crosses indicate the 1665 & 1667 OH masers.

References

C. Andre, M. C. Festou, L. Koechlin, A. Lannes, J.-P. Perez, J.-L. Prieur, and S. Roques. High Resolution Imaging of Comets and Asteroids Using Bispectral Techniques. *LPI Contributions*, 810:9–+, 1993.

E. Araya, P. Hofner, L. Olmi, S. Kurtz, and H. Linz. Arecibo Observations of Formaldehyde in L1551. *AJ*, 132:1851–1858, November 2006. doi: 10.1086/507599.

R. Bachiller. Molecular observations of shocks and outflows. In E. F. van Dishoeck, editor, *IAU Symp. 178: Molecules in Astrophysics: Probes & Processes*, pages 103–+, 1996.

R. Bachiller, J. Gomez-Gonzalez, A. Barcia, and K. M. Menten. The 44 GHz methanol masers - Results of an extensive survey in the 7(0)-6(1)A(+) line. *A&A*, 240:116–122, December 1990.

J. Bally. Observational Constraints on the Formation of Massive Stars. In P. Crowther, editor, *Hot Star Workshop III: The Earliest Phases of Massive Star Birth*, volume 267 of *Astronomical Society of the Pacific Conference Series*, pages 219–+, October 2002.

D. G. Barnes, L. Staveley-Smith, W. J. G. de Blok, T. Oosterloo, I. M. Stewart, A. E. Wright, G. D. Banks, R. Bhathal, P. J. Boyce, M. R. Calabretta, M. J. Disney, M. J. Drinkwater, R. D. Ekers, K. C. Freeman, B. K. Gibson, A. J. Green, R. F. Haynes, P. te Lintel Hekkert, P. A. Henning, H. Jerjen, S. Juraszek, M. J. Kesteven, V. A. Kilborn, P. M. Knezek, B. Koribalski, R. C. Kraan-Korteweg, D. F. Malin, M. Marquarding, R. F. Minchin, J. R. Mould, R. M. Price, M. E. Putman, S. D. Ryder, E. M. Sadler, A. Schröder, F. Stootman, R. L. Webster, W. E. Wilson, and T. Ye. The Hi Parkes All Sky Survey: southern observations, calibration and robust imaging. *MNRAS*, 322:486–498, April 2001.

A. H. Barrett, P. R. Schwartz, and J. W. Waters. Detection of Methyl Alcohol in Orion at a Wavelength of ˜1 Centimeter. *ApJL*, 168:L101+, September 1971. doi: 10.1086/180793.

W. Batrla and K. M. Menten. Detection of a strong new maser line of methanol toward DR 21(OH). *ApJL*, 329:L117–L120, June 1988. doi: 10.1086/185189.

A. J. Beasley, S. P. Ellingsen, M. J. Claussen, and E. Wilcots. A Methanol Maser Survey of IRAS-selected Regions in the Magellanic Clouds. *ApJ*, 459:600–+, March 1996. doi: 10.1086/176924.

R. A. Benjamin, E. Churchwell, B. L. Babler, T. M. Bania, D. P. Clemens, M. Cohen, J. M. Dickey, R. Indebetouw, J. M. Jackson, H. A. Kobulnicky, A. Lazarian, A. P. Marston, J. S. Mathis, M. R. Meade, S. Seager, S. R. Stolovy, C. Watson, B. A. Whitney, M. J. Wolff, and M. G. Wolfire. GLIMPSE. I. An SIRTF Legacy Project to Map the Inner Galaxy. *PASP*, 115:953–964, August 2003. doi: 10.1086/376696.

H. Beuther, T. K. Sridharan, and M. Saito. Caught in the Act: The Onset of Massive Star Formation. *ApJL*, 634:L185–L188, December 2005. doi: 10.1086/498867.

H. Beuther, Q. Zhang, E. A. Bergin, T. K. Sridharan, T. R. Hunter, and S. Leurini. Dust and gas emission in the prototypical hot core G29.96-0.02 at sub-arcsecond resolution. *ArXiv e-prints*, 704, April 2007.

L. Blitz. Local Group High-Velocity Clouds: Status of the Evidence. In J. E. Hibbard, M. Rupen, and J. H. van Gorkom, editors, *ASP Conf. Ser. 240: Gas and Galaxy Evolution*, pages 469–+, 2001.

I. A. Bonnell, M. R. Bate, C. J. Clarke, and J. E. Pringle. Accretion and the stellar mass spectrum in small clusters. *MNRAS*, 285:201–208, February 1997.

I. A. Bonnell, R. B. Mate, and H. Zinnecker, 1998.

I. A. Bonnell, M. R. Bate, C. J. Clarke, and J. E. Pringle. Competitive accretion in embedded stellar clusters. *MNRAS*, 323:785–794, May 2001. doi: 10.1046/j.1365-8711.2001.04270.x.

I. A. Bonnell, S. G. Vine, and M. R. Bate. Massive star formation: nurture, not nature. *MNRAS*, 349:735–741, April 2004. doi: 10.1111/j.1365-2966.2004.07543.x.

S. L. Breen, S. P. Ellingsen, J. L. Caswell, and B. E. Lewis. 12.2-GHz methanol masers towards 1.2-mm dust clumps: quantifying high-mass star formation evolutionary schemes. *MNRAS*, 401:2219–2244, February 2010. doi: 10.1111/j.1365-2966.2009.15831.x.

J. L. Caswell. Maser emission from OH at the 6035-MHz transition. *MNRAS*, 326: 805–820, September 2001. doi: 10.1046/j.1365-8711.2001.04745.x.

J. L. Caswell. Spectra of OH masers at 6035 and 6030 MHz. *MNRAS*, 341:551–568, May 2003. doi: 10.1046/j.1365-8711.2003.06418.x.

J. L. Caswell. A Galactic Centre survey for 6.6-GHz methanol masers. *MNRAS*, 283: 606–612, December 1996.

J. L. Caswell. Coincidence of maser emission from OH at 6.035 GHz and methanol at 6.668 GHz. *MNRAS*, 289:203–224, July 1997.

J. L. Caswell. Positions of hydroxyl masers at 1665 and 1667 MHz. *MNRAS*, 297: 215–235, June 1998. doi: 10.1046/j.1365-8711.1998.01468.x.

J. L. Caswell and R. F. Haynes. Star formation regions - their galactic distribution assessed from new OH maser surveys. *JRASC*, 77:257–+, October 1983a.

J. L. Caswell and R. F. Haynes. Survey of OH masers at 1665 MHz. II - Galactic longitude 340 deg to the galactic centre. *Australian Journal of Physics*, 36:361–399, 1983b.

J. L. Caswell and R. F. Haynes. An OH maser in the Large Magellanic Cloud. *MNRAS*, 194:33P–35P, March 1981.

J. L. Caswell and R. A. Vaile. Excited-state OH masers at 6.035 GHz. *MNRAS*, 273: 328–346, March 1995.

J. L. Caswell, G. A. Fuller, J. A. Green, A. Avison, S. L. Breen, K. J. Brooks, M. G. Burton, A. Chrysostomou, J. Cox, P. J. Diamond, S. P. Ellingsen, M. D. Gray, M. G. Hoare, M. R. W. Masheder, N. M. McClure-Griffiths, M. R. Pestalozzi, C. J. Phillips, L. Quinn, M. A. Thompson, M. A. Voronkov, A. J. Walsh, D. Ward-Thompson, D. Wong-McSweeney, J. A. Yates, and R. J. Cohen. The 6-GHz methanol multibeam maser catalogue - I. Galactic Centre region, longitudes $345\deg to 6\deg$. *MNRAS*, $404 : 1029 - -1060, May 2010. doi : 10.1111/j.1365 - 2966.2010.16339.x$.

X. Chen, S. P. Ellingsen, and Z.-Q. Shen. Class I methanol masers: masers with extended green objects. *MNRAS*, 396:1603–1609, July 2009. doi: 10.1111/j.1365-2966.2009.14818.x.

R. J. Cohen. Compact maser sources. *Reports of Progress in Physics*, 52:881–943, 1989.

R. J. Cohen. Masers in Star-Forming Regions. *Ap&SS*, 224:55–62, February 1995.

doi: 10.1007/BF00667821.

R. J. Cohen, G. C. Brebner, B. Hutawarakorn, and N. Gasiprong. OH Maser Discs at the Centre of Bipolar Molecular Outflows. In *IAU Symposium*, volume 221 of *IAU Symposium*, pages 168P–+, 2003.

R. J. Cohen, N. Gasiprong, J. Meaburn, and M. F. Graham. Hydroxyl maser disc and outflow in the Orion-BN/KL region. *MNRAS*, 367:541–552, April 2006. doi: 10.1111/j.1365-2966.2006.10021.x.

J. J. Condon, J. J. Broderick, and G. A. Seielstad. A 4.85 GHz sky survey. I - Maps covering delta between 0 and + 75 deg. *AJ*, 97:1064–1073, April 1989. doi: 10.1086/115049.

D. M. Cragg, A. M. Sobolev, and P. D. Godfrey. Modelling methanol and hydroxyl masers in star-forming regions. *MNRAS*, 331:521–536, March 2002. doi: 10.1046/j.1365-8711.2002.05226.x.

C. J. Cyganowski, B. A. Whitney, E. Holden, E. Braden, C. L. Brogan, E. Churchwell, R. Indebetouw, D. F. Watson, B. L. Babler, R. Benjamin, M. Gomez, M. R. Meade, M. S. Povich, T. P. Robitaille, and C. Watson. A Catalog of Extended Green Objects in the GLIMPSE Survey: A New Sample of Massive Young Stellar Object Outflow Candidates. *AJ*, 136:2391–2412, December 2008a. doi: 10.1088/0004-6256/136/6/2391.

C. J. Cyganowski, B. A. Whitney, E. Holden, E. Braden, C. L. Brogan, E. Churchwell, R. Indebetouw, D. F. Watson, B. L. Babler, R. Benjamin, M. Gomez, M. R. Meade, M. S. Povich, T. P. Robitaille, and C. Watson. A Catalog of Extended Green Objects in the GLIMPSE Survey: A New Sample of Massive Young Stellar Object Outflow Candidates. *AJ*, 136:2391–2412, December 2008b. doi: 10.1088/0004-6256/136/6/2391.

C. J. Cyganowski, C. L. Brogan, T. R. Hunter, and E. Churchwell. A Class I and Class II CH_3OH *Maser Survey of EGOs from the GLIMPSE Survey*. *ApJ*, 702 : 1615 – –1647, *September* 2009. *doi* : 10.1088/0004 – 637*X*/702/2/1615.

T. M. Dame and P. Thaddeus. A New Spiral Arm of the Galaxy: The Far 3 kpc Arm. *ApJL*, 683:L143–L146, August 2008. doi: 10.1086/591669.

T. M. Dame, D. Hartmann, and P. Thaddeus. The Milky Way in Molecular Clouds: A New Complete CO Survey. *ApJ*, 547:792–813, February 2001. doi: 10.1086/318388.

J. M. De Buizer, R. O. Redman, S. N. Longmore, J. Caswell, and P. A. Feldman. SiO outflow signatures toward massive young stellar objects with linearly distributed methanol masers. *A&A*, 493:127–143, January 2009. doi: 10.1051/0004-6361:200810907.

K. A. Edris, G. A. Fuller, R. J. Cohen, and S. Etoka. The masers towards IRAS 20126 + 4104. *A&A*, 434:213–220, April 2005. doi: 10.1051/0004-6361:20041872.

K. A. Edris, G. A. Fuller, and R. J. Cohen. A survey of OH masers towards high mass protostellar objects. *A&A*, 465:865–877, April 2007. doi: 10.1051/0004-6361:20066280.

M. Elitzur and T. de Jong. A model for the maser sources associated with H II regions. *A&A*, 67:323–332, July 1978.

S. P. Ellingsen. The relationship between class I and class II methanol masers. *MNRAS*, 359:1498–1516, June 2005. doi: 10.1111/j.1365-2966.2005.09010.x.

S. P. Ellingsen. Methanol Masers: Reliable Tracers of the Early Stages of High-Mass Star Formation. *ApJ*, 638:241–261, February 2006. doi: 10.1086/498673.

S. P. Ellingsen. A GLIMPSE-based search for 6.7-GHz methanol masers and the lifetime of their spectral features. *MNRAS*, 377:571–583, May 2007. doi: 10.1111/j.1365-2966.2007.11615.x.

S. P. Ellingsen, J. B. Whiteoak, R. P. Norris, J. L. Caswell, and R. A. Vaile. A Search for Methanol Masers in the Magellanic Clouds. *MNRAS*, 269:1019–+, August 1994.

Y. Fukui, N. Mizuno, R. Yamaguchi, A. Mizuno, and T. Onishi. On the Mass Spectrum of Giant Molecular Clouds in the Large Magellanic Cloud. *PASJ*, 53:L41–L44, December 2001.

G. Garay and S. Lizano. Massive Stars: Their Environment and Formation. *PASP*, 111:1049–1087, September 1999. doi: 10.1086/316416.

A. G. Gibb, M. G. Hoare, L. T. Little, and M. C. H. Wright. A detailed study of G35.2-0.7N: collimated outflows in a cluster of high-mass young stellar objects. *MNRAS*, 339:1011–1024, March 2003. doi: 10.1046/j.1365-8711.2003.06251.x.

P. Goldreich and D. A. Keeley. Astrophysical Masers. I. Source Size and Saturation. *ApJ*, 174:517–+, June 1972.

M. D. Gray. Pumping of OH main-line masers in star-forming regions. *MNRAS*, 375: 477–488, February 2007. doi: 10.1111/j.1365-2966.2006.11309.x.

J. A. Green, J. L. Caswell, G. A. Fuller, S. L. Breen, K. Brooks, M. G. Burton,

A. Chrysostomou, J. Cox, P. J. Diamond, S. P. Ellingsen, M. D. Gray, M. G. Hoare, M. R. W. Masheder, N. McClure-Griffiths, M. Pestalozzi, C. Phillips, L. Quinn, M. A. Thompson, M. Voronkov, A. Walsh, D. Ward-Thompson, D. Wong-McSweeney, J. A. Yates, and R. J. Cohen. Multibeam maser survey of methanol and excited OH in the Magellanic Clouds: new detections and maser abundance estimates. *MNRAS*, 385:948–956, April 2008. doi: 10.1111/j.1365-2966.2008.12888.x.

J. A. Green, J. L. Caswell, G. A. Fuller, A. Avison, S. L. Breen, K. Brooks, M. G. Burton, A. Chrysostomou, J. Cox, P. J. Diamond, S. P. Ellingsen, M. D. Gray, M. G. Hoare, M. R. W. Masheder, N. M. McClure-Griffiths, M. Pestalozzi, C. Phillips, L. Quinn, M. A. Thompson, M. A. Voronkov, A. Walsh, D. Ward-Thompson, D. Wong-McSweeney, J. A. Yates, and R. J. Cohen. The 6-GHz multibeam maser survey - I. Techniques. *MNRAS*, 392:783–794, January 2009a. doi: 10.1111/j.1365-2966.2008.14091.x.

J. A. Green, J. L. Caswell, G. A. Fuller, A. Avison, S. L. Breen, K. Brooks, M. G. Burton, A. Chrysostomou, J. Cox, P. J. Diamond, S. P. Ellingsen, M. D. Gray, M. G. Hoare, M. R. W. Masheder, N. M. McClure-Griffiths, M. Pestalozzi, C. Phillips, L. Quinn, M. A. Thompson, M. A. Voronkov, A. Walsh, D. Ward-Thompson, D. Wong-McSweeney, J. A. Yates, and R. J. Cohen. The 6-GHz multibeam maser survey - I. Techniques. *MNRAS*, 392:783–794, January 2009b. doi: 10.1111/j.1365-2966.2008.14091.x.

J. A. Green, N. M. McClure-Griffiths, J. L. Caswell, S. P. Ellingsen, G. A. Fuller, L. Quinn, and M. A. Voronkov. High-Mass Star Formation in the Near and Far 3 kpc Arms. *ApJL*, 696:L156–L158, May 2009c. doi: 10.1088/0004-637X/696/2/L156.

J. A. Green, N. M. McClure-Griffiths, J. L. Caswell, S. P. Ellingsen, G. A. Fuller, L. Quinn, and M. A. Voronkov. High-Mass Star Formation in the Near and Far 3 kpc Arms. *ApJL*, 696:L156–L158, May 2009d. doi: 10.1088/0004-637X/696/2/L156.

A. D. Haschick, K. M. Menten, and W. A. Baan. Detection of widespread strong methanol masers at 44 GHz. *ApJ*, 354:556–567, May 1990. doi: 10.1086/168715.

J. Hatchell, J. S. Richer, G. A. Fuller, C. J. Qualtrough, E. F. Ladd, and C. J. Chandler. Star formation in Perseus. Clusters, filaments and the conditions for star formation. *A&A*, 440:151–161, September 2005. doi: 10.1051/0004-6361:20041836.

R. F. Haynes and J. L. Caswell. A strong 1665-MHz OH maser in the Large Magellanic Cloud. *MNRAS*, 197:23P–25P, December 1981.

R. H. Hildebrand. The Determination of Cloud Masses and Dust Characteristics from Submillimetre Thermal Emission. *QJRAS*, 24:267–+, September 1983.

B. Hutawarakorn and R. J. Cohen. Magnetic field structure in the bipolar outflow source G 35.2-0.74N: MERLIN spectral line results. *MNRAS*, 303:845–854, March 1999. doi: 10.1046/j.1365-8711.1999.02286.x.

B. Hutawarakorn, R. J. Cohen, and G. C. Brebner. OH masers and magnetic fields in the bipolar outflow source W75N. *MNRAS*, 330:349–364, February 2002. doi: 10.1046/j.1365-8711.2002.05068.x.

F. P. Israel. Radio observations of H II regions in external galaxies. III - Thermal emission, H II regions and star formation in 14 late-type galaxies. *A&A*, 90:246–268, October 1980.

A.-K. Jappsen, Y. Li, M.-M. Mac Low, and R. S. Klessen. Effects of a Piecewise Polytropic Equation of State on Turbulent Fragmentation. In *Bulletin of the American Astronomical Society*, volume 35 of *Bulletin of the American Astronomical Society*, pages 1214–+, December 2003.

K. J. Johnston, R. Gaume, S. Stolovy, T. L. Wilson, C. M. Walmsley, and K. M. Menten. The distribution of the 6(2)-6(1) and 5(2)-5(1) E-type methanol masers in OMC-1. *ApJ*, 385:232–239, January 1992. doi: 10.1086/170930.

S. V. Kalenskii, R. Bachiller, I. I. Berulis, I. E. Valtts, J. Gomez-Gonzales, J. Martin-Pintado, A. Rodriguez-Franco, and V. I. Slysh. Search for Methanol Masers at 44-GHZ. *Soviet Astronomy*, 36:517–+, October 1992.

S. V. Kalenskii, L. E. B. Johansson, P. Bergman, S. Kurtz, P. Hofner, C. M. Walmsley, and V. I. Slysh. Search for Class I methanol masers in low-mass star formation regions. *MNRAS*, 405:613–620, June 2010. doi: 10.1111/j.1365-2966.2010.16484.x.

S. V. Kalenskiĭ, V. G. Promyslov, V. I. Slysh, P. Bergman, and A. Winnberg. The detection of class I methanol masers towards regions of low-mass star formation. *Astronomy Reports*, 50:289–297, April 2006. doi: 10.1134/S1063772906040032.

E. Keto. The Formation of Massive Stars by Accretion through Trapped Hypercompact H II Regions. *ApJ*, 599:1196–1206, December 2003. doi: 10.1086/379545.

M. R. Krumholz. High Mass Star Formation by Gravitational Collapse of Massive Cores. *ArXiv Astrophysics e-prints*, July 2006.

M. R. Krumholz, C. F. McKee, and R. I. Klein. Why Radiation Pressure Cannot Stop the Formation of Massive Stars. In *Bulletin of the American Astronomical*

Society, volume 36 of *Bulletin of the American Astronomical Society*, pages 1620–+, December 2004.

M. R. Krumholz, C. F. McKee, and R. I. Klein. How Protostellar Outflows Help Massive Stars Form. *ApJL*, 618:L33–L36, January 2005a. doi: 10.1086/427555.

M. R. Krumholz, C. F. McKee, and R. I. Klein. Bondi Accretion in the Presence of Vorticity. *ApJ*, 618:757–768, January 2005b. doi: 10.1086/426051.

S. Kurtz, P. Hofner, and C. V. Álvarez. A Catalog of $CH_3OH 7_0 - 6_1 A^+ Maser Sources in Massive Star - forming Regions$. *ApJS*, 155 : 149 – −165, *November* 2004. *doi* : 10.1086/423956.

C. J. Lada and B. A. Wilking. The nature of the embedded population in the Rho Ophiuchi dark cloud - Mid-infrared observations. *ApJ*, 287:610–621, December 1984. doi: 10.1086/162719.

C. J. Lada, J. Alves, E. A. Lada, and E. A. Bergin. Seeing Light Through the Dark: Probing the Structure of the Dense Molecular Cloud B68. In *Bulletin of the American Astronomical Society*, pages 914–+, May 2001.

G. M. Larionov, V. G. Promyslov, and I. E. Val'Tts. Mapping of Bipolar Outflows and Methanol Masers in the CS(2-1) Line. *Astronomy Reports*, 45:331–338, May 2001. doi: 10.1134/1.1369796.

F. J. Lockman. Star formation and ionization in the 3 kiloparsec arm. *ApJ*, 241:200–207, October 1980. doi: 10.1086/158332.

S. N. Longmore, M. G. Burton, P. J. Barnes, T. Wong, C. R. Purcell, and J. Ott. Multi-wavelength observations of southern hot molecular cores traced by methanol masers - I. Ammonia and 24-GHz continuum data. *MNRAS*, 379:535–572, August 2007. doi: 10.1111/j.1365-2966.2007.11850.x.

P. Manoj, P. T. P. Ho, N. Ohashi, Q. Zhang, T. Hasegawa, H.-R. Chen, H. C. Bhatt, and N. M. Ashok. An Evolved Disk Surrounding the Massive Main-Sequence Star MWC 297? *ApJL*, 667:L187–L190, October 2007. doi: 10.1086/522424.

P. Massey. MASSIVE STARS IN THE LOCAL GROUP: Implications for Stellar Evolution and Star Formation. *ARA&A*, 41:15–56, 2003. doi: 10.1146/annurev.astro.41.071601.170033.

C. F. McKee and J. C. Tan. The Formation of Massive Stars from Turbulent Cores. *ApJ*, 585:850–871, March 2003. doi: 10.1086/346149.

K. M. Menten. The discovery of a new, very strong, and widespread interstellar

methanol maser line. *ApJL*, 380:L75–L78, October 1991. doi: 10.1086/186177.

V. Minier, J. E. Conway, and R. S. Booth. VLBI observations of 6.7 and 12.2 GHz methanol masers toward high mass star-forming regions. II. Tracing massive protostars. *A&A*, 369:278–290, April 2001. doi: 10.1051/0004-6361:20010124.

V. Minier, M. Burton, T. Wong, C. Purcell, and R. Hill. Methanol Masers: Signposts of Massive Protostars. In F. Combes, D. Barret, T. Contini, and L. Pagani, editors, *SF2A-2003: Semaine de l'Astrophysique Francaise*, pages 211–+, 2003.

S. Molinari, J. Brand, R. Cesaroni, F. Palla, and G. G. C. Palumbo. A search for precursors of ultracompact H II regions in a sample of luminous IRAS sources. II. VLA observations. *A&A*, 336:339–351, August 1998.

M. Morimoto, T. Kanzawa, and M. Ohishi. New maser lines of methanol. *ApJL*, 288: L11–L15, January 1985. doi: 10.1086/184411.

F. Motte, P. Schilke, and D. C. Lis. From Massive Protostars to a Giant H II Region: Submillimeter Imaging of the Galactic Ministarburst W43. *ApJ*, 582:277–291, January 2003. doi: 10.1086/344538.

P. Murdin. *Encyclopedia of astronomy and astrophysics*. 2001.

J. D. Pandian, P. F. Goldsmith, and A. A. Deshpande. The Arecibo Methanol Maser Galactic Plane Survey. I. Data. *ApJ*, 656:255–274, February 2007. doi: 10.1086/510512.

Y.-S. Park, J.-F. Panis, N. Ohashi, M. Choi, and Y. C. Minh. Interferometric Observation of the L483 Molecular Core. *ApJ*, 542:344–351, October 2000. doi: 10.1086/309501.

N. Peretto and G. A. Fuller. The initial conditions of stellar protocluster formation. I. A catalogue of Spitzer dark clouds. *A&A*, 505:405–415, October 2009. doi: 10.1051/0004-6361/200912127.

M. Pestalozzi, M. Elitzur, and J. Conway. A differentially rotating disc in a high-mass protostellar system. *ArXiv e-prints*, April 2009.

M. R. Pestalozzi, V. Minier, and R. S. Booth. A general catalogue of 6.7-GHz methanol masers. I. Data. *A&A*, 432:737–742, March 2005. doi: 10.1051/0004-6361:20035855.

J. E. Pineda, E. W. Rosolowsky, and A. A. Goodman. The Perils of Clumpfind: The Mass Spectrum of Substructures in Molecular Clouds. *ApJL*, 699:L134–L138, July 2009. doi: 10.1088/0004-637X/699/2/L134.

R. L. Plambeck and K. M. Menten. 95 GHz methanol masers near DR 21 and DR 21(OH). *ApJ*, 364:555–560, December 1990. doi: 10.1086/169437.

P. Pratap, P. A. Shute, T. C. Keane, C. Battersby, and S. Sterling. Class i Methanol Masers: Signposts of Star Formation? *AJ*, 135:1718–1730, May 2008. doi: 10.1088/0004-6256/135/5/1718.

C. R. Purcell, R. Balasubramanyam, M. G. Burton, A. J. Walsh, V. Minier, M. R. Hunt-Cunningham, L. L. Kedziora-Chudczer, S. N. Longmore, T. Hill, I. Bains, P. J. Barnes, A. L. Busfield, P. Calisse, N. H. M. Crighton, S. J. Curran, T. M. Davis, J. T. Dempsey, G. Derragopian, B. Fulton, M. G. Hidas, M. G. Hoare, J.-K. Lee, E. F. Ladd, S. L. Lumsden, T. J. T. Moore, M. T. Murphy, R. D. Oudmaijer, M. B. Pracy, J. Rathborne, S. Robertson, A. S. B. Schultz, J. Shobbrook, P. A. Sparks, J. Storey, and T. Travouillion. A CH_3CN and HCO^+ survey towards southern methanol masers associated with star formation. *MNRAS*, 367:553–576, April 2006a. doi: 10.1111/j.1365-2966.2005.09921.x.

C. R. Purcell, R. Balasubramanyam, M. G. Burton, A. J. Walsh, V. Minier, M. R. Hunt-Cunningham, L. L. Kedziora-Chudczer, S. N. Longmore, T. Hill, I. Bains, P. J. Barnes, A. L. Busfield, P. Calisse, N. H. M. Crighton, S. J. Curran, T. M. Davis, J. T. Dempsey, G. Derragopian, B. Fulton, M. G. Hidas, M. G. Hoare, J.-K. Lee, E. F. Ladd, S. L. Lumsden, T. J. T. Moore, M. T. Murphy, R. D. Oudmaijer, M. B. Pracy, J. Rathborne, S. Robertson, A. S. B. Schultz, J. Shobbrook, P. A. Sparks, J. Storey, and T. Travouillion. A CH_3CN and HCO^+ survey towards southern methanol masers associated with star formation. *MNRAS*, 367:553–576, April 2006b. doi: 10.1111/j.1365-2966.2005.09921.x.

M. J. Reid, K. M. Menten, X. W. Zheng, A. Brunthaler, L. Moscadelli, Y. Xu, B. Zhang, M. Sato, M. Honma, T. Hirota, K. Hachisuka, Y. K. Choi, G. A. Moellenbrock, and A. Bartkiewicz. Trigonometric Parallaxes of Massive Star-Forming Regions. VI. Galactic Structure, Fundamental Parameters, and Noncircular Motions. *ApJ*, 700: 137–148, July 2009. doi: 10.1088/0004-637X/700/1/137.

N. A. Ridge and T. J. T. Moore. A single distance sample of molecular outflows from high-mass young stellar objects. *A&A*, 378:495–508, November 2001. doi: 10.1051/0004-6361:20011180.

T. P. Robitaille, B. A. Whitney, R. Indebetouw, and K. Wood. Interpreting Spectral Energy Distributions from Young Stellar Objects. II. Fitting Observed SEDs Using a Large Grid of Precomputed Models. *ApJS*, 169:328–352, April 2007. doi:

10.1086/512039.

E. Scalise, Jr. and M. A. Braz. H2O maser survey in the Magellanic Clouds. *AJ*, 87: 528–531, March 1982. doi: 10.1086/113125.

P. Schilke, D. M. Mehringer, and K. M. Menten. A Submillimeter HCN Laser in IRC +10216. *ApJL*, 528:L37–L40, January 2000. doi: 10.1086/312416.

F. Schuller, K. M. Menten, Y. Contreras, F. Wyrowski, P. Schilke, L. Bronfman, T. Henning, C. M. Walmsley, H. Beuther, S. Bontemps, R. Cesaroni, L. Deharveng, G. Garay, F. Herpin, B. Lefloch, H. Linz, D. Mardones, V. Minier, S. Molinari, F. Motte, L.-Å. Nyman, V. Reveret, C. Risacher, D. Russeil, N. Schneider, L. Testi, T. Troost, T. Vasyunina, M. Wienen, A. Zavagno, A. Kovacs, E. Kreysa, G. Siringo, and A. Weiß. ATLASGAL - The APEX telescope large area survey of the galaxy at 870 μm. *A&A*, 504:415–427, September 2009. doi: 10.1051/0004-6361/200811568.

M. W. Sinclair, G. J. Carrad, J. L. Caswell, R. P. Norris, and J. B. Whiteoak. A methanol maser in the Large Magellanic Cloud. *MNRAS*, 256:33P–+, May 1992.

V. I. Slysh, S. V. Kalenskii, I. E. Valtts, and R. Otrupcek. The Parkes Survey of Methanol Masers at 44.07-GHz. *MNRAS*, 268:464–+, May 1994.

D. P. Smits. New Detections of Excited OH Masers at 5-CENTIMETER Wavelength. *MNRAS*, 269:L11+, July 1994.

L. Staveley-Smith, S. Kim, M. R. Calabretta, R. F. Haynes, and M. J. Kesteven. A new look at the large-scale HI structure of the Large Magellanic Cloud. *MNRAS*, 339: 87–104, February 2003. doi: 10.1046/j.1365-8711.2003.06146.x.

J. Stutzki and R. Guesten. High spatial resolution isotopic CO and CS observations of M17 SW - The clumpy structure of the molecular cloud core. *ApJ*, 356:513–533, June 1990. doi: 10.1086/168859.

Y.-N. Su, Q. Zhang, and J. Lim. Bipolar Molecular Outflows from High-Mass Protostars. *ApJ*, 604:258–271, March 2004. doi: 10.1086/381880.

M. Szymczak, A. J. Kus, and G. Hrynek. A blind survey of the 6.7 GHz methanol maser line. In V. Migenes & M. J. Reid, editor, *Cosmic Masers: From Proto-Stars to Black Holes*, volume 206 of *IAU Symposium*, pages 143–+, 2002.

A. R. Thompson. Fundamentals of Radio Interferometry. In G. B. Taylor, C. L. Carilli, & R. A. Perley, editor, *Synthesis Imaging in Radio Astronomy II*, volume 180 of *Astronomical Society of the Pacific Conference Series*, pages 11–+, 1999.

D. M. Tideswell, G. A. Fuller, T. J. Millar, and A. J. Markwick. The abundance of

HNCO and its use as a diagnostic of environment. *A&A*, 510:A85+, February 2010. doi: 10.1051/0004-6361/200810820.

A. G. G. M. Tielens. *The Physics and Chemistry of the Interstellar Medium*. The Physics and Chemistry of the Interstellar Medium, by A. G. G. M. Tielens, pp. . ISBN 0521826349. Cambridge, UK: Cambridge University Press, 2005., September 2005.

I. E. Val'Tts and G. M. Larionov. A general catalog of class I methanol masers. *Astronomy Reports*, 51:519–530, July 2007. doi: 10.1134/S1063772907070013.

M. Voronkov, A. Sobolev, S. Ellingsen, A. Ostrovskii, and A. Alakoz. Maser Action in Methanol Transitions. *Ap&SS*, 295:217–223, January 2005. doi: 10.1007/s10509-005-3692-z.

M. A. Voronkov, K. J. Brooks, A. M. Sobolev, S. P. Ellingsen, A. B. Ostrovskii, and J. L. Caswell. Class I methanol masers in the outflow of IRAS16547-4247. *MNRAS*, 373:411–424, November 2006. doi: 10.1111/j.1365-2966.2006.11047.x.

A. J. Walsh, A. R. Hyland, G. Robinson, and M. G. Burton. Studies of ultracompact HII regions - I. Methanol maser survey of IRAS-selected sources. *MNRAS*, 291: 261–278, October 1997.

A. J. Walsh, M. G. Burton, A. R. Hyland, and G. Robinson. Studies of ultracompact HII regions - II. High-resolution radio continuum and methanol maser survey. *MNRAS*, 301:640–698, December 1998. doi: 10.1046/j.1365-8711.1998.02014.x.

A. J. Walsh, M. G. Burton, A. R. Hyland, and G. Robinson. Studies of ultracompact HII regions - III. Near-infrared survey of selected regions. *MNRAS*, 309:905–922, November 1999. doi: 10.1046/j.1365-8711.1999.02890.x.

A. J. Walsh, G. H. Macdonald, N. D. S. Alvey, M. G. Burton, and J.-K. Lee. Observations of warm dust near methanol masers. *A&A*, November 2003.

S. Weinreb. Radio Observations of OH in the Interstellar Medium. *Nature*, 200:829–831, November 1963. doi: 10.1038/200829a0.

J. B. Whiteoak and F. F. Gardner. Observations of H2O masers in nearby galaxies. *MNRAS*, 222:513–523, October 1986.

J. B. Whiteoak, K. J. Wellington, D. L. Jauncey, F. F. Gardner, J. R. Forster, J. L. Caswell, and R. A. Batchelor. Observations of H2O maser emission in the Large Magellanic Cloud. *MNRAS*, 205:275–279, October 1983.

J. P. Williams, E. J. de Geus, and L. Blitz. Determining structure in molecular clouds.

ApJ, 428:693–712, June 1994. doi: 10.1086/174279.

D. O. S. Wood and E. Churchwell. The morphologies and physical properties of ultracompact H II regions. *ApJS*, 69:831–895, April 1989a. doi: 10.1086/191329.

D. O. S. Wood and E. Churchwell. Massive stars embedded in molecular clouds - Their population and distribution in the galaxy. *ApJ*, 340:265–272, May 1989b. doi: 10.1086/167390.

Y. Wu, Y. Wei, M. Zhao, Y. Shi, W. Yu, S. Qin, and M. Huang. A study of high velocity molecular outflows with an up-to-date sample. *A&A*, 426:503–515, November 2004. doi: 10.1051/0004-6361:20035767.

H. W. Yorke and C. Sonnhalter. On the Formation of Massive Stars. *ApJ*, 569:846–862, April 2002. doi: 10.1086/339264.

Q. Zhang, T. R. Hunter, T. K. Sridharan, and P. T. P. Ho. A Disk/Jet System toward the High-mass Young Star in AFGL 5142. In *Bulletin of the American Astronomical Society*, volume 33 of *Bulletin of the American Astronomical Society*, pages 1504–+, December 2001.

H. Zinnecker and H. W. Yorke. Toward Understanding Massive Star Formation. *ARA&A*, 45:481–563, September 2007. doi: 10.1146/annurev.astro.44.051905.092549.